UNIVERSITY OF THE FREE STATE
UNIVERSITEIT VAN DIE VRYSTAAT
YUNIVESITHI YA FREISTATA

SENSITIVITY ANALYSIS OF THE INTEGRAL QUALITY MONITORING SYSTEM® FOR RADIOTHERAPY VERIFICATION USING MONTE CARLO SIMULATION

A thesis submitted in fulfilment of the requirements for the degree of ***Doctor of Philosophy*** *in Medical Physics*

Department of Medical Physics

Faculty of Health Science

University of the Free State

By

Oluwaseyi Michael Oderinde

Supervisor: Dr. F.C.P. du Plessis

July 2017.

DECLARATION

AUTHOR: Oluwaseyi Michael ODERINDE

DEGREE: Doctor of Philosophy

TITLE: Sensitivity Analysis of the Integral Quality Monitoring System® for Radiotherapy Verification using Monte Carlo Simulation

ETHICS NUMBER: ECUFS NR 224/2015

DATE OF DEPOSIT: July 2017

I, Oluwaseyi Michael ODERINDE, declare that the doctorate's research thesis or publishable, interrelated articles that I herewith submit at the University of the Free State, is my independent work and that I have not previously submitted it for a qualification at another institution of higher education.
I at this moment declare that I am aware that the copyright is vested in the University of the Free State.
I at this moment claim that all royalties as regards intellectual property that was developed during and in connection with the study at the University of the Free State will accrue to the University.
I at this moment declare that I am aware that the research may only be published with the dean's approval.

SIGNATURE: …….. OM ODERINDE.

TABLE OF CONTENTS

DEDICATION

I dedicate this research to the Almighty God (the source of my strength and the provider of my help in times of needs [Isaiah 41:10]) and my dearest mother who died in the last year of my PhD program.

GLOSSARY

2D: Two-dimensional

3D: Three-dimensional

4D: Four-dimensional

AAPM: American Association of Physicist in Medicine

ART: Adaptive radiotherapy

ASTRO: American Society of therapeutic radiology and oncology

BEAMDP: Beam Data Processor

CM: Component Module

COIN: Clinical Oncology Information Network

CPU: Central processing unit

CRT: Conformal radiotherapy

CT: Computer Tomography

DD: Dose difference

DNA: Deoxyribonucleic acid

DTA: Distance-to-agreement

EPID: Electronic portal imaging device

ESTRO: European Society for Radiotherapy and Oncology

FORTRAN: Formula Translation

FS: Field size

GeV: Giga electron volts

IAEA: International Atomic Energy Agency

IGRT: Image-guided radiotherapy

IMRT: Intensity modulated radiotherapy

IQM: Integral quality monitor

ISO: International Organization Standardization

kV: kilovolts

Linac: Linear accelerator

MLC: Multileaf Collimator

MORTRAN: More of FORTRAN

MRI: Magnetic resonance imaging

MU: Monitor Unit

MV: Megavolt

MVCT: Megavolt cone beam CT

NTCP: Normal tissue complication probability

NRCC: National Research Council Canada

OAR: Organ at risk

OS: Operation system

PET: Positron emission tomography

QA: Quality assurance

QC: Quality control

ROF: Relative output factor

RT: Radiotherapy

SRC: Standard regression coefficient

SASQART: South Africa Standards for Quality Assurance in Radiotherapy

SBRT: Stereotactic body radiotherapy

SFS: Square field size

SLIC: scanning liquid ionization chamber

SSD: Source to surface distance

SRS: stereotactic radiosurgery

TCL: Tool command language

TCP: Tumour control probability

TK: Tool kit

TP: Treatment plan

TPS: Treatment planning system

VMAT: Volumetric modulated arc therapy

WHO: World Health Organization

XVI: X-ray volume imaging

STATEMENT OF ORIGINALITY

The contents of this thesis are the summary of the research conducted by the author during his PhD programme in Medical Physics, University of the Free State.

The research outcomes have been submitted for publication and presented at National and International conferences. Due to the nature of this study, a technical report is submitted to the Department of Medical Physics, the University of the Free State for internal use only.

Manuscripts

1. Technical note: A new wedge-shaped ionization chamber component module for BEAMnrc to model the integral quality monitoring system® (*In Production at Journal of Radiation Physics and Chemistry*).
2. Sensitivity analysis of the integral quality monitoring system using Monte Carlo simulation (*In Press at Computational and Mathematical Methods in Medicine Journal*)

Conference presentations

1. Monte Carlo study of an Integral quality monitoring system. 53rd National Congress of the SAAPMB; Theme: Cancer Imaging; September 2015; Bloemfontein, South Africa [*Abstract in Physica Medica European Journal of Medical Physics*].
2. Accurate Monte Carlo modelling of an Elekta Synergy linac equipped with an Agility 160-leaf MLC. 54th National Congress of the SAAPMB; Theme: Education and Training for the Millennials; September 2016; Cape Town, South Africa [*Abstract in Physica Medica European Journal of Medical Physics*].
3. Monte Carlo modelling of a prototype beam delivery check system for Intensity Modulated Radiation therapy plan. 54th National Congress of the SAAPMB; Theme: Education and Training for the Millennials; September 2016; Cape Town, South Africa [*Abstract in Physica Medica European Journal of Medical Physics*].

4. Variance-based sensitivity analysis study of a prototype beam delivery check system using Monte Carlo simulation. Engineering and Physical Science in Medicine Conference (EPSM); November 2016; Sydney, Australia.
5. On the sensitivity of the integral quality monitoring system to MLC positional error using BEAMnrc Monte Carlo simulation. 55th National Congress of the SAAPMB; September 2017; Durban, South Africa (The abstract was *accepted by the Physica Medica European Journal of Medical Physics*)

Technical report

1. Design of an Integral Quality Monitor (IQM) component module using BEAMnrc Monte Carlo simulation platform. Department of Medical Physics, University of the Free State; July 2015.

ABSTRACT

Advanced radiotherapy (RT) techniques have improved the quality of radiation treatment. Notwithstanding, advanced RT techniques have generated complexities in their quality assurance (QA). Therefore, there is a huge interest to verify treatment plan data in real-time treatment. The Integral quality monitoring (IQM) system® (iRT Systems GmbH, Koblenz, Germany) is an independent real-time treatment verifying system which checks the integrity and validates the accuracy of the treatment plan data. The IQM also functions as a pre-treatment quality assurance tool for radiotherapy. The prototype system (IQM) is currently undergoing its beta testing, and contributions from researchers across the globe are pivotal to its integration into the clinical workflow. The IQM is a large wedge-shaped ionization chamber that is attached to the treatment head of the linear accelerator (linac) for signal measurement in real-time treatment. The aim of this innovative study was to determine how sensitive the IQM is for small alterations in the multileaf collimator (MLC) leaf positions using Monte Carlo (MC) simulation. The sensitivity of the IQM system is essential for its integration into clinical workflow. The MC simulation technique is an accurate dose calculation engine that could score dose in regions that seem complicated for physical measurement.

A new component module (CM) called IQM was successfully developed using TCL/TK, and MORTRAN codes. The newly created CM was added-on to the BEAMnrc MC User code.

Also, a linac source model of an Elekta Synergy linac equipped with an Agility 160-leaf MLC head was developed using the EGSnrc/BEAMnrc. Accurate MC calculations for percentage depth doses, lateral beam profiles, and relative output factors were benchmarked with physical measurements using the Gamma analysis criterion of 2%/2 mm. Characterised photon beams of 10 MV for 1 × 1 up to 30 × 30 cm^2 fields using the BEAMnrc MC Code were simulated. Photon beam data stored in the phase space files after the source model simulations were calculated in a homogeneous water phantom using the DOSXYZnrc MC Code.

For the square field sizes considered, MC dosimetry features (percentage depth doses and lateral beam profiles) passed the gamma (γ) index criterion of 2%/2 mm. MC calculations and physical measurements agreed to approximate local difference of 1.44% for relative output factors. This accurate source model is suitable for the sensitivity study. It also has the potential to be used for dose calculation in advanced radiotherapy treatment planning.

The accurate source model with the IQM CM positioned with its central electrode plate fixed perpendicularly to the photon beam in subsequent simulations was used. The spatial integral dose in the air region of the IQM CM was calculated. The IQM MC dose was calculated for 1 × 1 up to 30 × 30 cm^2 fields at 10 MV photon beams and then correlated with physical measurement of the prototype IQM system. Secondly, systematic positional errors of 1, 2 and 3 mm were subtracted and added to the whole MLC bank of 1 × 1, 3 × 3, 5 × 5 and 10 × 10 cm^2 fields. Thirdly, the IQM signal response for 1, 2, 3, 4 and five leaves shifted out of a 5 × 5 cm^2 field for positional error of 1, 2, 3, 5, and 10 mm was calculated. Fourthly, the signal response was calculated for segments along the gradient of the IQM CM for 3 × 3, 5 × 5 and 7 × 7 cm^2 fields at 10 MV photon beams. Lastly, eleven segments (regular and irregular) were altered randomly within ±1, ±2 and ±3 mm regarding its individual leaf positions as defined at the isocentre. Sensitivity analyses of leaf positioning errors were studied by using the following techniques such as scatter plots, brute force, variance-based and standard regression coefficient.

The normalised IQM signal increases with an increase in square field sizes for the MC calculation and the physical measurement. The IQM model is highly sensitive to alterations of 1 × 1 cm^2 more than other fields considered. For the segments considered, the magnitude of the signal response decreased and increased when systematic positional errors were subtracted from and added to individual MLC leaves. An increase in numbers of leaves shifted out causes an increase in IQM signal response and an increase in the position of moving leaves causes a further increase in the IQM signal. The sensitivity of the IQM model increases along the gradient of the IQM up to a noticeable plateau. The sensitivity analysis techniques utilised in this study

deduced that the IQM model is highly sensitive to leaf positions of small segments compared to large apertures.

The newly developed IQM MC model can now serve as a basis for researchers that have an interest in dose monitoring and MLC calibration using the wedge-shaped ionization chamber. The IQM model shows a potential platform for further study on advanced radiotherapy quality control.

Application of MC techniques to dose monitoring is authentic. It demonstrates that the MC radiation transport method is virtually unlimited when it comes to solving radiation transport and dose calculation challenges.

LIST OF TABLES AND FIGURES

List of Figures

List of Tables

ACKNOWLEDGEMENTS

I sincerely thank the Lord Almighty for the success of this research. If it had not been the Lord on my side, where would I have been (Psalm 124)?

My in-depth gratitude goes to my supervisor Dr FCP du Plessis, for his relentless effort in correcting and putting me through the nitty-gritty of a quality thesis. His constructive criticism is beyond measure. I learnt from him how to conduct an independent research.

I appreciate Prof. William Rae's for his advice and interest in this study.

I am grateful to the members of staff and colleagues (Dr. Willie, Mrs Dedril, Mr Cobus, Mr Lourens, Mr Itumeleng, Dr. Nicholas, Mr Stalyn and Mr Courage) at the Medical Physics Department, Universitas of the Free State Annex District Hospital, Bloemfontein for their support and contributions during the research meetings and our daily interactions.

My friends and family have substantially assisted me during this study. In particular, my parents (Daddy and Late Mummy Oderinde, Daddy and Mummy Adebiyi) and my brothers (Tolu and Iyanu) who have supported me beyond measure. You have been the best family have ever wished.

My profound gratitude goes to my dearest wife for her support in all ramification. I appreciate her patience, calmness and understanding even when I denied her a befitting honeymoon due to my busy schedule during this study. Thank you for believing in me. I share the joy of completing this research with you and our newborn baby.

This research project was funded by the South Africa Medical Research Council (MRC) with funds from National Treasury under its Economic Competitive and Support package. This research and the publication thereof are the results of funding provided by the SAMRC under the High Energy Advanced Radiation (HARD) sponsorship programme *SAMRC-RFA-UFSP-01-2013/HARD*.

CHAPTER 1

1.0 INTRODUCTION

1.1 BACKGROUND

Africa, the worlds' second largest and second most- populous continent in the world is suffering from malignant tumour (cancer). This life-threatening disease is projected to terminate over 970,000 lives in Africa by 2030 (American Cancer Society 2011). South Africa, where prostate cancer is mostly prevalent in men and breast cancer tops the list of cancer occurrences in women could experience an increase of 78% cancer cases by 2030 (Sitas et al. 2006; Rogo et al. 2006). Cancer outbreak could be as a result of behavioural and dietary risk, overweight, ageing and natality increase in South Africa. Strict and professional measures have being introduced in combating this deadly disease in Africa at large (Parkin et al. 2003; IAEA 1998; Cook & Burkitt 1971; IAEA 2003). The most traditional cancer treatments are surgery, radiotherapy (RT), and chemotherapy. Approximately 50% of cancer patients will receive radiation treatment during the course of their treatment with about 40% curative strength (Fig. 1.1 depicts the epidemic cancers that undergo radiotherapy) (Baskar et al. 2012; Roopashri & Baig 2013). This study is a radiation oncology physics research.

Radiotherapy is the treatment of cancer using high-energy radiation, usually x-rays. However, the radiation oncology facilities are not well distributed within this continent (Levin et al. 1999; Petereit 2015; Adewuyi et al. 2013). Governments and influential, magnanimous and passionate individuals are daily called upon to contribute their quota towards equipping our hospitals with radiotherapy facilities. The major types radiation treatments are external beam radiotherapy and brachytherapy. In external radiation beam, the high-energy source irradiates the target volume from a defined distance to the tumour target. External beam radiotherapy employs the use of high energy machines (such as cobalt unit and linear accelerators) to irradiate the tumour site either with photons, protons or electrons. While in brachytherapy, the radioisotope source sealed in a seed is positioned inside the targeted volume to emit particles that could damage the deoxyribonucleic acid (DNA) structure of the tumour. External photon beams are recommended for radiotherapy treatment compare to external electron

beams which are efficient for shallow treatment and external proton beams which are limited because of its high expenses (Benedict 2004; Ma et al. 2006; Virnig et al. 2002).

It is a continual effort to improve the quality of radiotherapy treatment and increase the number of cancer survivors. This research channels towards enhancing the quality of radiation treatment in Universitas annex Hospital, Bloemfontein, South Africa and impacting its neighbouring countries in a similar way.

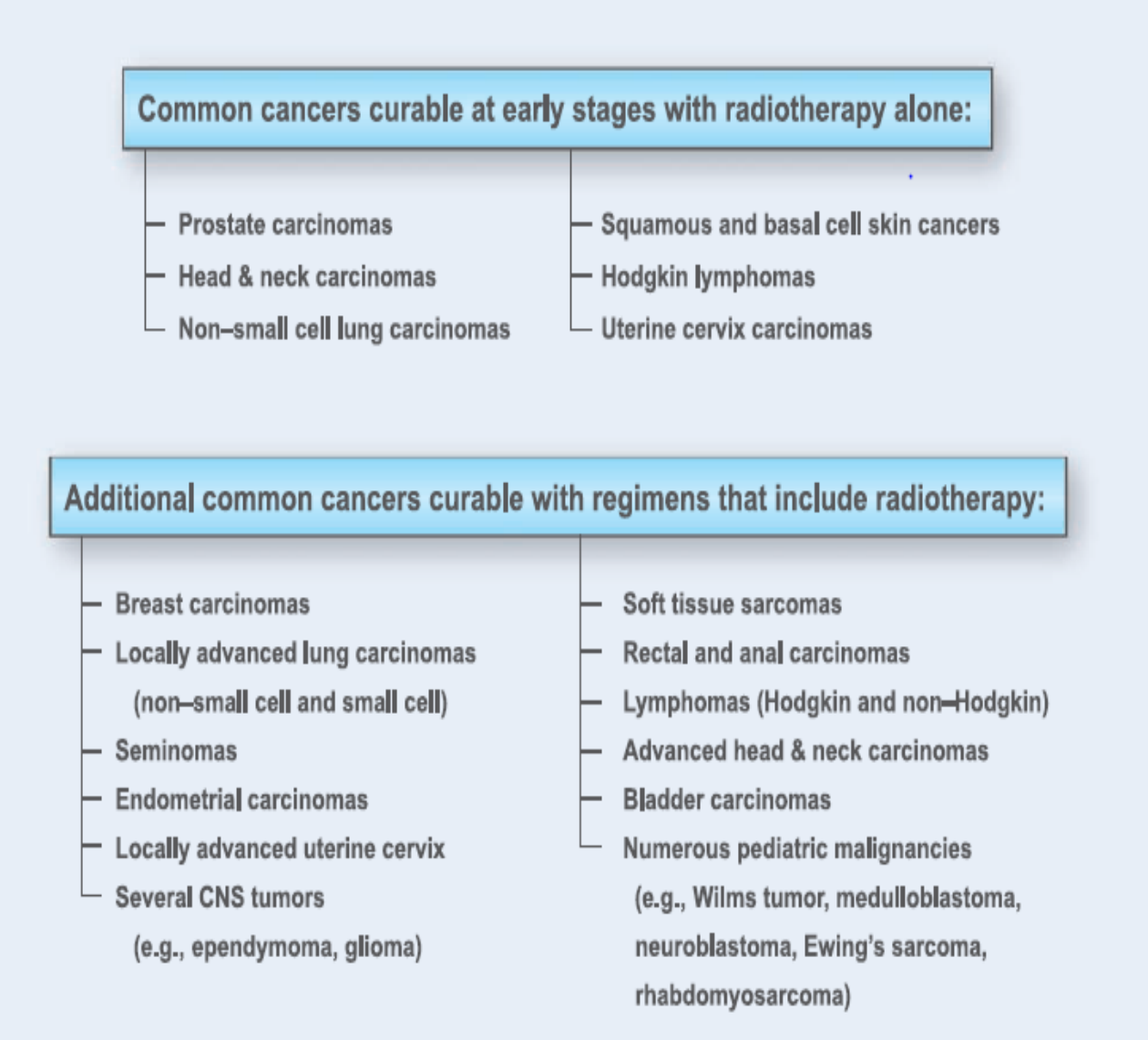

Figure 1.1: List of common cancer treated with radiotherapy (Connell & Hellman 2009)

1.2 ADVANCES IN EXTERNAL BEAM RADIOTHERAPY

Over the years, technological innovation has driven advances in external-beam radiotherapy (EBRT). It is for the purpose of care (healthy tissue sparing), cure (optimised treatment), and cost (inexpensive). It is an improvement on treatment beam, total delivery dose, safest delivery angle, treatment volume and irradiated region. Wilhelm Conrad Röentgen's (a German Professor of Physics) pioneered radiotherapy research (Hellman 1996). He discovered the electromagnetic radiation in a wavelength range called X-rays in November 1895 while studying the cathode ray production. In his further quest, he used x-ray beam to image his wife's finger (popularly called Röentgen photography) (Coutard 1934; Fletcher 1978). Nearly seven (7) months after, they conducted the first radiation treatment and the first superficial tumour treatment was carried out approximately 18 months after this discovery. However, the X-ray tubes treatment was limited to 150 kV. In 1900, palliative treatment using an X-ray machine was successful. This discovery gave birth to the field of radiology and radiation oncology (Clark 1992). Since then it has been stated that x-ray machines function as diagnostic and therapeutic tools. It could as well work as a palliative treatment and symptom control tool in complicated or recurrent tumours. Since Roentgen's discovery, advancement has emanated from x-ray on several occasions to improve and upgrade radiotherapy treatment (Mayles et al. 2007; Haffty & Wilson 2009; Kupelian et al. 2004).

Earlier discoveries were unable to generate high-energy treatment machines for deep-seated tumours without excessive skin dose. The beginning of the 1950s brought in Cobalt 60 for high energy EBRT. Cobalt 60 makes use of Gamma γ rays from radioisotopes of Cobalt 60. It is proficient of treating tumours with 1.25 MeV, which make it possible to deliver 45- 60 Gy doses to a deep-seated tumour (tumour like Hodgkin lymphoma). However, it is limited to low Megavolt and risky to manage. It needs an efficient radioactive waste management. Cobalt 60 is widely used today since it is reliable and straightforward to maintain (Thariat et al. 2013).

Excitement came to the world in the 1960s with the development of high energy (Megavolt) treatment machine called a linear accelerator (linac). It could conveniently

treat deep-seated tumours (such as Pelvic of an obese patient) without damaging the healthy tissues or wreak havoc in the overlying skin tissues (Bucci et al. 2005; Emami et al. 1991). Linacs have the potential to produce X-ray beams up to 20 MV and electron beams for superficial treatments.

1.2.1 TWO- DIMENSIONAL CONVENTIONAL RADIOTHERAPY

In Two- dimensional (2D) (plain X-ray images) conventional RT, a single beam of one to four coplanar directions are used. This treatment approach is quite simple regarding equipment, infrastructure, and training. 2D RT utilises four parallel opposing fields "boxes" as depicted in figure 1.2(a). Despite the fact that X-ray simulator film is used to develop the treatment portals, and 2D treatment planning system is used to calculate the dose distributions, 2D RT gives an excessive dose to healthy tissues around the treatment site (Bucci et al. 2005; Oh et al. 1999).

1.2.2 THREE- DIMENSIONAL CONFORMAL RADIOTHERAPY

Technological advancement in computing has improved imaging techniques, generating powerful software for high spatial image resolution. The 1970s saw the transition from two-dimensional (2D) conventional RT (planar x-ray images) to three-dimensional (3D) conformal radiotherapy (3D-CRT) (computer tomography (CT) images) (Ryu et al. 2002; Michalski et al. 2003; Baglan et al. 2003). Figure 1.2(b) shows an example of 3D-CRT. The purpose of radiotherapy treatment is to attain the highest level of cure with least morbidity. A CT scanner can conveniently image the axial anatomy and complex irregular shapes. CT-based simulation and planning allow better radiation dose delivery. Magnetic resonance imaging (MRI) has also been introduced which some researchers suggested that it should be used alongside with CT-scan to increase the therapeutic ratio of head and neck malignancies (Roach et al. 1996; Kagawa et al. 1997). Over the years, X-ray, CT, MRI with or without spectroscopy, positron emission tomography (PET), and ultrasound have been introduced for tumour identification (Roopashri & Baig 2013; Baskar et al. 2012; Langen et al. 2003).

3D-CRT reduces radiation dose to surrounding critical structures and also increases the efficiency of dose calculation with fewer sequelae compared to 2D RT (Sale et al.

2005). With CT-based simulation and plan, RT delivery dose is accurate on a 3D sculpture of the target with minimal dose to organs at risk (OARs). The arrival of multileaf collimators (MLCs) and treatment planning system (TPS), influenced an efficient beam orientations; displaying beam-eye-views (BEVs). A computerised algorithm on the TPS drives the geometric beam shaping device (MLCs). Despite the capabilities of 3D-CRT, there are limitations in target conformity due to the uniform intensity of the treatment beams.

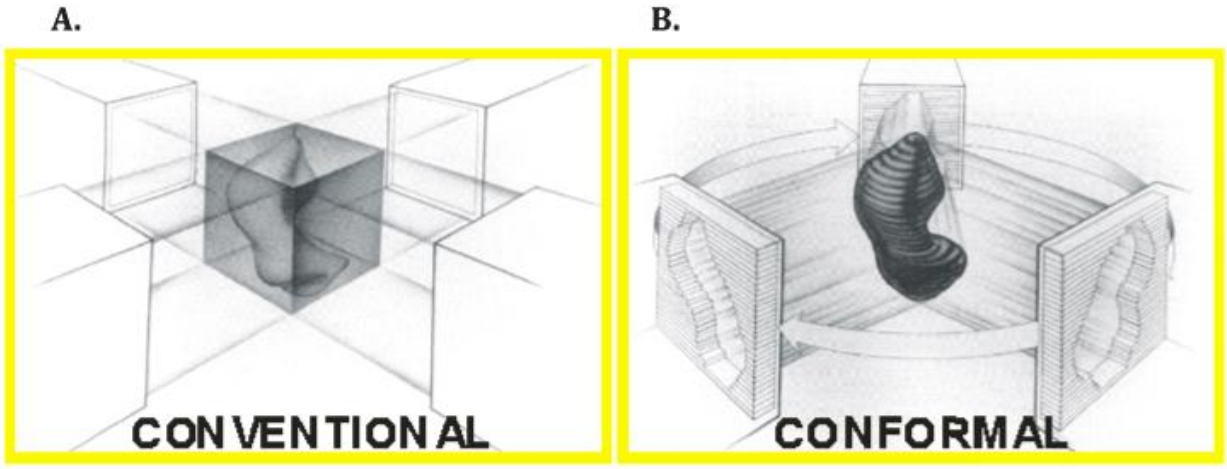

Figure 1.2: planned radiotherapy field, (a) for 2D RT and (b) for 3D CRT (Dj 2014)

1.2.3 INTENSITY-MODULATED RADIOTHERAPY

The intensity modulated radiotherapy (IMRT) tolerates treatment of complex irregular shapes by modulating the photon beam intensity of fractions in the same field (Nakamura et al. 2014; Bindhu et al. 2009; Mundt & Roeske 2005). This technique optimises the therapeutic ratio and surrounding organs-at-risk (OAR) (Boutilier et al. 2015; Amit et al. 2015; Hansen et al. 2006). The IMRT is made possible through inverse planning software and computer controlled motion of the MLC during beam-on-time (Huang et al. 2002; Intensity modulated radiotherapy collaborated working group 2001; Xia et al. 2000; Zelefsky et al. 2000). The MLCs are metallic leaves located in the linac head; they move independently for beam intensity optimisation (Mohan 1995; Palta et al. 2003; Thilmann et al. 2004; St Clair et al. 2004). The IMRT technique has the

potential to improve dose delivery in many clinical complicated circumstances. It treatment delivery is done by using static (step and shoot) or dynamic MLC (DMLC) or TomoTherapy® machines (Fenwick et al. 2006; Oldham et al. 1995; Hall 2006; Lee et al. 2002). Furthermore, the innovative IMRT technology has improved the treatment rate by using dynamic therapy (Thariat et al. 2013). IMRT is inadequate to identify microscopic tumours and unable to immobilise the patient, organ and tumour during the treatment session (about 15-30 minutes) (Bucci et al. 2005).

1.2.4 FOUR- DIMENSIONAL RADIOTHERAPY

In the early 1990s, it is apparent that patients, organs, and tumours could move during radiation treatment. These voluntary and visceral movements (including respiration and digestion) during the treatment may lead to suboptimal treatment and unplanned dose to the OARs. Four-dimensional (4D) RT was introduced to reduce geometrical uncertainties that are influenced by these movements during RT. The time (t) to measure the target motion and anatomical change is the fourth dimension beyond the 3D-space (x,y,z). In 4D (t,x,y,z) RT, imaging, planning and delivery of RT are designed precisely to account for provisional variations in the anatomy (Keall et al. 2005). 4D CT scan obtains series of images for movement cycles and 4D TPS plans for each of the received images of the movement phases. In 4D RT, there is continual beam delivery of the 4D treatment plans to the patient. 4D RT has been tested to enhance dosimetry than 3D CRT (Keall et al. 2005). In thoracic RT, where respiratory motion influences the position of the lungs, breast and heart, five strategic approaches are currently utilised to reduce respiratory motion. They are; breath-holding techniques (active or voluntary), respiratory gating techniques, DMLC tracking technologies, forced shallow breathing with abdominal compression and integration of respiratory motion into the treatment planning (Giraud & Houle 2013). In 4DRT, IGRT radiation beams are harmonised with series of the movement cycle beams for an efficient real-time treatment. 4DRT shows the capabilities of reducing dosimetry and sequelae than IGRT (Li et al. 2008). The image guided radiotherapy (IGRT) uses successive images during the radiation treatment. These images are to identify anatomical changes and movements of the target when positioned and immobilised on the treatment couch. IGRT technique allows

accurate and precise delineation of both the target and surrounding critical structures. Re-planning is necessary if the target gets out of tolerance corridor of the initial treatment plans (this technique is called ART). IGRT images could be sculptured using scanners such as 3D CT, MRI and PET. The cone beam CT (CBCT) allows reconstruction of the tumour geometries in real-time treatment and onboard kilovolt (kV) imaging. CBCT is a faster and safer version of 3D CT which requires a lesser time for the full scan. Treatment with IGRT is based on the actual daily dose as opposed to the planned dose and this has improved dose delivery accurately (Dj 2014; Bissonnette et al. 2012).

1.2.5 STEREOTACTIC RADIOTHERAPY

Series of technical development has occurred in EBRT from the generation of 2D CRT to the era of 4D CRT, allowing the possibility of delivering a very narrow beam with a high dose to a deep-seated small volume tumour with high positional accuracy using a stereotactic frame (Thariat et al. 2013). Stereotactic radiosurgery (SRS) enables the delivery of an ablation dose in a single fraction with the narrow radiation beam. It is efficient in treating the intra-cranial oligometastatic (brain tumour) using, for example, the Gamma Knife (Andrews et al. 2004; Bondiau et al. 2013; Weichselbaum & Hellman 2011). This surgery is painless, effective, and safe with an increased therapeutic ratio. Stereotactic body radiotherapy (SBRT) is used for small deep-seated tumours in the body (extracranial tumours) such as in the spine, lung, prostate, renal, hepatic, and pancreatic regions (Freeman & King 2011; Wu et al. 2008; M. Kim et al. 2014). SRS/ SBRT has shown excellent outcome in previous treatments (Davis et al. 2015; Hoyer et al. 2006).

1.3 INFLUENCE OF ADVANCED EXTERNAL RADIOTHERAPY TECHNIQUES ON QUALITY ASSURANCE PROGRAM

Radiation treatment community has spent its past five decades improving the quality of radiotherapy treatment, minimising the dose given to surrounding OARs and developing an efficient protocol for personnel safety (Khan 2014; Paliwal et al. 1996). To every radiotherapy improvement, there is an advanced radiation treatment technique. This enhancement can be attributed majorly to inventions of treatment planning using multiple imaging modalities to define the tumour volume in three to four dimensions (a series of similar images over time or treatment fractions). The treatment machines have also been kept up to date to deliver the advanced radiotherapy techniques with the help of excellent computerised software packages. Over the years, we have realised that advances in EBRT techniques have accompanied complex quality assurance (QA) practices and protocols (Pawlicki & Mundt 2007).

Radiotherapy QA (RTQA) program is to prevents the likelihood of errors and to raises the level of confidence of each treatment (LoSasso et al. 2001). Quality control (QC) program, on the other hand, is one part of the overall QA program, it identifies possible errors by validating its test result with the existing standard just before treatment (Rosenberg 2008; Haffty & Wilson 2009). Overall, a systematic QA program makes sure that deviation within ± 5% of patient's delivery dose and spatial uncertainty within ± 5 mm is accepted according to TG 40's recommendation. In TG 142, deviations within ± 1 mm for the stereotactic machine and ± 2 mm for other treatment machines were additionally recommended (Klein et al. 2009). It is a necessary procedure that has clinical, physical and administrative components and it involves the professional teamwork of the Radiation Oncologists, Medical Physicists, Dosimetrists, Radiotherapy Technologists, Engineering Technologists and Radiotherapy Nurses. These professionals, work hand-in-hand to achieve an efficient QA program (Podgorsak & Hendee 2006; Benedict 2004). The RTQA program goes through the subsequent processes depicted in figure 1.3 since RT errors can occur at any point along the planning and the treatment. Possible errors could be: wrong patient or body part

treated, dosage miscalculation error, corrupt software files, set-up error of equipment or patient, and beam not reaching the target. Each of the subsequent processes in figure 1.3 requires QA and QC for effective and efficient treatments.

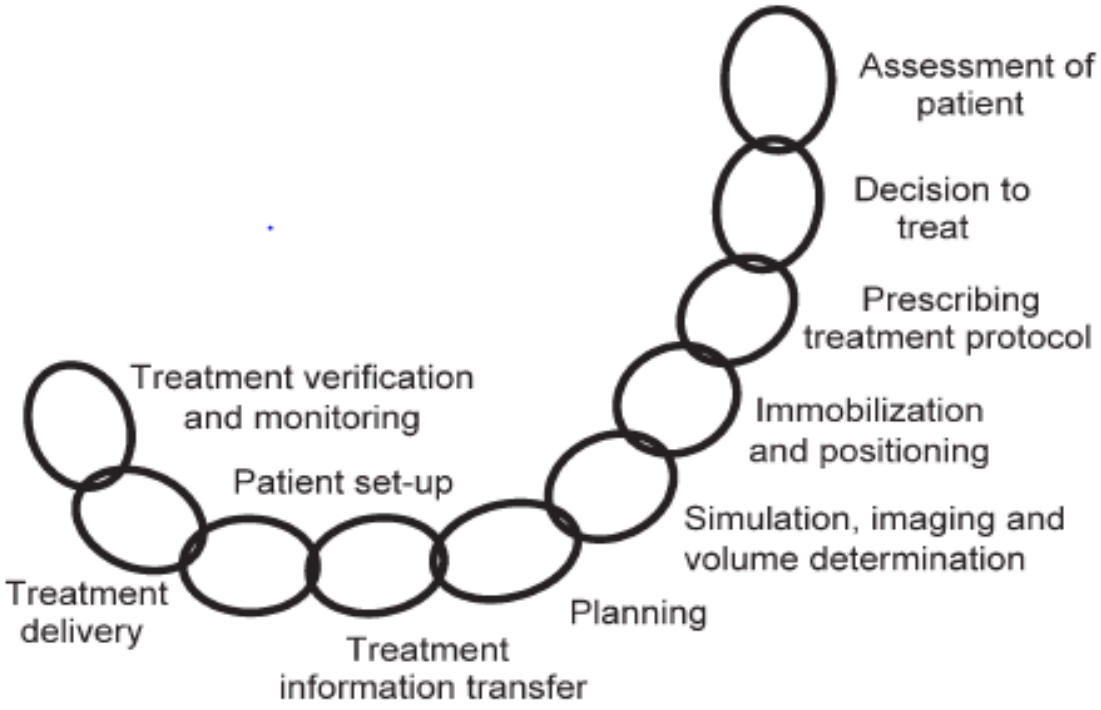

Figure 1.3: The following processes utilised for QA in radiotherapy (Ishikura 2008)

Prominent organisations have raised several benchmarks for periodic quality activities in radiation treatment. They are: World Health Organization (WHO) (World Health Organization Technical Manual 2008); American Association of Physicist in Medicine (AAPM) in series of task group (TG) documents like TG 40, 43, 53, 56, 60, and 64 (Kutcher et al. 1994; Saw et al. 1998; Fraass et al. 1998; Nath et al. 1997; Kubo et al. 1998; Nath et al. 1999; Nath et al. 2009); International Atomic Energy Agency (IAEA) (IAEA 1997); European Society for Radiotherapy and Oncology (ESTRO) (Thwaites et al. 1995); Clinical Oncology Information Network (COIN); International Organization Standardization (ISO) (Señal et al. 2008),and South Africa Standards for Quality Assurance in Radiotherapy (SASQART). These organisations' quality activities in radiotherapy checked and updated regularly. However, not all of these organisations have updated their RTQA programs to align with IMRT, IGRT and SRS/SBRT that

requires a sophisticated test and measurement for quality improvement (Dezarn 2008; Williamson et al. 2008; Palta et al. 2008).

Systematic QA for advanced radiotherapy techniques demands much time, experienced professionals, continuous training of staff, the dynamic research team, huge capital, and sophisticated dose monitors. Unfortunately, the QA technologies for radiotherapy dose monitoring have not been kept up to date with advances in radiotherapy (Rosenberg 2008; Islam et al. 2009). Advanced RT techniques and complexities in their QA have raised the interest of clinicians and researchers to verify and monitor the dose giving to patients in real-time treatment. If there will be any online beam delivery check system, the system must be highly sensitive to errors.

The QA for advanced radiotherapy techniques is time-consuming, and the continuous increase in workload at various radiotherapy centres has limited the time for QA. QA is carried out before the first treatment session, and the next QA is done after thirty to forty treatment session even though pre-treatment plan QA has been done(Islam et al. 2009) This is evident that error introduced within each treatment session could go undetected. Fast QA per patient and online dose verification seem to be the most appropriate modality for this challenge. Fast QA device should be able to verify patient's data, plan parameters alongside with radiation beam shape, gantry position, patient's position and dose within few minutes.

1.4 ONLINE DOSE VERIFICATION OF EXTERNAL PHOTON BEAM RADIOTHERAPY

The goal of every radiotherapy intervention is to improve the quality of radiation treatment and minimise the surrounding normal tissue dose. The quest for an optimum treatment made Paliwal (Paliwal et al. 1996) to introduce the concept of an online beam delivery check for non-computerised linacs. He introduced a transmission chamber to address the possible errors in treatment delivery within a short period of time and also to serve as pre-treatment QA (Pre-treatment QA is an offline procedure of cross checking the accuracy of treatment plan (TP) data before treatment.). This concept is to

attach the record-and-verify system to the linac head. Since then, vendors have developed and suggested few online dose monitoring devices to aid a thorough QA for external photon beam radiotherapy. Online dose verification is a process whereby the delivery TP data is checked with the reference TP data when the patient is right on the treatment bench (during treatment). This process is to checkmate discrepancies that may have crept in between the planning phase and treatment stage.

1.4.1 ELECTRONIC PORTAL IMAGING DEVICES

Electronic portal imaging devices (EPID®) are pre-treatment verifying systems that validates the dosimetry setup of TP data, and serve as a QA tools (Greer 2013; Wendling et al. 2006; Xing & Li 2000). EPIDs are incorporated into modern medical linacs and they verify the patient set-up position by taking images of the treatment site using radiation beam from the linac. The patient portal images will then be verified with reference images (simulator or digitally reconstructed radiography (DRR) images) for dosimetric and anatomic errors (Bastida-Jumilla et al. 2011). Types of EPIDs are: amorphous-silicon based EPID (aSI-EPID), Scanning liquid ion chamber EPID (SLIC-EPID), fluoroscopic portal, Kodar CR reader and fluorescence screen, mirror and charge couple device (CCD) camera imaging. SLIC-EPID images can be converted into transmitted dose map (Mohammadi & Bezak 2012). EPID set-up is fast and the portal images are acquired within a short period. It is utilised within treatment fractions even in a high workload environment (Partridge et al. 2002; van Elmpt et al. 2005; Langmack 2001).

The modern EPID is provided with a photo-stimulated phosphor plate that gives a high image resolution. Fast EPID-based real-time dose verification that could display the images within few seconds for clinical practice has been pronounced recently for IMRT and VMAT treatments (Boyer et al. 1992; Benedict 2004; Herman et al. 2001; Greer 2013; Fuangrod et al. 2011; Woodruff et al. 2015). However EPID devices can be damaged by Mega Volts since its fluence recording is behind the patient.

1.4.2 DEVICE FOR ADVANCED VERIFICATION OF IMRT DELIVERIES

A device for advanced verification of IMRT deliveries (DAVID™) system is a product of PTW, Freiburg, Germany. DAVID system is a transparent harp multi-wire ionization chamber that allows the transmission of light field when mounted on the linac head in practice (Poppe et al. 2006; Stelljes et al. 2015). It verifies the delivery dose by measuring the MLC pair signal to check for leaf positioning error (PTW 2013). DAVID is placed between the patient and MLC and its signals are generated by the MLC opening. Each measurement wire monitors the opening of each leaf pair "each wire for each MLC pair" (Poppe et al. 2008; Riegel et al. 2011). The measured wires of 4.4 mm spacing are parallel to the direction of the MLC opening and the number of MLC pairs determines the numbers of chamber wire. The sum of all wire signals is equivalent to patient's delivery dose. Pre-treatment QA which serves as a reference for DAVID is required. DAVID system compares the measured signals with the reference values that were previously obtained from the TP verification. TP verification is carried out by using 2D-ARRAY (PTW, Freiburg, Germany) of 729 chambers with centre region spacing of 10 mm (Poppe et al. 2010). This is done in order to verify the integrity of the dose given to the patient during treatment. Any detected deviations from the pre-treatment QA will not be given to the patient unless it is within tolerance (Looe et al. 2010; Chandraraj et al. 2011; Myers et al. 2013).

The DAVID system is sensitive to MLC shifts within ± 1 mm at 20 × 20 cm^2 and ± 0.5 mm at 10 × 10 cm^2 fields, but not yet recommended for adaptive warning where there is a movement of organs during the treatment because the uniform multi-wires are not spatially sensitive (Chang et al. 2013).

1.4.3 DOLPHIN® ONLINE TREATMENT MONITORING

Dolphin® is a pre-treatment/ machine QA system for advanced EBRT (Beam Applications (IBA) Dosimetry, Uppsala, Sweden). It has the potential to be used for online treatment monitoring and for adaptive RTQA (IBA 2014). The time efficient transmission detector is mounted on the linac head when in use. The wireless system has an inbuilt angular sensor which measures the beam segments per gantry angle.

The signal is a measure of photon fluence deposited in the parallel ionization chambers of the Dolphin® system. It has 1513 ionization chambers with 5 mm spacing at the centre region. Dolphin® is capable of capturing the fluence map up to 40 × 40 cm^2 field size. After every fraction, the measured dose is transmitted wirelessly for analysis in the QuickCheck workstation which verifies the accuracy of the output dose with the reference dose from the TP and immediately confirms the accuracy of the dose in a matter of second (Thoelking et al. 2015; IBA 2014).

Alternatively, the measured fluence map from the linac is compared with predicted response from the COMPASS (Beam Applications (IBA). COMPASS verifies the patient's TP with clinical significance and reconstructs the plan based on dose analysis.

Dolphin® is a new detector that is currently waiting for approvals from linac manufacturers for online monitoring.

1.4.4 BEAM DELIVERY CHECK SYSTEM

Pre-treatment QA for advanced EBRT has experienced giant strides in the past, but little has been achieved for online treatments verification (Paliwal et al. 1996). The sensitivity of any online detector will definitely prove its capability to verify TP data and detect errors during the treatment. This research makes use of a new verifying system called integral quality monitoring (IQM) system®.

The major interest of utilised the prototype IQM device in this study is its ability to function as a beam delivery check system in real-time treatment (Islam et al. 2009; Chang et al. 2013). Another interest of choosing the IQM system over others (such as dolphin®) is its sophisticated double wedge-shaped ionization chamber which is innovative in the world of radiation detectors. This is the first idea about a wedge-shaped ionization chamber. The IQM is a monitoring system that validates the dose-area product of conformal and IMRT treatment plan data (segment by segment) as well as VMAT. It can also function as pre-treatment QA for advanced radiotherapy like other RT detectors.

1.5 AIM OF THE RESEARCH

The aim of this study was to determine how sensitive the IQM is for small alterations in the MLC leaf positions using Monte Carlo (MC) simulation.

To achieve this study, the following four objectives were met:

One: Creation of the more of FOTRAN (MORTRAN) codes for the IQM component module (CM) that was incorporated into the EGSnrc MC code and the tool command language/ tool kit (TCL/TLK) code for the IQM CM to be accessible on the BEAMnrc interface.

Two: Development of an accurate source model of an Elekta Synergy linac equipped with Agility 160-leaf multileaf Collimator (MLC) using the standard BEAMnrc MC simulation.

Three: Simulation of the altered segments in the BEAMnrc and calculation of spatial integral dose for each alteration in the IQM model.

Four: Analysis of the IQM output data using the sensitivity analysis techniques.

1.6 THESIS SCOPE

This thesis is arranged as follows:

Chapter one is the introductory part of this research. It was deduced that cancer is an epidemic disease in Africa. An effective and efficient treatment measure is necessary to combat this life-threatening disease. It was further stated that technological innovation has been the bedrock of advances in EBRT over the years. No doubt, advances in EBRT has enhanced radiation treatment and minimised the surrounding healthy tissue dose. However, RTQA program has been challenging and complicated due to advanced treatment techniques. Future projection of cancer occurrences will definitely increase daily workload in our cancer centres and there is an urgent need for fast RTQA and online verification system. In this chapter, fast, automated and online verification systems were described.

Chapter two comprises the Literature review of IQM system, photon interactions, external photon beam radiotherapy, Monte Carlo simulation technique for radiotherapy and analysing techniques.

Chapter three covers the detailed methods and materials used in this research.

Chapter four presents the outcome of each method applied to this study.

Chapter five is focused on the discussion and the interpretation of the results in chapter four.

Chapter six concludes and summarises the outcome of this research. It also states the future work.

CHAPTER 2

2.0 LITERATURE REVIEW

2.1 INTEGRAL QUALITY MONITORING SYSTEM®

The Integral quality monitoring® (IQM) system is an independent real-time treatment verifying system that validates the integrity and accuracy of treatment plan data. It also functions as a pre-treatment quality assurance tool for IMRT and dynamic arc photon dose delivery. IQM is a large wedge-shaped ionization chamber that is attached to the linac head in real-time radiotherapy (Islam et al. 2009; Chang et al. 2013; iRT Systems 2014). The wedge-shaped ionization chamber leads to a gradient in the leaf travel direction. The prototype IQM system was released in 2014 by iRT Systems, Koblenz, Germany and is currently in its beta testing phase. Figure 2.1 depicts the IQM set-up when in use.

The system consists of a large wedge-shaped ionization chamber of 550 cm^3. The shape was built with three electrode plates; a collecting plate and two polarising plates that are kept at 500 V during operation. These polarising plates define the wedge-shaped of the IQM system as shown in figure 2.2. The three plates are made of aluminum

Figure 2.1: IQM set up in practice on Elekta Synergy Linac

and the total separation distance between the polarised electrodes varies linearly across the chamber. The thickness of the chamber is approximately 4 cm.

The IQM system generates the spatial output integral signal scored in the spatial sensitive area of the ionization chamber. The integral signal is based on the linac aperture beam (segment beam) defined by the treatment plan. The spatial sensitivity area of the chamber is 26 × 26 $cm^{2,}$ and it is capable of monitoring a maximum field size of 40 × 40 cm^2 defined at the isocenter. The gradient of the ion chamber was produced to be spatially sensitive at approximately 0.5% mm^{-1} at the centre of the slope.

The signal output is recorded by an electrometer that is incorporated into the IQM system. It has an inbuilt Inclinometer that reads the gantry angle of the linac during VMAT treatment. The recorded data is transferred to the dosimetry control with the aid of Bluetooth that is also incorporated into the IQM system. The measured data are then verified with the expected data (reference data) in the IQM database that is display during the online treatment. The expected data is the preliminary measurement which verifies the accuracy of the online treatment.

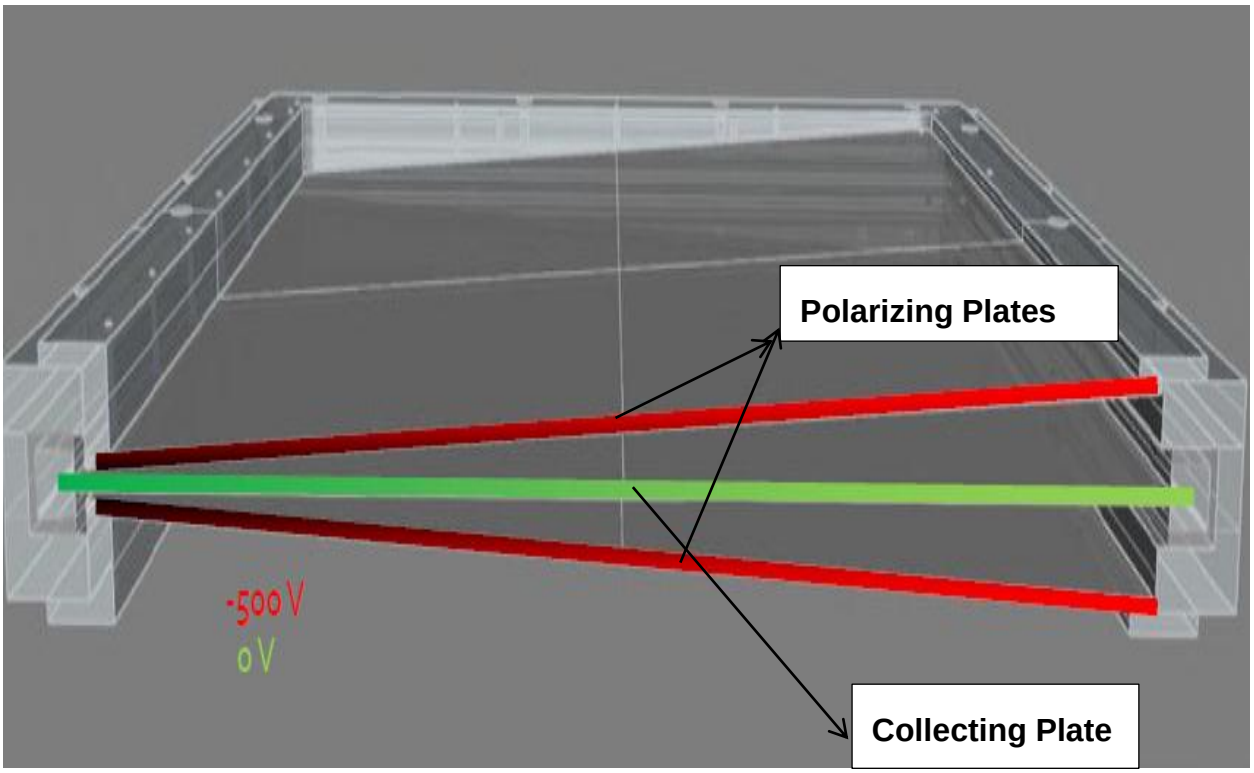

Figure 2.2: IQM model

The transmission ionization chambers of fourth and fifth generation linacs were constructed for monitoring purposes just like the IQM system. They were built with parallel plates. The transmission ionization chamber reads the resultant electronic signals created by the voltage of the plate. The linac monitoring chamber is situated just below the flattening filter, while the IQM chamber is mounted on the last layer of the beam defining structure. Therefore, IQM is capable of monitoring patient-specific treatment beams.

$$V = \int_a^b E\, dx \qquad 1.1$$

V Is the voltage of the electrode (plate)

E is the electric field in the parallel plates

dx is the distance between the plates

A uniform electric field is generated in the parallel plate of the transmission ionization chamber. In the case of the IQM system that has a wedge-shaped chamber (gradient plates), the electric field is uneven, and the field strength depends solely on the distance between the plates.

$$E = \frac{dV}{dx} \qquad 1.2$$

An increase in the distance between the electrodes along the gradient of the IQM system causes a decrease in the electric field strength. As the electric field strength decreases along the slope, there will be an increase in recombination of ion pair in the air chamber of the IQM system. The recombination effect reduces the ion current along the wedge-shaped chamber. Therefore, it could be assumed that the sensitivity of the IQM system decreases along its gradient. It could also be assumed that the gradient of the IQM system makes it sensitive to small field alterations. If a patient's delivery-beam is altered, the altered beam will be covering different local electric field strength on the IQM system.

It should be noted that the IQM electronic signal cannot be converted to gray (Gy) just like the way the transmission ionization chamber in the linac head could not be

converted to dose. However, it can be preset to dose in such a way that one monitor unit (MU) of the transmission ionization chamber relates to a dose of 1 cGy at maximum depth dose in a water phantom for 10 × 10 cm^2 at 100 SSD (Rosenberg 2008).

Report from iRT systems and Islam *et al.* (2009) state that the influence of the IQM system on beam attenuation is minuscule and the effect on surface dose and beam quality is negligible. Notwithstanding, the TP could be set to account for beam attenuation.

However, mounting of the IQM on the linac head obstructs the light field and the surface-to-source distance mark on the patient. Likewise, the IQM system will not be able to detect the source of error in the dose delivery, but it can save the patient from suboptimal treatment and overdose.

At ASTRO annual meeting in Boston (September 2016), iRT systems introduced a new beam delivery check system called IQM+. IQM+ functions like the IQM but with extensive features of automated logfile analysis. This proposed system presents the analysis results to state the possible source of error (iRT Systems 2016).

2.2 PHOTON INTERACTIONS

Photons are elementary particles of electromagnetic radiation (light). Electromagnetic radiation is a form of energy that is produced by oscillating electric and magnetic fields. These fields are vectorially perpendicular to each other and the direction of propagation. Electromagnetic radiation is characterised as ionising radiation when it has sufficient energy to eject an electron from its atom or molecule. X-rays and Gamma rays are the only types of electromagnetic radiation that can eject electrons from the absorbing medium during interaction (Attix 1986; Kelsey 2016; Khan 2014; Podgorsak & Hendee 2006; Rosenberg 2008).

The stochastic interaction of photons with the matter may involve either electrons or nuclei of the absorbing medium. During the photon interaction, the incident photon releases charged particles in the medium. The released charged particles will either deposit energy to the medium close to the interaction site through direct Coulomb

interaction with orbital electrons of the atoms of the absorbing medium or radiate their kinetic energy away through bremsstrahlung interaction with nuclei of the absorbing medium. Photon fluence and energy fluence are influenced inside and around the irradiated matter when they generate secondary charge particles (Benedict 2004).

The photon fluence (Φ) is the quotient of *dN* by *da*. Where *dN* is the number of photons that enters the irradiated matter of the cross-sectional area *da.* It has a unit of per centimetre square (cm^{-2}).

$$\Phi = \frac{dN}{da} \qquad (2.1)$$

The energy fluence (Ψ) is the quotient of dE_f by *da,* where dE_f is the sum of all the energies of all the photons that enter the irradiated matter of the cross-sectional area *da.* It has a unit of Joule per centimetre square (Jcm^{-2}).

$$\Psi = \frac{dE_f}{da} \qquad (2.2)$$

Photon interactions are classified as absorption and scattering processes. In absorption process, the intensity $I_{(x)}$ of the photon beam is attenuated by an attenuating material of thickness *x*, which is given as:

$$I_{(x)} = I_{(0)} e^{-\mu(h\nu,Z)x} \qquad (2.3)$$

Where

$I_{(0)}$: Original intensity of the unattenuated beam

$\mu(h\nu, Z)$: Linear attenuation coefficient depends on the photon energy *hv* and attenuator atomic number *Z*

The half-value layer (HVL) is the thickness of an attenuator that attenuates the intensity of photon to half of the original intensity of the unattenuated beam.

$$HVL = \frac{\text{In}2}{\mu} \qquad (2.4)$$

During the attenuation of the photon beam by the attenuator, photons may completely disappear which is called the absorption process (photoelectric *(pe)* absorption, pair *(pr)* and triplet *(tp)* production) or it may undergo the scattering process (coherent *(coh)* and incoherent *(ich)* scattering). The nuclear photo-effect *(ph)* is an absorption process that is mostly ignored but referred to in some cases. The total attenuation coefficient is the sum of all the individual attenuation coefficients of the considered processes (Mayles et al. 2007; Khan 2014; Podgorsak 2005).

$$\mu = \mu_{pe} + \mu_{pr} + \mu_{tp} + \mu_{ch} + \mu_{ich} + \mu_{ph} \qquad (2.5)$$

2.3 EXTERNAL PHOTON BEAM RADIOTHERAPY

Treatment with external photon beams is the most common form of radiation treatment. Photons have no charge or rest mass. The photons are released as electrons in the targeted volume. In radiotherapy, only ionising photons are used for treatment. There are only two sources of ionising photons which are part of the electromagnetic spectrum. The gamma rays that originate from nuclear disintegration and the x-rays that originate from the bombardment of suitable targets by an electron beam resulting in the production of bremsstrahlung x-rays and characteristics x-rays (Benedict 2004). Clinical X-ray beams could have energies between 10kVp (produced in an X-ray tube) and 50 MV (generated in a linear accelerator) (Madsen & Ponto 1992; Blomquist et al. 1998; Sätherberg & Karlsson 1998)

The bremsstrahlung x-rays are produced when a bombarding electron interacts with the atomic nucleus. The bombarding electron decelerates and loses part of its kinetic energy (radioactive loss) in the form of an x-ray photon which is called bremsstrahlung x-ray while the characteristic x-ray is emitted when bombarding electron interacts with an orbital electron of the targeted material (collision loss). There will be ejection of an electron from the inner shell, hence creating a vacancy. The vacant electron shell is

filled with an electron from the outer shell, emitting a quantized photon (characteristic x-ray) whose kinetic energy is the resultant energy difference between the higher energy level (inner shell) and the lower energy level (outer shell) of the atom.

Clinically, x-ray beams are used for studying the internal structure of non-conformity and opaque structure making use of energy range of 10-150 kV. It has also been used to treat malignant tumours with the use of Megavolt energy range (1-50 MV). Most of the diagnostic photons are produced 90^0 from the direction of the accelerated electron while photons of megavoltage energy are produced in the direction of the accelerated electron (Podgorsak 2005).

2.3.1 LINEAR ACCELERATOR

A Linear accelerator (linac) is an external beam radiation treatment machine producing high-energy x-rays. The linac treatment is efficient for deep-seated tumours since the maximum dose caused by its x-rays is below the skin surface. The linac is a type of cyclic particle accelerator that produces high energy (electrons). It makes use non-conservative microwave radio-frequency (RF) fields in the frequency range of 2- 4 MHz (medical linac RF fields operate at S-band either 2856 MHz or 2998 MHz frequencies) that are produced through magnetrons and klystrons (Karzmark 1984). The waveguide guides the accelerated electrons. The final kinetic energy created determines the length of the accelerating waveguide, which is approximately from 30 cm at 4 MeV to 150 cm at 25 MeV (Benedict 2004). The accelerating electrons can be used to create bremsstrahlung photons through its interaction with a high-atomic-number (thick) target, or the accelerated electron is used directly to treat the patient. Treatment with 15 MeV electron beam can only be efficient with the tumour seated at no more than 7 cm below the skin surface. For deeper depth, the photon beam from the linac is applied. The clinical linac is efficient in generating high photon energies of 6 MV, 10 MV, 15 and 18 MV and also could generate several electron energies between 4 MeV and 22 MeV.

Over decades, linac production has experienced different brands; from machines that produce low photon energies to devices that are capable of producing high photon energies with incorporated multileaf collimators for conformal treatments. The last sophisticated generation of linacs has accompanied complexities that could be

electrical, mechanical and in its treatment planning approach (Ahmad et al. 2012). These raise concerns for safety operation in favour of patients (Benedict 2004).

2.3.1.1 LINAC HEAD COMPONENTS FOR PHOTON BEAM TREATMENT

Linac head components are the independent materials that control, modify and monitor the generation of clinical radiotherapy beam. After obtaining the desired kinetic energy in the waveguide, the accelerated electrons channels into the linac head. The major components developed lately are:

1. *The x-ray targets*: X-ray targets are made of high atomic number metal, mostly tungsten or laminated copper-tungsten alloy. Clinical photon beams are generated when the high energy accelerated electrons are focused on the target; bremsstrahlung radiations are emitted in a forward direction, through which photon beams are produced. The x-ray target retracts for electron beam treatment.

2. *The flattening filters*: Flattening filters are high atomic number materials that make up for non-scattering of forwarding direction bremsstrahlung beams in radiation treatment. They are positioned in the rotating carousel or sliding drawer along with the path of the beam. The Therapy Emerging Technology Assessment Work Group of the AAPM reported that flattening Filter-free (FFF) linac is efficient (high dose rate) for SRS/SRT and appropriate IMRT since small field dose profile may be sufficiently flat for both flattening filter linacs and FFF linacs. The FFF linac will not be suitable for conventional 3D radiotherapy of a large tumour due to the heterogeneity of treatment site. This could be accounted for if modulated (Xiao et al. 2015; Prendergast et al. 2013).

3. *The light field is a* visual beam marking system, which defines the actual patient position for radiation treatment. A high-intensity filament produces the light fields and a mirror is used to project it such that it coincides with the radiation source position.

4. *The collimators*: Collimators are materials that define the structure of the patient irradiated beams. It is achieved by two to three of these independent devices:

4a.The primary collimators are collimators that define the globular field shape of the radiation beam. They seem to be smaller than the diagonal of the maximum square field size (they define the maximum circular field size) to form the corner beams for enhanced resolution.

4b.The secondary collimators are sometimes called the diaphragm. They are flat faced shaped blocks that could form upper jaws and lower jaws of the collimator. The blocks tend to move to align with the field divergent edges. Asymmetrical blocks could be used with a view to generate asymmetrical fields. Notwithstanding, the purpose of producing a sharp beam should not be compromised.

4c.The multileaf collimators (MLCs) could be optional in the linac head setup. They account for conformal radiotherapy; defining the irregular shapes of the beam during the radiation treatment. MLCs make use of leaf pairs (Agility 160-Leaf MLC has 80 pairs) that are independently movable to conform to the irregular shape of the planning target volume (Jeraj & Robar 2004).

5. *The dual transmission ionization chambers:* Dual transmission ionization chambers serve as a monitoring system for beam output during radiotherapy. The primary chamber is used for beam monitoring while the secondary chamber acts as a backup for the failure of the main chamber.

2.4 MONTE CARLO SIMULATION

The Monte Carlo (MC) simulation technique is a computational approach that obtains its numerical result through repeated random sampling technique (Andreo 1991). The MC technique is faithful in using pseudo-random numbers to sample probability distribution of various quantities. The MC method has been used to solve complex radiation transport challenges. In previous studies, MC techniques had accurately calculated the dose distributions for clinical radiotherapy (Rogers et al. 1995; Kawrakow 2000; Jarkko 2014; Usmani et al. 2014; Ishihara et al. 2014; Paganetti et al. 2004).

In MC simulation for radiotherapy, tracked particles are transported randomly to interact with media and geometries. The type of interaction particles undergo depends on the particle type, transport medium, and particle energy. Each particle's interaction obeys the physics of interaction probabilities. Particles may change directions and energies after the first interaction to create new particles. The new particles undergo further random interaction. These procedures are repeated until the particles reach specified cut-off energy or a defined boundary. The outcome of every simulation is the average behaviour of tracked particles.

MC method is a stochastic procedure which requires a large number of events (particles) called history [N] to reduce its uncertainty (variance [σ^2]). A large number of an event increases the computational time. An increase in the computational time will be appreciated if the efficiency [ε] of the simulation is improved (Mayles et al. 2007; Kawrakow 2000). For [N] histories of an independent event [x_i], the mean [μ], the variance [σ^2] and the statistical uncertainty of the mean (standard variance of the mean) [ϑ] are calculated thus:

$$\mu = \frac{1}{N}\sum_{i=1}^{N} x_i \qquad (2.6),$$

$$\sigma^2 = \frac{1}{N-1}\sum_{i-1}^{N}(x_i - \mu)^2 \qquad (2.7)$$

And

$$\Im = \frac{\sigma}{\sqrt{N}} \qquad (2.8)$$

The efficiency [ε] is calculated as follows:

$$\varepsilon = \frac{1}{\mathrm{T}\cdot\sigma^2} \qquad (2.9)$$

[T]: Computational time and [σ] is standard deviation

Thousands of charge particle's interactions do occur and it is unreasonable to track each interaction individually for time sake. The condensed history technique could be applied, in which thousands of interactions are condensed and considered as a single particle step (I Kawrakow & Bielajew 1998; Kawrakow 2000).

There are various general purpose MC codes which could be used to simulate photon, electron/positron, proton and neutron transports, for example EGSnrc (Kawrakow et al. 2013), MCNP (Jabbari & Seuntjens 2014; Brown 2003), PENELOPE (Baro et al. 1995; Sempau et al. 2001), and GEANT4 (Agostinelli et al. 2003; Archambault et al. 2003) (Chetty et al. 2007). This research makes use of the EGSnrc MC system.

2.4.1 EGSnrc SYSTEM

The EGSnrc system which is a continuous development of the EGS4 (Electron-Gamma Shower) was developed by National Research Council Canada NRCC (Kawrakow et al. 2013; Walters et al. 2010). The major Improvement on EGSnrc is to calculate dose in an ion chamber meticulously and to accurately model low energy physics of photon and electron transport (Kawrakow 1999; Kawrakow 2000). Additional features of the EGSnrc systems over the EGS4 are: NIST data for photon cross section and bremsstrahlung cross section, Rayleigh scattering, photoelectron angular sampling, binding effects in Compton scattering, relaxation cascades after creation of atomic vacancies, electron impact ionization, spinning effect of electron scattering, improved bremsstrahlung angular sampling and improved inelastic collision. The EGSnrc was benchmarked against the EGS4 for relevant features common to radiotherapy (Walters et al. 2010). The EGSnrc applied the knowledge of basic physics to accurately simulate photon and electron transport in various media and geometries. The EGSnrc user codes are BEAMnrc, DOSXYZnrc, DOSRZnrc, FLURZnrc, CAVRZnrc, SPRRZnrc, CAVSPHnrc, EDKnrc. Each of the EGSnrc user codes applied the knowledge of basic physics, but they model different geometries and score different quantities (Kawrakow et al. 2013). This research makes use of BEAMnrc, DOSXYZnrc, and data analysis packages that accompanied the EGSnrc user codes.

2.4.1.1 EGSnrc MONTE CARLO CODE

The EGSnrc Monte Carlo (MC) code is a general purpose package for electron and photon transport simulation. EGSnrc takes cognizance of radiation transport physics and its interaction with matter. This code is user-friendly, and it handles particles up to several hundred Giga electron volts (GeV). The EGSnrc code was written in MORTRAN (more of FORTRAN) programming language. It is a trusted MC technique which has been in use for decades. It can calculate dose distribution in locations where physical measurement seems complex or even impossible.

The EGSnrc code comprised of two user-callable subroutines, HATCH and SHOWER which in turn call other subroutines; HOWFAR, HOWNEAR, and AUSGAB. The user interacts with the code using COMMON variables detailed in (Kawrakow et al. 2013; Nelson et al. 1985). The user as well could write the MAIN program that usually performs any initialization needed for the geometry routines, HOWFAR and HOWNEAR and the set media, cut-off energies and positions for particle deposition.

Functions of subroutines are:

HATCH: To establish media data.

SHOWER: To initiate the cascade.

HOWFAR: To specify the position of the geometry.

HOWNEAR: To specify the perpendicular distance to the geometry boundary.

AUSGAB: To score and output the results and to control variance reduction.

2.4.2 BEAMnrc

The BEAMnrc which was built around the core EGSnrc MC simulation software is used to simulate the particle beams for various clinical linacs and other external beam radiotherapy machines. It models the geometries of the independent and reusable component modules (CMs) of a specified linac (Rogers et al. 2011). There were twenty-five (25) different CMs on BEAMnrc platform utilised for several external beam radiotherapy simulation (this study added a new CM to have a total number of twenty-six (26) CMs).

The linac model is constructed by stacking the CMs perpendicularly in the beam's direction. After that, the output of the BEAMnrc simulation could be in the form of a listing file, graphic file, and phase space data file. The graphic file and the phase space data file could be optional. Listing file is considered as the main output file that contains the basic information of the simulation written in text file format. The scoring plane which is positioned below any of the model's CMs contains the phase space file after simulation. A phase space file functions as a data record for every particle that crosses the scoring plane which could be used for further analysis of beam energy, position, direction, weight and types of particles. The phase space file can also serve as an input file for Beam Data Processor (BEAMDP) and particle dosimetry in phantoms (Heath & Seuntjens 2003; Rogers et al. 1995).

2.4.3 DOSXYZnrc

The DOSXYZnrc is one of the EGSnrc user codes designed for calculating dose distributions in a Cartesian geometry. It has an input file that consists of a text file which defines the parameter of the primary particle source (nine (9) sources available in DOSXYZnrc), phantom geometries, simulation control, and variance reduction of the model. The Cartesian voxel is in three dimensions and each voxel, its size, density, and media are defined. A phantom geometry could also be defined by patient CT data converted into readable code using CTcreate. The DOSXYZnrc simulation output is stored in 3D dose file (*.*3ddose*) which contains the dose deposited and statistical uncertainty in each voxel. The dose deposited in the phantom could be analysed to calculate the percentage depth doses, relative output factors, and lateral beam profiles. The particle transport in DOSXYZnrc is controlled by the core EGSnrc code (Rogers et al. 2011).

2.4.4 VARIANCE REDUCTION

The variance reduction is a process required to reduce the time of simulation and to raise the confidence level of the simulation outcome. An efficient simulation is been determined by the precision of its output. It demands more computational time due to a large number of events. The variance reduction techniques play a significant role in the computational time reduction in agreement with the statistical efficiency of the

simulation. The variance reduction techniques employed in this research are range rejection, photon forcing, bremsstrahlung photon splitting and Russian roulette (Rogers et al. 2011; Rogers et al. 1995).

2.4.5 DEVELOPMENT OF A NEW COMPONENT MODULE

The BEAMnrc GUI was developed with the tool command language (TCL) / toolkit (TK) code. The TCL is a scripting language, powerful and easy to learn. It is suitable for a wide range of applications and website development (Brent et al. 2003; Roger & Jr 1996). It accompanies the TK code for GUI development to the higher level of understanding of users. The TCL/TK commands are descriptive, and highly extensible.

A MORTRAN (More FORTRAN) is a string processor that produces a FORTRAN 77 code. It is a user code for EGSnrc and BEAMnrc. It could mean a structured language, a translator for the language and a macro processor. The MORTRAN code is needed to code the radiation transport and subroutines of a new CM that is necessary for EGSnrc MC Simulation.

To develop a new CM on the EGSnrc platform, the developer should follow these steps:

1. Understand the geometry of the new CM.
2. Write the TCL/TK code for the new CM.
3. Add-on the TCL/TK code to the BEAMnrc GUI file.
4. Write the MORTRAN code for the new CM.
5. Add on the MORTRAN code to the EGSnrc files in BEAMnrc file location.

The add-on location is `$HEN_HOUSE/OMEGA/BEAMnrc/CMs`.

The new CM must have two MORTRAN source files. The MORTRAN macros specific for the CM are contained in `CM_macros.mortran`. The BEAMnrc and EGSnrc subroutines for the CM make use of these macros. The set of subroutines specific for the CM is contained in `CMNAME_cm.mortran`. The major subroutines are:

HOWFAR_$CMNAME: It is used during the simulation to define the geometry of the CM at boundaries and set region-dependent parameters.

HOWNEAR_$CMNAME: It is used to calculate perpendicular distance to the nearest boundary in the horizontal plane.

WHERE_AM_I_$CMNAME: It is used to determine the region of particles upon entry into CM CMNAME.

INPUT_$CMNAME: It prompts for and digests input from the interactive user or the parameter definition file for information related to CM CMNAME.

ISUMRY_$CMNAME: It writes the summary of input for CM CMNAME to listing file.

2.4.6 VALIDATION OF A NEW COMPONENT MODULE GEOMETRY

The ray tracing method is used to test the geometry of a new CM (Heath & Seuntjens 2003). Macros (`nrcaux.mortran`) in the BEAMnrc code allow an output detail of particle interaction when crossing boundaries. It outputs the geometric detail to the `.egsgeom` file that could be displayed by using EGS_Windows or a normal graph plot. This file is available when the IWATCH is set to four (4) (Rogers et al. 2011).

2.5 GAMMA EVALUATION METHOD

The gamma (γ) evaluation method has generally been accepted as the gold standard method for dose distribution comparison. Its produces a quantitative measure that is based on both dose and spatial criteria (Ceberg 2013; Van Dyk et al. 1993; J.-I. Kim et al. 2014; Park et al. 2011; Li et al. 2013). This method incorporates pass-fail criteria for both dose-difference (DD) and distance-to-agreement (DTA) of dose distributions to calculate a dimensionless metric called the gamma index (Hussein et al. 2013; Persoon et al. 2011). It shows the magnitude of agreement between DD and DTA (Spezi & Lewis 2006; Huang et al. 2014). This evaluation method can be used for one, two or three spatial dimensional metric.

Van Dyk (Van Dyk et al. 1993) stated that using DTA measure in low dose gradient region(such as a central axis region of lateral dose profile) is inefficient and needs to

work in conjunction with DD measure in composite analysis. Likewise, using DD in high dose gradients such as lateral dose penumbra and buildup regions may be misleading, and the concept of DTA is used for accurate evaluation (Low et al. 1998). The composite analysis works in both low and high dose gradient regions, where DD and DTA evaluation complement each other when used in conjunction (Bak et al. 2012; Xing et al. 2015).

The gamma evaluation concept as explained by Low *et al* (Low 2010; Low & Dempsey 2003; Low et al. 1998), is designed to compare two dose distributions (reference dose distribution and evaluated dose distribution). Fig. 2.3 shows a systematic representation of dose distribution evaluation criteria using the combined 2D ellipsoidal DD and DTA. Tab. 2.1 presents the function of each symbol.

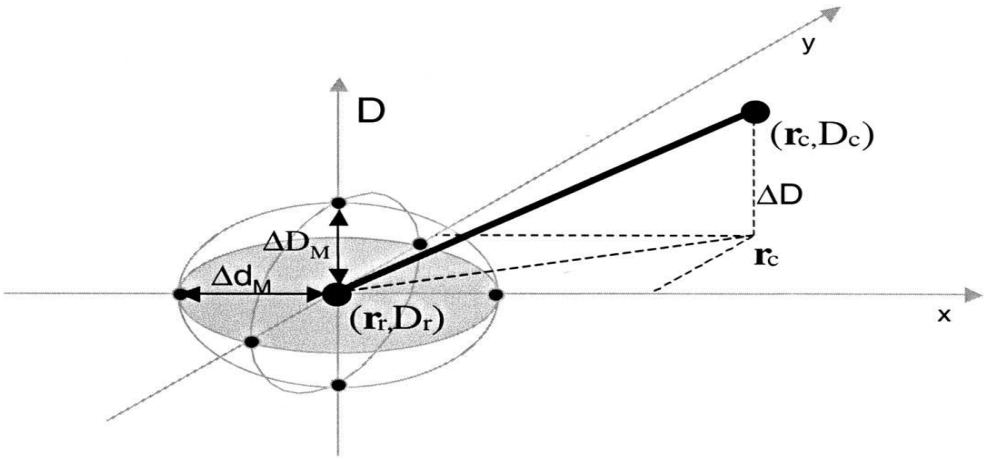

Figure 2.3: 2D representation of Gamma evaluation method for dose distribution (Depuydt et al. 2002)

Table 2.1: Definition of Gamma Evaluation symbols(Low & Dempsey 2003)

Symbol	Equation	Description
$D_m(\vec{r}_m)$		Evaluation dose D_m at position. $\vec{r}_m$
$D_r(\vec{r}_r)$		Reference dose D_r at position $\vec{r}_r$
ΔD		Dose difference criterion, can either be local or global. It is selected to be 2% of

		the maximum dose in this research.
Δd		Distance-to-agreement criterion. It is selected to be 2mm for this research.
$r(\vec{r}_m, \vec{r}_r)$	$r(\vec{r}_m, \vec{r}_r) = \lvert \vec{r}_m - \vec{r}_r \rvert$	Spatial distance between evaluated and reference dose points.
$\delta(\vec{r}_m, \vec{r}_r)$	$\delta(\vec{r}_m, \vec{r}_r) = D_m(\vec{r}_m) - D_r(\vec{r}_r)$	The difference between evaluated dose $D_m(\vec{r}_m)$ at position $(\vec{r}_m)$ and reference dose $D_r(\vec{r}_r)$ at position $(\vec{r}_r)$.
$\Gamma(\vec{r}_m, \vec{r}_r)$	$\Gamma(\vec{r}_m, \vec{r}_r) = \sqrt{\frac{r^2(\vec{r}_m, \vec{r}_r)}{\Delta d^2} + \frac{\delta^2(\vec{r}_m, \vec{r}_r)}{\Delta D^2}}$	Generalised Γ function, computed for all evaluated positions $\vec{r}_m$ and reference positions $\vec{r}_r$.
$\gamma(\vec{r}_r)$	$\gamma(\vec{r}_r) = \min\{\Gamma(\vec{r}_m, \vec{r}_r)\} \forall \{\vec{r}_m\}$	γ Function, the minimum generalised Γ function in the set of evaluated points.

If $\gamma(\vec{r}_r)$ is ≤ 1, DD/ DTA criterion is passed (correspondence is within specified acceptance criteria);

If $\gamma(\vec{r}_r)$ is >1, DD/ DTA criterion is failed (correspondence is not within specified acceptance criteria).

Commonly acceptance criteria are ΔD = 2 or 3 % and Δd =2 or 3 mm (J.-I. Kim et al. 2014; Xing et al. 2015; Huang et al. 2014; Low & Dempsey 2003). A 3%/ 3 mm criterion was the international clinical standards for photon beams (Low et al. 1998).

CHAPTER 3

3.0 MATERIALS AND METHODS

3.1 INTRODUCTION

A sensitivity study of the IQM system using MC simulation needs the IQM model which has not been developed on BEAMnrc hitherto. This study starts off by focusing on how to develop the IQM CM and to incorporate it into the standard BEAMnrc codes of the EGSnrc system (EGSnrc system was explained in section 2.4.1).

Secondly, the BEAMnrc code was utilised to simulate the Elekta Synergy equipped with Agility 160-Leaf MLC linac head using the manufacturer's specification for characterising the photon beams of the linac model. An accurate source model is essential in order to know that there are no discrepancies upstream of the IQM model.

Thirdly, the effect of various intentional alterations of leaf positions on the IQM integral dose was studied.

Lastly, signal outputs were analysed using the sensitivity analysis techniques described in section 3.6.

3.2 WRITING THE IQM COMPONENT MODULE

For the IQM component module (CM) to function on the BEAMnrc GUI, a special iqm code was written using TLC script. The TLC script on BEAMnrc GUI allows the user to interact with the BEAMnrc code and to simplify the task of creating the input file. The `IQM.tcl` was added to `$HEN_HOUSE/ OMEGA/ progs/ gui/beamnrc`. Two MORTRAN source files were written namely, `IQM_macros.mortran` and `IQM_cm.mortran`. The MORTRAN files allow the simulation of the IQM CM. It contains subroutines that define the calculation of geometry, and boundary crossing. The source files were added to `$HEN_HOUSE/OMEGA/BEAMnrc/CMs`.

3.2.1 IQM COMPONENT MODULE SUBROUTINES AND INPUT FILE

IQM CM (Fig. 3.1) was designed to fully model the wedge-shaped ionization chamber. The geometry of the ionization chamber model requires three layers to define the electrode plates. Above the first layer is the ZMIN and below the third layer is the

ZMAX, while the ZTHICK defines the height of the modelled ionization chamber in Z-axis and the perpendicular distance for z-axis to boundary surrounding component (RMAX). Three regions were created in each layer for effective dose calculation; front air region, material region, and back air region. Regions were created in IQM_cm.mortran and in IQM_macro.mortran; coding HOWFAR, HOWNEAR, DNEAR, WHERE AM I, the mass dose zone and all other subroutines in order to define the IQM geometry and dose scoring regions. Like other CMs on the BEAMnrc GUI, the IQM CM requires input from the user for accurate geometry. The manufacturer's specification was used to model the IQM on BEAMnrc.

The constant parameters to be filled by the user are:

Half-width of outer square boundary (cm)

Number of layers

Distance from front to reference plane

Distance from back to reference plane

Positive x dimension of opening at front (cm)

Positive x dimension of opening at back (cm)

Negative x dimension of opening at front (cm)

Negative x dimension of opening at back (cm)

Positive y dimension of opening at front (cm)

Positive y dimension of opening at back (cm)

Negative y dimension of opening at front (cm)

Negative y dimension of opening at back (cm)

Outer x edge (cm)

Outer y edge (cm)

Dose scoring regions, media, energy cut-off, latch and all other EGSnrc parameters. Appendix 1 depicts the full constant parameters location in the BEAMnrc GUI.

The filling of these constant parameters is sufficient to define the IQM's geometry as drawn in fig. 3.1.

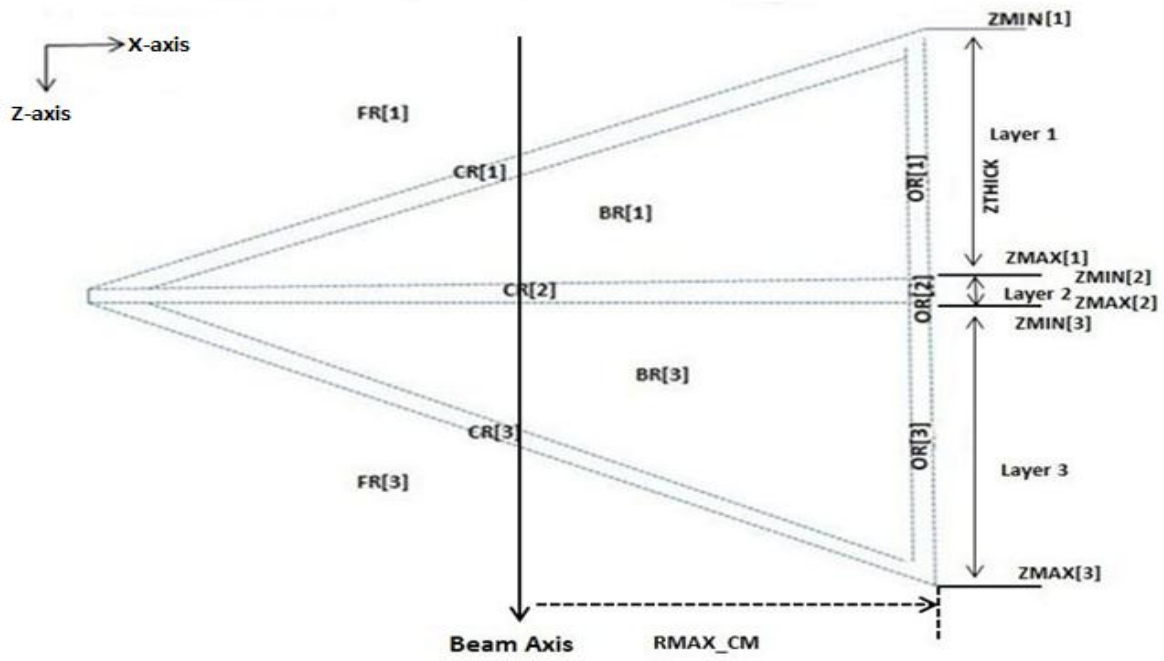

Figure 3.1: The IQM CM model showing the three regions and layers of its main construction

The Dose regions, energy cut-off, and region materials were defined for the central and outer region, the front region and the back region for each layer. The dose scoring regions numerical value is used to differentiate one region from another and materials for each medium in every layer. An aluminium, vacuum, and air were the materials used. These input parameters are flexible and user-friendly which could be adjusted to suit the user's purpose.

3.2.2 VALIDATION OF IQM CM GEOMETRY BY RAY TRACING

Validation of the IQM geometry was done by ray-tracing of the particle track through the IQM model. This method allows graphical display of the simulation coordinates of the IQM model. The ray-tracing method tests the correctness of the IQM's geometry in BEAMnrc MC. This geometry could be seen in `egsgeom.file` after running the simulation (Heath & Seuntjens 2003; Dorner 2012).

3.3 PROCEDURES TO BUILD A CODE FOR LINAC SIMULATION

The BEAMnrc code forms part of the associated code used in the EGSnrc MC Simulation platform. It makes use of single component modules (CM) which were designed to generate each part of the radiotherapy machine. The CMs are reusable and independent components that interact with every part of the radiotherapy system. All materials needed for the radiotherapy machine must exist in the PEGS4 data file. This file contains the cross section data of the modelled materials.

To compile the code for the Elekta Synergy linac head, the input for each CM geometry and media were entered into the BEAMnrc user interface using the manufacturer's specification. The EGSnrc radiation transport parameters were also defined. After compilation, an input file that contains the specification of the virtual machine's geometry was created for further simulations. The input file was stored in `myaccel.module` file that resides in the user's `$EGS_HOME/beamnrc/ spec_modules` subdirectory. The model has an executable code called `BEAM_myaccel`. The central processing unit (CPU) time to complete an execution depends on the number of histories, particle type, EGSnrc parameters, the number of components required to model a machine and desired efficiency. Particle histories within the range of 12 – 15 Billion were used for the simulation of square field sizes characterised photon beams in BEAMnrc. This was done in order to achieve a variance that was less than 1 % for all fields (I. Kawrakow & Bielajew 1998; Systems 2012).

Complete simulation generates `.egsphsp1 (2 or 3)`, `.egslst`, and `.egsplot`.

`.egsphsp1`: It contains information of all particles crossing the scoring planes. These files were used as a source for further MC simulation and for further analysis in the BEAMDP.

`.egslst`: It contains all the dose and fluence results of the simulation.

`.egsplot`: It contains the dose versus depth for all dose components when a CHAMBER CM is used as depth dose phantom.

The BEAMnrc graphical user interface (GUI) makes it possible for users to communicate with BEAMnrc code. “Specifying accelerator” means that the myaccel.module would be built from the scratch. Once the accelerator has been specified, the concatenated source codes of all the CMs to be created are filed in $EGS_HOME/BEAM_myaccel/BEAM_myaccle_cm.mortran and $EGS_HOME/BEAM_myaccel/BEAM_myaccle_marcos.mortran. If the code is modified, the accelerator needs to be re-built. The accelerator was built with the MORTRAN code beam_build.mortran. The beam_build creates the files Makefile, module.make, sources.make and Beam_myaccel.io and stores them in the Beam_myaccel subdirectory. Makefile, module.make, and sources.make were used for beam compilation while Beam_myaccel.io was used for proper output file nomenclature.

3.4 SOURCE MODEL SIMULATION

As mentioned earlier, BEAMnrc and DOSXYZnrc were utilised in this study. The Elekta synergy linear accelerator (linac) head was modelled according to the manufacturer’s specification. For the dosimetry, the Agility 160-leaf MLC of the Elekta synergy linac operating at 10 MV photon energy beam, was used. The Linac was modelled using the BEAMnrc software package and the dose was calculated using the DOSXYZnrc software package. In order to know the accuracy of the characteristic photon beams achieved from MC simulation, the MC output was validated by physical measurement. The MC simulation data (percentage depth doses (PDDs), dose profiles and output factors) for 1 × 1 up to 30 × 30 cm^2 square field sizes (SF) were validated by physical measurement as stated in articles without the IQM CM in place (Jabbari et al. 2013; Tayalati et al. 2013; Mesbahi et al. 2007; Oliveira et al. 2013; Juste et al. 2007).

3.4.1 LINAC HEAD SIMULATION PARAMETERS

The Elekta synergy linac head model was simulated using the independent and repeatable CMs of the BEAMnrc. The components simulated and geometries include:

a. *X-ray target (SLABS CM):* made of 9 mm thin sheet of tungsten alloy (density, 17.6 $gcm^{-3)}$ and rhenium with 5 mm diameter of bremsstrahlung target.

b. *Primary conical collimator (CONS3R CM):* comprised of 10 cm thick material of tungsten alloy, nickel and iron, located just below and within 0.5 cm from the X-ray target.
c. *X-ray beam flatten filter (FLATFILT CM):* composed of stainless steel material of height that varies with photon energy. This CM is positioned below the CONS3R CM.
d. *Anti-back scattering plate (SLAB CM):* made of 0.3 mm aluminium alloy and it is located below the FLATFIT CM.
e. *Multi-leaf collimator (MLCE CM):* made of tungsten alloy, nickel, and iron. This CM is about 9.1 cm thick and it is positioned just below the backscattering plate.
f. *Asymmetric Jaws (JAWS CM):* made of tungsten alloy, nickel, and iron. It is about 7.0 cm thick and it is positioned just below the MLCE CM.

The x-ray target, primary collimator, flattening filter and backscattering plates are the major components that influence the photon spectrum. Only the components that are influential to photon spectrum are modelled as suggested in the literature (Oliveira et al. 2013; Fix et al. 2004). Figure 3.2 shows examples of the systematic geometry and component modules used for linac model and figure 3.3 shows the eye view of the Elekta Agility 160 MLC.

After the linac model was designed without the IQM, the model is saved, compiled and executed using the core EGSnrc code (Rogers et al. 2011). The simulation output was scored in phase space files for further analysis.

3.4.2 WATER TANK SIMULATION PARAMETERS

A Water tank model was simulated using the DOSXYZnrc software package. For most of the BEAMnrc simulations, approximately (10-15) × 10^8 particles were scored in the phase space files and these particles were used as radiation sources incident on the water phantom as setup in DOSXYZnrc to simulate the phase space particles transport. The three-dimensional water tank phantom of 40 × 40 × 40 cm^3 which was also recommended in IAEA teachers handbook (Rosenberg 2008) was used in this study. The phantom was situated at 100 cm SSD from the reference source of the linac as

depicted in Fig. 3.4. The inner part of the homogeneous water tank phantom was defined by voxels; small voxel sizes of 0.2 × 0.2 × 0.2 cm^3 were used for penumbra region and large voxel sizes of 0.5 × 0.5 × 0.5 cm^3 were used at the central axis region for better resolution. This homogeneous water tank simulation technique was used to deduce the relative output factors, percentage depth doses and off- axis profiles of the photons crossing the phase space of 10 MV photon beams and square fields considered for linac model validation.

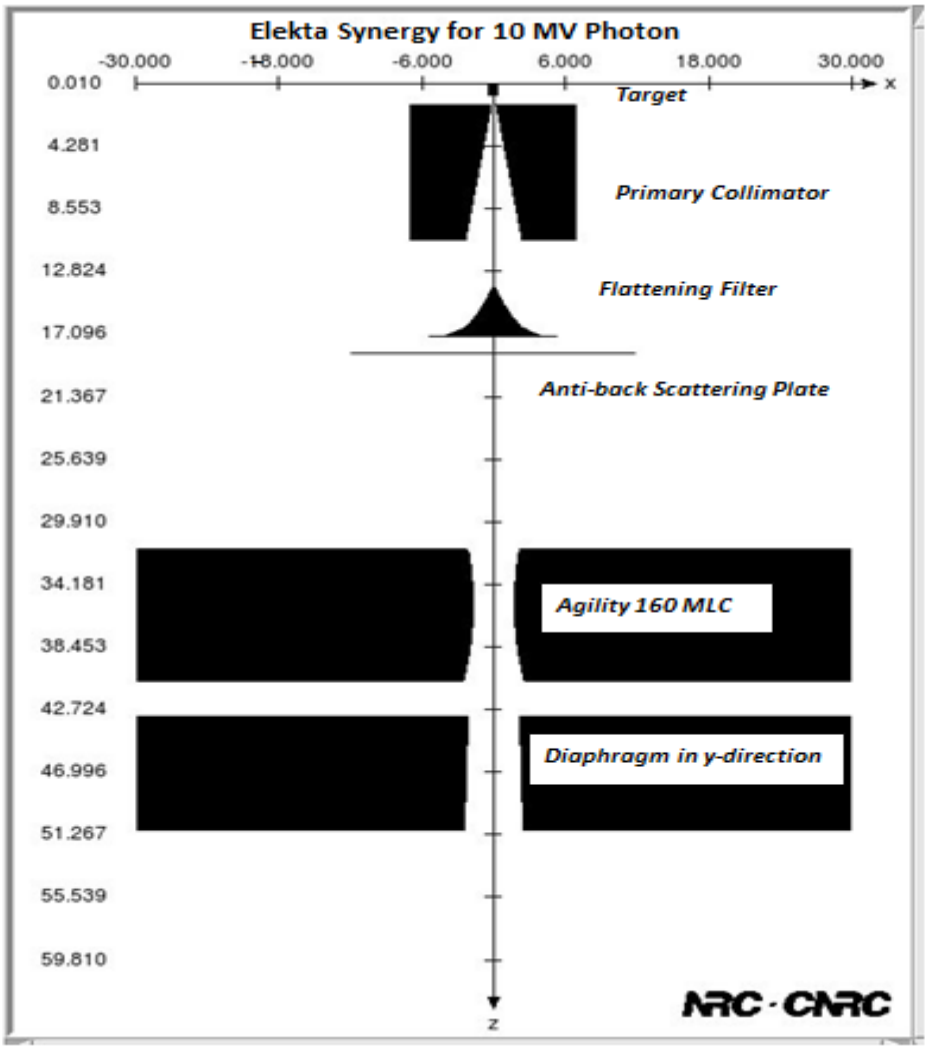

Figure 3.2: Elekta Synergy linac for 10 MV Photon Beam using BEAMnrc MC Simulation

3.4.3 SIMULATOR AND SIMULATION PARAMETERS

All the simulations in this study were carried out on a Linux OS workstation super microcomputer, equipped with 24 Intel(R) Xeon(R) core processors, each with CPU time of 2.10 GHz and 64 GB RAM accompanied with an X8 slot for the hard disk.

For the simulations, the number of histories was defined in order to make uncertainties less than 1% in the useful beam area. The following parameters were utilised for the electrons and/or photons transport in BEAMnrc and Dosxyznrc:

Global electron cut-off energy (ECUT) was set to 0.7 MeV;

Global photon cut-off energy (PCUT) was set to 0.01 MeV. In order not to distort the high energy transport and to reduce the effect of low dominant energy transport during tracking, a predetermined low energy limit was carefully set for ECUT and PCUT (Chetty, Curran, Cygler, DeMarco, Ezzell, Faddegon, Kawrakow, Keall, Liu, C. M. C. Ma, et al. 2007).

Maximum step size (SMAX) defines the maximum step electron in centimetre (cm). It was set to 1.e10 cm because we use EXACT and PRESTA II in our boundary algorithm;

Maximum fraction energy loss/step (ESTEPE) defines the maximum fractional energy loss per electron step. It was set to 0.25 (25%) for accurate electron transport.

Maximum first elastic scattering moment per step (Xlmax) is the maximum first multiple elastic scattering moments per electron step. It was set to 0.5.

Boundary cross algorithm (bca_ algorithm) was set to EXACT. It defines the algorithm that is used for transporting electron across the region boundaries.

Skin depth for boundary cross algorithm (skindepth_for_bca) was set to 1e10 cm. the entire simulation will be done in a single scattering mode since EXACT is set on.

Electron-step algorithm (transport_algorithm) was set to PRESTA II. This makes use of the new and more accurate algorithm to reconstruct of elastic scattering.

Spin effects for electron elastic scattering (spin_effects) was turned on for appropriate backscattering calculation. It accounts for relativistic spinning effect of electron transport.

Electron impact ionization (eii_flag) was turned off because Kawrakow's theory was not used for the BEAMnrc simulation (Kawrakow 2002).

Bremsstrahlung angular sampling (IBRDST) determines the angular sampling set when bremsstrahlung is created. It was set to simple (default) so that the sampling can use a modified equation 2BS of Koch and Motz (Bielajew et al. 1989; Rogers & Bielajew 1990)

Bremsstrahlung crossing sections were set to BH (default). It determines the cross-section utilized for bremsstrahlung interactions.

Bound Compton scattering (IBCMP) was turned on. It detects the binding effects and Doppler broadening simulations in Compton scattering histories.

Compton cross-sections (Cross_xsections) were set to default;

Pair angular sampling (IPRDST) was set to BH (simple [default]). It is used in pair production event for sampling positron and electron angles.

Photoelectron angular sampling (IPHTER) determines the sampling techniques in photoelectrons' angle of emission during EGSnrc simulation. It was turned off.

Rayleigh scattering (IRAYLR) was turned off. It determines the presence of Rayleigh scattering in the simulation.

Atomic relaxations (IEDGFL) were turned on. It determines the presence of atomic relaxation in the ground state after Compton and Photoelectric simulation.

Photon cross-sections (photon_xsections) were set to use PEGS4 dataset that we designed.

Photon cross-sections output (xsec_out) was turned off (default). All EGSnrc simulation parameters were conventionally set for a better reflection of realistic radiation transport (Rogers et al. 2011).

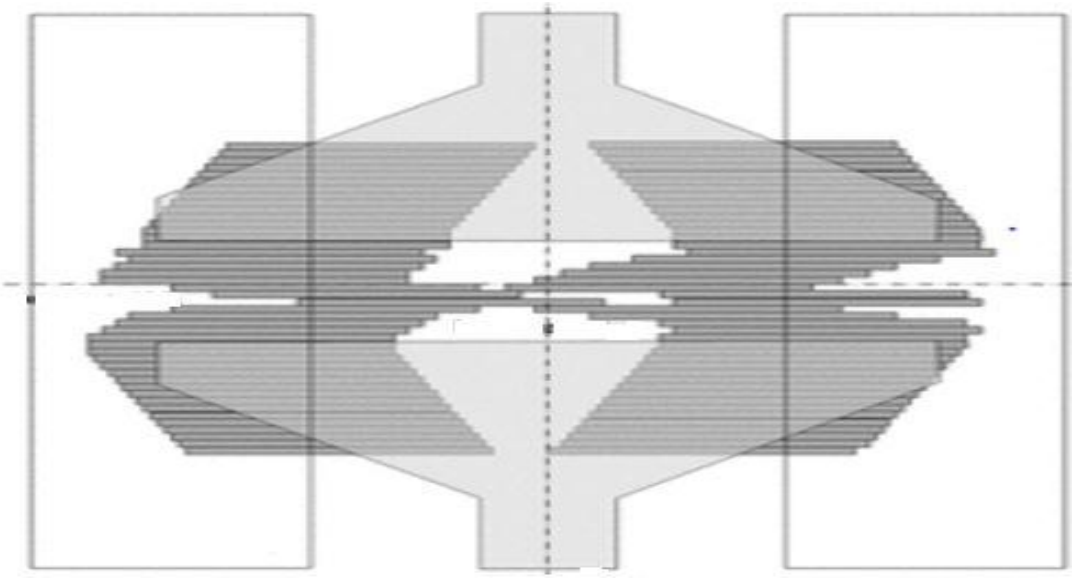

Figure 3.3: Beam's eye views of Agility 160-leaf MLC (Bedford et al. 2016)

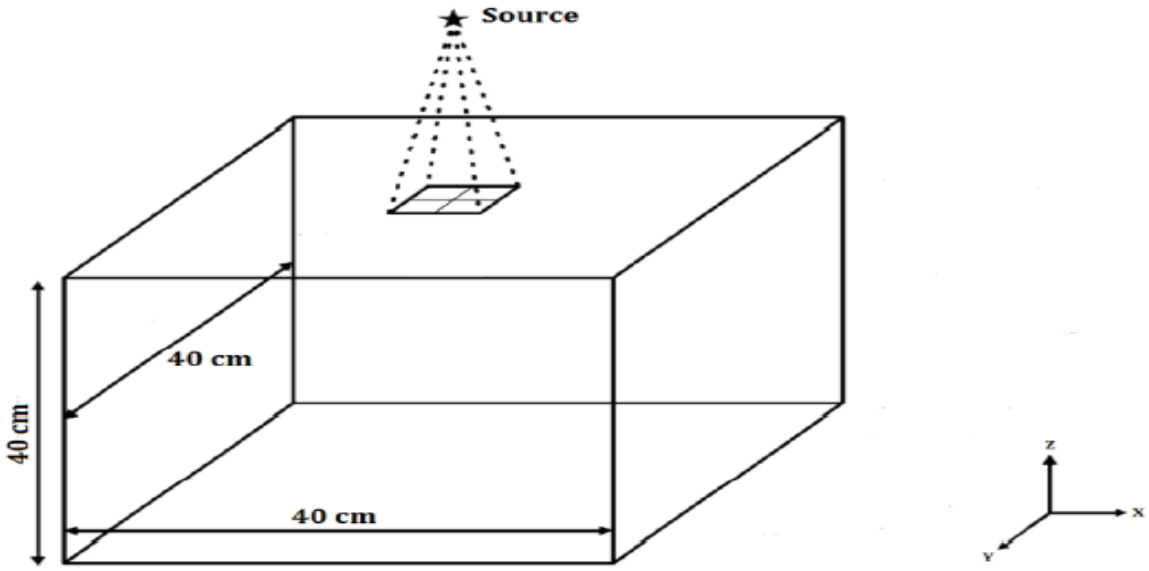

Figure 3.4: Water phantom model using DOSXYZnrc

3.4.4 WATER TANK MEASUREMENTS

The physical dose measurements were carried out by using CC01 ionization chamber inserted into the water tank for 1 × 1 to 5 × 5 cm^2 fields dosimetry and CC13 ionization chamber was also inserted into the water tank for larger square field sizes (SFS) dosimetry (Table 3.1 depicts the notable features of CC01 and CC13 chamber and figure 3.5 illustrates the physical water tank). Measurement data for 1 × 1 cm^2 to 30 × 30 cm^2 fields at 10 MV photon beams were obtained in a Scanditronics Wellhofer Blue Phantom using OmniPro^{TM} Accept 6.4a (IBA Dosimetry GmbH, Schwarzenbruck, Germany) scanning software. The least square smoothing and linear interpolation of 2 mm step width were performed on the water tank data. PDDs for 1 × 1 cm^2 to 30 × 30 cm^2 fields were recorded for the first 30 cm depth from the water tank surface at 10 MV photon beams for 100 SSD. The lateral beam profiles for 5 × 5 cm^2 to 30 × 30 cm^2 fields were registered at 2, 5, 10 and 20 cm depth in the water phantom at 100 SSD. Lastly, relative output factors were obtained at 10cm depth in water tank at 90 SSD for all the fields considered. These were the measurement procedures to obtain the commissioning data used in this study (the MC simulations were limited to available measured data).

Table 3.1: Notable features of CC01 and CC13 ionization chamber (IBA Dosimetry)

Features	CC01	Cc13
Cavity volume (mm^3)	0.01	0.13
Cavity length (mm)	3.6	5.8
Cavity radius (mm)	1.0	3.0
Wall material	C-552	C-552
Wall thickness (g/cm^2)	0.088	0.070
Sensitivity (nC/Gy)	~0.4	~3.8
Steam material	PEEK	PEEK
Outer electrode material	C-552	C-552
Inner electrode material	Steel	C-552

PEEK: Polyester ester ketone; C-552: Air equivalent plastic (1.76 g/cm^3)

3.4.5 COMPARISON OF MEASUREMENT AND MC SIMULATION DOSIMETRY FOR ELEKTA SYNERGY LINAC HEAD MODEL

The following dosimetry features were utilised for comparison:

a. *Percentage depth dose (PDD) curves*: Normalised vertical doses deposited within the first 30 cm from the skin surface considered. The buildup region and dose maximum (D_{max}) of measured data were compared with simulated data for 1 × 1 cm^2 to 30 × 30 cm^2 fields at 10 MV photon beams using Gamma criterion of 2%/2 mm.

b. *Lateral dose profiles:* Off- axis dose both in-line beam profiles and cross-line beam profiles at 2, 5, 10 and 20 cm depth were considered for measured data and compared with simulated data for 5 × 5 cm^2 to 30 × 30 cm^2 fields at 10 MV photon beams using Gamma criterion of 2%/2 mm.

c. *Relative output factors (ROF):* Relative output factors were considered at 90 cm SSD while 10 x 10 cm^2 fields were utilised as the reference field for relative output factor. The measured ROF were compared with simulated ROF for 1 × 1 cm^2 to 30 × 30 cm^2 fields at 10 MV photon beams. Relative output factors were recorded at 10 cm depth in water for all field sizes because at 10 cm depth; there is less effect of back scattering and electron contamination on the relative output factors (Wieslander 2000). The AAPM TG 74 report (Zhu et al. 2009) recommended that the relative output factors should be measured at 10 cm depth and according to Thomadsen et al. (Frye et al. 1995; Thomadsen et al. n.d.).

Figure 3.5: Water Tank used for physical measurements

3.5 SENSITIVITY STUDY OF IQM COMPONENT MODULE

For the sensitivity study of the IQM CM, the accurate source model of the Elekta Synergy equipped with Agility 160-Leaf MLC was simulated alongside with IQM CM in place (It is depicted in figure 4.3; continuation of the first research objective). In the model, IQM CM was located just below the lower diaphragm (4.5 cm) of the linac treatment head using the manufacturer's specification. In the air region of the wedge-shaped chamber, the spatial integral dose was scored after every simulation. The spatial MC dose were calculated in the air region of an open beams for every segment. Larger field will cover a large air region vice versa.

This IQM model should be able to detect leaf-positioning errors before the errors become clinically relevant. To determine the sensitivity of the IQM using BEAMnrc MC Simulation:

Firstly, 1 × 1 up to 30 × 30 cm^2 fields were modelled and dose was recorded in the air chamber of the IQM CM for square fields. The simulation outputs for all the fields were correlated with physical measured signal of the air chamber system. Physical measurements were taken by using the prototype IQM system for 1 × 1 up to 30 × 30

cm^2 fields. The output of the physical measurement is an electronic signal. The prototype IQM system used in this study is in its beta testing. Further development, definitions, and upgrades are expected such as to pre-set the electronic signal response of the IQM system to dose.

Secondly, MC simulated dose was calculated for alteration of open leaves. Each of the open leaves of 1 × 1, 3 × 3, 5 × 5 and 10 ×10 cm^2 fields was moved in and out of the central axis of the isocentre by the same amount of 1, 2, and 3 mm error regarding its individual leaf positions for 10 MV beams. The IQM dose response quantifies the leaf-positioning error. The effect of these positional errors when added to each leaf position influenced the field size only in the x-direction because the Agility 160-MLC leaf moves in the x-direction. Figure 3.6 depicts the graphical effect of systematic positional errors on a field size. This procedure is done to study the percentage change in IQM signal when all the MLC leaves are moved uniformly in and out of the defined fields within few millimetres and to compare the effect of alteration in the small field to large field. Simulations of these positional errors were done and the signal response in the IQM was calculated for all the fields considered. The magnitude of signal response for the altered field was calculated with respect to the unaltered field. The numbers of histories for these simulations for all the fields considered were chosen in order to have an output variance that is within 1%.

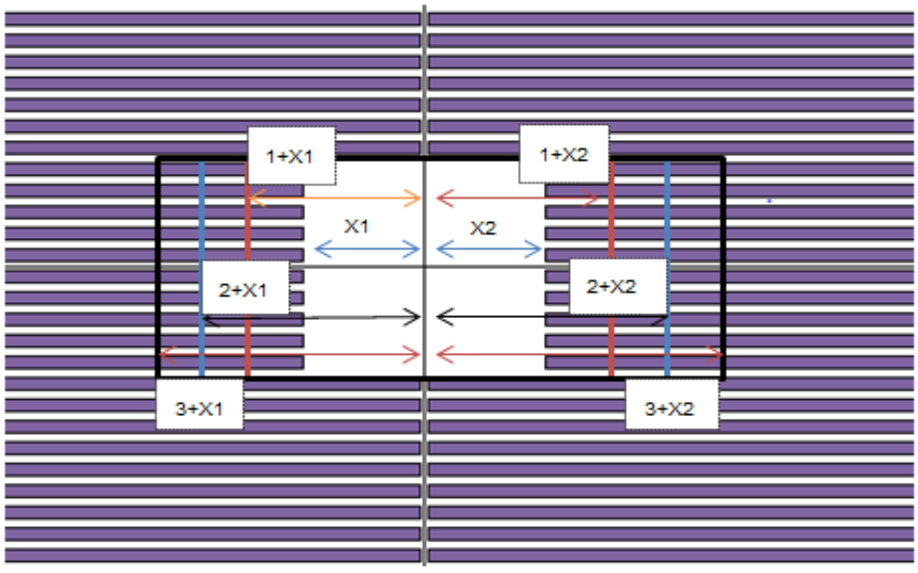

Figure 3.6: Positional errors of 1, 2 and 3 mm added to whole MLC leaves bank

Thirdly, the simulated dose response was scored for offsets of 1, 2, 3, 4 and 5 leaves shifted from the central axis of 5 × 5 cm^2 field by 1, 2, 3, 5 and 10 mm positions. Simulations were done to study the dose-response effect of numbers of misaligned leaves on offset positions. A 5 × 5 cm^2 field that has fourteen (14) opened leaves was used for this study. This is to note the IQM signal response to positional errors of 1, 2, 3, 5 and 10 mm when a single leaf out of fourteen leaves is out of place in the field considered. The IQM signal response of altered fields was normalised to IQM signal response of unaltered field. More leaves were also moved out of position as shown in Tab. 3.2. Each output variance of all the MC simulations is within 1%.

Table 3.2: Fraction of altered MLC leaves to unaltered leaves of 5 × 5 cm^2 field

Number of leaves altered	Fraction of leaf altered
1	1/14 = 0.0714
2	2/14 = 0.1429
3	3/14 = 0.2143
4	4/14 = 0.2857
5	5/14 = 0.3514

Fourthly, 3 × 3, 5 × 5, 7 × 7, 7 × 5 and 5 × 7, 5 × 3 and 3 × 5 cm^2 fields were simulated and moved along the gradient of the IQM. Figure 3.7 shows how a single segment was moved along the slope of the IQM. Dose responses were recorded along the gradient at positions of interest. The MLC defined field size remains unchanged along the IQM gradient, but the spot of the radiation beams on the IQM model were changed at every interval.

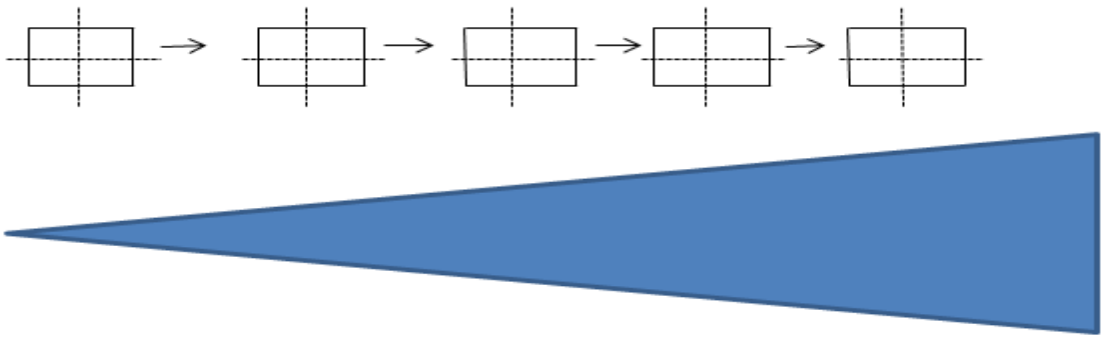

Figure 3.7: Movement of segment along the gradient of the IQM model

The signal response along the gradient of the IQM model is of great importance to this study. The gradient response is to give a better understanding of how the IQM signal responds to the positional change of the same field along the gradient of the wedge-shaped model. This is to see the signal response to an aperture that has not lost its beam shape but has experienced a complete positional change on the gradient, or its beam is covering another part on the slope. Several fields along the gradient of the IQM model were moved to study the sensitivity of the IQM model along the slope. The signal response for moving each segment along the slope of the IQM model was normalised to the centre segment.

Lastly, MLC positions of eleven segments (regular and irregular segments) were altered at random within ±1, ±2 and ±3 mm as defined at isocenter for 10 MV photon beams. The offset leaves were also selected at random. The four-pair guard leaves (two-pair at left and right side) were also simulated alongside with the open leaves for each aperture. However, the y-jaw positions for each segment (as depicted in Table 3.3) were modelled to overlap the Agility MLC guard leaves for accurate simulation. The regular and irregular segments were chosen for fair evaluation. For example, ±1 mm alteration means that any randomly generated value between -1 mm and +1 mm is the residual error value that influences the leaf's position. Note that, there is a probability of having zero value from the random generator which means that the particular leaf will not be altered. Each defined segment was altered 30 times to have a total number of 330 modified apertures. Each of the 160 leaves of the Agility MLC model was altered according to the random value generated. Altered and unaltered segments' IQM signals are scored and analysed using the scatter plots, brute force, variance-based and standard regression coefficient sensitivity analysis. (Appendix 2 contains the examples of brute force, variance-based and standard regression coefficient sensitivity techniques calculation).

The numbers of histories chosen for the entire altered segments were within 10 - 16 × 10^9 particles. The numbers of histories were carefully chosen after several iterations in order to have a variance that is within 1%. This is to raise the level of confidence in the simulation. Uncertainty should be within 1% of mathematical computation.

Table 3.3: Y- jaw positions for simulated segments

Segment	Segment area (cm^2)	- y jaw position (cm)	+y jaw position (cm)
One	49.00	- 3.5	+ 3.5
Two	25.00	- 2.5	+ 2.5
Three	9.00	- 1.5	+ 1.5
Four	19.99	- 2.5	+ 2.5
Five	36.66	- 3.0	+ 3.0
Six	25.83	- 2.5	+ 2.5
Seven	70.82	- 3.5	+ 3.5
Eight	47.49	- 3.5	+ 3.5
Nine	4.00	- 1.0	+ 1.0
Ten	1.00	- 0.5	+ 0.5
Eleven	38.74	-3.5	+ 3.5

3.6 SENSITIVITY ANALYSIS

Sensitivity analysis is the process of undertaking a systematic review involved in sequential decisions (Satelli et al. 2008; Sobol 2001). It is also called a cause-effect analysis and it identifies and determines the impact of inputs on its outputs (Confalonieri et al. 2010; Tiede 2005; Saltelli et al. 2010; Bucher 2009; Homma & Saltelli 1996; Ishigami & Homma 1990). This builds a theory that relates the input variables with the output variables. There are sensitivity analysis techniques stated in various articles (Saltelli & Annoni 2010; Zhao & Tiede 2011; Becker et al. 2011; Hamby 1994; Schwieger 2004; Confalonieri et al. 2010; Liu & Zou 2012). The sensitivity ranking of the input for several techniques may vary slightly but the focus is based on the consistent parameter that is most effective on output (Helton et al. 2006; Hamby 1994; Bucher 2009). The choice of method of sensitivity analysis is guided by the problem constraints. The constraint can be correlated inputs, nonlinearity, multiple outputs, input interaction, given data, random variables (for example, simple random sampling, Monte Carlo, Latin Hypercube, Morris method, quasi- random sequence). Random sampling, which is the constraint of this research majorly requires the application of scatter plots, brute force, variance-based and standard regression coefficient sensitivity analysis techniques which are efficiently independent of one another (Saltelli & Annoni 2010; Saltelli & Bolado 1998; Liu & Zou 2012; Becker et al. 2011; Saltelli & Tarantola 2002; Homma &

Saltelli 1996) .These four sensitivity analysis techniques were used for an in-depth study of the consistent input parameters that influenced the output value.

3.6.1 SCATTER PLOTS SENSITIVITY ANALYSIS

The scatter plots can be utilised in a quick determination of a model's sensitivity by correlating the effect of input on its output. It is often recommended as the first step of sensitivity analysis. Scatter plot is a qualitative analysis which can determine the most sensitive analysis technique for its analysis. It is achieved by plotting the graph of the input value against the output values. In this study our input values will be the alteration of segment shapes (areas) and the output will be the corresponding simulated IQM signals. The linearity of the scatter plots determines the sensitivity of the model. An increase in gradient of the linear equation of the output signal means that the model is more sensitive to the segment (Most 2011; Saltelli et al. 2004).

The linear equation: $y = mx + c$ (3.1)

where m is the gradient and c is the y-intercept.

For this research scatter plots of the randomly altered segment area were plotted against the integral dose scored in the IQM air chamber.

3.6.2 BRUTE FORCE SENSITIVITY ANALYSIS

The brute force sensitivity analysis is a local sensitivity analysis; it is based on non-interactive input variables whereby you vary the input variable and study the effect on the output value. It generates the sensitivity of a model due to perturbation of the input variables (Zhou & Lin 2008). This study quantifies the input parameter as the area of the segment. Sensitivity index was calculated based on the change in output (integral dose (I)) over the change in input (segment area (A)).

$$S_i = \left| \frac{d(I)}{d(A)} \right|_i \qquad (3.2)$$

Where $d(I) = d(I - I_i)$ and $d(A) = d(A - A_i)$.

dI - Unaltered spatial integral dose

dI_i - Altered spatial integral dose

dA - Unaltered segment area

dA_i - Altered segment area

S_i Is the sensitivity value for a single shift, $d(I)$ is the change in IQM dose and $d(A)$ is the change in segment area. In summary, the brute force sensitivity could be stated as the rate of change of the IQM signal (I) per unit change of the segment area (A) (Hwang et al. 1997; Hakami et al. 2003; Cohan et al. 2005).

3.6.3 VARIANCE- BASED SENSITIVITY ANALYSIS

The variance-based sensitivity analysis is a global sensitivity analysis; it is based on the idea that one can deduce the sensitivity of a model through its variance V. It is a probability distribution of the output uncertainties. It focuses on interactions between the input variables and the effect of each of the input variables on the output value. It is a measure of the importance of input variables on the outputs. The sensitivity of the output to the input variable is therefore measured by the amount of variance in the output caused by the inputs (Gan et al. 2014; Chan et al. 1997; Kamp et al. 2014).

$$Y = f(X_i) \qquad (3.3)$$

In equation (3.3) Y is the IQM integral dose value and X_i is the MLC shifts generated at random for a given segment (table 1). It should be noted that since only one input variable plays a role in the IQM output in this study, index i = 1 in equation (3.3). If some other input variable also played a role then index i = 1, 2.

The sensitivity measure of conditional variance V_i for a single input variable is given by:

$$V_i = V(E[Y \mid X_i]) \qquad (3.4)$$

The sensitivity measure of sensitivity index S_i is given by:

$$S_i = \frac{V_i}{V(Y)} \qquad (3.5)$$

$V(Y)$ can be decomposed thus:

$$V(Y) = V(E[Y \mid X_i]) + E[V(Y \mid X_i)] \qquad (3.6)$$

Where

$V(E[Y \mid X_i])$ is the variance of the conditional expectation of Y (output) conditioned on X_i (fixed input). It is termed as the explained variance.

$E[V(Y \mid X_i)]$ is the expectation of the conditional variances of Y (output) conditioned on X_i (fixed input). It is termed as the "unexplained variance".

The sensitivity index S_i is also called the main effect index. S_i is also called the first order sensitivity index, correlation ratio, it describes the main effect of the given data X_i on the IQM response value Y (Saltelli et al. 2004; Zhao & Tiede 2011; Plischke 2012).

In this study, effects of other input variables on the IQM output value are not present. Therefore, an extension for the total effect index is not applicable since the focus is on only one input variable; randomly altered segments. The sensitivity of the output to the input variable is therefore measured by the amount of variance in the output integral dose caused by the input segment area. The variance-based sensitivity indices were plotted against the randomly altered segments.

3.6.4 STANDARD REGRESSION COEFFICIENT

This is a regression analysis that tests the significance of an independent variable (input) on its dependent variable (output) by using both the mean and variance of the independent and dependent variables across the observable model. It is generally been used for linear regression model (Gan et al. 2014; Iooss & Lemaître 2015).

The generalised linear regression model is:

$$Y = b_0 + \sum_{i=1}^{n} b_i X_i \qquad (3.7)$$

The normalised regression model for an input variable is:

$$\frac{b_i s_i}{s} = \left| \frac{\frac{Y_i - \overline{Y}}{s}}{\frac{X_i - \overline{X}}{s_i}} \right| \qquad (3.8)$$

Where the standard regression coefficient (SRC) $\mathrm{SRC} = \frac{b_i s_i}{s}$ and b_i is the regression coefficient for the ith sample of the input X.

Where

$$s = \sqrt{\frac{1}{N-1}\sum_{i=1}^{N}(Y_i - \overline{Y})^2}$$

and

$$s_i = \sqrt{\frac{1}{N-1}\sum_{i=1}^{N}(X_i - \overline{X})^2}$$

are the standard deviation of Y and X respectively. The sensitivity of the model is determined by the SRC value. The higher the SRC value, the more sensitive is the input parameter on the output value. The SRC values were plotted against the randomly altered segments.

3.7 CORRELATION OF THE MONTE CARLO SIMULATION DOSE WITH MEASUREMENT

In order to relate the measured IQM electronic signal and the MC dose in the chamber, the IQM signal was divided by the product of relative output factor (ROF) and monitor unit (MU) of the MC dose. This is shown in steps below. The spatial response of the wedge-shaped chamber (electronic signal S_{IQM}) is predicted as (iRT Systems 2014; Islam et al. 2009)

$$S_{IQM} = MU.AOF(x,y) \oint_{Area} I_{field}.S(x,y) \qquad (3.9)$$

From equation 3.8, *MU* is the monitor unit, $AOF(x,y)$ is the area integrated output factor for the collimator setting which is a function of square or equivalent square fields (It is the variation in the machine output that increases with an increase in square field size), I_{field} is the fluence distribution, and $S(x,y)$ is the spatial chamber response function. The IQM electronic signal corresponds to the spatial sensitive dose-area product for each beam segment (Islam et al. 2009; iRT Systems 2014). If the electronic signal is divided by the ROF for the segment size and the MU of the MC dose, then we can relate $\oint_{Area} I_{field}.S(x,y)$ with MC dose-area product (calculated signal).

To calculate the MU and ROF for the MC dose, the following steps were followed:

Step 1: MC relative dose distribution $R(x,y,z)$ was calculated by normalising the spatial integral dose scored for each simulated field $D_i(x,y,z)$ in the wedge-shaped chamber to the MC reference dose $D^{ref}_{cax,\max}$ for 10 MV photon beams (Ma et al. 2004). The MC reference dose in this study was defined as the depth of maximum dose scored in a water phantom along the central axis for the 10 × 10 cm^2 field at 100 cm source-to-surface distance (SSD) for 10 MV photon beams as used clinically (Rosenberg 2008; Khan 2014).

$$R(x,y,z) = \frac{D_i(x,y,z)}{D^{ref}_{cax,\max}} \qquad (3.10)$$

Step 2: The MC relative output factor (ROF) in equation 3.11 is the ratio of the depth of maximum dose $D_{i,cax,\max}$ scored in water phantom along the central axis for a simulated field to the MC reference dose $D^{ref}_{cax,\max}$.

$$ROF = \frac{D_{i,cax,\max}}{D^{ref}_{cax,\max}} \qquad (3.11)$$

Step 3: The MU for any spatial simulated field *(x,y,z)* transmitted through the wedge-shaped ionization chamber using MC is:

$$MU = \frac{D_{\mathrm{p}}(x,y,z)}{R(x,y,z).ROF} \qquad (3.12)$$

Where $D_p(x,y,z)$ is the prescribed dose, $R(x,y,z)$ is the relative dose distribution, and ROF is the MC relative output factor as stated in equation 3.10 and 3.11 respectively (Ma et al. 2004). For example; if the prescribed dose is 100 cGy for an MC relative dose distribution of 0.8 and relative output factor of 1.1, then the amount of MU needed to be delivered to this dose will be 113.64 based on equation 3.12.

Step 4: To relate the MC simulated dose in the wedge-shaped ionization chamber with the physical measured electronic signal in the IQM system, the measured electronic signal S_{mes} is divided by the product of MU calculated in equation 3.12 and ROF calculated in equation 3.11.

$$S_{cal} = \frac{S_{mes}}{MU.ROF} \qquad (3.13)$$

Where S_{cal} is now the new value of the measured signal (an electronic signal) that will be correlated with the MC signal (MC simulated dose).

Equation 3.13 can be restated using equations 3.11 and 3.12 as:

$$S_{cal} = \frac{S_{mes}.R(x,y,z)}{D_p(x,y,z)} \qquad (3.14)$$

The calculated electronic signals S_{cal} and the MC calculated dose were normalised to their respective 10 × 10 cm^2 field.

CHAPTER 4

4.0 RESULTS

4.1 IQM COMPONENT MODULE DESIGN

4.1.1 TCL/TK CODE FOR THE IQM COMPONENT MODULE

The IQM CM TCL/TK code was written to display the IQM model on BEAMnrc Graphical User Interface (GUI). This user code was used to incorporate the IQM CM into the BEAMnrc GUI as shown in Fig. 4.1 and 4.2. The full Linac head model with the new IQM CM attached to the linac head is depicted in Fig. 4.3. In Fig. 4.1, the IQM on the BEAMnrc GUI is the last CM on the selective options which is circled in pink for easy identification. This is a necessary addition to BEAMnrc code for the essence of this study since previously no wedge-shaped rectangular ionization chamber with a central electrode plate could be built in BEAMnrc. The IQM control tool in the BEAMnrc GUI allows the user to define the geometry parameters of the IQM model as displayed graphically in Fig 4.2. The TCL/TK script file `iqm.tcl` is available on request ***because it is too large to be included in this thesis.***

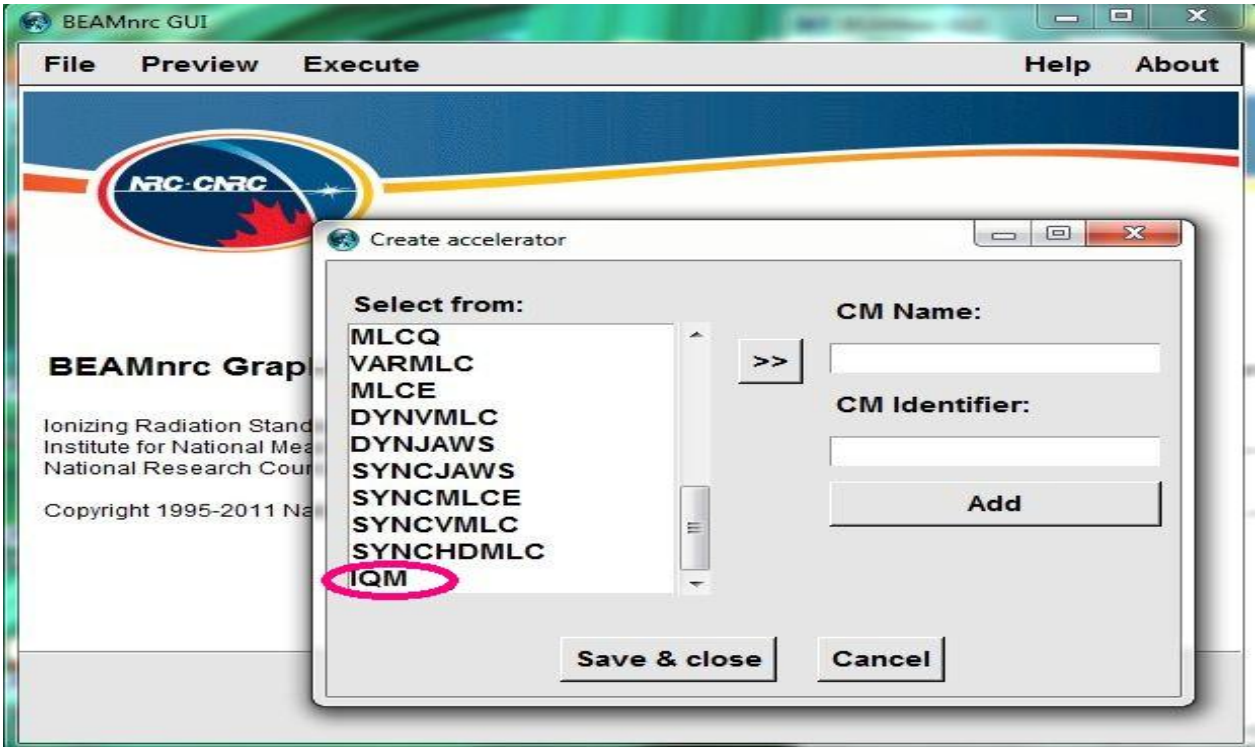

Figure 4.1: Addition of IQM to the BEAMnrc GUI

To obtain the graphical display of the IQM CM in figure 4.3 which is on x and z-axis, the parameters were defined in table 4.1.

Table 4.1: Parameters that defined the IQM model in Fig.4.3

Reference Parameters	**Variable parameters**
Half-width of outer square boundary (RMAX_CM)	13 cm
Number of layers	3
Distance from front to reference plane (ZMIN[1])	55.5 cm
Distance to back to reference plane (ZMAX[1])	57.4 cm
Positive x dimension of opening at front (XFP[1])	12.8 cm
Positive x dimension of opening at back (XBP[1]]	-12.6 cm
Negative x dimension of opening at front (XFN[1])	12.6 cm
Negative x dimension of opening at back (XBN[1])	12.8 cm
Outer x edge (XMAX[1])	12.9 cm
Distance from front to reference plane (ZMIN[2])	57.4 cm
Distance to back to reference plane (ZMAX[2])	57.6 cm
Positive x dimension of opening at front (XFP[2])	12.8 cm
Positive x dimension of opening at back (XBP[2]]	12.8 cm
Negative x dimension of opening at front (XFN[2])	-12.8 cm
Negative x dimension of opening at back (XBN[2])	-12.8 cm
Outer x edge (XMAX[2])	12.9 cm
Distance from front to reference plane (ZMIN[3])	57.6 cm
Distance to back to reference plane (ZMAX[3])	59.5 cm
Positive x dimension of opening at front (XFP[3])	-12.6 cm
Positive x dimension of opening at back (XBP[3]]	12.8 cm
Negative x dimension of opening at front (XFN[3])	-12.8 cm
Negative x dimension of opening at back (XBN[3])	12.6 cm
Outer x edge (XMAX[3])	12.9 cm

4.1.2 MORTRAN CODE FOR THE IQM COMPONENT MODULE

The IQM CM MORTRAN codes were written to simulate the integral quality monitoring (IQM) model using the BEAMnrc MC Simulation platform. The subroutines and macros used in the MORTRAN code of the CM were carefully compiled and debugged. The MORTRAN source files `IQM_cm.mortran` and `IQM_macros.mortran` are available on request ***because the files are too large to be included in this thesis***.

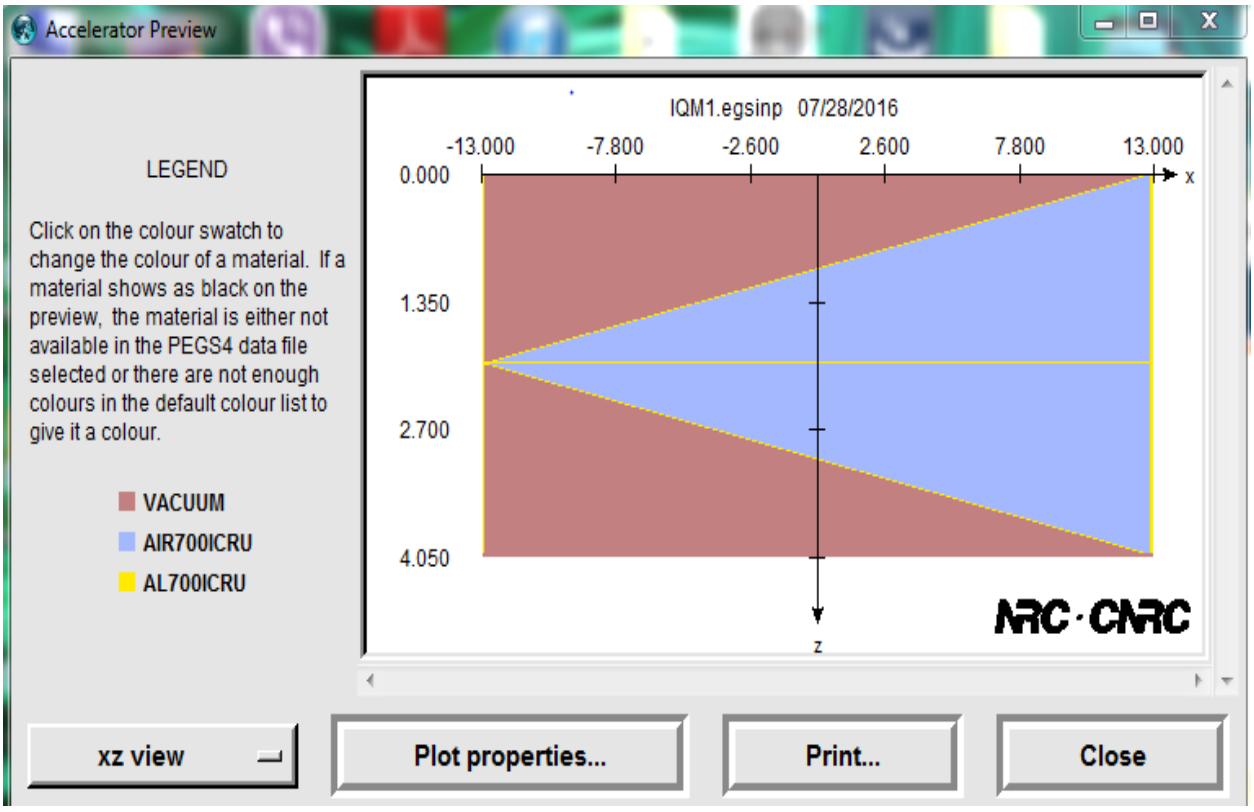

Figure 4.2: Illustration of the IQM CM coordinates on BEAMnrc GUI

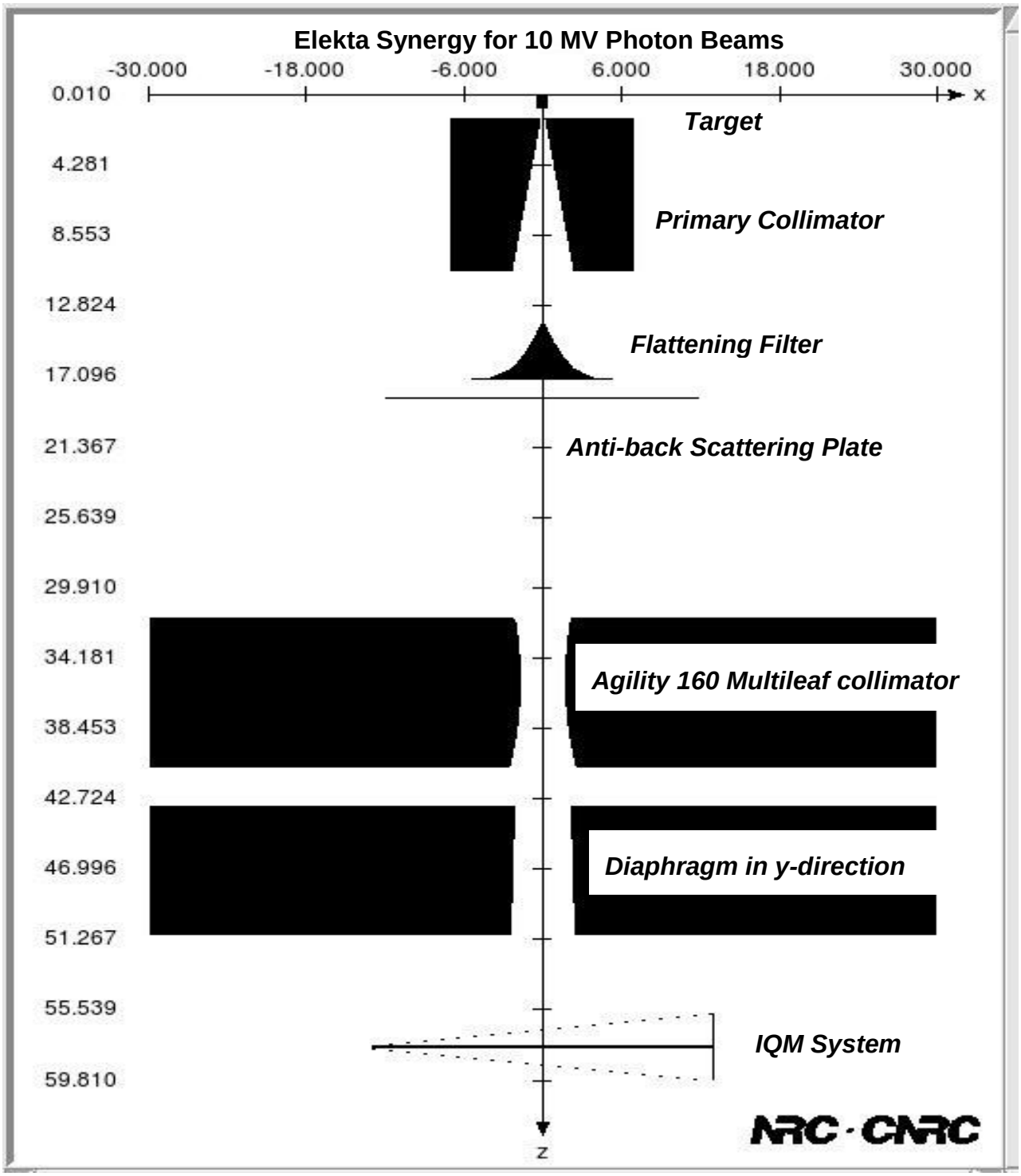

Figure 4.3: Depiction of a complete Linac head model with the IQM CM fixed to the linac head tray using the BEAMnrc GUI

4.1.3 VALIDATION OF THE IQM CM GEOMETRY BY RAY-TRACING

Fig 4.4 shows a two-dimensional ray tracing graph of the IQM CM coordinates. It specifies the boundaries of the IQM model in the simulation. All the arrows on Fig 4.4 were used to trace out the actual image of IQM model on the specified boundaries.

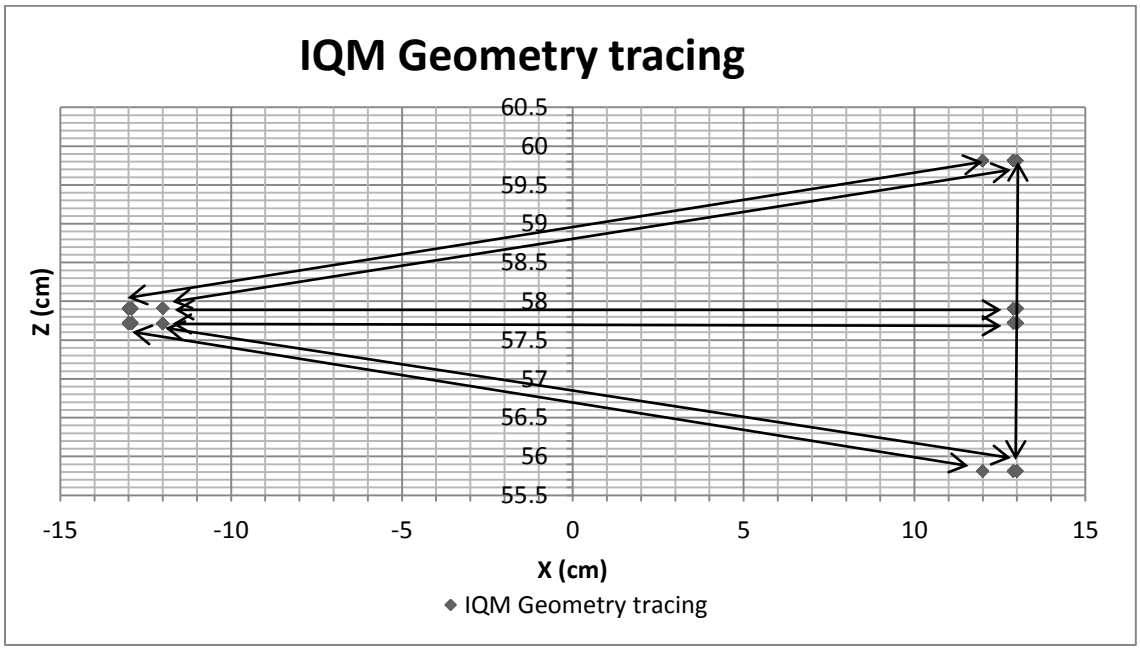

Figure 4.4: 2D (z and x- axis) projection of a ray tracing of the IQM CM. The z-axis represents the thickness of the IQM model parallel to the photon incident beam direction while the x-axis represents the perpendicular side of the IQM model across the incident beam

4.2 ACCURATE MONTE CARLO MODEL OF A LINAC

4.2.1 VALIDATION OF ELEKTA SYNERGY LINAC MODEL

4.2.1.1 PERCENTAGE DEPTH DOSE CURVES

Figs. 4.5 - 4.7 show the comparison between commissioned data and MC data for percentage depth dose (PDD) curves of 1 x 1 to 30 x 30 cm^2 fields obtained at 100 cm SSD using 10 MV photon beams.

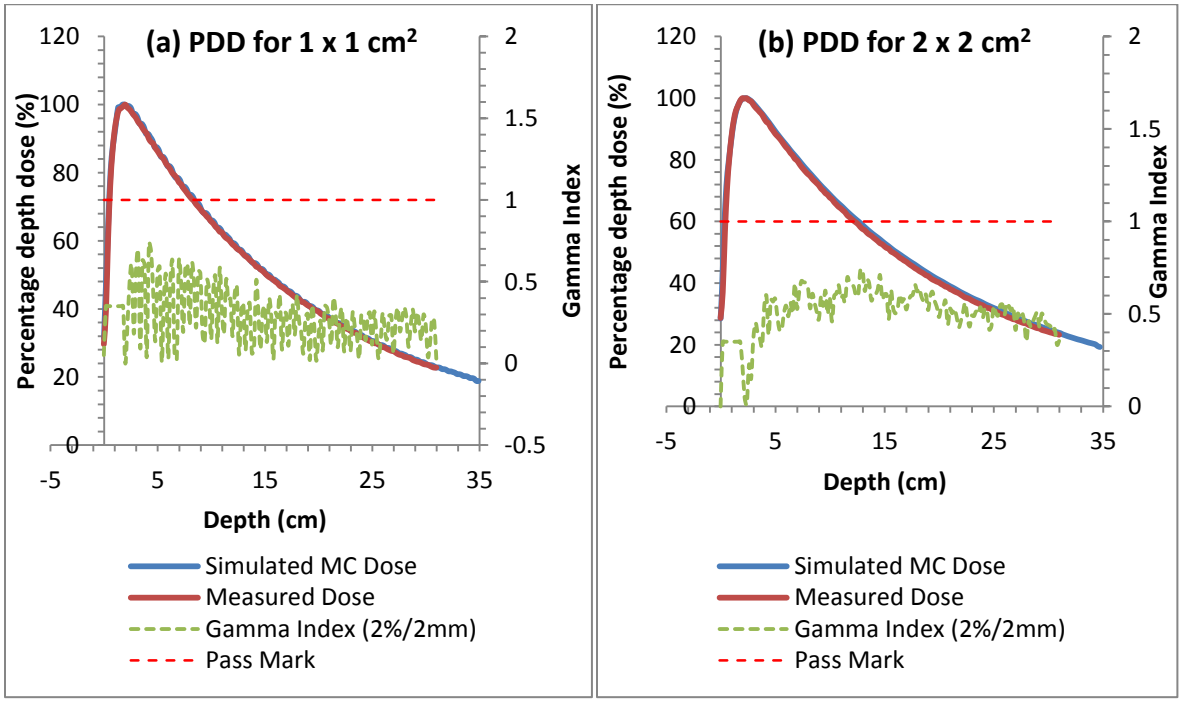

Figure 4.5: Comparison between measurement and MC percentage depth dose curves at 100 cm SSD for 10MV photon beams for 1 × 1 cm^2 and 2 × 2 cm^2

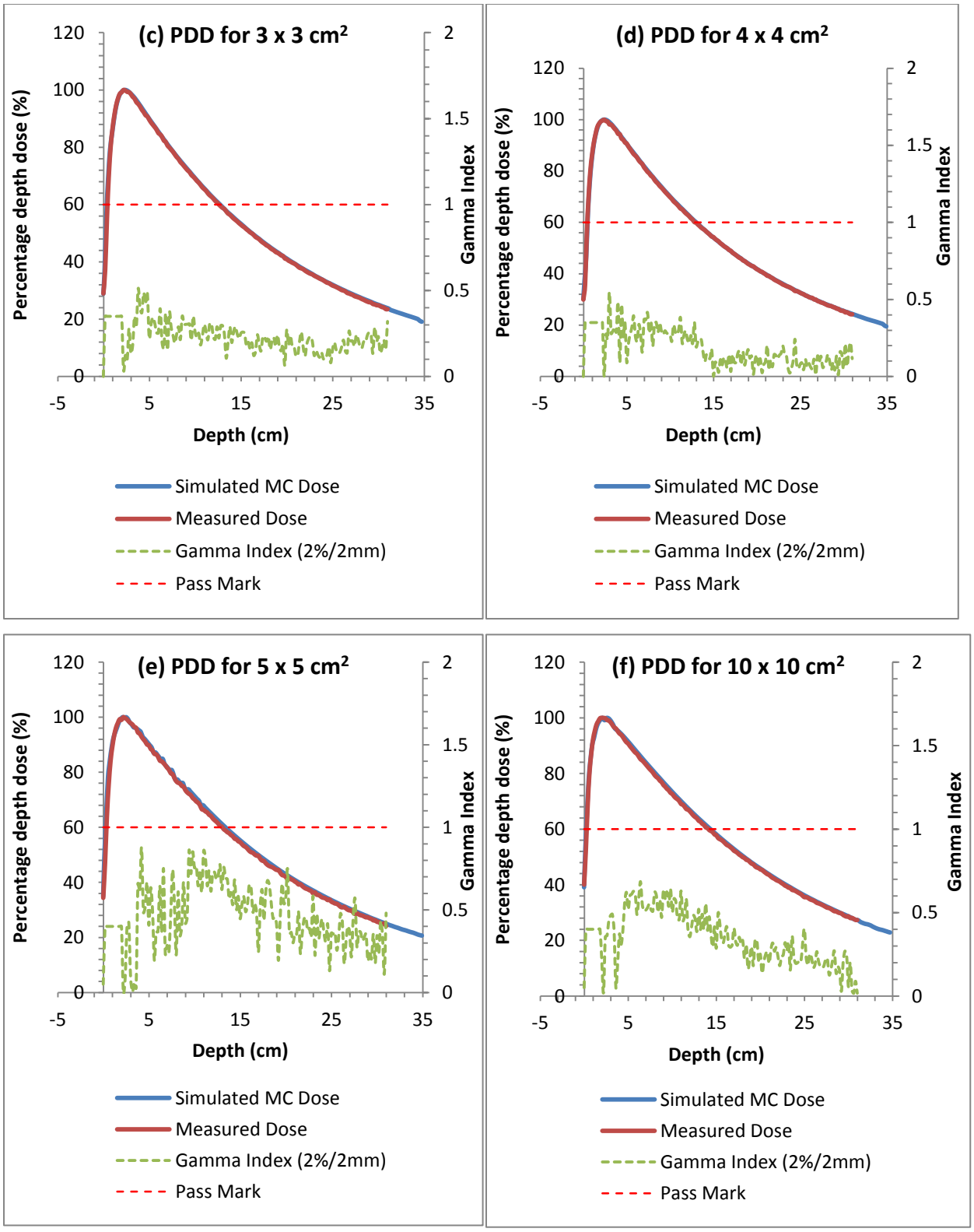

Figure 4.6: Comparison between measurement and MC percentage depth dose curves at 100 cm SSD for 10MV photon beams for 3 × 3 cm² and 10 × 10 cm²

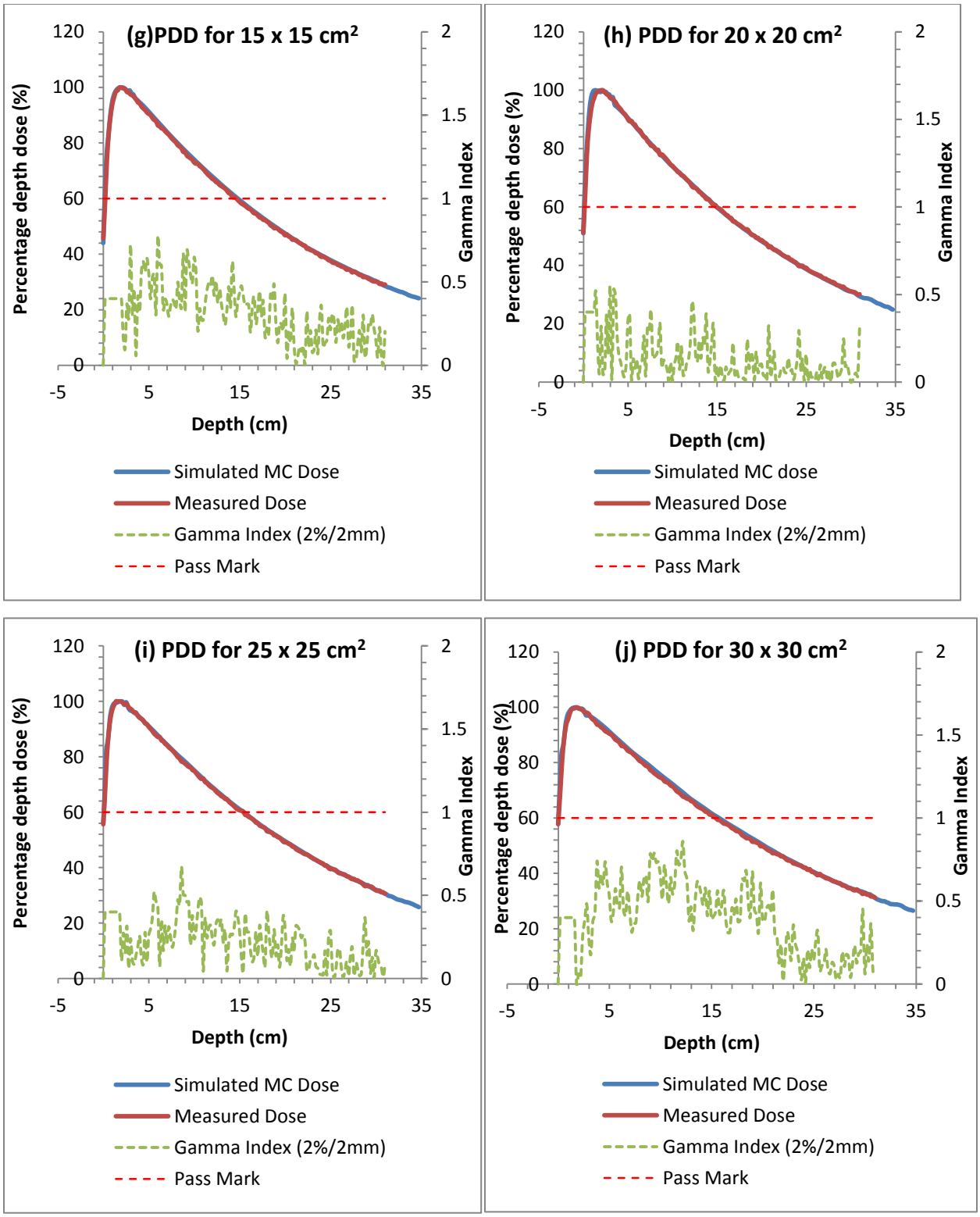

Figure 4.7: Comparison between measurement and MC percentage depth dose curves at 100 cm SSD for 10MV photon beams for 15 × 15 cm² to 30 × 30 cm²

4.2.1.2 DOSE PROFILES

Figs. 4.8 – 4.19 show the comparison between commissioning data and MC data cross-lines and in-lines dose profile curves of 5 × 5 to 30 × 30 cm^2 field sizes obtained at 100 cm SSD for 10 MV photon beams.

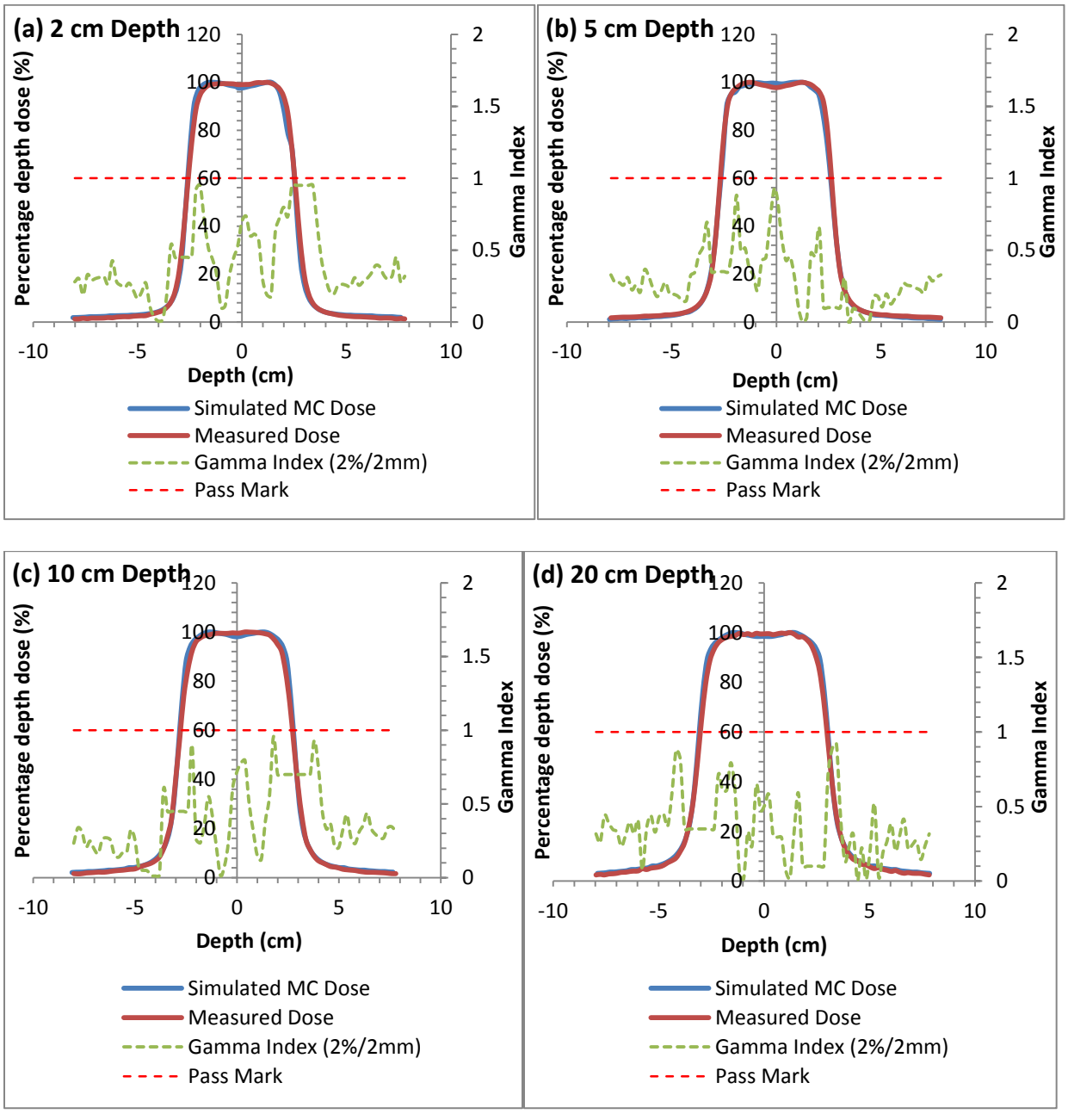

Figure 4.8: Comparison between measurement and MC cross-line profile curves for a 5 × 5 cm^2 field obtained at 100 cm SSD for 10MV photon beams

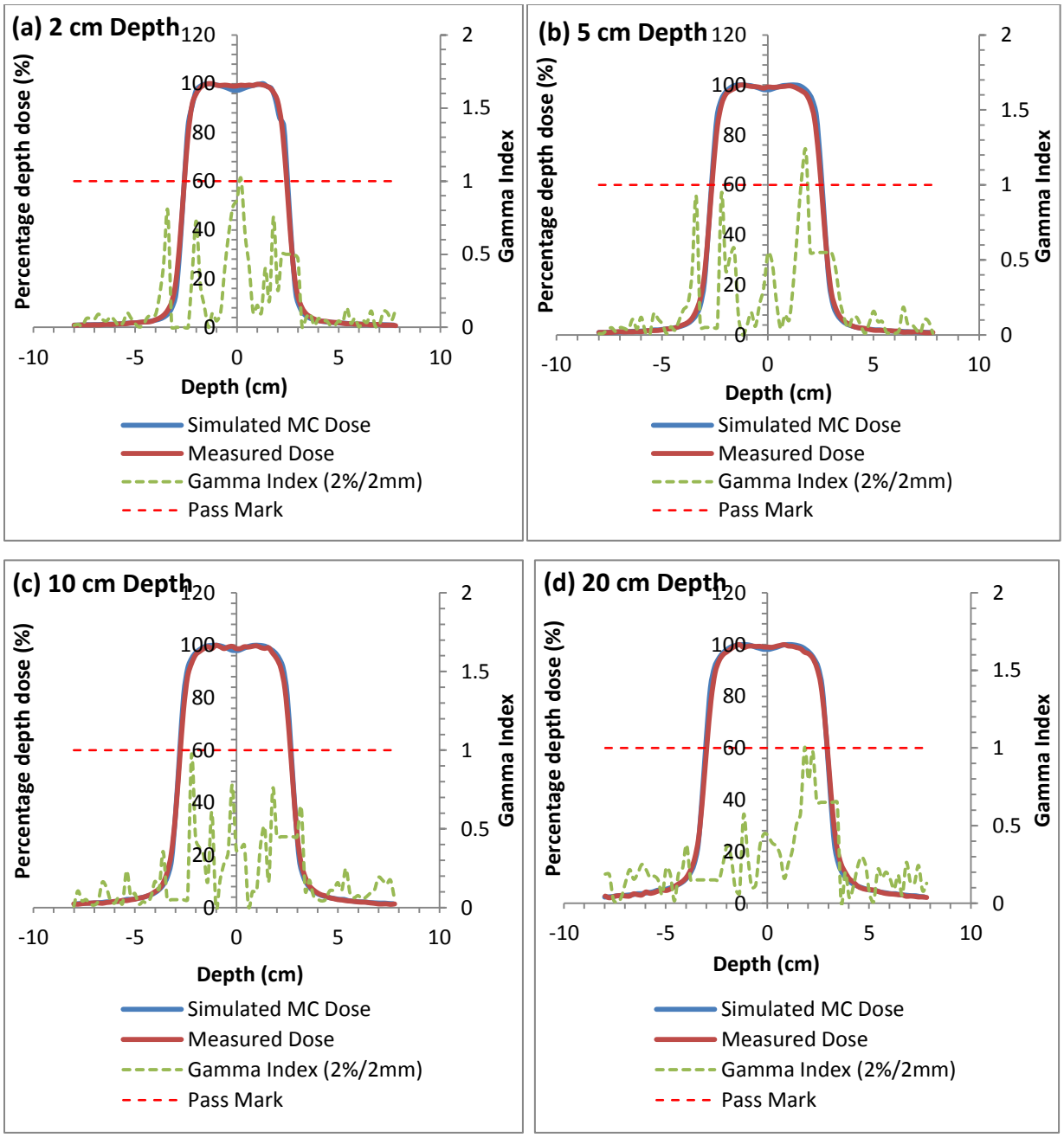

Figure 4.9: Comparison between measurement and MC in-line profile curves for a 5 × 5 cm^2 field obtained at 100 cm SSD for 10MV photon beams

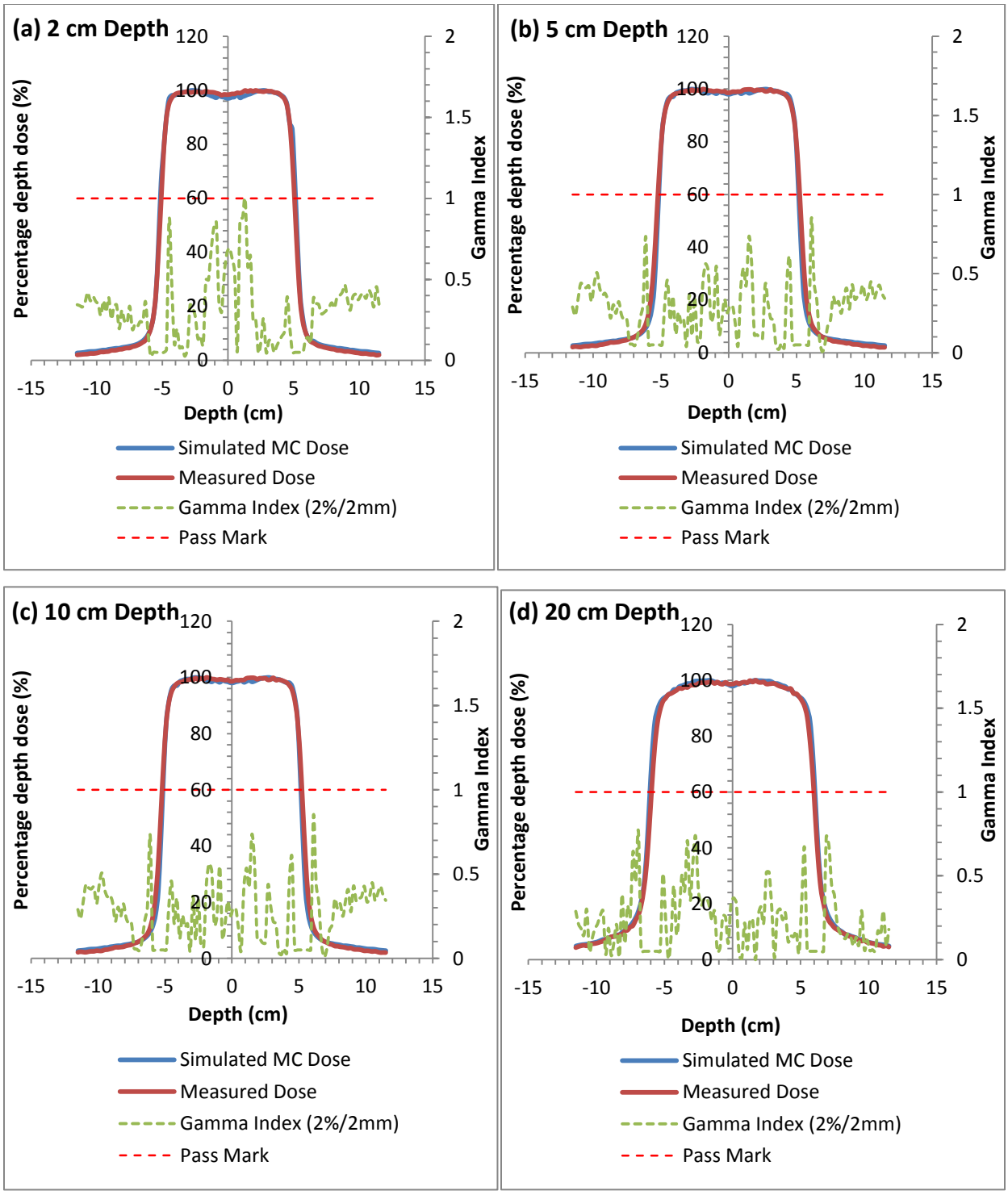

Figure 4.10: Comparison between measurement and MC cross-line profile curves for a 10 × 10 cm^2 field obtained at 100 cm SSD for 10MV photon beams

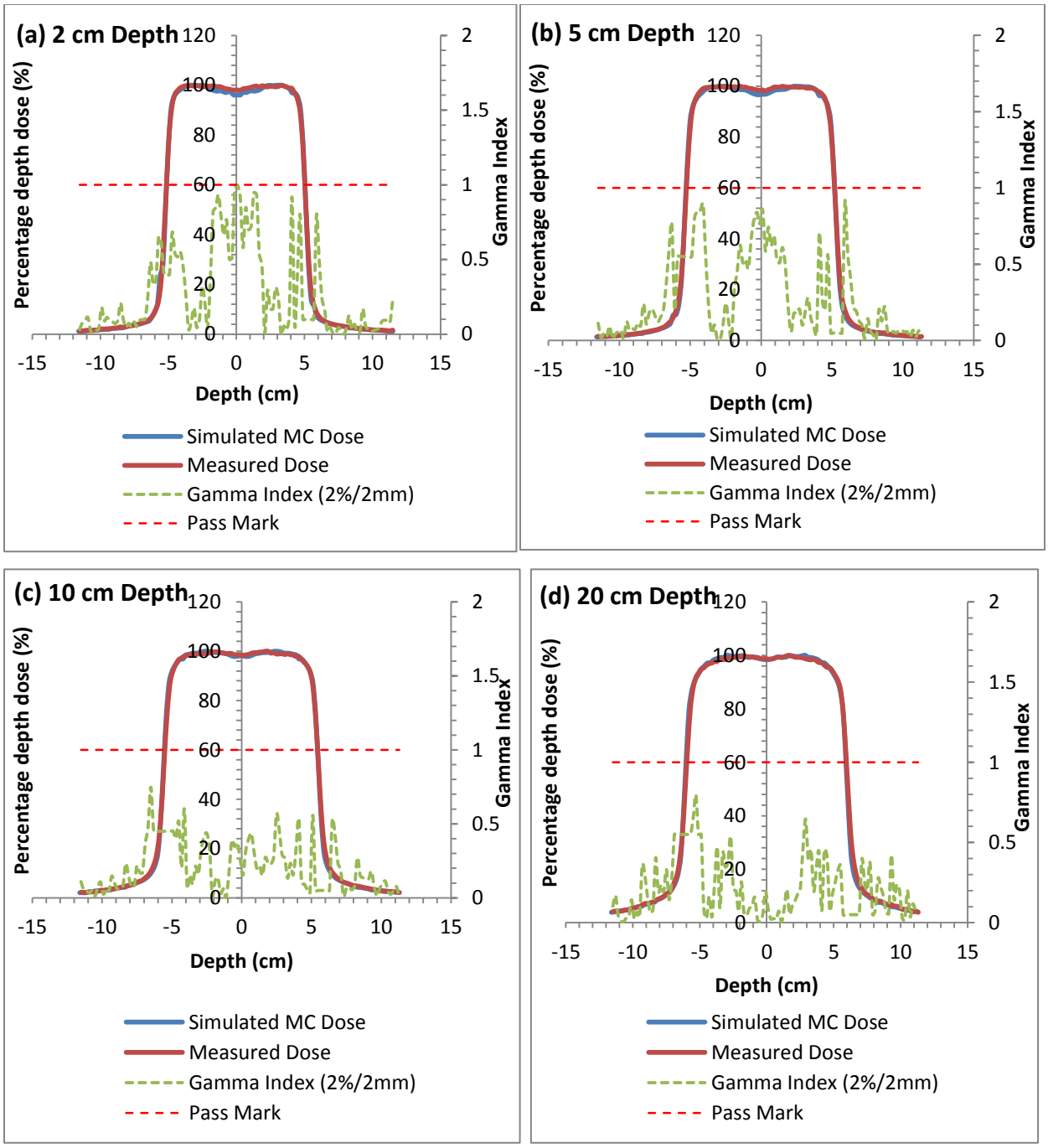

Figure 4.11: Comparison between measurement and MC inline-line profile curves for a 10 × 10 cm^2 field obtained at 100 cm SSD for 10MV photon beams

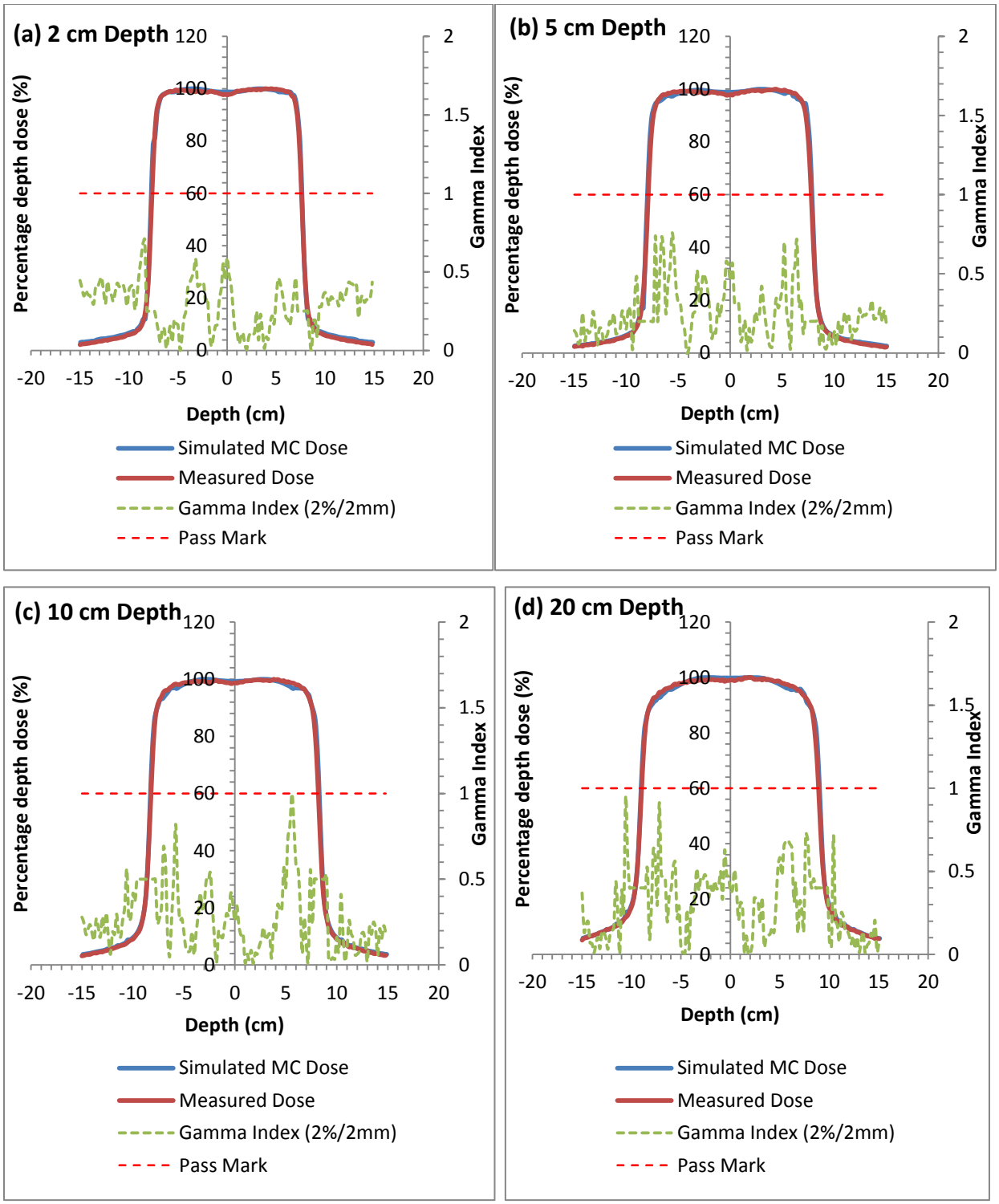

Figure 4.12: Comparison between measurement and MC cross-line profile curves for a 15 × 15 cm^2 field obtained at 100 cm SSD for 10MV photon beams

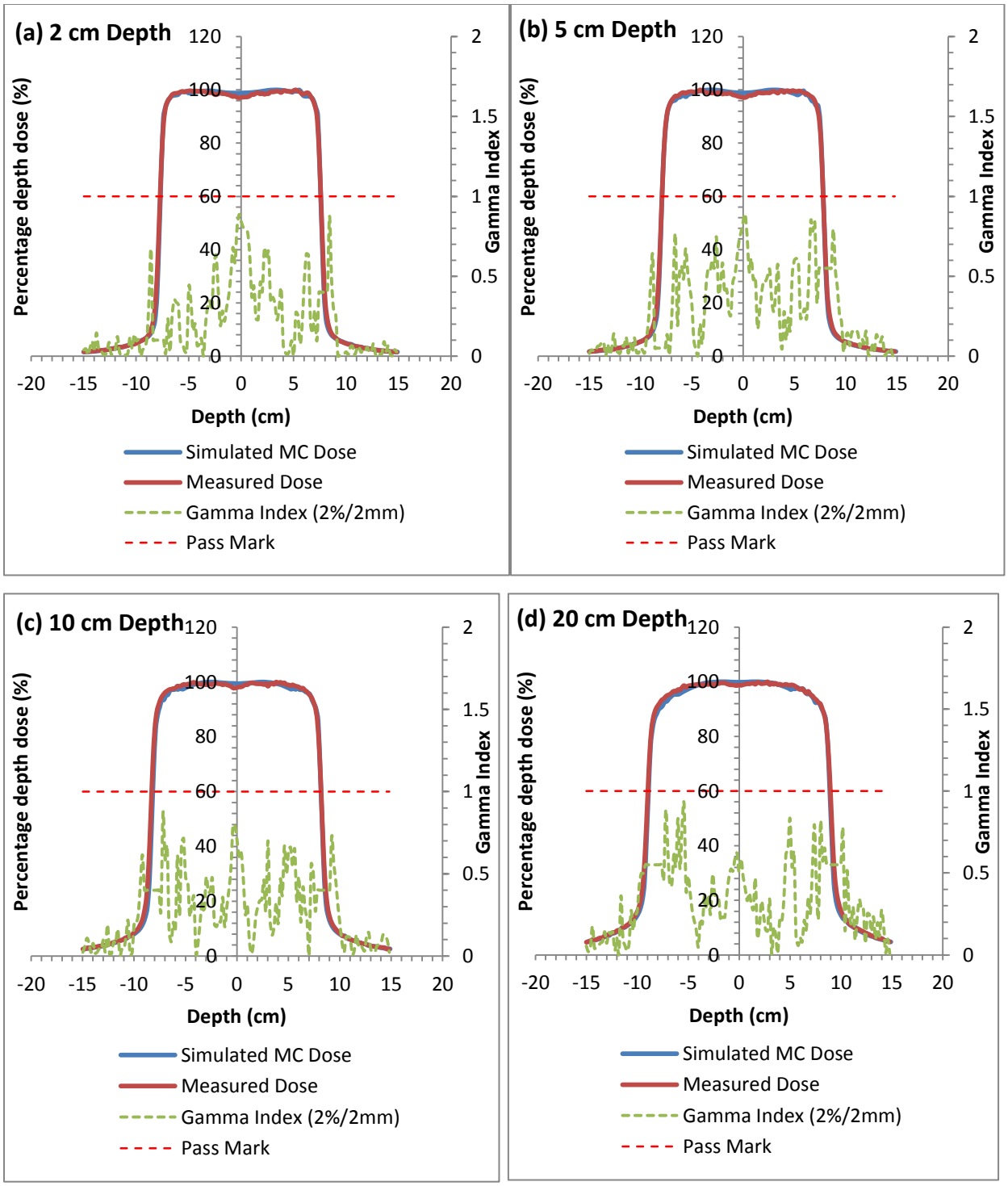

Figure 4.13: Comparison between measurement and MC inline-line profile curves for a 15 × 15 cm^2 field obtained at 100 cm SSD for 10MV photon beams

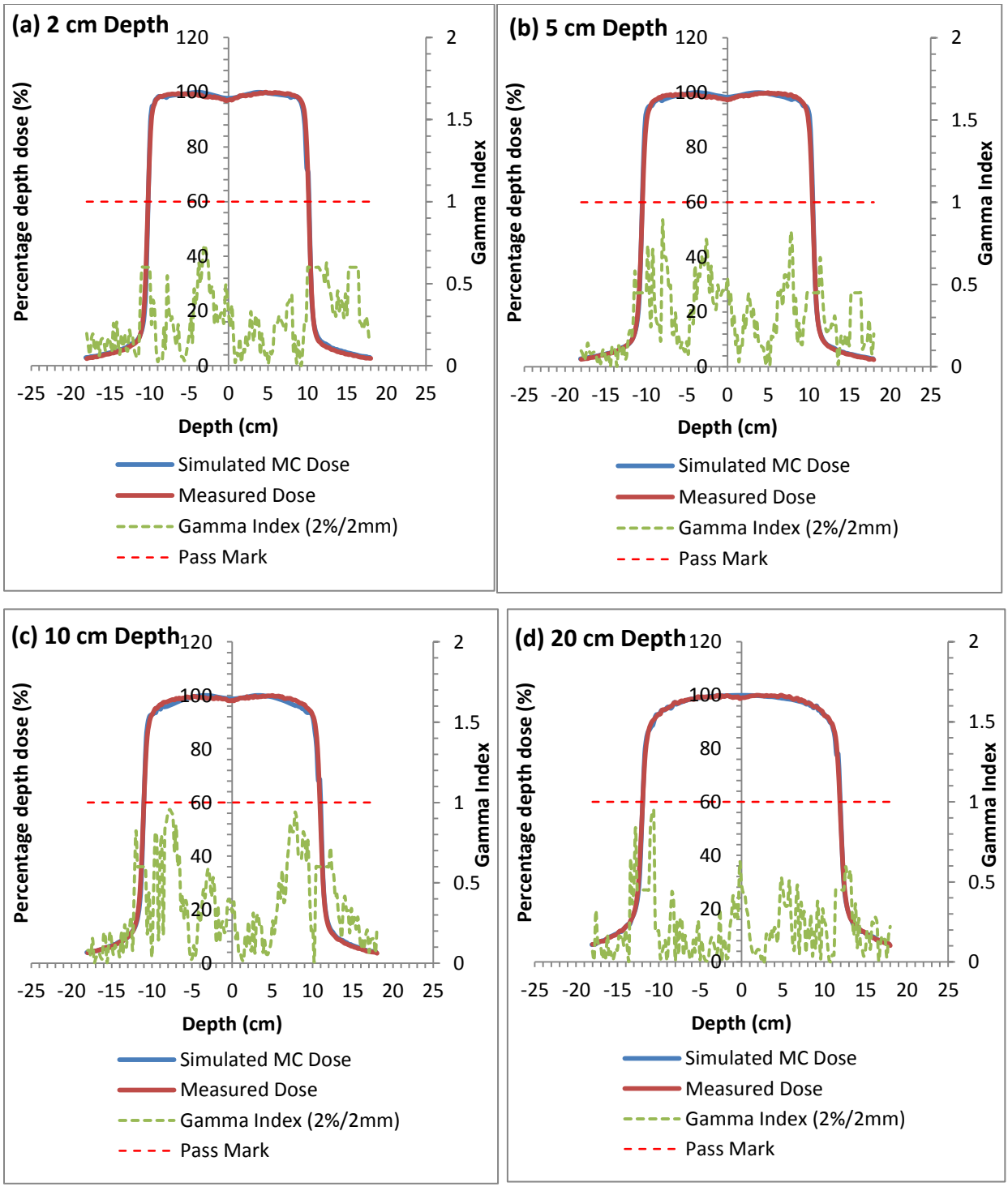

Figure 4.14: Comparison between measurement and MC cross-line profile curves for a 20 × 20 cm^2 field obtained at 100 cm SSD for 10MV photon beams

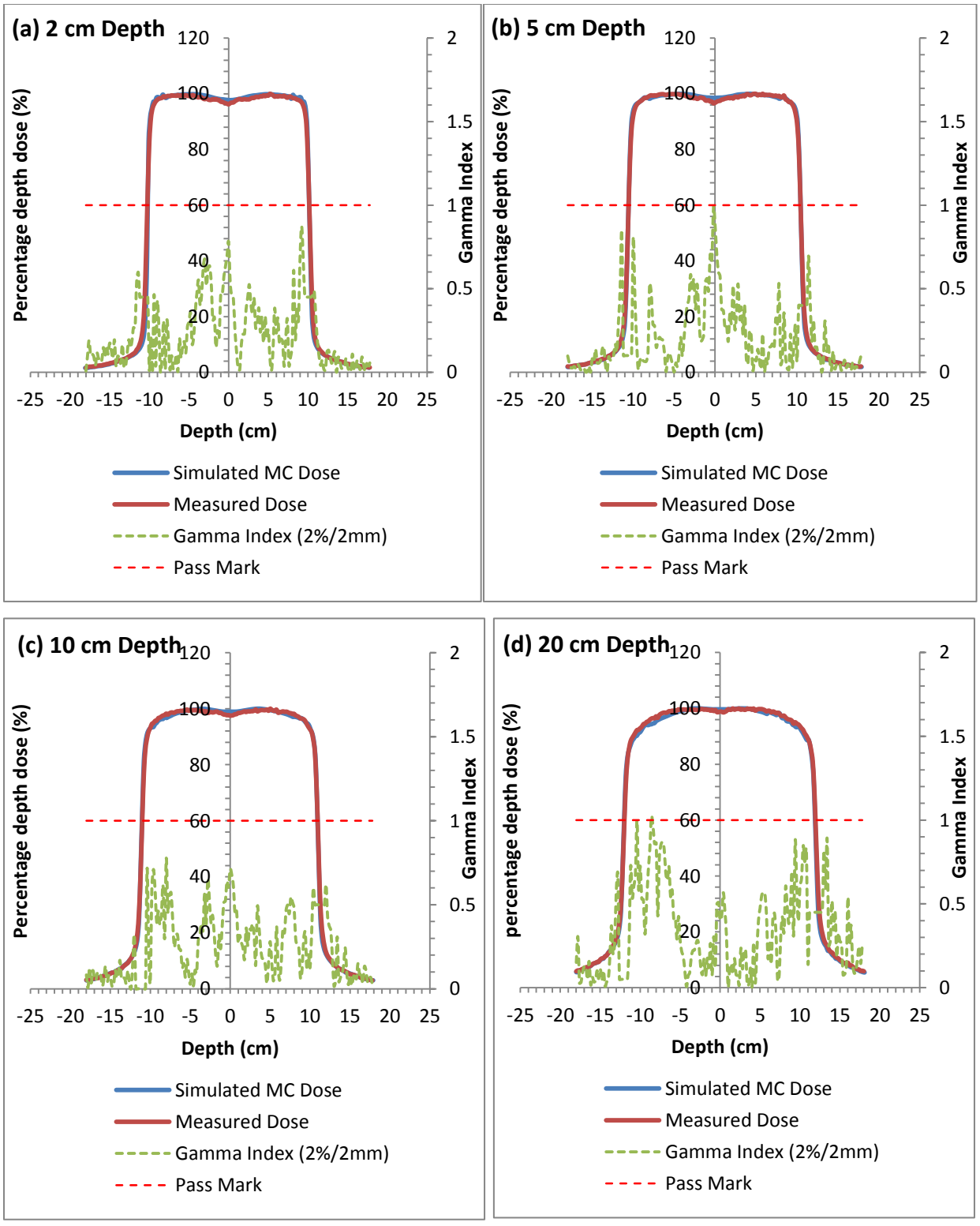

Figure 4.15: Comparison between measurement and MC in-line profile curves for a 20 x 20 cm^2 field obtained at 100 cm SSD for 10MV photon beams

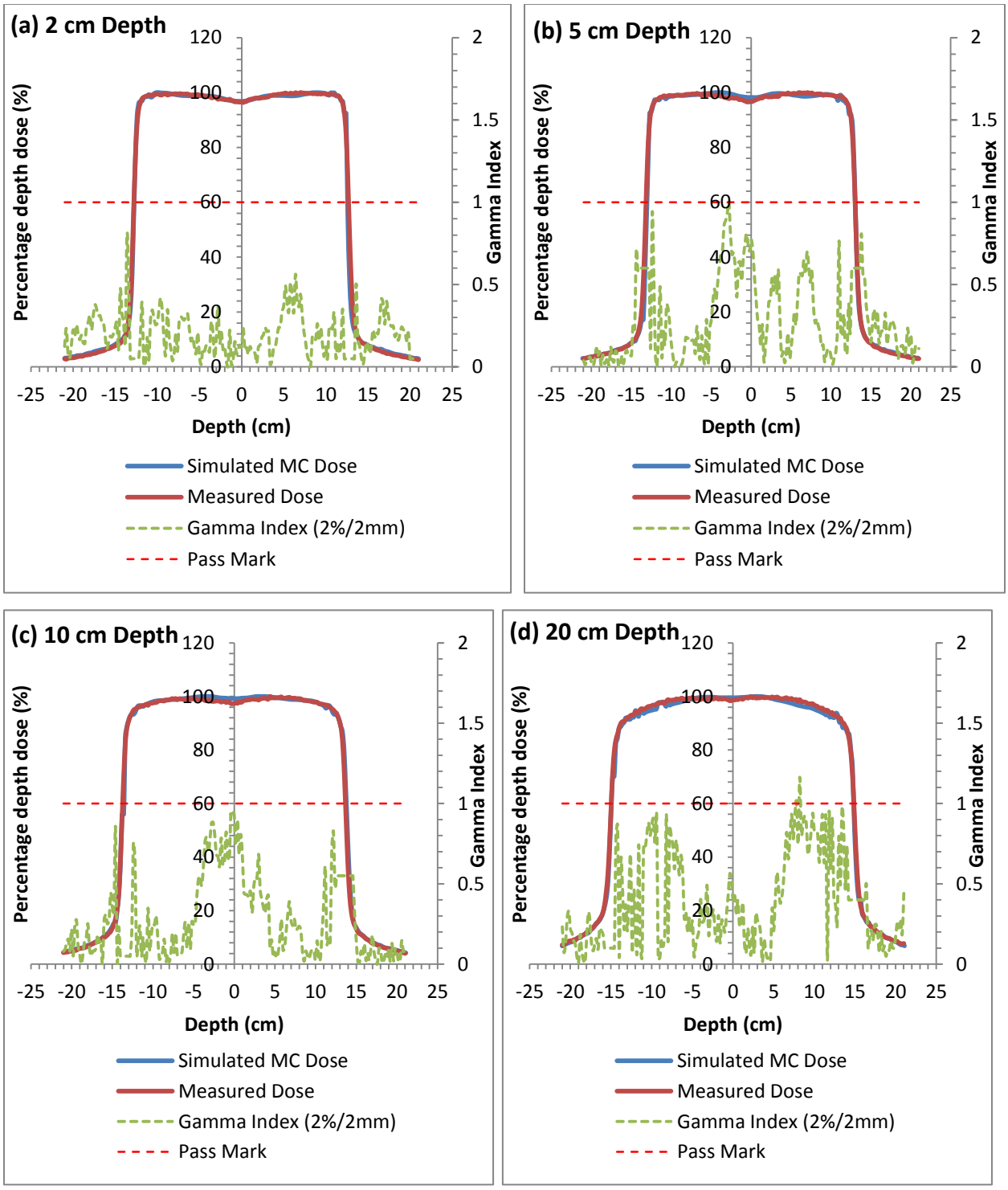

Figure 4.16: Comparison between measurement and MC cross-line profile curves for a 25 × 25 cm^2 field obtained at 100 cm SSD for 10MV photon beams

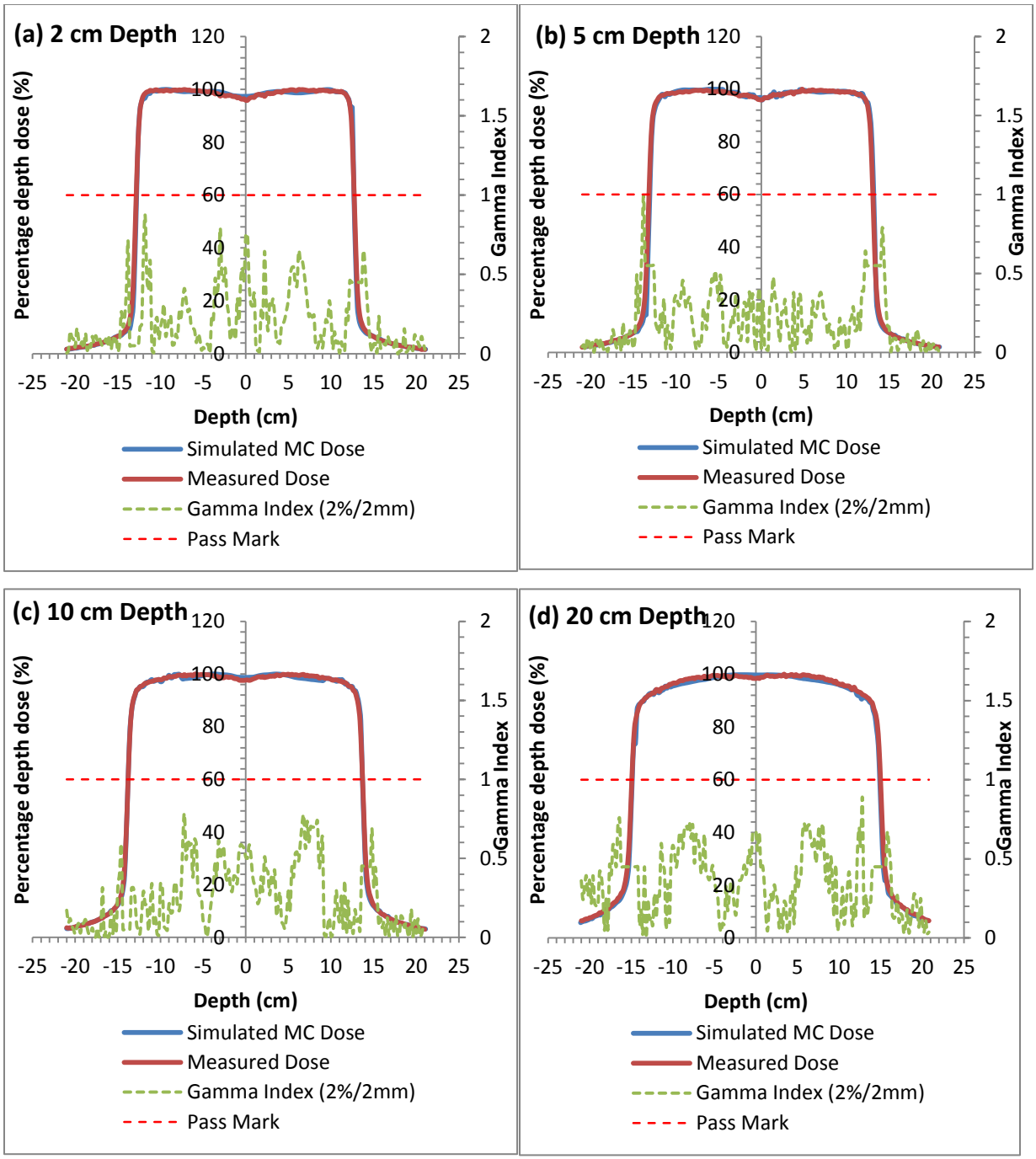

Figure 4.17: Comparison between measurement and MC in-line profile curves for a 25 × 25 cm^2 field obtained at 100 cm SSD for 10MV photon beams

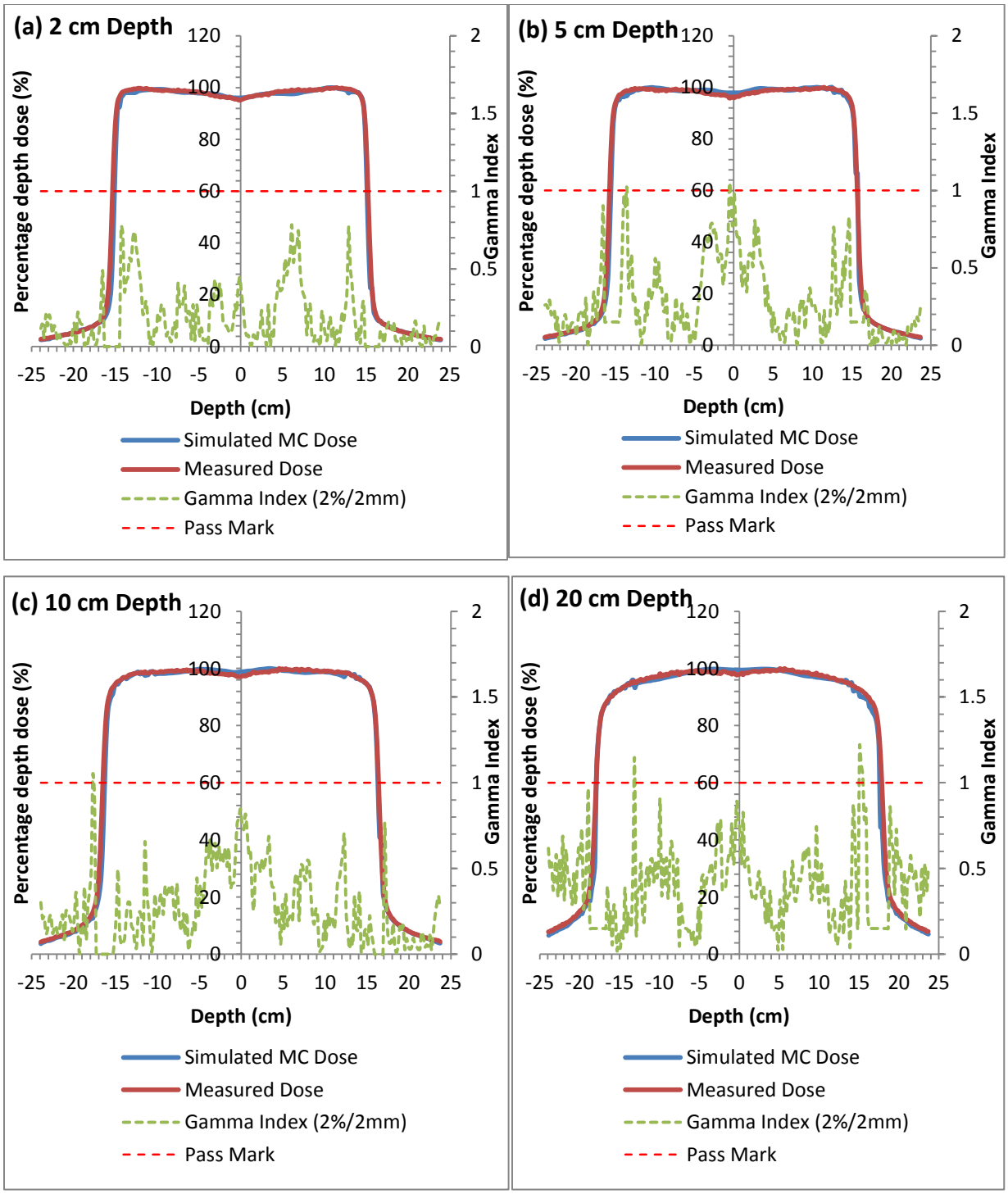

Figure 4.18: Comparison between measurement and MC cross-line profile curves for a 30 × 30 cm^2 field obtained at 100 cm SSD for 10MV photon beams

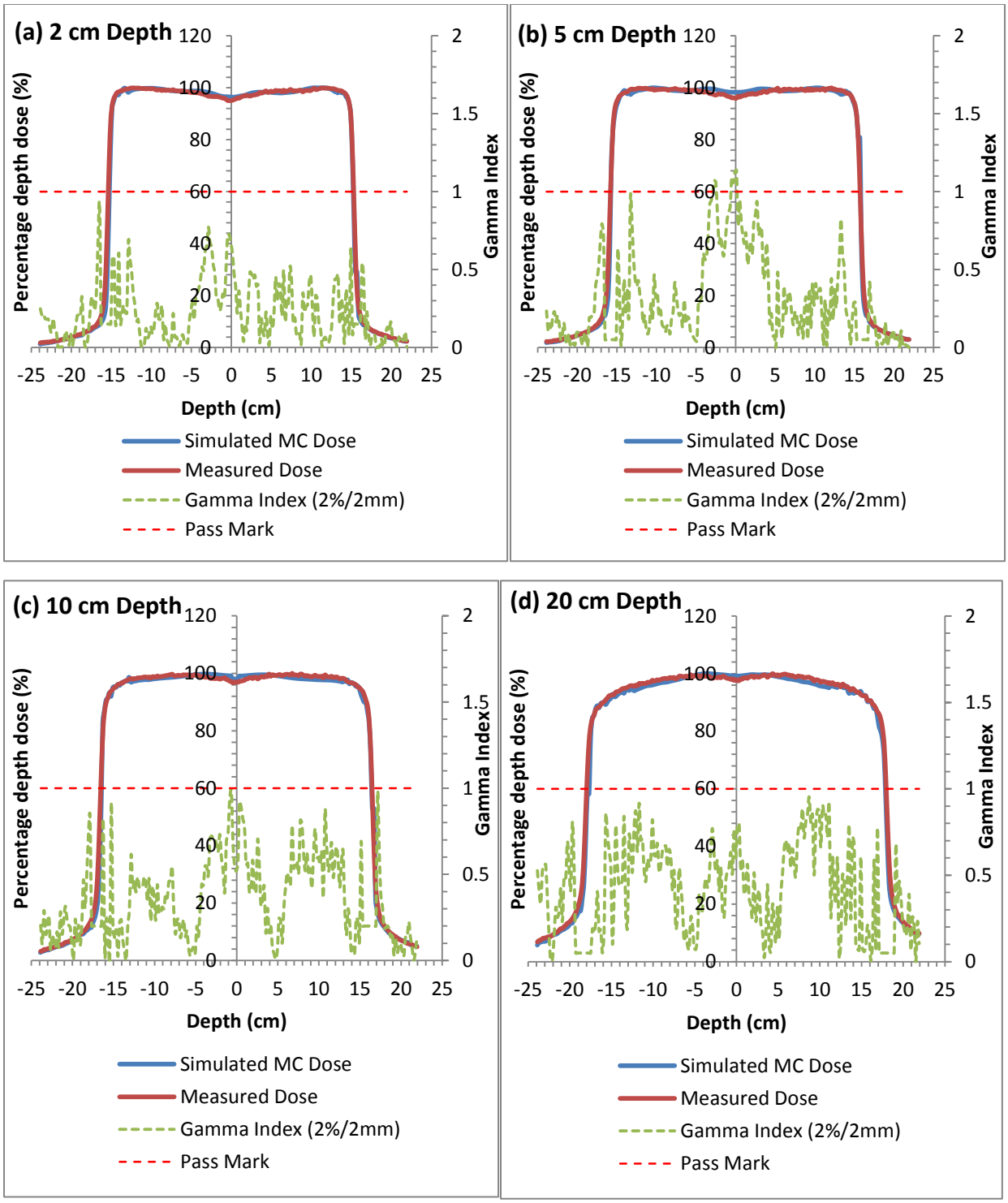

Figure 4.19: Comparison between measurement and MC in-line profile curves for a 30 × 30 cm^2 field obtained at 100 cm SSD for 10MV photon beams

4.2.1.3 RELATIVE OUTPUT FACTORS

Tab. 4.2 shows the comparison between commissioning and MC relative output factors of 1 x 1 to 30 x 30 cm^2 field sizes at 90 cm SSD for 10 MV photon beams.

Table 4.2: Relative output factor at 90 cm SSD for 10 MV photon beams

SQAURE FIELD SIZE (cm^2)	SIMULATED	MEASURED	LOCAL DIFF (%)
1 X 1	0.6792	0.6714	1.1648
2 X 2	0.8224	0.8115	1.3543
3 X3	0.8771	0.8647	1.4422
4 X 4	0.9200	0.8964	2.6318
5 X 5	0.9244	0.9205	0.4172
10 X 10	1.0000	1.0000	-
15 X 15	1.0559	1.0460	0.9436
20 X 20	1.0608	1.0759	1.4082
25 X 25	1.0842	1.0960	1.0770
30 X 30	1.1194	1.1100	0.8455

In Fig. 4.5- 4.19, the MC simulation benchmarked against measurement agreed to 2%/2 mm criterion for the percentage depth dose curves and for the lateral beam profiles. Most of the dose points analysed passed the criterion.

In Tab. 4.2, accurate ROF data is presented. The majority of the MC simulated data and the physically measured data for the square fields' relative output factors agreed to less than 1.5% of local dose difference. 4 × 4 cm^2 field has a local difference of 2.63% which could have been caused by discrepancies in commissioning data whereby an additional electron source in the linac head for the field size or effect of contaminant electrons after the buildup region in the water phantom or chamber positioning or changes in chamber responses at small fields and shallow depth.

The characterised photon beam of the Elekta Synergy equipped with Agility 160-Leaf MLC model is accurate having passed the universal criteria. This accurate source model is suitable for MC sensitivity simulation.

4.3 SENSITIVITY STUDY OF THE IQM COMPONENT MODULE

As stated in earlier chapters, the purpose of this study was to know how sensitive the integral dose of a double wedge-shaped ionization chamber can be for altered segments using the EGSnrc MC code. This will show the relationship between the altered field and IQM signal response and will also create awareness to detector manufacturers the essence of having a future wedge-shaped ionization chamber that could give its reading in dose or be rescaled to dose. The measurement output is an electronic signal while the simulation output is an integral dose. This study was able to correlate the electronic signal with MC dose (IQM signal). Ability to use MC to calculate dose in the ionization chamber is one of the advantages of the EGSnrc code that was used in this study over the EGS4.

Fig. 4.20 shows the correlation between the measurement and the simulation output which increases with an increase in field size. The physical measurements and MC simulations are not measured in the same unit. Normalisation allows rescaling of both outputs. Validation of the linac model used in this study gives the confidence that there are no discrepancies in the photon beams upstream of the IQM model. In order words simulated response is possible since the MC and real photon beam have the same ROFs, PDDs and profiles over the fields studied.

Tab 4.3 shows the numbers of histories used for the square field of IQM simulation that is depicted in Fig. 4.20.

Fig. 4.20 shows the normalised IQM response for 1 × 1 to 30 × 30 cm^2 fields for 10 MV photon beams measured (calculated signal) and simulated (dose-area product).

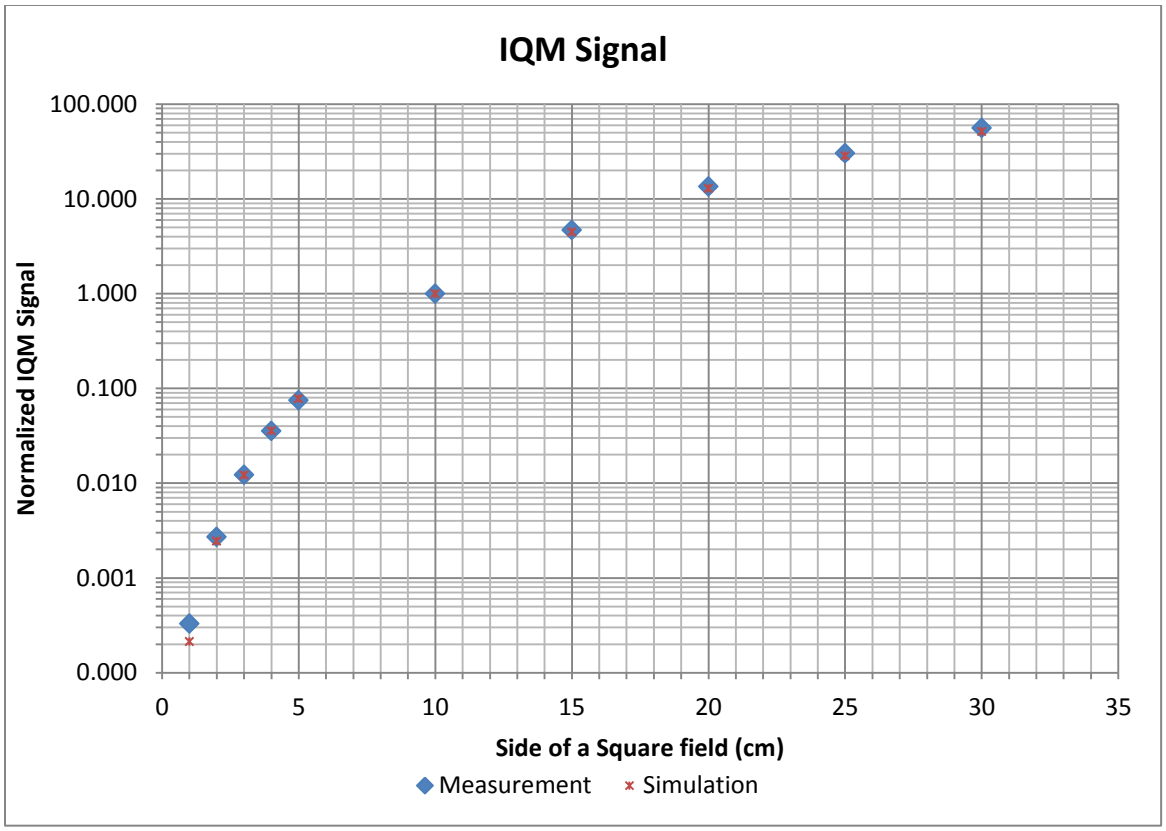

Figure 4.20: IQM signal response plotted on a semi-log scale for 1 × 1 to 30 × 30 cm^2 fields for 10 MV photon beams

Table 4.3: Number of histories used in MC simulation of field sizes

Field size	Number of histories ($\times 10^9$)
1 ×1 cm^2	14.00
2 × 2 cm^2	14.50
3 × 3 cm^2	14.80
4 × 4 cm^2	14.85
5 × 5 cm^2	15.00
10 × 10 cm^2	15.20
15 × 15 cm^2	15.60
20 × 20 cm^2	15.82
25 × 25 cm^2	15.87
30 × 30 cm^2	15.95

4.3.1 SYSTEMATIC POSITIONAL ERROR ANALYSIS

Figure 4.21 shows the magnitude of the normalised IQM signal for MLC segments of 1 × 1, 3 × 3, 5 × 5 and 10 × 10 cm^2 when systematic positional errors of 1, 2 and 3 mm were uniformly added and also subtracted from open leaves of fields as defined at the isocentre for 10 MV beams. In figure 4.21, miss-calibration of 1 × 1 cm^2 field has the highest magnitude of the normalised IQM signal when its open leaves were uniformly altered. The wedge-shaped ionization chamber is sensitive to positional errors. An increase or decrease in positional, causes an increase or decrease in normalised IQM magnitude. Each of the altered-field signal was normalised to its individual unaltered-field signal.

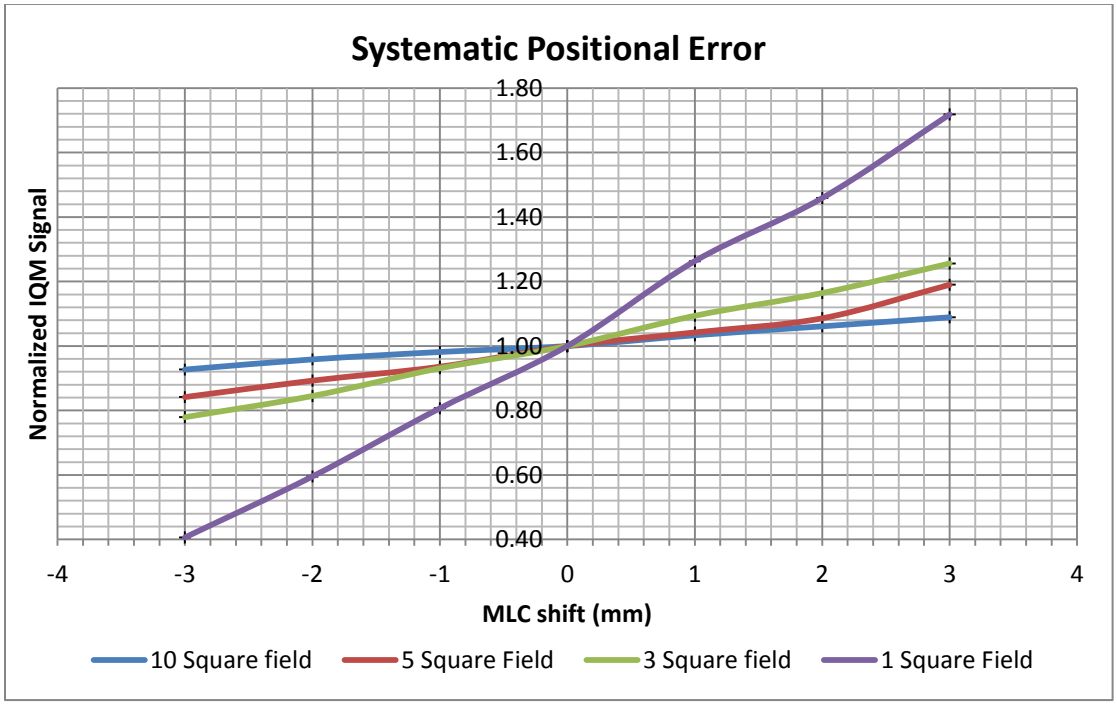

Figure 4.21: Sensitivity of the IQM model when the open leaves of segments 1 × 1, 3 × 3, 5 × 5 and 10 × 10 cm^2 are altered uniformly by -3, -2, -1, 1, 2 and 3 mm

Tab. 4.4 displays the normalised IQM signal for misalignments 1, 2, 3, 4 and 5 leaves when shifted from the central field axis by 1, 2, 3, 5 and 10 mm for 5 × 5 cm^2 field. Misalignment results in different dose variation. It shows that the wedge-shaped ionization chamber model responds to 1 mm offsets of a single leaf. An increase in the number of leaves altered causes an increase in signal response. The signal response was approximated to three decimal places. An increase in positional error causes an increase in IQM signal response. These values were normalised to signal of unaltered 5 × 5 cm^2 field. There were inconsistencies in column one, row four and five, also in column 4, row two and three.

Table 4.4: IQM signals for 1, 2, 3, 4 and 5 leaves shifted out of field for 1, 2, 3, 5 and 10 mm positional shift for a 5 × 5 cm^2 field (± standard deviations)

Number of leaves shifted	Leaf shifted position				
	1 mm	**2 mm**	**3 mm**	**5 mm**	**10 mm**
1	1.003±0.008	1.007±0.008	1.012±0.008	1.020±0.008	1.030±0.008
2	1.007±0.008	1.009±0.008	1.015±0.008	1.038±0.008	1.065±0.008
3	1.012±0.008	1.015±0.008	1.018±0.008	1.038±0.008	1.076±0.008
4	1.020±0.008	1.021±0.008	1.032±0.008	1.057±0.008	1.095±0.009
5	1.020±0.008	1.026±0.008	1.034±0.009	1.067±0.009	1.129±0.009

4.3.2 GRADIENT POSITIONAL ERROR ANALYSIS

Fig 4.22a shows the sensitivity gradient profiles for 3 × 3, 5 × 5 and 7 × 7 cm^2 fields at 10 MV photon beams. This is to compare the gradient response between different segments. Fig 4.22b and 4.22c show the sensitivity gradient profiles of 7 × 5 cm^2 and 5 × 7 cm^2 fields and 5 × 3 cm^2 and 3 × 5 cm^2 fields respectively at 10 MV photon beams.

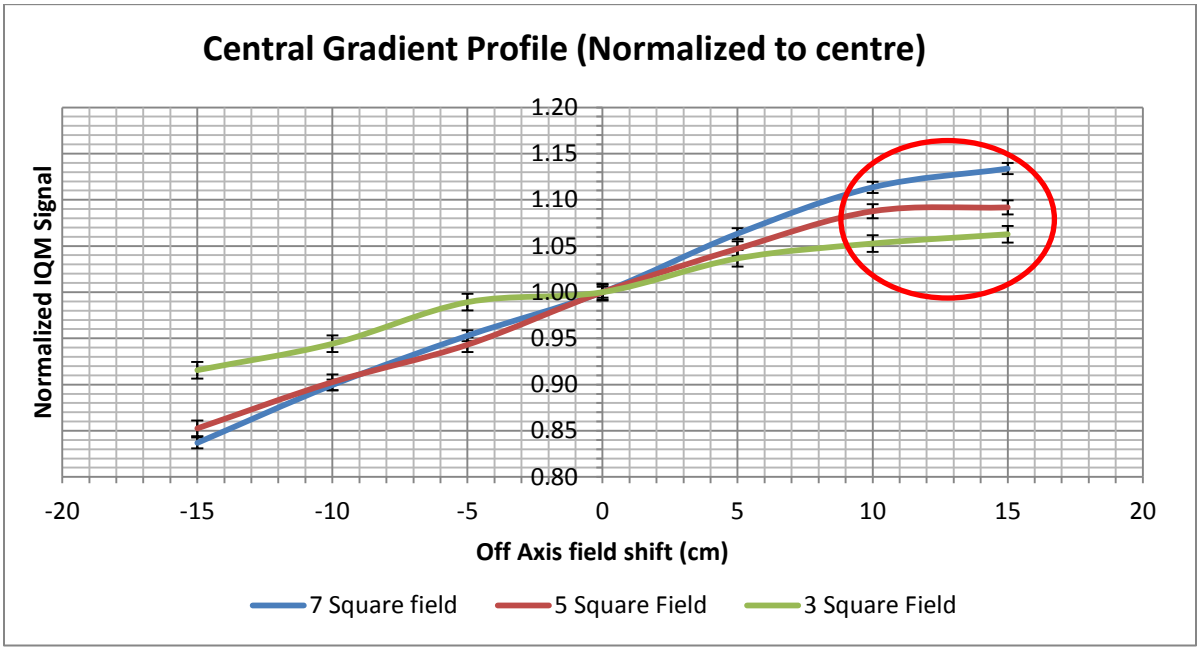

Figure 4.22a: Sensitivity factor along the IQM CM gradient for 3 × 3, 5 × 5 and 7 × 7 cm^2 fields (trend gradients are 0.005, 0.009, and 0.010)

In Fig. 4.22a, b, and c, the sensitivity profile increases along the gradient of the IQM model. There is a noticeable plateau region in the sensitivity profile. This is the region of the higher separation distance between the collecting plate and the polarising plate. It should also be noted that the photon beam of a field that is incident on the IQM model is not the same along the gradient of the IQM. The incident aperture changes along the gradient. The combined effect of non-uniform incident aperture and the separation distance between the plates gives the sensitivity profile. In figure 4.22a, the gradient of the trend line increases with an increase in field sizes. In figures 4.22b and c, gradients of the trend lines increase with an increase in the side of the field that is parallel to the IQM slope.

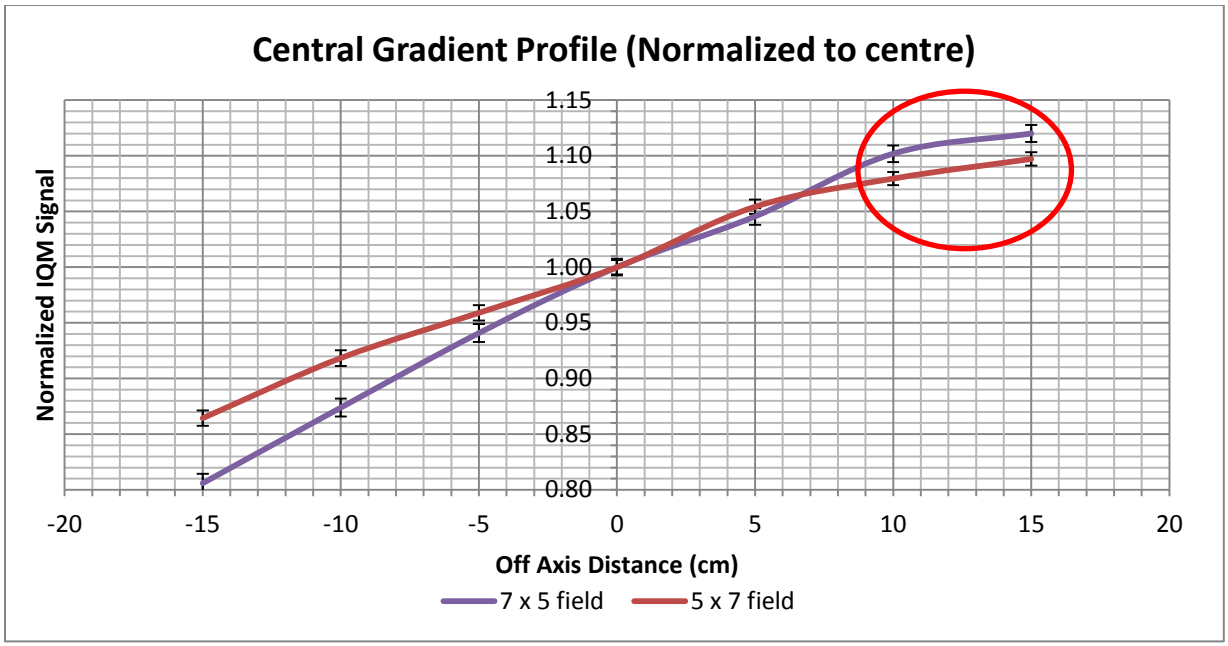

Figure 4.22b: Sensitivity factor along the IQM CM gradient for 7 x 5 and 5 x 7 cm^2 fields (trend gradients are 0.011 and 0.008)

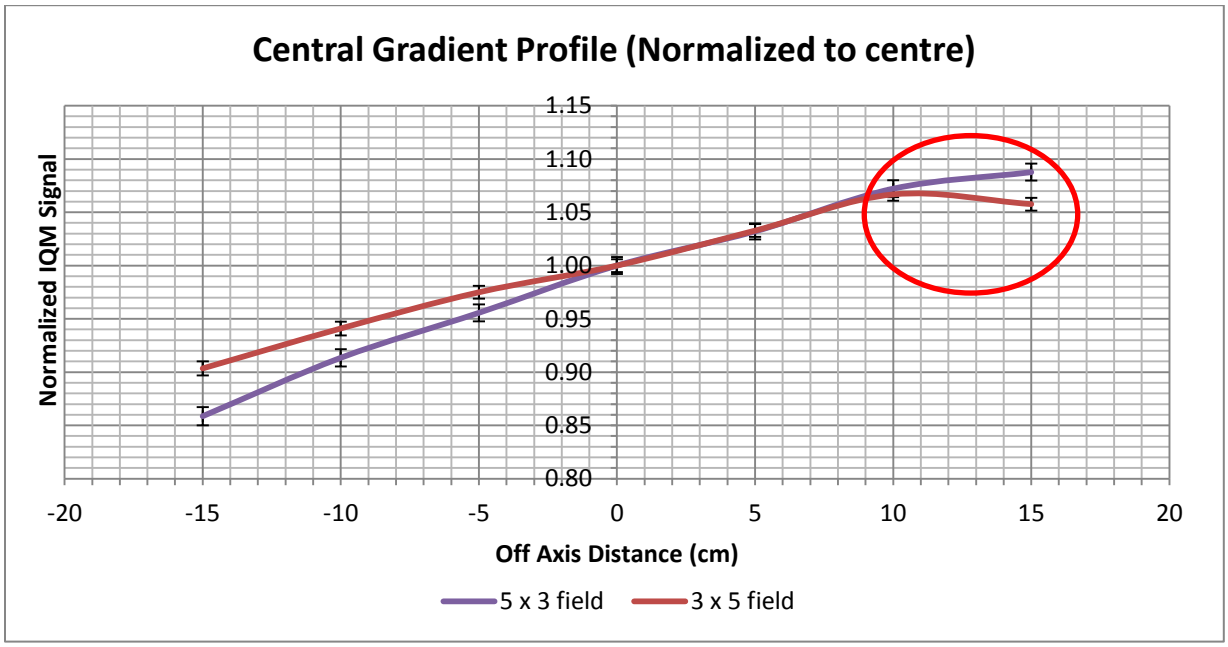

Figure 4.22c: Sensitivity factor along the IQM CM gradient for 5 × 3 and 3 × 5 cm^2 fields (trend gradients are 0.008 and 0.006)

4.3.3 RANDOM POSITIONAL ERROR ANALYSIS

To conclude this sensitivity study of the IQM CM, eleven segments (regular and irregular segments) were altered at random within ±1, ±2 and ±3 mm positional errors defined at the isocentre for 10 MV beams.

4.3.3.1 SEGMENT ONE

Segment one is a regular 7 × 7 cm^2 field. This field was altered at random 30 times and analysed. IQM signals were normalised to the unaltered segment which has a segment area of 49 cm^2.

Fig. 4.23a shows the example of an unaltered field, and the examples of fields altered at random within ±1, ±2, and ±3 mm regarding its individual leaf positions.

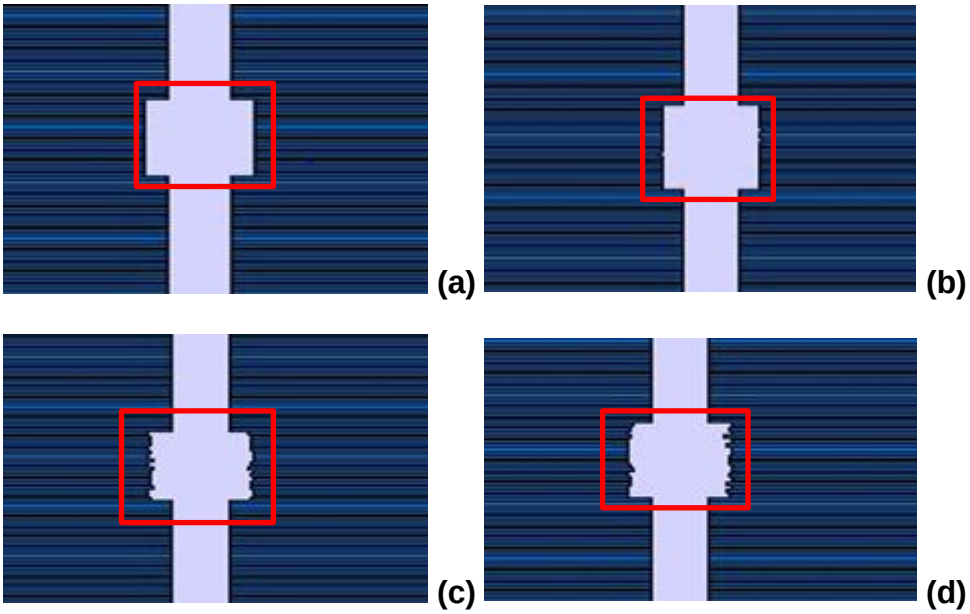

Figure 4.23a: Depicts the examples of randomly altered MLC leaf positions for Segment 1 (7 × 7 cm^2 field) (a) Unaltered segment; (b) within ± 1 mm alteration; (c) within ± 2 mm alteration; (d) within ± 3 mm alteration

SENSITIVITY ANALYSIS OF SEGMENT ONE

In segment one, the altered segments size range depends on the allowed alteration limit. For the ± 3mm randomly altered case the segment area ranged between 48.42 cm^2 to 49.68 cm^2. The original unaltered segment size is exactly 49.00 cm^2. For the ±

2mm case, this range shrank to between 48.63 cm^2 and 49.41 cm^2. For the ± 1 mm case, there is an even spread around the 49.00 cm^2 unaltered segment size.

A. SCATTER PLOTS SENSITIVITY ANALYSIS

Scatter plots is an analysis technique that plots the graph of the output against the input. This is used in this study to plot the graph of the normalised IQM signal against the area of the segment for segment one. The linearity of scatter plots determines the sensitivity of the graph.

Fig. 4.23b shows the scatter plots of a regular segment of 7 × 7 cm^2 that were altered at random within ±1, ±2, and ±3 mm regarding its individual leaf positions.

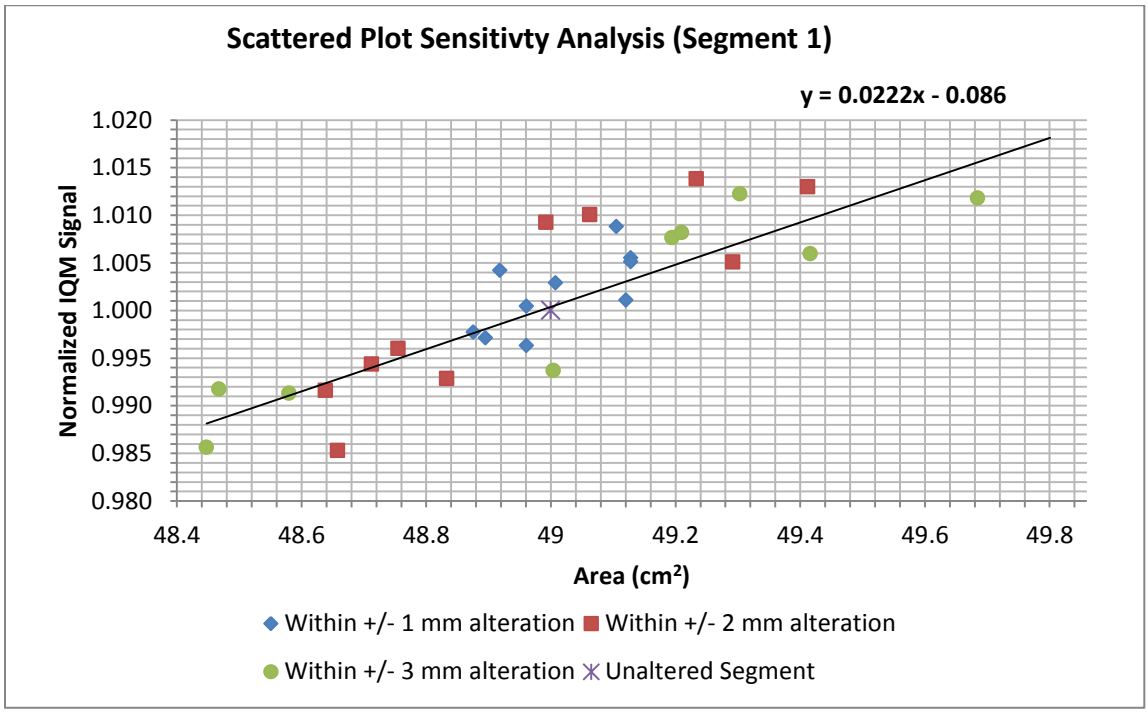

Figure 4.23b: Scatter plots Sensitivity Analysis of Segment one, for random alterations within +/- 1, +/- 2, +/- 3 mm

In Fig. 4.23b, the scatter plots for 7 × 7 cm^2 field shows a degree of linearity (linear trend gradient of 0.0222). The IQM model is sensitive to random alterations within few millimetres. An increase in the area of segment causes an increase in the normalised IQM signal. The normalised IQM signals scatter around the linear trend line.

B. BRUTE FORCE SENSITIVITY ANALYSIS

Brute force sensitivity analysis is a local technique which bases on the non-interactive input variable. It studies the effect of perturbation of an input variable on an output value. The sensitivity index of segment one was determined by calculating the change in output value (normalised IQM signal) per change in input variable (area of the segment). High sensitive index means that the perturbation (change in segment size) has a significant impact on the output (scored dose in the large wedge-shaped ionization chamber).

Fig 4.23c shows the graph of sensitivity index plotted against the area of the segment for segment one.

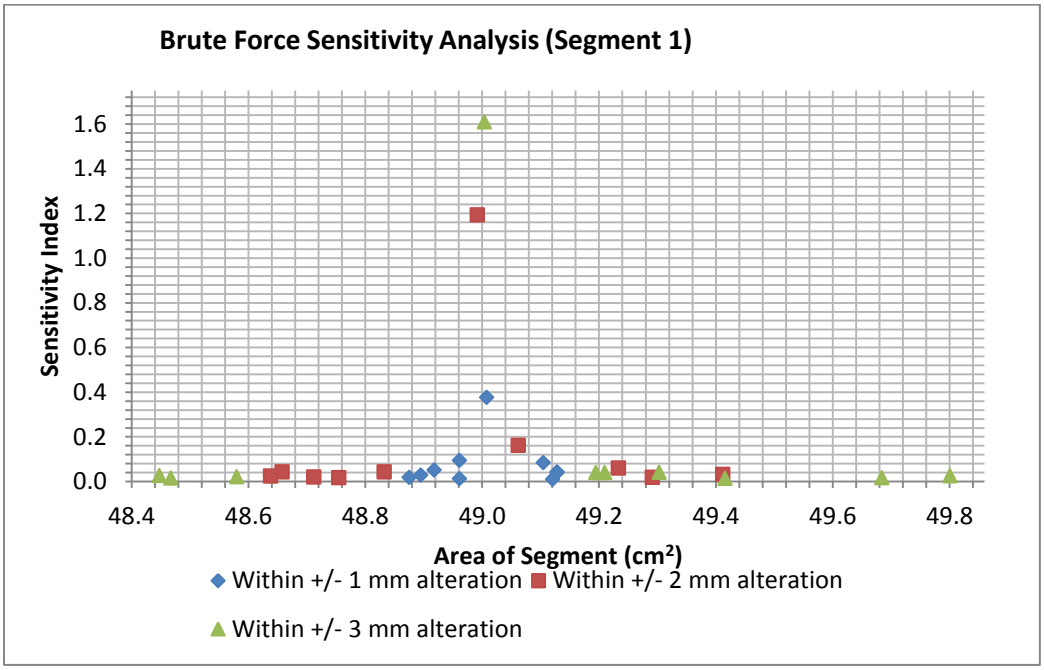

Figure 4.23c: Brute force Sensitivity Analysis of Segment one, for random alterations within +/- 1, +/- 2, +/- 3 mm

In Fig. 4.23c, the brute force technique on random alterations of a 7 × 7 cm^2 field shows that the most sensitive altered segments are majorly the segments with minimal alterations around the region of unaltered segment (49.00 cm^2). The highest sensitivity index falls within ± 3 mm variations. None of the indices is zero, which means that they are all sensitive.

C. VARIANCE-BASED SENSITIVITY ANALYSIS

The variance-based sensitivity analysis (SA) is a global technique that uses the variance of the output value to determine the sensitivity of a model. For this MC simulation, the variance is within 1%, which probably will not be a constraint. Sensitivity index for segment one is defined as the variance of the altered segment per unit variance of the unaltered segment. First order variance techniques were used in this study with the absence of interactive input parameters. A sensitive parameter should have a sensitive index between zero and one. If the sensitivity index is zero, then the input variable does not influence the output value. Fig. 4.23d shows the variance-based sensitivity index of randomly altered segments of segment one.

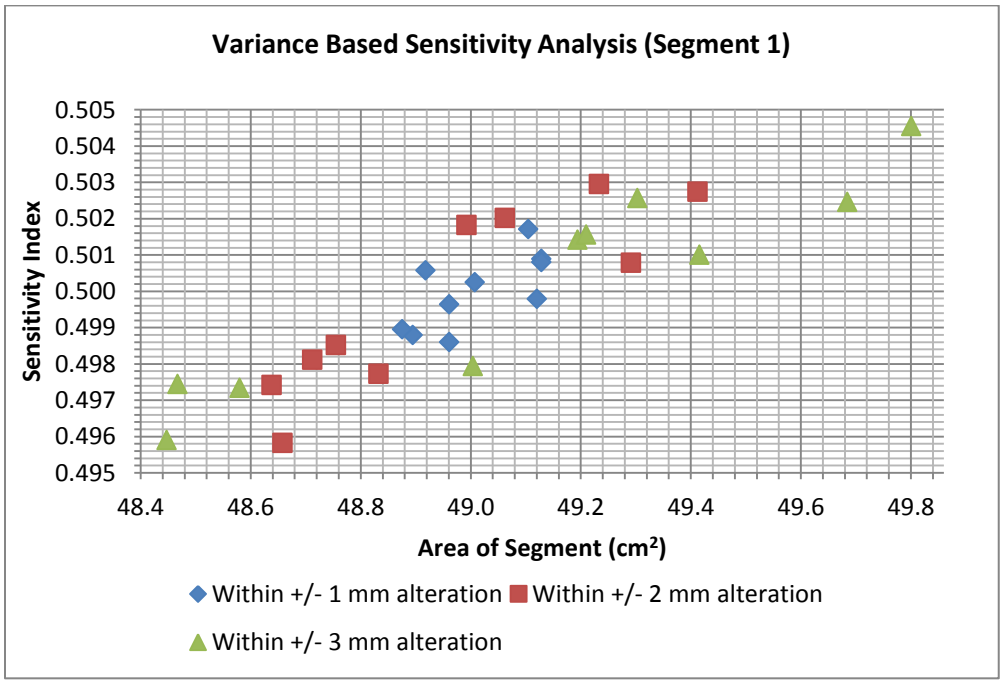

Figure 4.23d: Variance-based Sensitivity Analysis of Segment one, for random alterations within +/- 1, +/- 2, +/- 3 mm

In Fig. 4.23d, none of the sensitivity indices is zero. The IQM model could detect misalignment of MLC. Quantification of offset fields increases with an increase in offset sizes. This shows that the IQM model is sensitive to randomly altered segments of 7 × 7 cm^2 field.

D. STANDARD REGRESSION COEFFICIENT

This is a linear regression analysis that tests the significance of the input variable on the output value. The higher the SRC value, the more sensitive is the input parameter (Gan et al. 2014). This technique was used to analyse the IQM signal for segment one (7 × 7 cm^2).

Fig. 4.23e shows the standard regression coefficient values of all the randomly altered segments of segment one

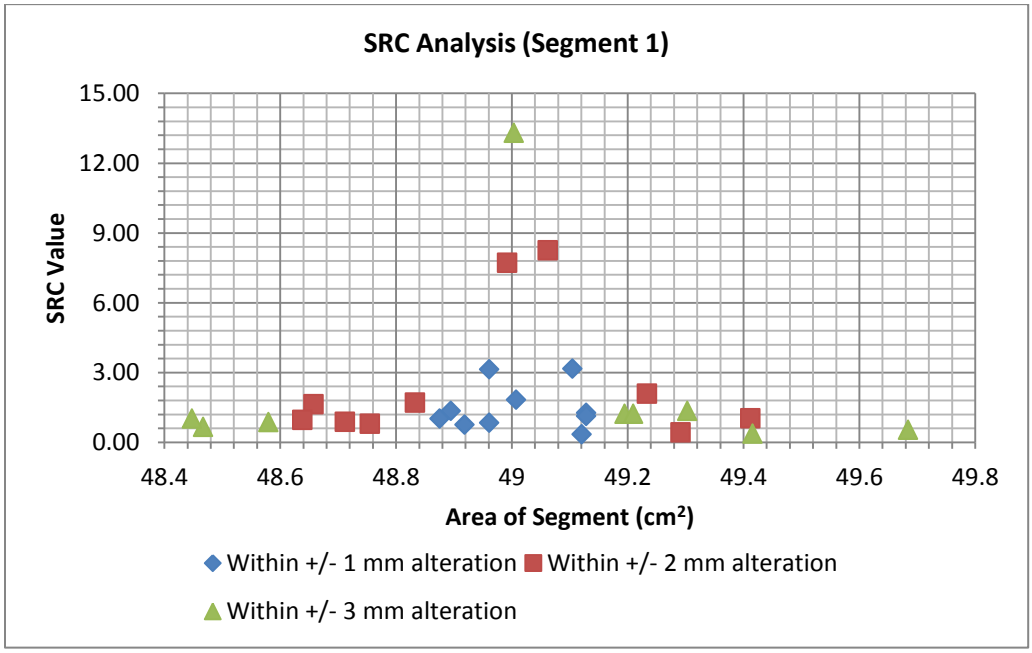

Figure 4.23e: SRC graph of Segment one, for random alterations within +/- 1, +/- 2, +/- 3 mm

In Fig. 4.23e, the SRC value for random alterations of a 7 × 7 cm^2 field depicts higher SRC values around the region of the unaltered area of the segment (49 cm^2). SRC test agrees that the wedge-shaped air chamber is sensitive to leaf positioning errors. The four sensitivity analysis techniques prove that the wedge-shaped chamber is sensitive to residual errors of a 7 × 7 cm^2 field.

4.3.3.2 SEGMENT TWO

Segment two is a regular segment of 5 × 5 cm^2 which was randomly altered. The IQM signals were calculated for unaltered and altered segments. The IQM signals were normalised to the unaltered segment which has a segment area of 25 cm^2. Fig. 4.24a shows the example of an unaltered field of segment 2, and the examples of fields altered at random within ±1, ±2, and ±3 mm regarding its individual leaf positions.

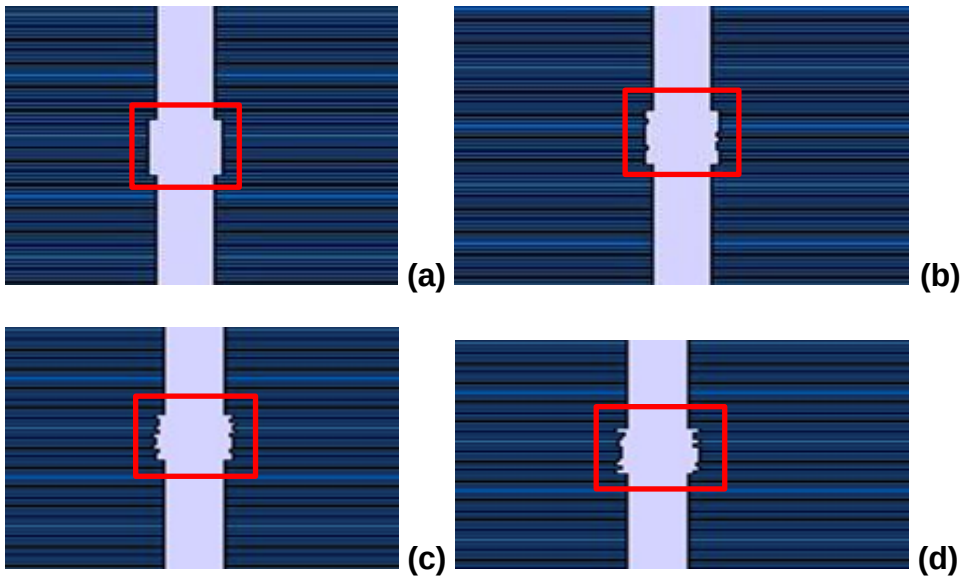

Figure 4.24a: Depicts the examples of randomly altered MLC leaf positions for Segment 2 (5 × 5 cm^2 field) (a) Unaltered segment; (b) within ± 1 mm alteration; (c) within ± 2 mm alteration; (d) within ± 3 mm alteration

SENSITIVITY ANALYSIS OF SEGMENT TWO

Alterations of 5 × 5 cm^2 were able to randomly generate 10 data points within 24.91 cm^2 and 25.76 cm^2 for ± 3 mm leaf positioning error, while ± 2 mm MLC alteration generated 10 data values between 24.54 cm^2 to 25.48 cm^2 where ± 1 mm alterations were dispersed around the unaltered segment area (25. 00 cm^2).

A. SCATTER PLOT SENSITIVITY ANALYSIS

Fig. 4.24b shows the scatter plots of a regular segment of 5 × 5 cm^2 that were altered at random within ±1, ±2, and ±3 mm regarding its individual leaf positions.

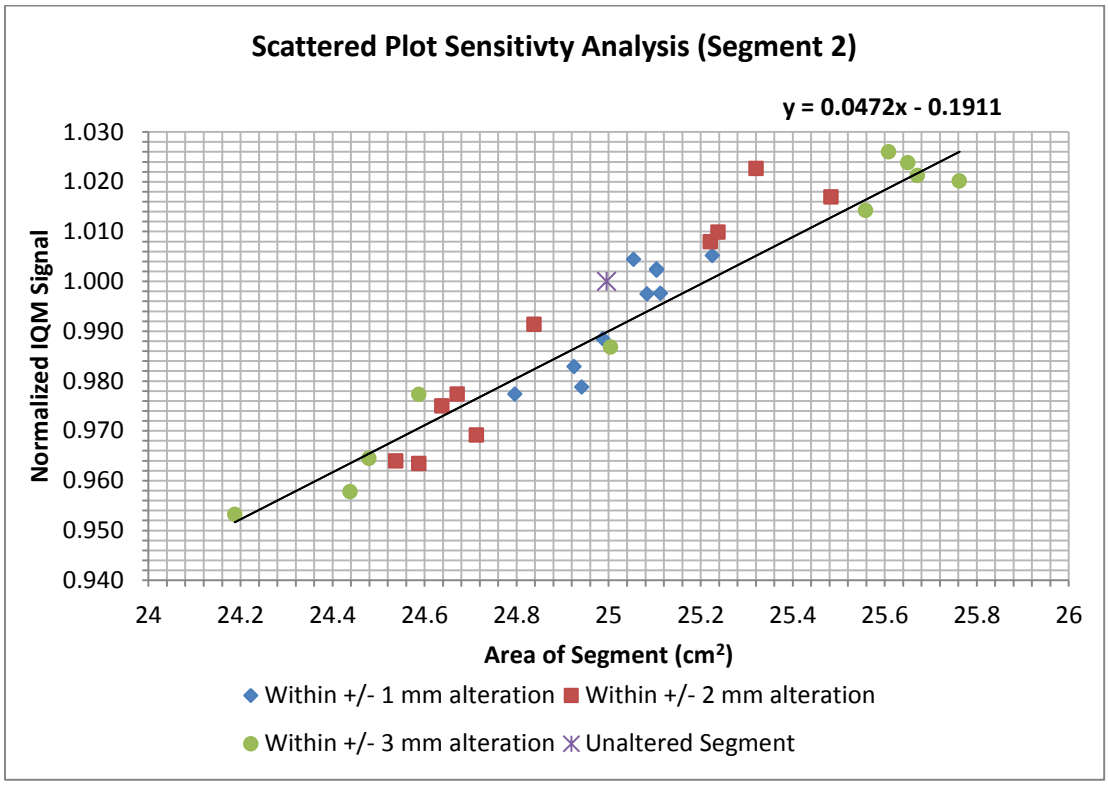

Figure 4.24b: Scatter plot Sensitivity Analysis of Segment two, for random alterations within +/- 1, +/- 2, +/- 3 mm

In Fig. 4.24b, the scatter plots for 5 × 5 cm^2 field is presented with trend gradient of 0.0472. The degree of linearity tends to reduce above the area of segment 25.30 cm^2. An increase in the area of segment causes an increase in the normalised IQM signal.

B. BRUTE FORCE SENSITIVITY ANALYSIS

Fig 4.24c shows the brute force analysis for segment two. In the graph, sensitivity index was plotted against the area of the segment for the altered segments.

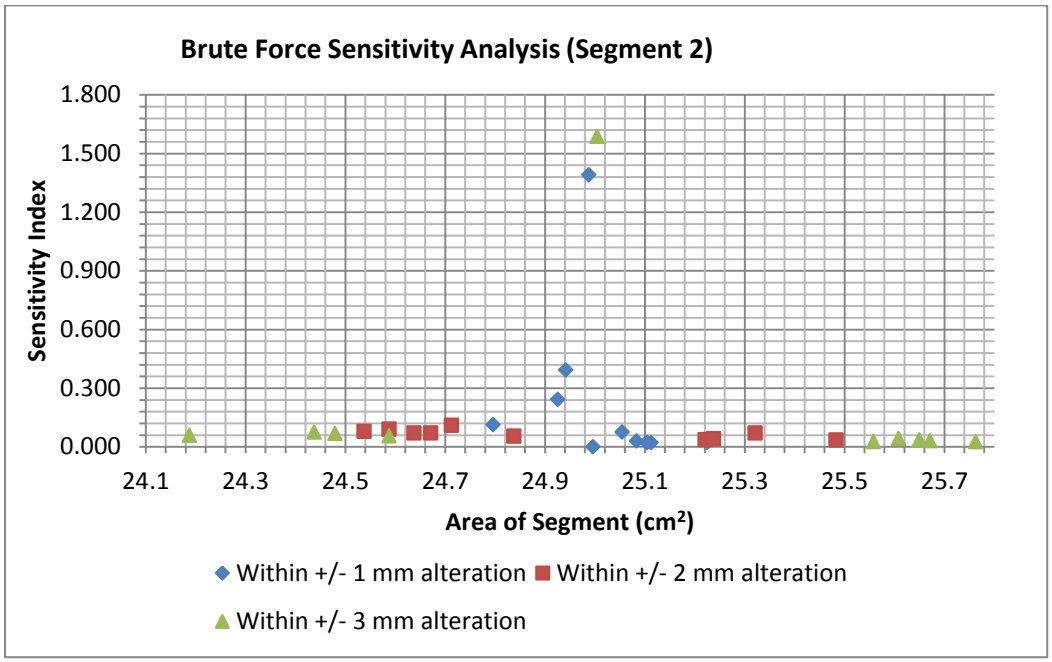

Figure 4.24c: Brute force Sensitivity Analysis of Segment two, for random alterations within +/- 1, +/- 2, +/- 3 mm

In Fig. 4.24c, the brute force analysis technique on random alterations of a 5 × 5 cm^2 field shows a peak region around the unaltered segment area. The most sensitive altered segments are majorly the segments with minimal alterations which are closer to the unaltered area of segment (25 cm^2).

C. VARIANCE-BASED SENSITIVITY ANALYSIS

Fig 4.24d shows the variance-based analysis for segment two. It displays the sensitivity indices for all the randomly altered segments of segment two.

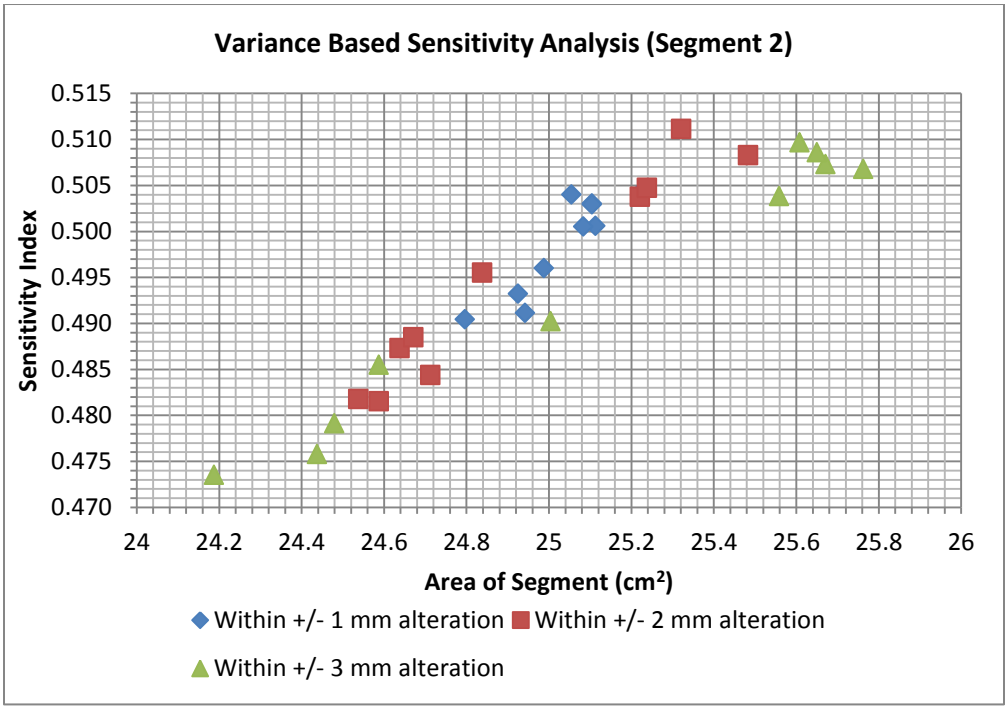

Figure 2.24d: Variance based Sensitivity Analysis of Segment two, for random alterations within +/- 1, +/- 2, +/- 3 mm

In Fig. 2.24d, the sensitivity index for all the altered segments is above zero. The variance-based sensitivity indices of ± 1 mm alterations shrank within ± 2 mm alterations. IQM model is sensitive to segment areas.

D. STANDARD REGRESSION COEFFICIENT

Fig. 4.24e shows the standard regression coefficient values of all the randomly altered segments of segment two (5 × 5 cm^2).

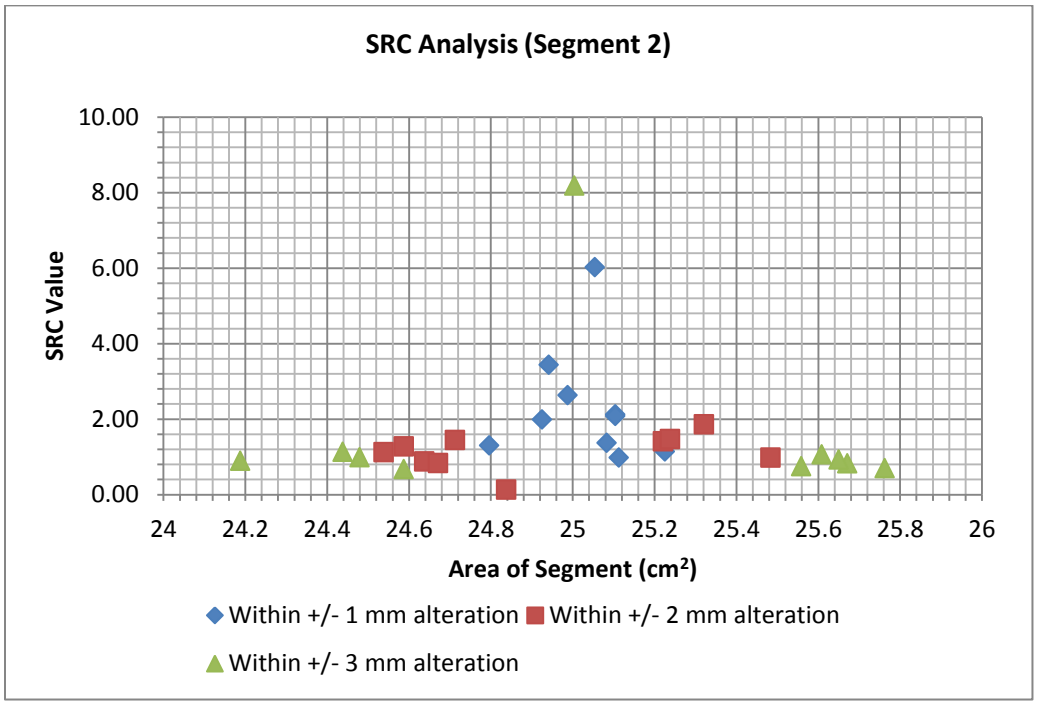

Figure 4.24e: SRC graph of Segment two, for random alterations within +/- 1, +/- 2, +/- 3 mm

In Fig. 4.24e, the SRC values show that the IQM is sensitive to alterations of 5 × 5 cm^2 field. The most sensitive offset parameters are displayed around the region of the actual leaf position (segment area of 25 cm^2).

4.3.3.3 SEGMENT THREE

Segment three is a regular segment of 3 × 3 cm^2 field. This small field was chosen in order to compare it with other smaller and bigger fields. The IQM signal of altered segments was normalised to the unaltered segment (segment area of 9 cm^2). Fig. 4.25a shows the example of an unaltered field of segment three, and the examples of fields altered at random within ±1, ±2, and ±3 mm regarding its individual leaf positions.

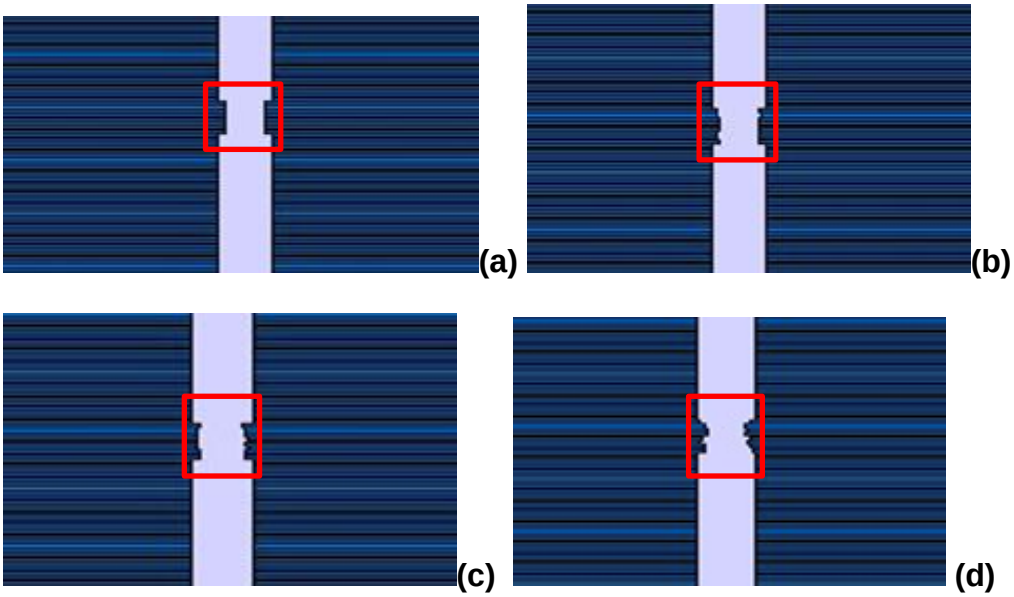

Figure 4.25a: Depicts the examples of randomly altered MLC leaf positions for Segment 3 (3 × 3 cm^2) (a) Unaltered segment; (b) within ± 1 mm alteration; (c) within ± 2 mm alteration; (d) within ± 3 mm alteration

SENSITIVITY ANALYSIS OF SEGMENT THREE

The leaf positioning errors within ± 3 mm randomly produced segments area from 8.37 cm^2 to 9.35 cm^2 and for other alterations within ± 2 and ± 1 mm, data points between 8.66 cm^2 and 9.28 cm^2 were created. The original field size is exactly 3 × 3 cm^2.

A. SCATTER PLOTS SENSITIVITY ANALYSIS

Fig. 4.25b shows the scatter plots of a regular segment of 3 × 3 cm^2 that was altered at random within ±1, ±2, and ±3 mm regarding its individual leaf positions.

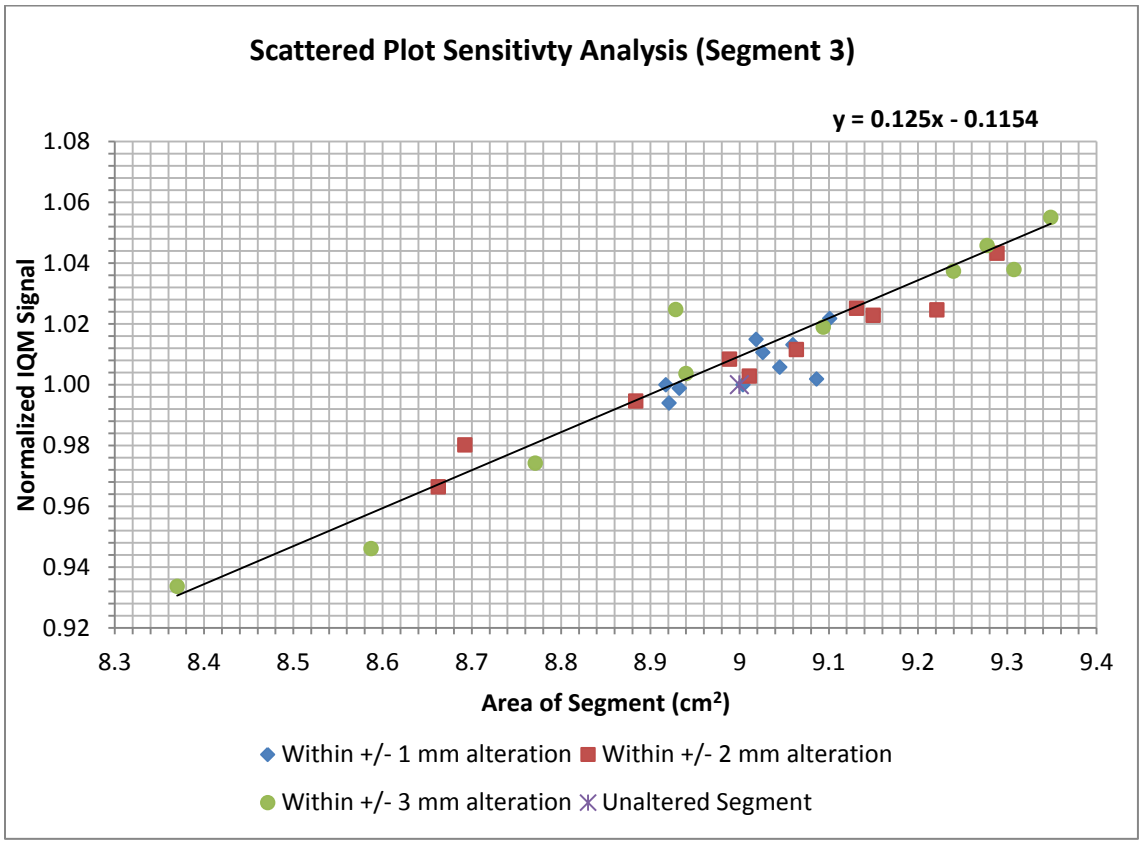

Figure 4.25b: Scatter plots Sensitivity Analysis of Segment three, for random alterations within +/- 1, +/- 2, +/- 3 mm

In Fig. 4.25b, the scatter plots for 3 × 3 cm^2 field shows a high degree of linearity with 0.125 gradient of the graph. It is expected of a small field as deduced in previous results in this study. An increase in the area of segment causes an increase in the normalised IQM signal. The normalised IQM signals are scattered around the linear trend line.

B. BRUTE FORCE SENSITIVITY ANALYSIS

Fig 4.25c shows the graph of the brute force sensitivity index plotted against the area of the segment for the altered segments of 3 × 3 cm^2 field.

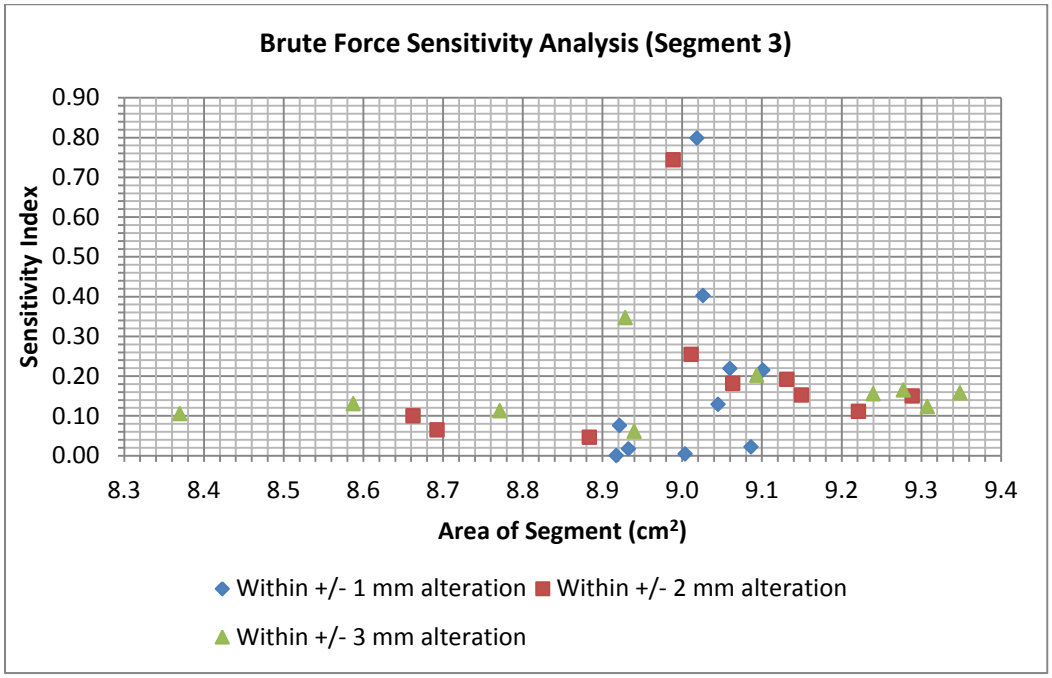

Figure 4.25c: Brute force Sensitivity Analysis of Segment three, for random alterations within +/- 1, +/- 2, +/- 3 mm

In Fig. 4.25c, the brute force technique on random alterations of a 3 × 3 cm^2 field shows that the most sensitive altered segments are majorly the segments with minimal alterations which are closer to the unaltered area of segment (9 cm^2). This shows that the wedge-shaped chamber model is highly sensitive to minimal leaf alterations

C. VARIANCE-BASED SENSITIVITY ANALYSIS

Fig. 4.25d shows the variance-based sensitivity indices for all the randomly altered segments of segment three which were altered randomly within ±1, ±2 and ±3 mm.

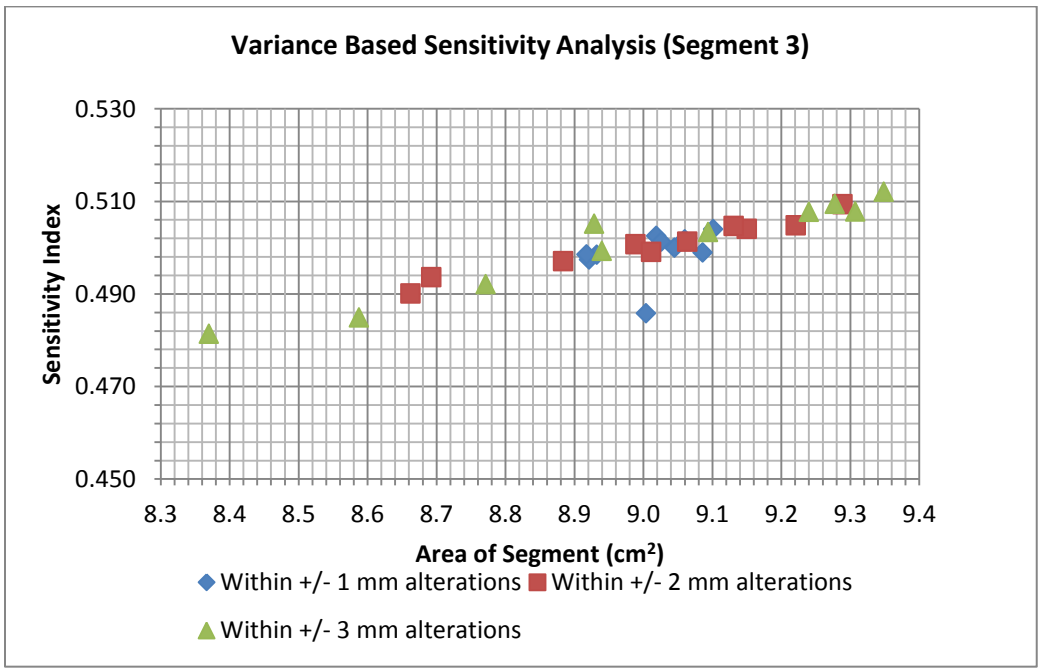

Figure 4.25d: Variance based Sensitivity Analysis of Segment three, for random alterations within +/- 1, +/- 2, +/- 3 mm

In Fig. 4.25d, for the entire segments considered, the variance based sensitivity indices are greater than zero. It shows that variance-based sensitivity analysis of random alterations of 3 × 3 cm^2 field for all the altered segments is sensitive. An increase in the area of segment causes an increase in the sensitivity index for this aperture.

D. STANDARD REGRESSION COEFFICIENT

Fig. 4.25e shows the standard regression coefficient values for all the randomly altered segments of segment three (3 × 3 cm^2) which were altered within ±1, ±2 and ±3 mm

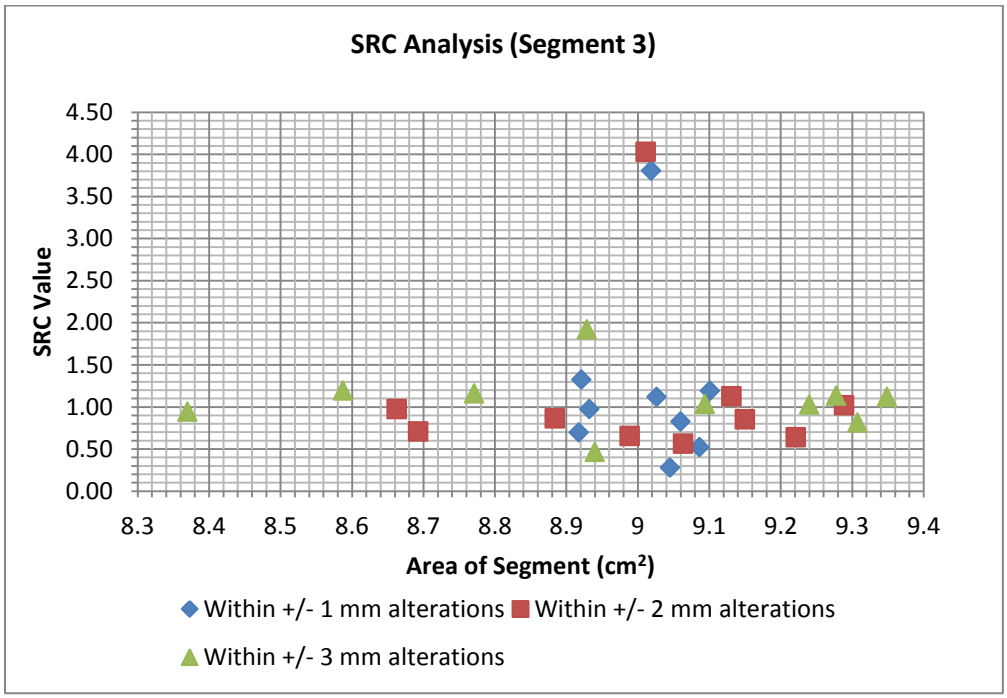

Figure 4.25e: SRC graph of Segment three, for random alterations within +/- 1, +/- 2, +/- 3 mm

In Fig. 4.25e, the SRC values of segment areas closer to the unaltered region are higher than others. This means that they are the most sensitive offset parameters of the randomly altered segments of segment three (segment area of 9 cm^2).

4.3.3.4 SEGMENT FOUR

Segment four is an irregular segment that was altered randomly. The IQM signal was calculated for all the altered and unaltered segments and then normalised to the unaltered segment which has a segment area of 19.99 cm^2. Fig. 4.26a shows the example of an unaltered field, and the examples of fields altered at random within ±1, ±2, and ±3 mm regarding its individual leaf positions.

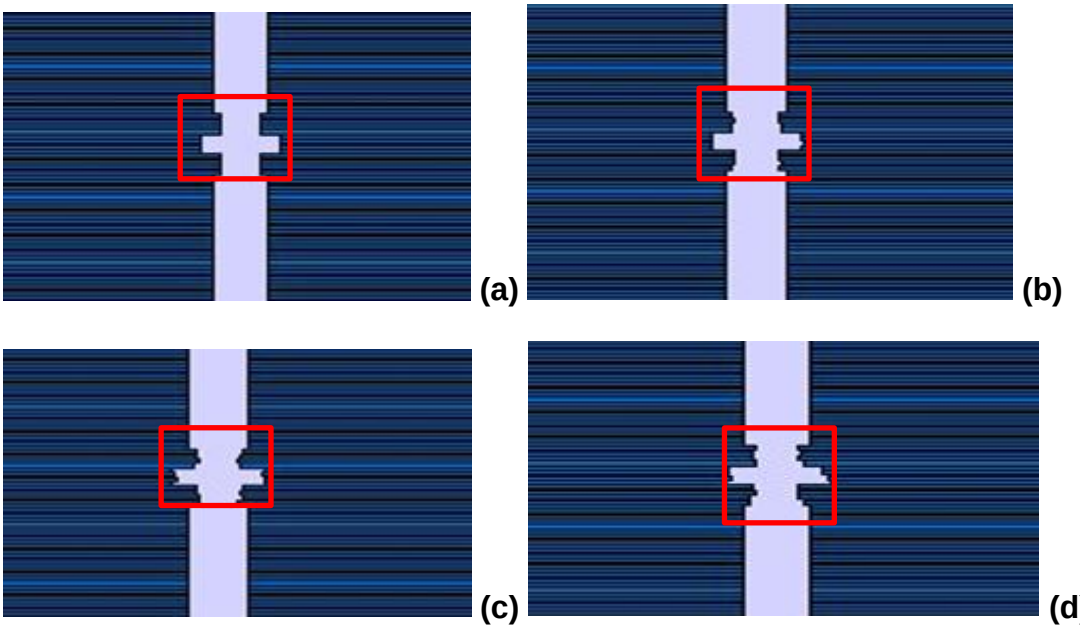

Figure 4.26a: Depicts the examples of randomly altered MLC leaf positions for Segment 4 (area of 19.99 cm^2) (a) Unaltered segment; (b) within ± 1 mm alteration; (c) within ± 2 mm alteration; (d) within ± 3 mm alteration

SENSITIVITY ANALYSIS OF SEGMENT FOUR

Random MLC alterations of an irregular segment generated 30 data points that fall within the range of 19.22 cm^2 – 20.78 cm^2. The original unaltered segment size is exactly 19.99 cm^2.

A. SCATTER PLOTS SENSITIVITY ANALYSIS

Fig. 4.26b shows the scatter plots of an irregular segment that was altered at random within ±1, ±2, and ±3 mm regarding its individual leaf positions.

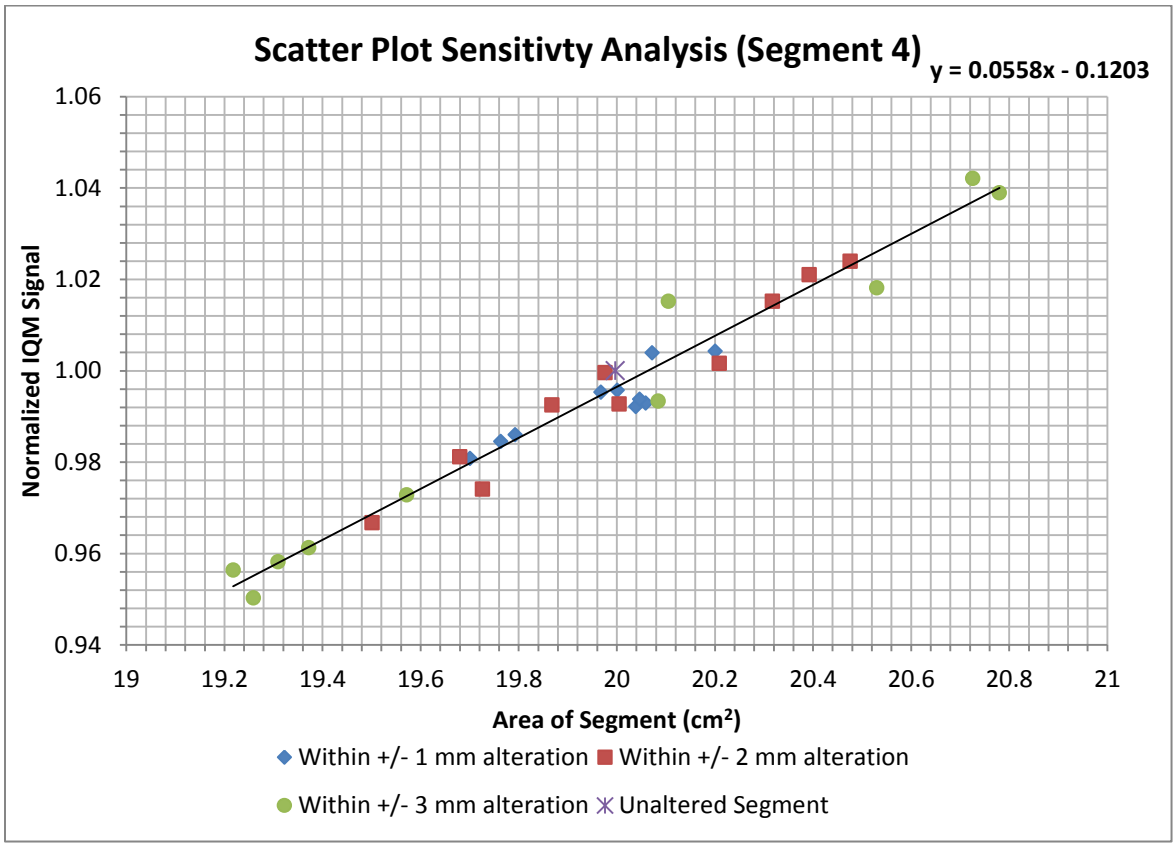

Figure 4.26b: Scatter plots Sensitivity Analysis of Segment four, for random alterations within +/- 1, +/- 2, +/- 3 mm

In Fig. 4.26b, the scatter plots for this irregular segment (area of 19.99 cm^2) show a degree of linearity (gradient of 0.0558). The IQM model is sensitive to random positional errors. An increase in the area of segment causes an increase in the normalised IQM signal. The normalised IQM signals are scattered around the linear trend line.

B. BRUTE FORCE SENSITIVITY ANALYSIS

Fig 4.26c shows the graph of brute force sensitivity index plotted against the area of the segment for altered segments of irregular aperture.

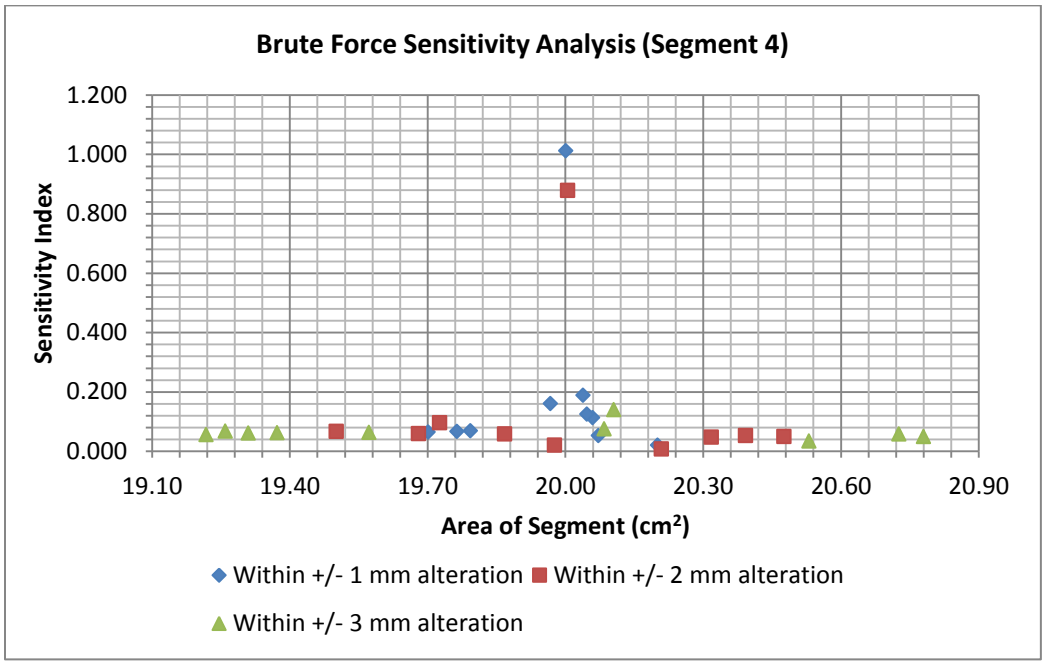

Figure 4.26c: Brute force Sensitivity Analysis of Segment four, for random alterations within +/- 1, +/- 2, +/- 3 mm

In Fig. 4.26c, the brute force analysis technique on random alterations of an irregular field shows that the most sensitive altered segments are majorly the segments with minimal MLC alterations surrounding the unaltered segment area (19.99 cm^2). This shows that the wedge-shaped chamber model can detect misalignment of leaves for the irregular segment of 19.99 cm^2.

C. VARIANCE-BASED SENSITIVITY ANALYSIS

Fig. 4.26d shows the variance-based sensitivity indices for all the randomly altered segments of segment four which is an irregular segment.

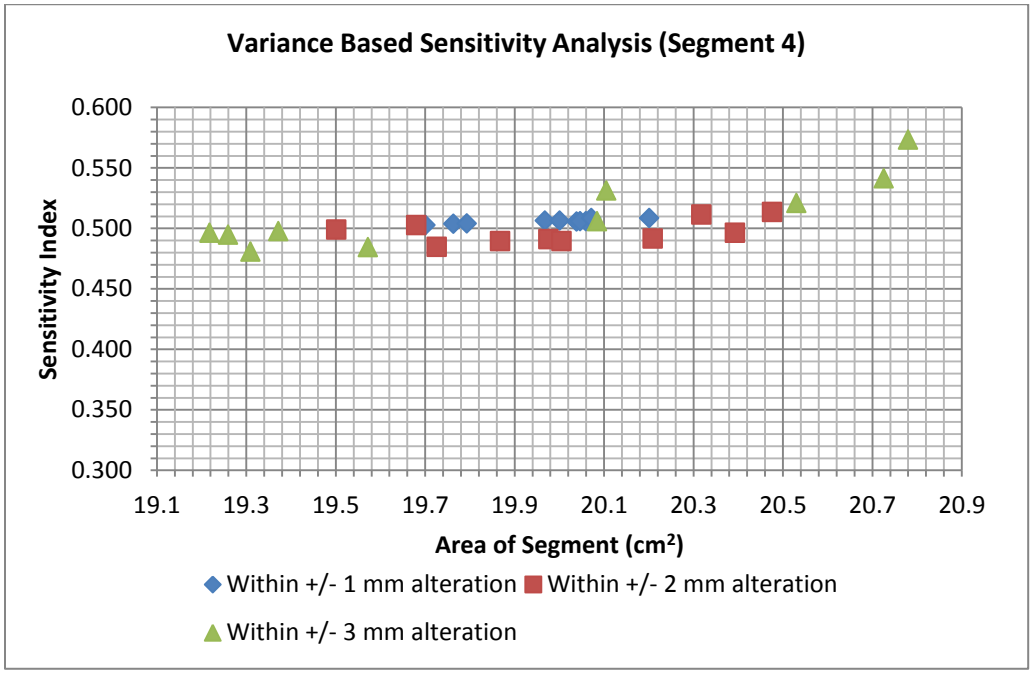

Figure 4.26d: Variance based Sensitivity Analysis of Segment four, for random alterations within +/- 1, +/- 2, +/- 3 mm

In Fig. 4.26d, the sensitivity indices are greater than zero. This shows that variance-based sensitivity analysis of random alterations of an irregular field (19.99 cm^2) for all the altered segments are sensitive. The graph has not shown a corresponding steep plot, but there are generated sensitivity indices for all altered segment. It shows that the shape of a segment is not a major determining factor for wedge-shaped chamber sensitivity.

D. STANDARD REGRESSION COEFFICIENT

Fig. 4.26e shows the standard regression coefficient values for all the randomly altered segments of segment four which is an irregular aperture (segment area of 19.99 cm^2).

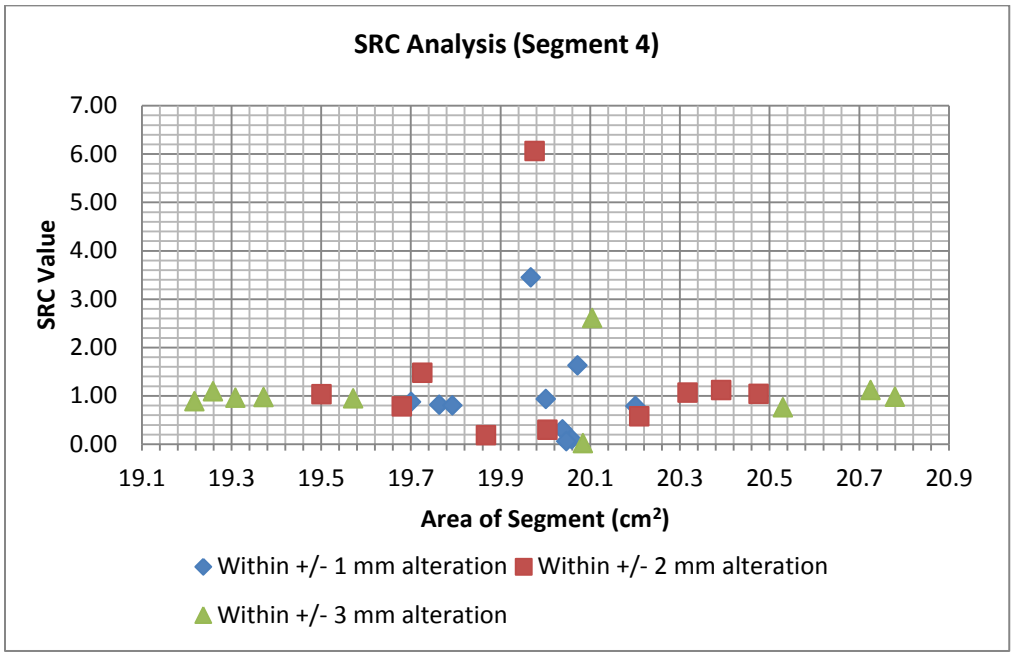

Figure 4.26e: SRC graph of Segment four, for random alterations within +/- 1, +/- 2, +/- 3 mm

In Fig. 4.26e, the most sensitive input parameter (segment area) is the segment that is closer to the unaltered segment area (19.99 cm^2) due to its high SRC value.

4.3.3.5 SEGMENT FIVE

Segment five is an irregular segment that was randomly altered 30 times. The IQM signal was calculated for all the altered and the unaltered segments of segment five. The IQM signals were normalised to the unaltered segment which has a segment area of 36.66 cm^2. Fig. 4.27a shows the example of an unaltered field, and the examples of fields altered at random within ±1, ±2, and ±3 mm regarding its individual leaf positions.

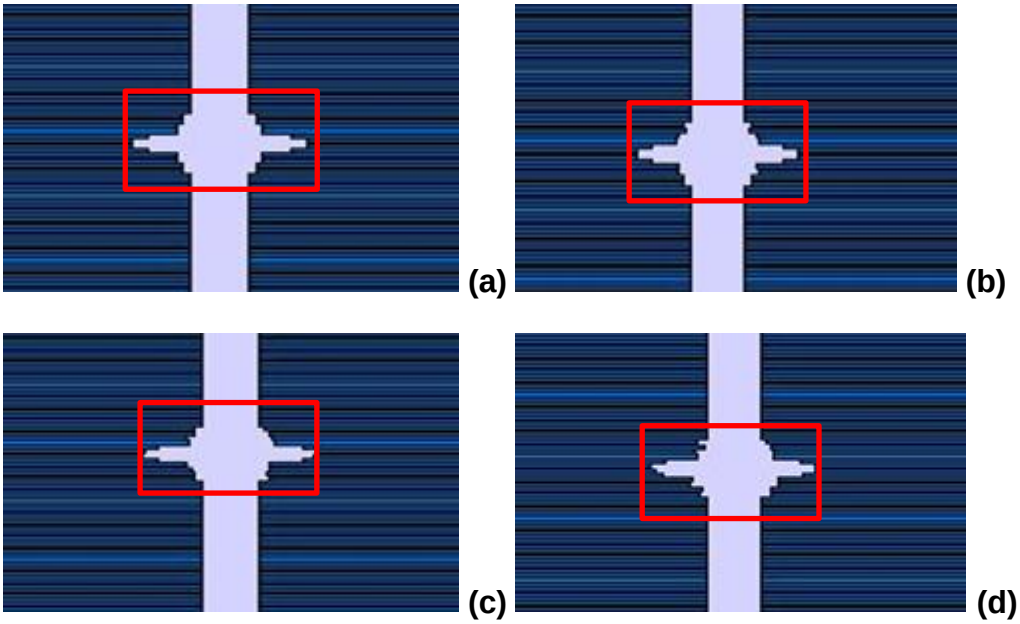

Figure 4.27a: Depicts the examples of randomly altered MLC leaf positions for Segment 5 (area of 36.66 cm^2) (a) Unaltered segment; (b) within ± 1 mm alteration; (c) within ± 2 mm alteration; (d) within ± 3 mm alteration

SENSITIVITY ANALYSIS OF SEGMENT FIVE

The ranges for segment five misalignment apertures are: 35.97 cm^2 – 37.39 cm^2 for ± 3 mm, 36.05 cm^2 – 37.18 cm^2 for ± 2 mm, and 36.50 cm^2 -36.82 cm^2 for ± 1 mm. the unaltered segment size is 36.66 cm^2.

A. SCATTER PLOTS SENSITIVITY ANALYSIS

Fig. 4.27b shows the scatter plots of an irregular segment that was altered randomly within ± 1, ± 2, and ± 3 mm regarding its individual leaf positions.

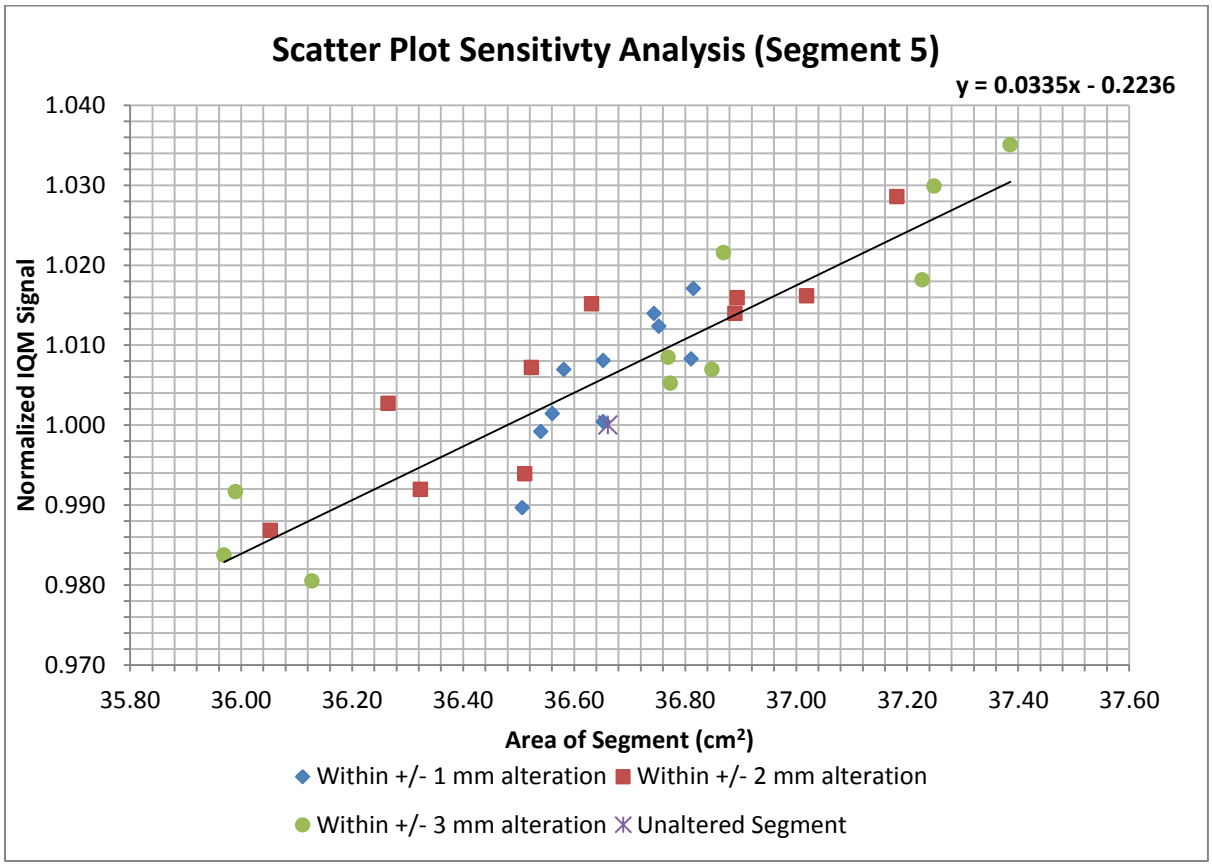

Figure 4.27b: Scatter plots Sensitivity Analysis of Segment five, for random alterations within +/- 1, +/- 2, +/- 3 mm

In Fig. 4.27b, the scatter plots for this irregular segment (area of 36.66 cm^2) shows a degree of linearity with a slope of 0.0335. The IQM model is sensitive to random leaves alterations of segment five. The normalised IQM signals scatter around the linear trend line.

B. BRUTE FORCE SENSITIVITY ANALYSIS

Fig 4.27c shows the graph of brute force sensitivity index plotted against the area of the segment for segment five altered at random within few millimetres.

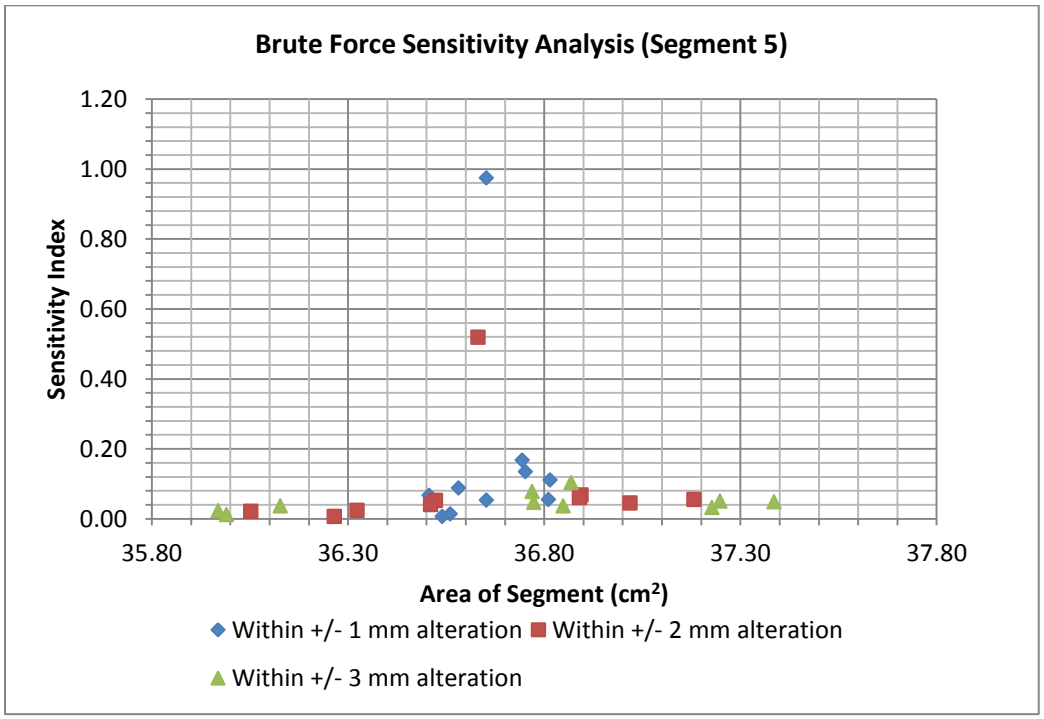

Figure 4.27c: Brute force Sensitivity Analysis of Segment five, for random alterations within +/- 1, +/- 2, +/- 3 mm

In Fig. 4.27c, the brute force analysis of randomly altered irregular field shows that the most sensitive altered segments are majorly the segments with slight alterations which are closer to the unaltered area of the segment (segment area of 36.66 cm^2).

C. VARIANCE-BASED SENSITIVITY ANALYSIS

Fig. 4.27d shows the variance-based sensitivity indices for all the randomly altered segments of segment five.

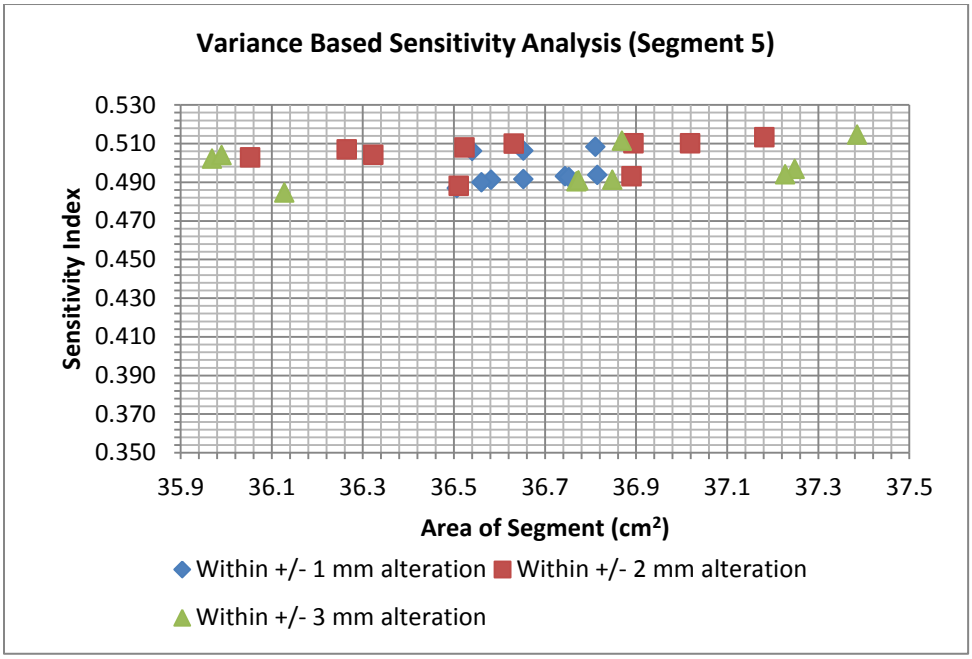

Figure 4.27d: Variance based Sensitivity Analysis of Segment five, for random alterations within +/- 1, +/- 2, +/- 3 mm

In Fig 4.27d, the uncertainties of IQM signals of segment five shows that the MC model is sensitive to random alterations since all the sensitivity indices are greater than zero. The variance-based sensitivity analyses of random alterations of an irregular field (36.66 cm^2) for all the altered segments proved that the IQM model is sensitive to this irregular segment.

D. STANDARD REGRESSION COEFFICIENT

Fig. 4.27e shows the standard regression coefficient values for all the randomly altered segments of segment five (segment area of 36.66 cm^2) which were altered within ±1, ±2 and ±3 mm

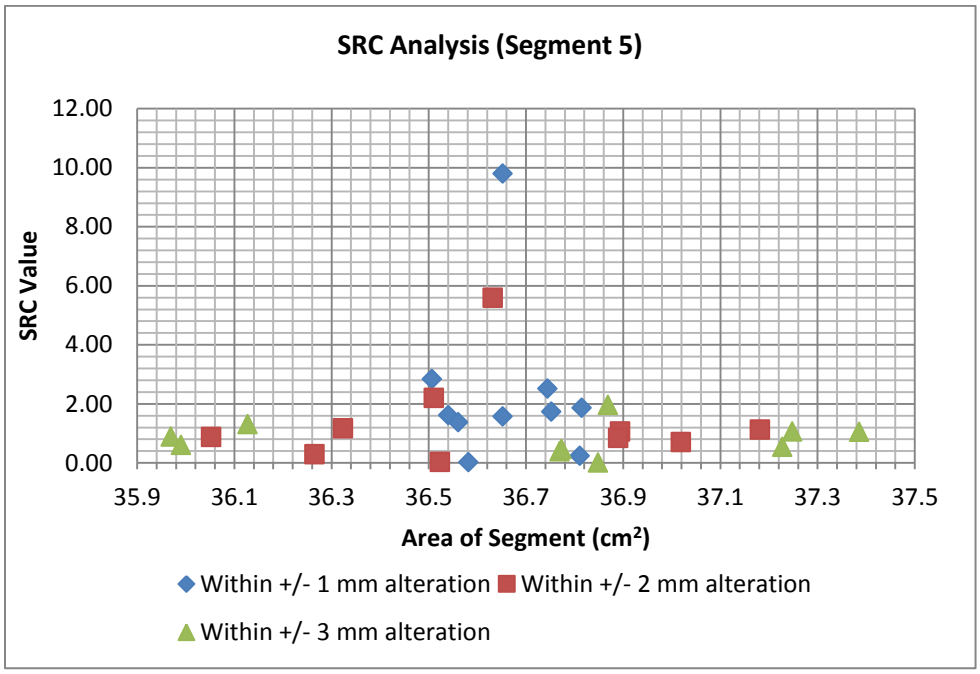

Figure 4.27e: SRC graph of Segment five, for random alterations within +/- 1, +/- 2, +/- 3 mm

In Fig. 4.27e, the SRC values show that the most sensitive input parameters are for the segment areas surrounding the unaltered segment (segment area of 36.66 cm^2).

4.3.3.6 SEGMENT SIX

Segment six is an irregular segment that was randomly altered. The IQM signals for altered segments were normalised to the IQM signal of the unaltered segment which has a segment area of 25.83 cm^2. Fig. 4.28a shows the example of an unaltered field, and the examples of fields altered at random within ±1, ±2, and ±3 mm regarding its individual leaf positions.

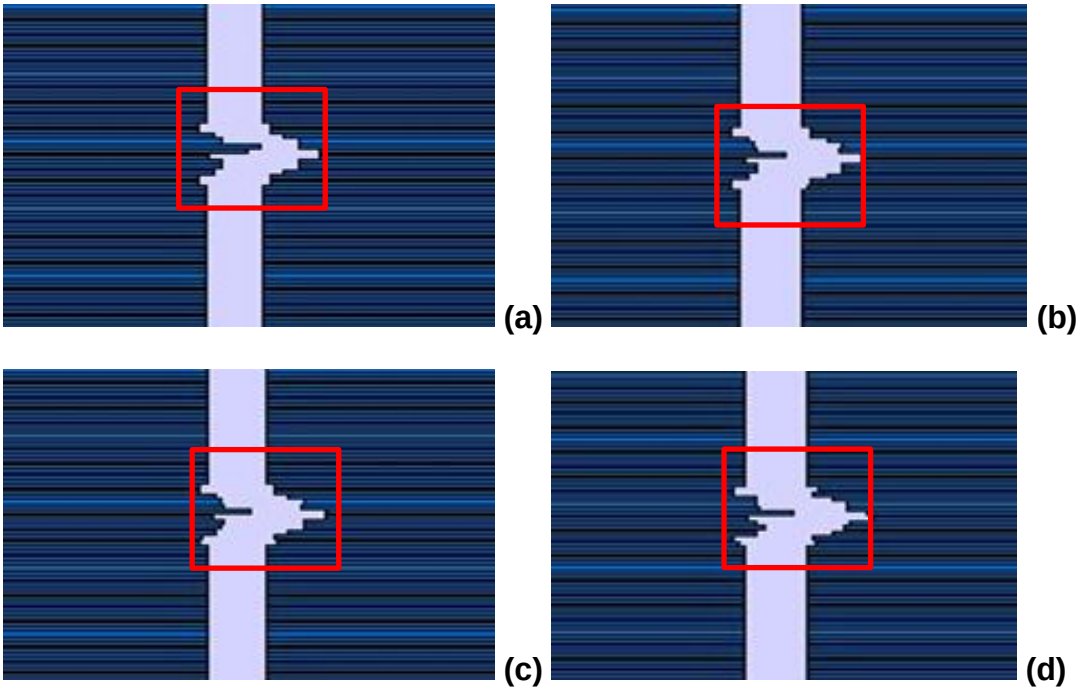

Figure 4.28a: Depicts the examples of randomly altered MLC leaf positions for Segment 6 (area of 25.83 cm^2) (a) Unaltered segment; (b) within ± 1 mm alteration; (c) within ± 2 mm alteration; (d) within ± 3 mm alteration

SENSITIVITY ANALYSIS OF SEGMENT SIX

In segment six, the offset segments size for ± 3mm randomly altered segment area ranged between 25.06 cm^2 to 26.47 cm^2. The original unaltered segment size is exactly 25.83 cm^2. For the ± 2mm case, this range fell between 25.42 and 26.23 cm^2. For the ± 1 mm case, there is an even spread within 25.61 cm^2 and 26.04 cm^2 unaltered segment size.

A. SCATTER PLOTS SENSITIVITY ANALYSIS

Fig. 4.28b shows the scatter plots of an irregular segment that was altered at random within ±1, ±2, and ±3 mm regarding its individual leaf positions.

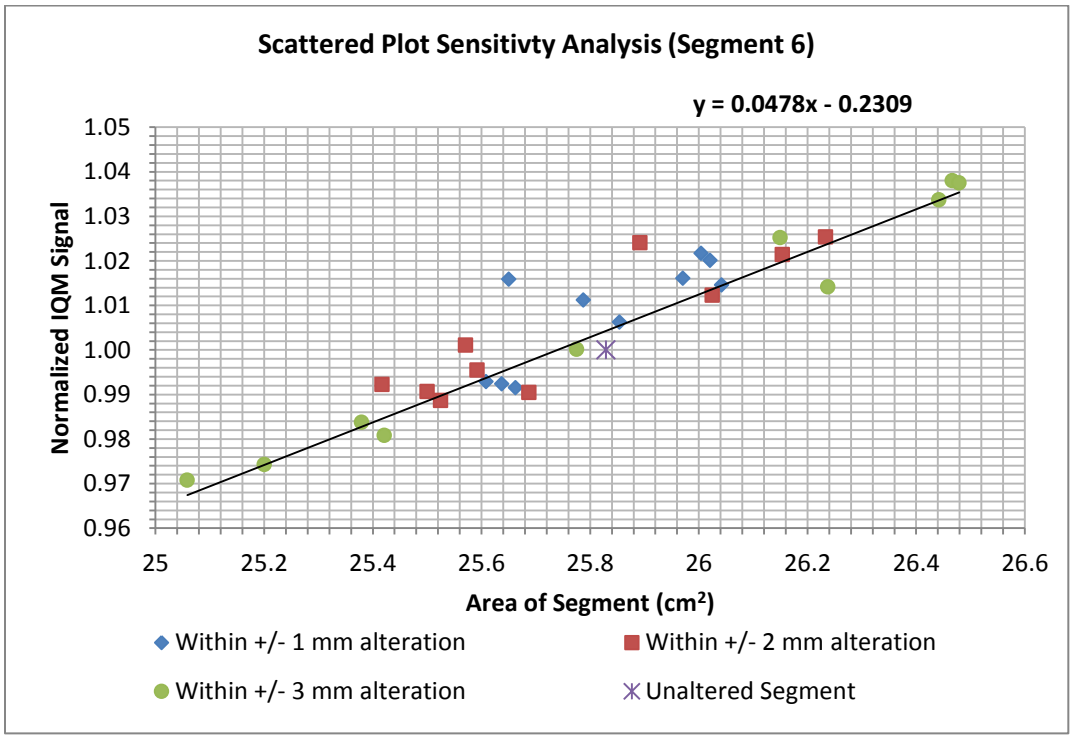

Figure 4.28b: Scatter plots Sensitivity Analysis of Segment six, for random alterations within +/- 1, +/- 2, +/- 3 mm

In Fig. 4.28b, the scatter plots for this irregular segment (area of 25.83 cm^2) shows a degree of linearity with a slope of 0.0478. The IQM model is sensitive to random alterations of segment six as analysed by scatter plots SA. An increase in the area of segment causes an increase in the normalised IQM signal.

B. BRUTE FORCE SENSITIVITY ANALYSIS

Fig. 4.28c shows the graph of brute force sensitivity index plotted against the area of the segment for segment six.

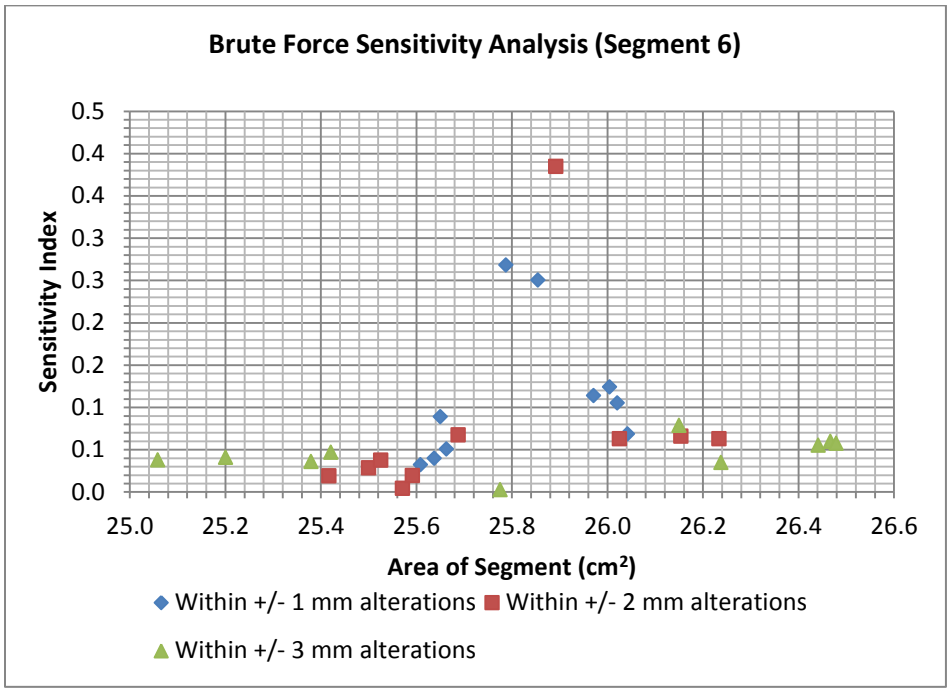

Figure 4.28c: Brute force Sensitivity Analysis of Segment six, for random alterations within +/- 1, +/- 2, +/- 3 mm

In Fig. 4.28c, the brute force analysis on random alterations of an irregular field shows a peak of the sensitive index around the unaltered segment area (25.83 cm^2). This peak region is the most sensitive region as analysed by the brute force SA. The region experiences a high rate of change in the normalised IQM signal per the segment area.

C. VARIANCE-BASED SENSITIVITY ANALYSIS

Fig. 4.28d shows the variance-based sensitivity indices for all the randomly altered segments for segment six.

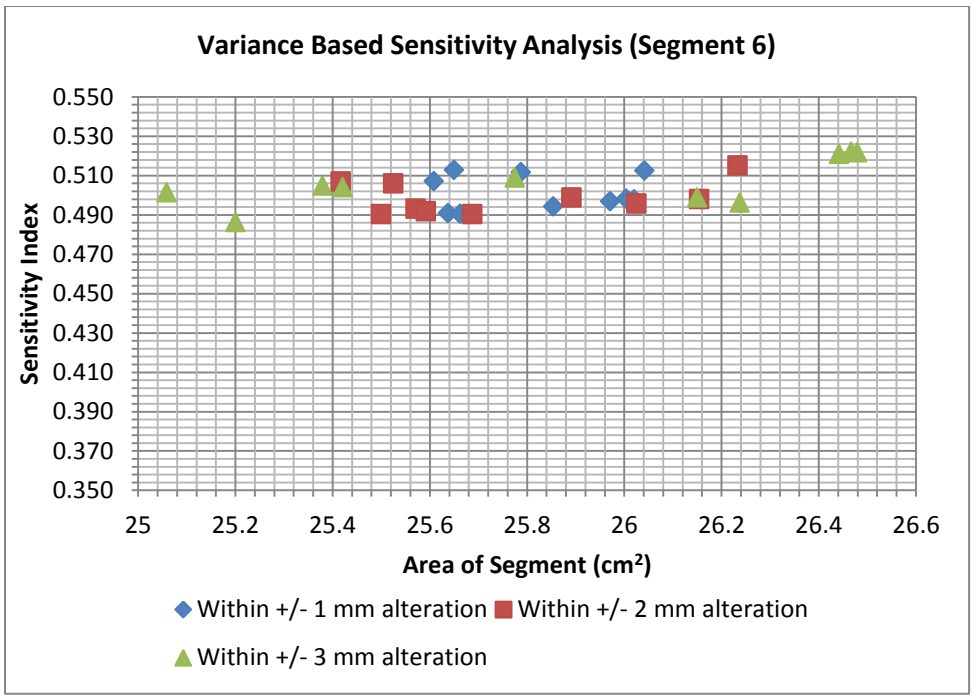

Figure 4.28d: Variance based Sensitivity Analysis of Segment six, for random alterations within +/- 1, +/- 2, +/- 3 mm

In Fig. 4.28d, the variance-based sensitivity indices show that random alterations of an irregular field (25.83 cm^2) for all the altered segments are sensitive. This proves that the wedge-shaped chamber is sensitive to random alterations of an irregular segment.

D. STANDARD REGRESSION COEFFICIENT

Fig. 4.28e shows the standard regression coefficient values for all the randomly altered segments of segment six (segment area of 25.83 cm^2) which was altered within ±1, ±2 and ±3 mm

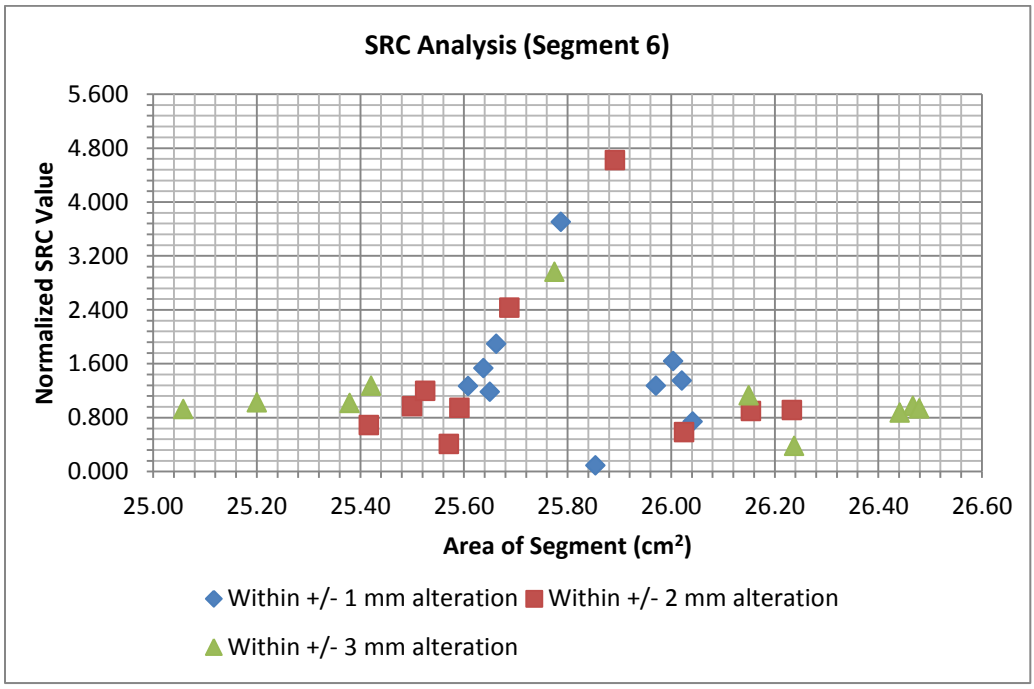

Figure 4.28e: SRC graph of Segment six, for random alterations within +/- 1, +/- 2, +/- 3 mm

In Fig. 4.28e, the SRC values for random alterations of this irregular segment displayed high SRC values around the region of the unaltered segment (segment area of 25.83 cm^2). The IQM model is sensitive to leaf shifts of segment six.

4.3.3.7 SEGMENT SEVEN

Segment seven is an irregular segment which was altered randomly. The IQM signals of the altered and unaltered segments were calculated after the MC simulation, and the IQM dose for altered segments was normalised to the unaltered segment (segment area of 70.82 cm^2). Fig. 4.29a shows the example of an unaltered field, and the examples of fields altered at random within ±1, ±2, and ±3 mm regarding its individual leaf positions.

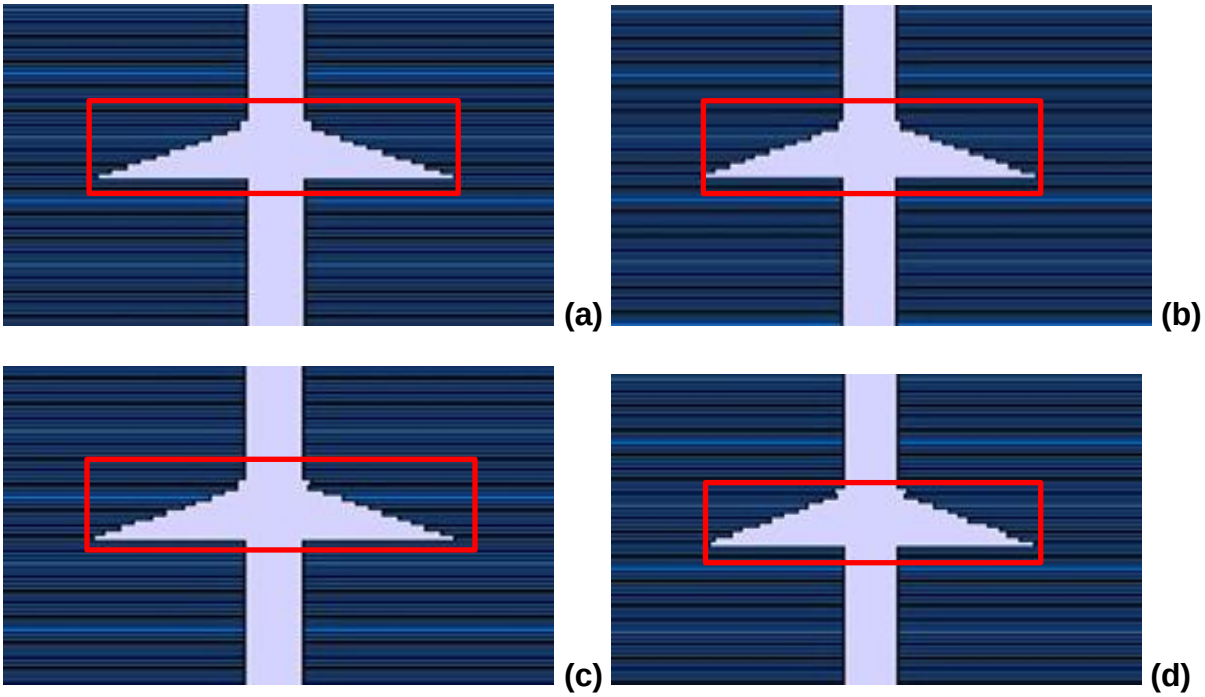

Figure 4.29a: Depicts the examples of randomly altered MLC leaf positions for Segment 7 (area of 70.82 cm^2) (a) Unaltered segment; (b) within ± 1 mm alteration; (c) within ± 2 mm alteration; (d) within ± 3 mm alteration

SENSITIVITY ANALYSIS OF SEGMENT SEVEN

The umbrella-shaped segment area of 70.82 cm^2 has offsets segments that ranged between 70.50 cm^2 and 70.97 cm^2 for random alterations within ±1 mm. Misalignment segments between 70.32 cm^2 and 71.35 cm^2 were obtained for random alterations within ±2 mm, and altered segment areas between 70.16 cm^2 and 71.58 cm^2 were created with random alterations within ±3 mm.

A. SCATTER PLOTS SENSITIVITY ANALYSIS

Fig. 4.29b shows the scatter plots of an irregular segment that was altered at random within ±1, ±2, and ±3 mm regarding its individual leaf positions.

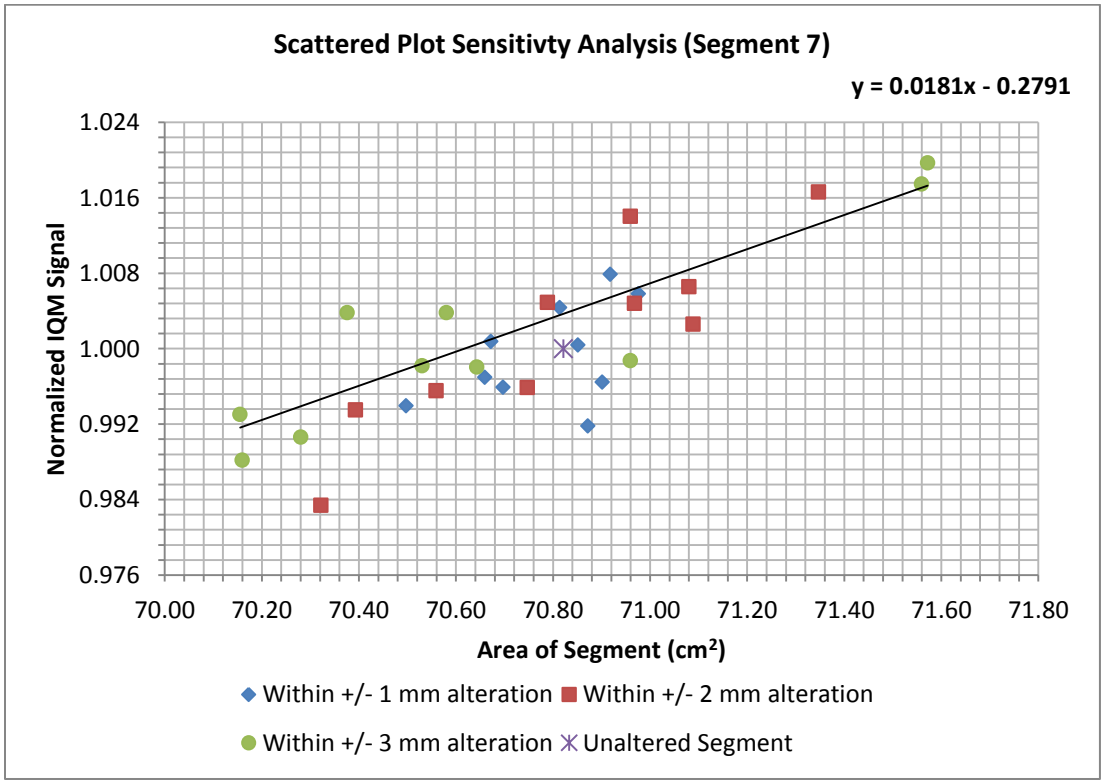

Figure 4.29b: Scatter plots Sensitivity Analysis of Segment seven, for random alterations within +/- 1, +/- 2, +/- 3 mm

In Fig. 4.29b, the scatter plots for this irregular segment (area of 70.82 cm^2) shows a small degree of linearity (gradient of 0.0181). An increase in the area of segment causes an increase in the normalised IQM signal for the largest segment considered in this study. The normalised IQM signals are much scattered around the linear trend line.

B. BRUTE FORCE SENSITIVITY ANALYSIS

Fig. 4.29c shows the graph of brute force sensitivity index plotted against the area of the segment for the altered segment of segment seven.

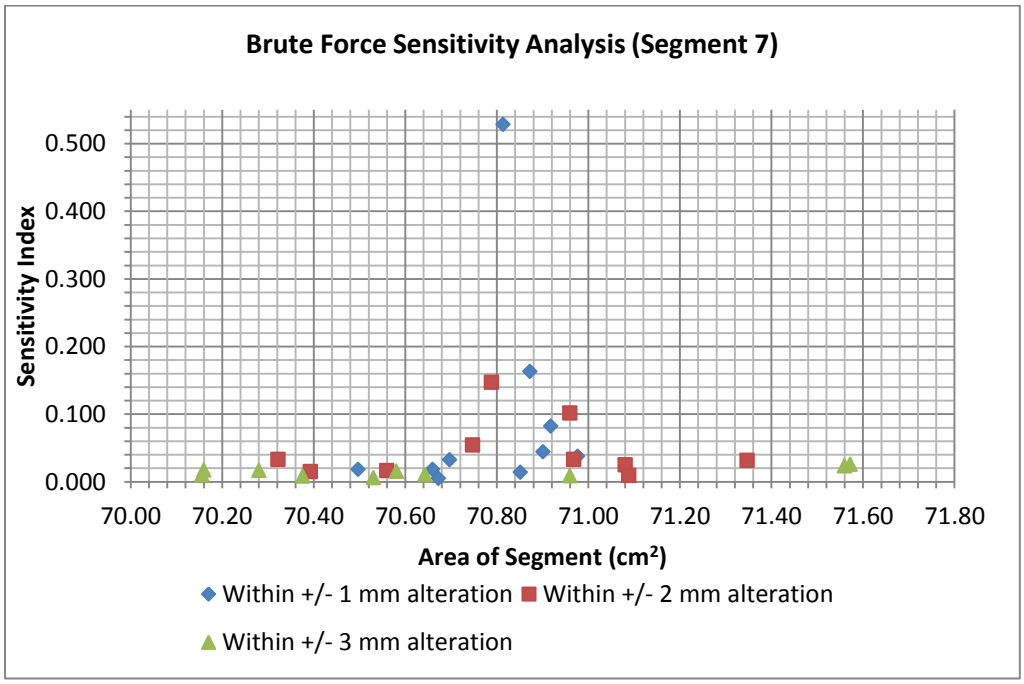

Figure 4.29c: Brute force Sensitivity Analysis of Segment seven, for random alterations within +/- 1, +/- 2, +/- 3 mm

In Fig. 4.29c, the brute force analysis on random alterations of an irregular field has the highest sensitive index around the unaltered area of segment (70.82 cm^2). This does not mean that the model is not sensitive to all other areas of segments. If the brute force sensitive index is zero, then the model is not sensitive to the area of the segment.

C. VARIANCE- BASED SENSITIVITY ANALYSIS

Fig. 4.29d shows the variance-based sensitivity indices for all the randomly altered segments of segment seven which is an irregular segment.

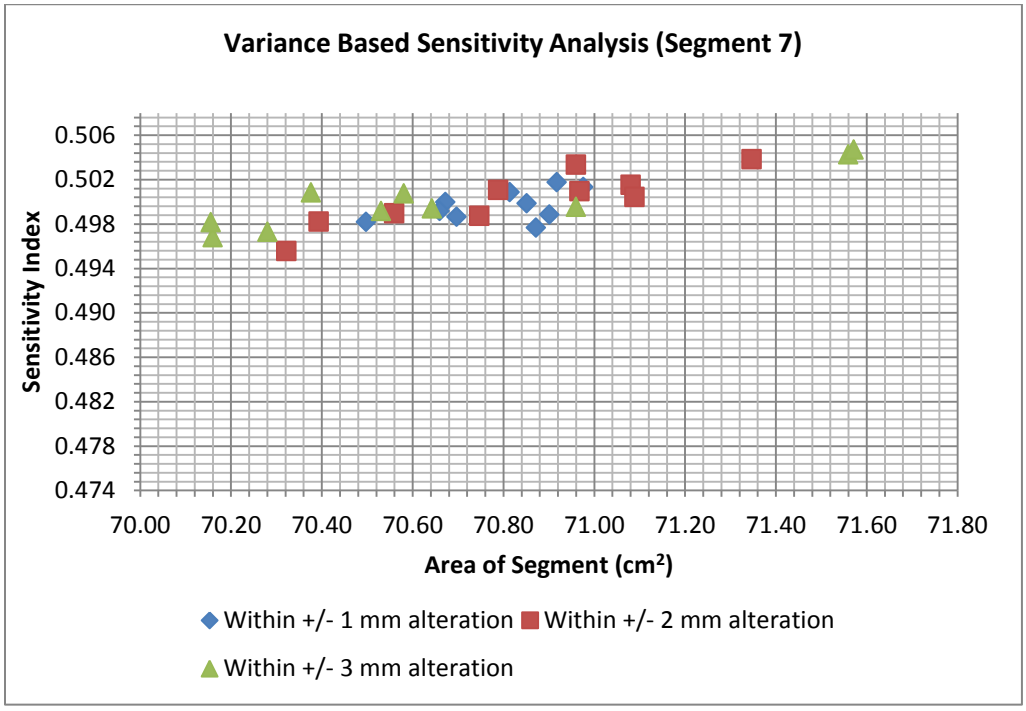

Figure 4.29d: Variance based Sensitivity Analysis of Segment seven, for random alterations within +/- 1, +/- 2, +/- 3 mm

In Fig. 4.29d, none of the sensitive indices is zero, and the indices increase with an increase in the area of the segment. This shows that variance-based sensitivity analysis technique of random alterations of an irregular field (70.82 cm^2) for all the altered segments are sensitive.

A. STANDARD REGRESSION COEFFICIENT

Fig. 4.29e shows the standard regression coefficient values for segment seven (segment area of 70.82 cm^2) that was randomly altered within ±1, ±2 and ±3 mm

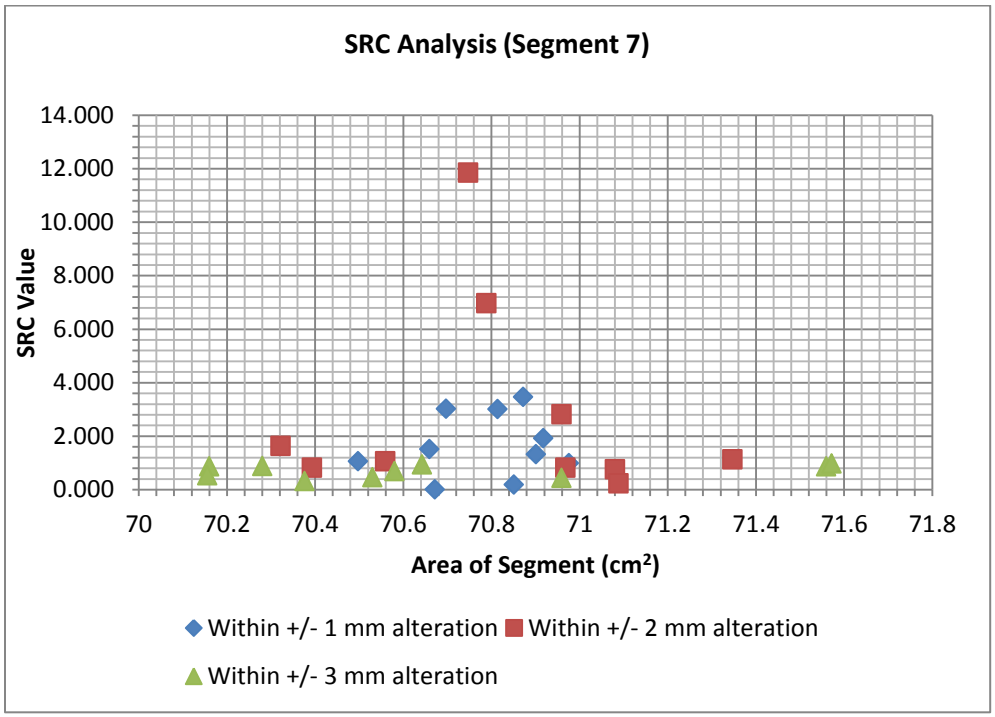

Figure 4.29e: SRC graph of Segment seven, for random alterations within +/- 1, +/- 2, +/- 3 mm

In Fig. 4.29e, the most sensitive input parameters are for the areas of altered irregular segment that are surrounding the region unaltered area of the segment (segment area of 70.82 cm^2).

4.3.3.8 SEGMENT EIGHT

Segment eight is an irregular segment and it was randomly altered 30 times. The IQM signal for altered segments was normalised to the unaltered segment which has a segment area of 47.49 cm^2.

Fig. 4.30a shows the example of an unaltered field, and the examples of fields altered at random within ± 1, ± 2, and ± 3 mm in terms of its individual leaf positions.

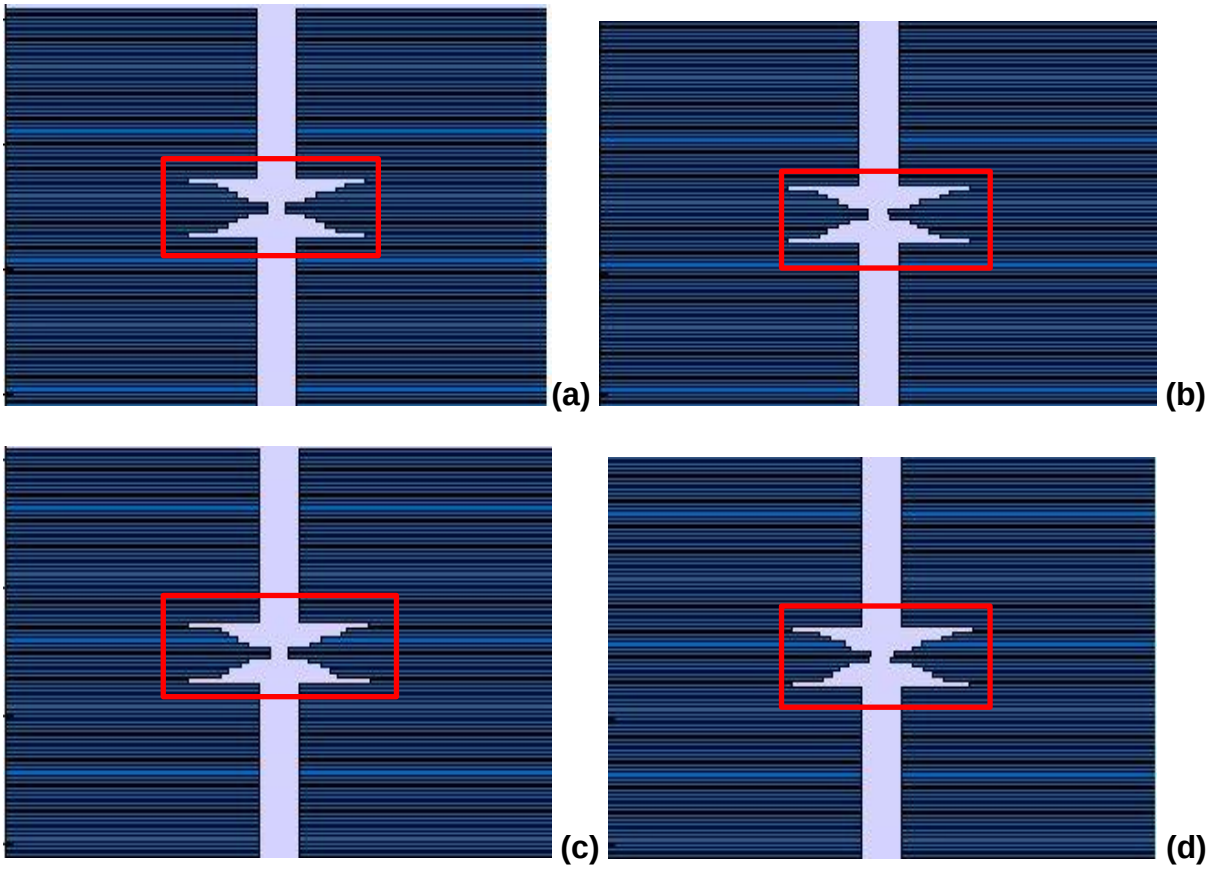

Figure 4.30a: Depicts the examples of randomly altered MLC leaf positions for Segment 8 (area of 47.49 cm^2) (a) Unaltered segment; (b) within ± 1 mm alteration; (c) within ± 2 mm alteration; (d) within ± 3 mm alteration

SENSITIVITY ANALYSIS OF SEGMENT EIGHT

In segment eight, the leaf positioning errors within ± 3 mm randomly produce segments area between 46.63 cm^2 to 48.53 cm^2 and for other alterations within ± 2 and ± 1 mm, data points between 46.99 cm^2 – 47.99 cm^2 were generated.

A. SCATTER PLOTS SENSITIVITY ANALYSIS

Fig. 4.30b shows the scatter plots of an irregular segment that was altered at random within ±1, ±2, and ±3 mm regarding its individual leaf positions.

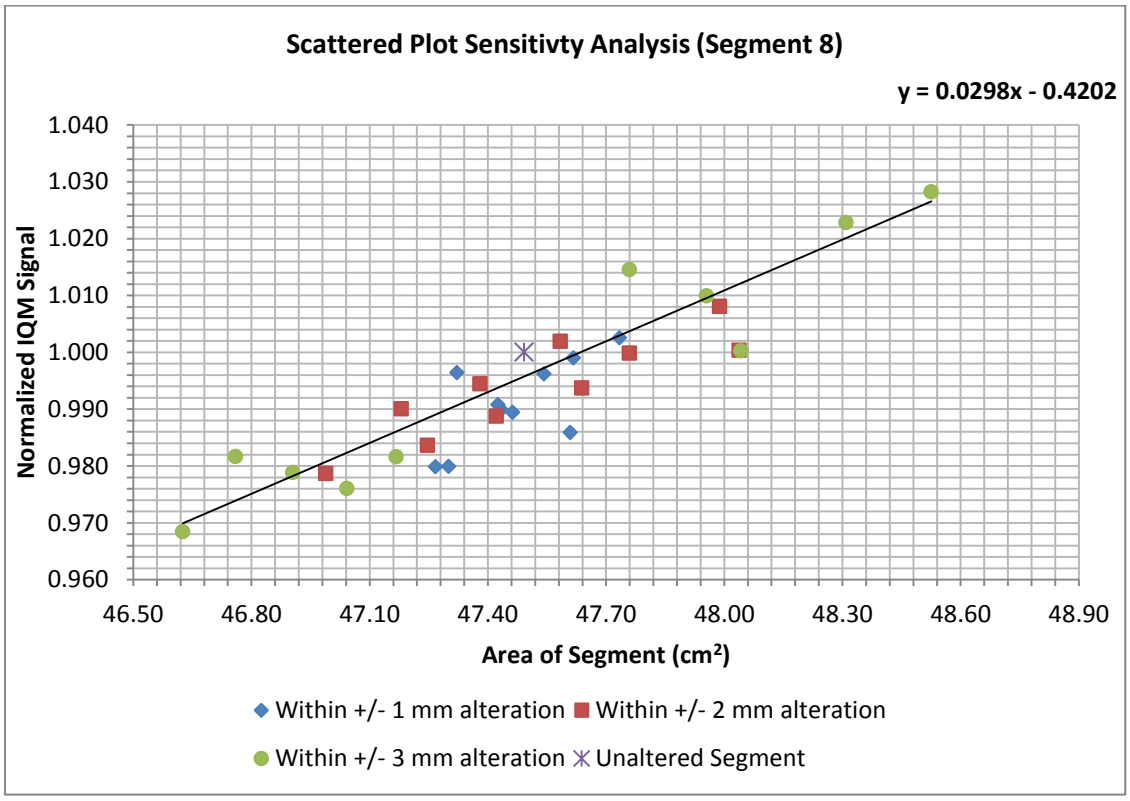

Figure 4.30b: Scatter plots Sensitivity Analysis of Segment eight, for random alterations within +/- 1, +/- 2, +/- 3 mm

In Fig. 4.30b, the graph displayed a gradient of 0.0298. The scatter plots for this irregular segment (area of 47.49 cm^2) that was altered randomly shows that an increase in the area of segment causes an increase in the normalised IQM signal. The normalised IQM signals scatter around the linear trend line.

B. BRUTE FORCE SENSITIVITY ANALYSIS

Fig. 4.30c shows the graph of brute force sensitivity index plotted against the area of the segment for segment eight.

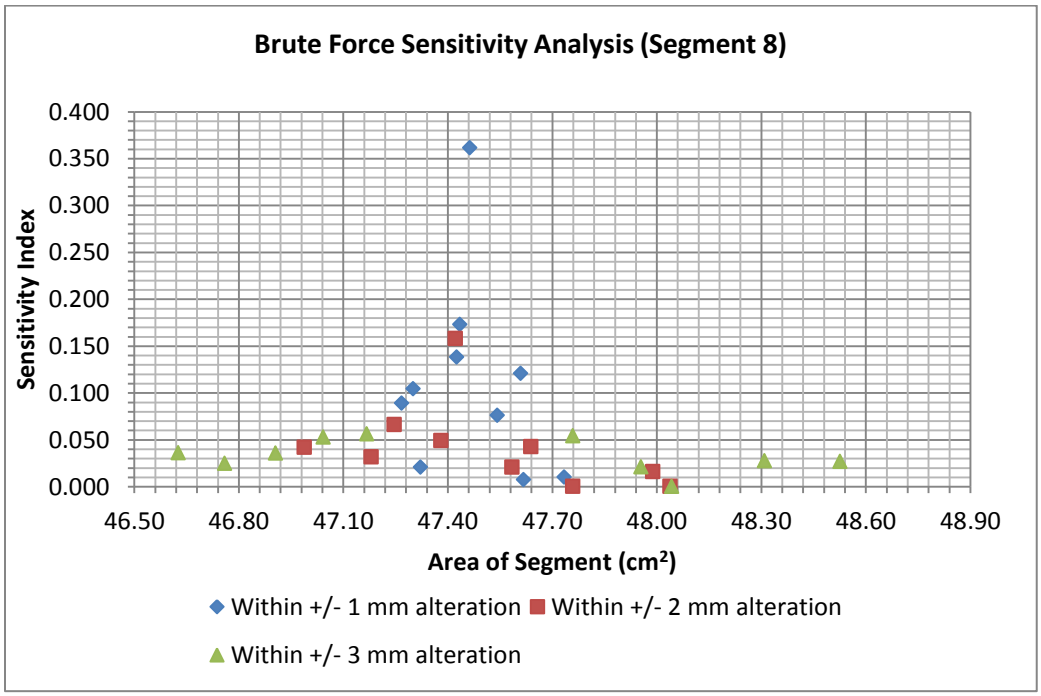

Figure 4.30c: Brute force Sensitivity Analysis of Segment eight, for random alterations within +/- 1, +/- 2, +/- 3 mm

In Fig. 4.30c, the brute force analysis on random alterations of an irregular field shows that the highest value of sensitivity index is located within the region of the unaltered segment (segment area of 47.49 cm^2). This shows that the IQM is mostly sensitive to minimal alterations.

C. VARIANCE-BASED SENSITIVITY ANALYSIS

Fig. 4.30d shows the variance-base sensitivity indices for all the randomly altered segments of segment eight.

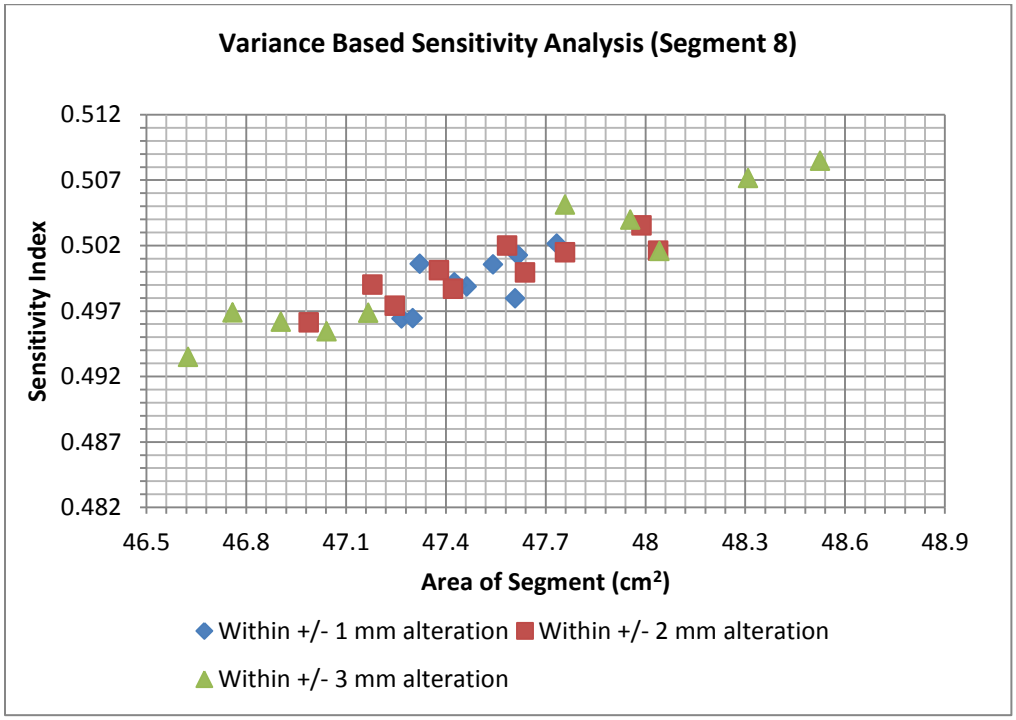

Figure 4.30d: Variance based Sensitivity Analysis of Segment eight, for random alterations within +/- 1, +/- 2, +/- 3 mm

In Fig. 4.30d, the variance-based sensitivity indices increase with an increase in the area of the segment. This shows that the model is sensitive to segment eight (segment area of 47.49 cm^2) according to variance-based sensitivity analysis.

D. STANDARD REGRESSION COEFFICIENT

Fig. 4.30e shows the standard regression coefficient values for segment eight (segment area of 47.49 cm^2) that was randomly altered within ±1, ±2 and ±3 mm

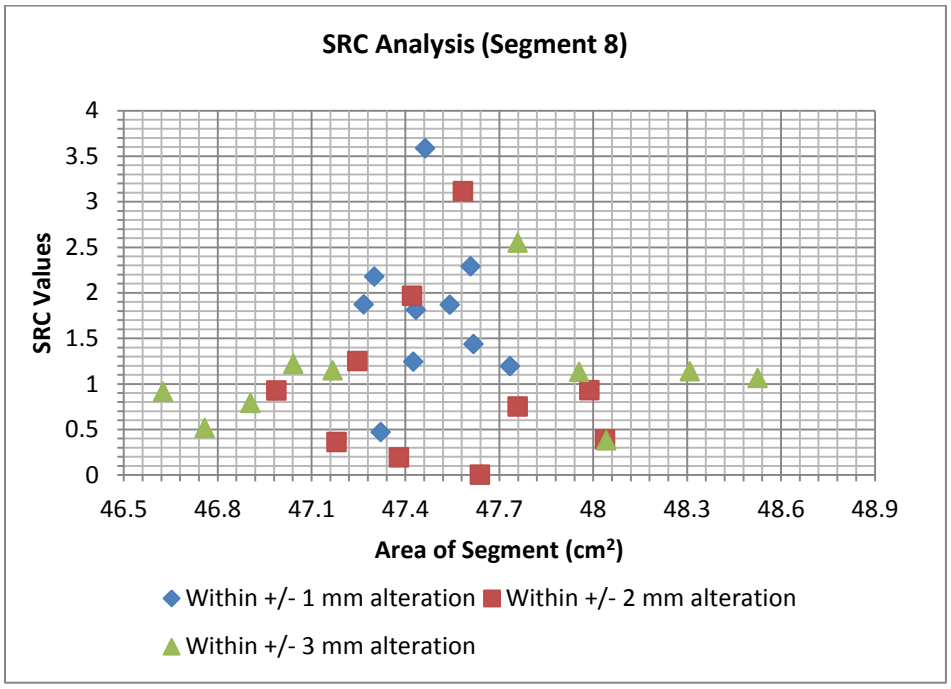

Figure 4.30e: SRC graph of Segment eight, for random alterations within +/- 1, +/- 2, +/- 3 mm

In Fig. 4.30e, the SRC values for the input parameters around the region of the unaltered segment (segment area of 47.49 cm^2) display the highest values.

4.3.3.9 SEGMENT NINE

Segment nine is a regular segment of 2 × 2 cm^2. This segment was altered randomly, and the signal response was calculated in the air region of the IQM model. The IQM signal of the unaltered segment was normalised to the unaltered segment which has a segment area of 4 cm^2. Fig. 4.31a shows the example of an unaltered field, and the examples of fields altered at random within ±1, ±2, and ±3 mm regarding its individual leaf positions.

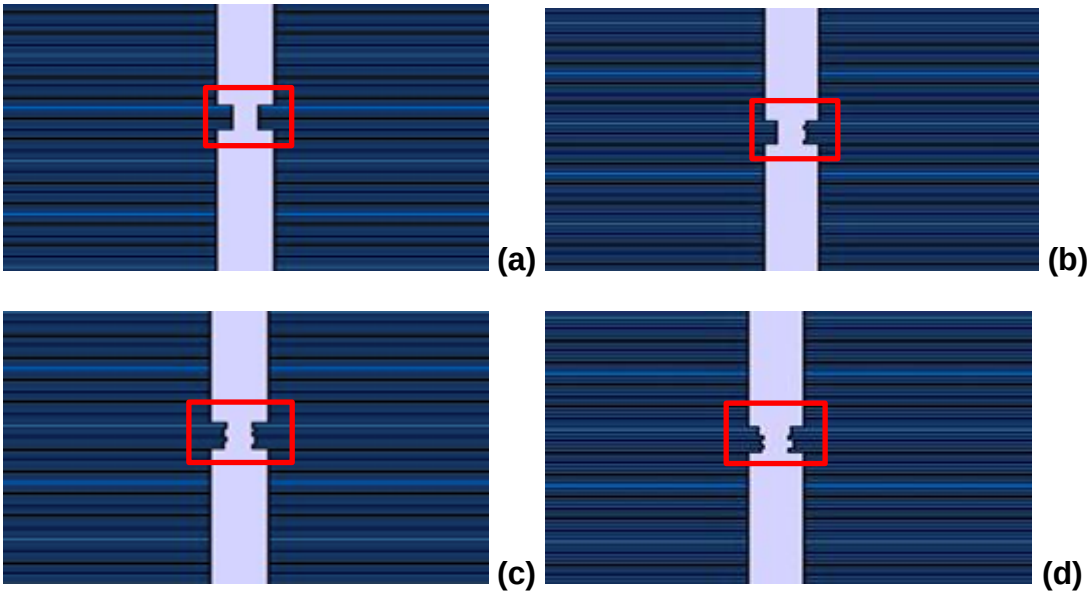

Figure 4.31a: Depicts the examples of randomly altered MLC leaf positions for Segment 9 (2 × 2 cm^2) (a) Unaltered segment; (b) within ± 1 mm alteration; (c) within ± 2 mm alteration; (d) within ± 3 mm alteration

SENSITIVITY ANALYSIS OF SEGMENT NINE

Alterations of 2 × 2 cm^2 were able to randomly generate 10 data points between 3.52 cm^2 and 4.35 cm^2 for ± 3 mm leaf positioning error. The ± 2 mm MLC alteration generated 10 data values within 3.70 cm^2 to 4.30 cm^2 where ± 1 mm alterations were packed around the unaltered segment area (4. 00 cm^2).

A. SCATTER PLOT SENSITIVITY ANALYSIS

Fig. 4.31b shows the scatter plots of a regular segment of 2 × 2 cm^2 that was altered at random within ±1, ±2, and ±3 mm regarding its individual leaf positions.

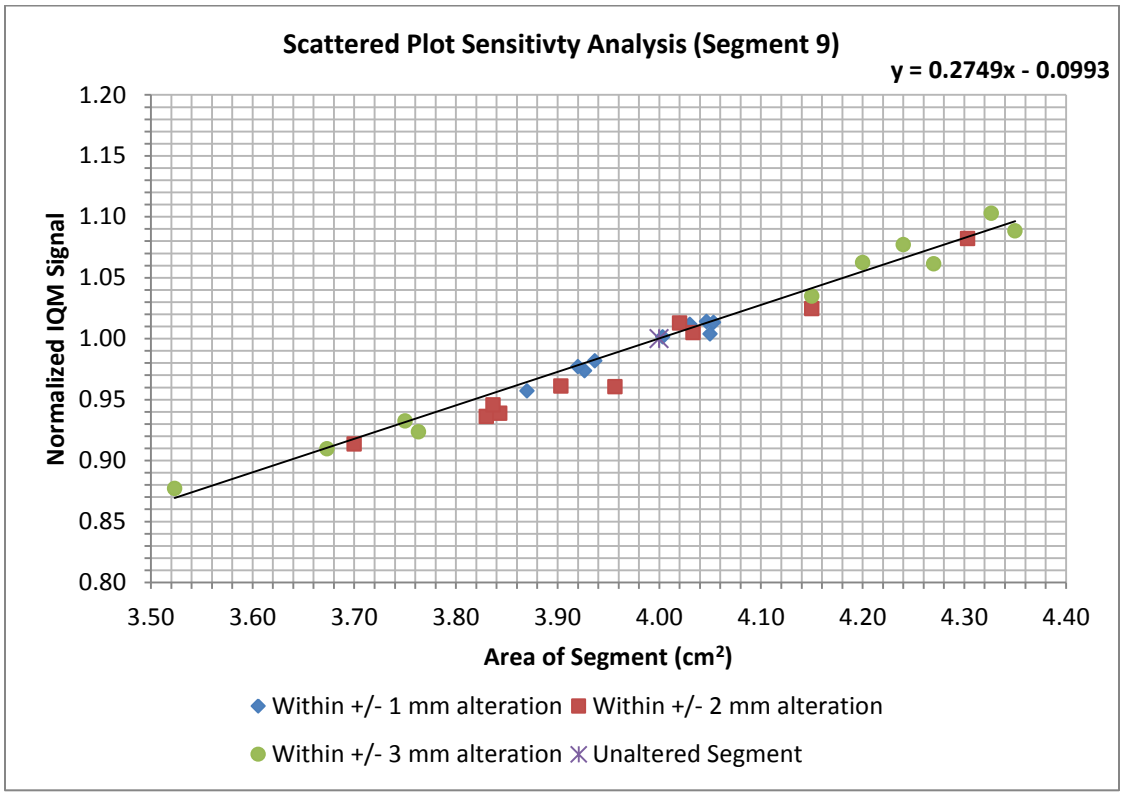

Figure 4.31b: Scatter plots Sensitivity Analysis of Segment nine, for random alterations within +/- 1, +/- 2, +/- 3 mm

In Fig. 4.31b, the scatter plots for this regular segment (area of 4 cm^2) shows a high degree of linearity (gradient of 0.2749). This means that the IQM model is very sensitive to small fields than large fields. The normalised IQM signals align on the linear trend line.

B. BRUTE FORCE SENSITIVITY ANALYSIS

Fig. 4.31c shows the graph of brute force sensitivity index plotted against the area of the segment for 2 × 2 cm^2 field.

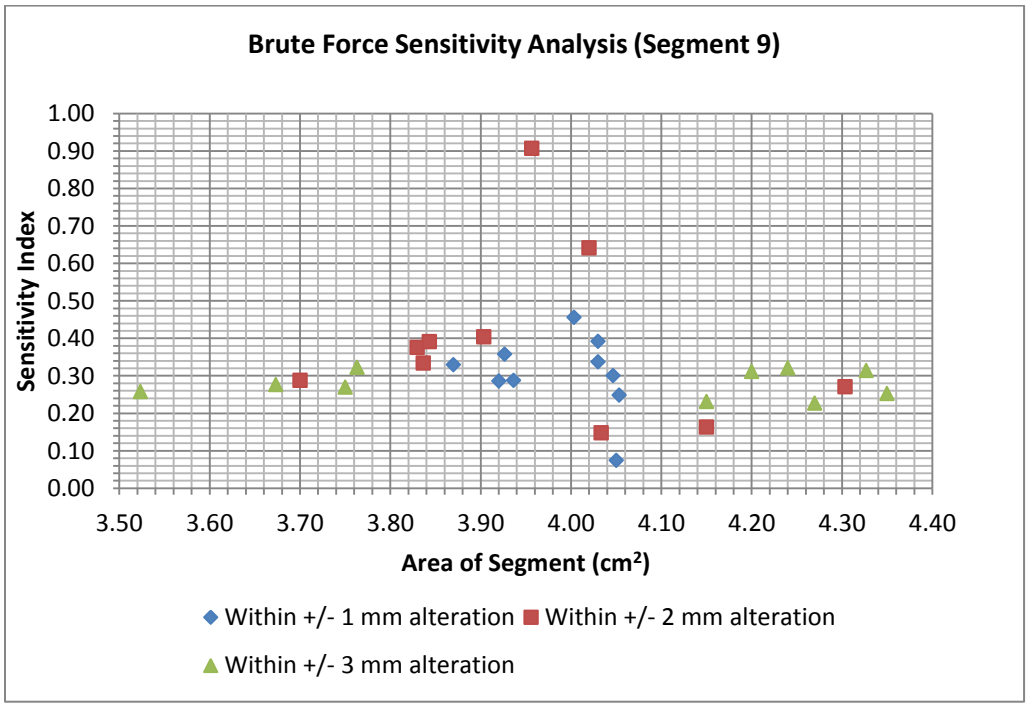

Figure 4.31c: Brute force Sensitivity Analysis of Segment nine, for random alterations within +/- 1, +/- 2, +/- 3 mm

In Fig. 4.31c, the brute force analysis on random alterations of a regular field of 2 × 2 cm^2 field shows an increased value of indices for all the altered segments compared to other segments (larger fields) considered in this study. This is due to high degree linearity in Fig. 4.31b, the rate of change in the IQM signal per change in the segment area (definition of the brute force sensitivity index) will almost be uniform.

C. VARIANCE-BASED SENSITIVITY ANALYSIS

Fig. 4.31d shows that the variance-based sensitivity indices for all the randomly altered segments of segment nine.

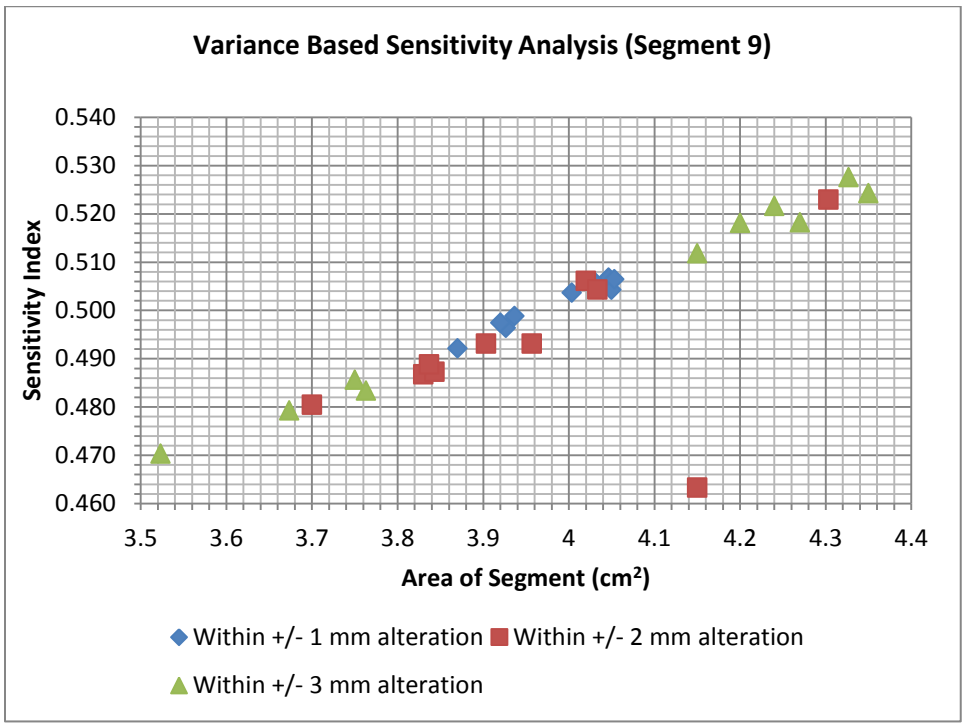

Figure 4.31d: Variance based Sensitivity Analysis of Segment nine, for random alterations within +/- 1, +/- 2, +/- 3 mm

In Fig. 4.31d, the sensitive index increases with an increase in the area of the segment. This shows that the wedge-shaped model is sensitive to random alterations of 2 × 2 cm^2 field.

D. STANDARD REGRESSION COEFFICIENT

Fig. 4.31e shows the standard regression coefficient values for a randomly altered segment of 2 × 2 cm^2 which was altered within ±1, ±2 and ±3 mm.

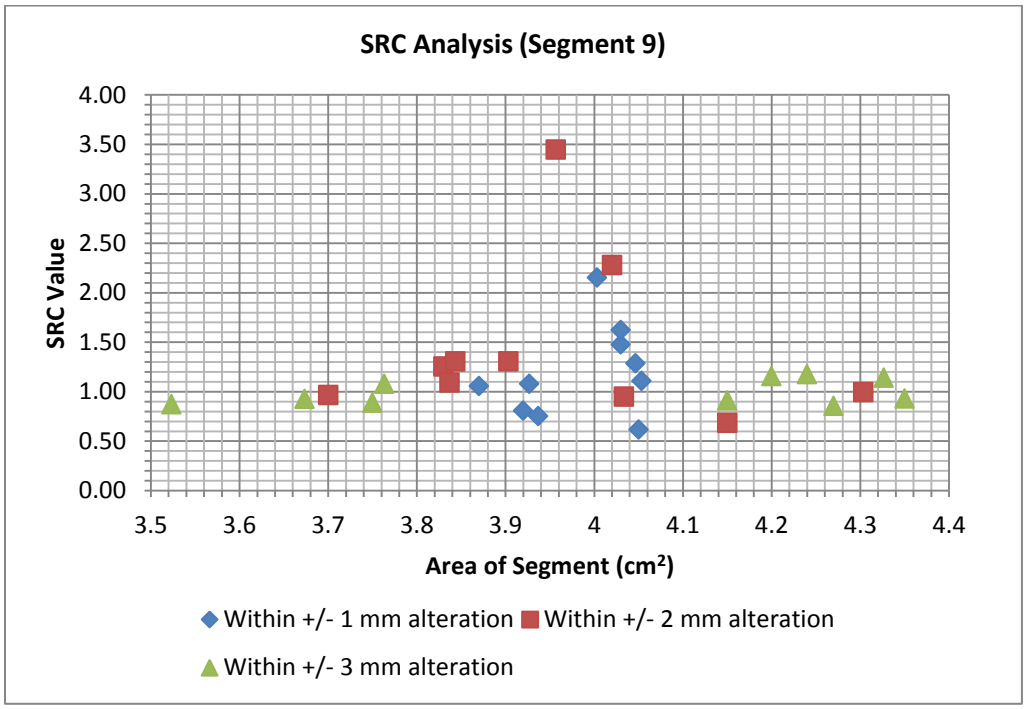

Figure 4.31e: SRC graph of Segment nine, for random alterations within +/- 1, +/- 2, +/- 3 mm

In Fig. 4.31e, the SRC values for 2 × 2 cm^2 field that was altered randomly shows the most sensitive input parameters around the region of the unaltered segment. The SRC values for all the altered segments shows a good response compared to larger segments considered in this study.

4.3.3.10 SEGMENT TEN

Segment ten is a regular segment of 1 × 1 cm^2. This is the smallest segment considered in this study. It was altered randomly, and the IQM signal of the altered segment was normalised to the unaltered segment.

Fig. 4.32a shows the example of an unaltered field, and the examples of fields altered at random within ± 1, ± 2, and ± 3 mm in terms of its individual leaf positions.

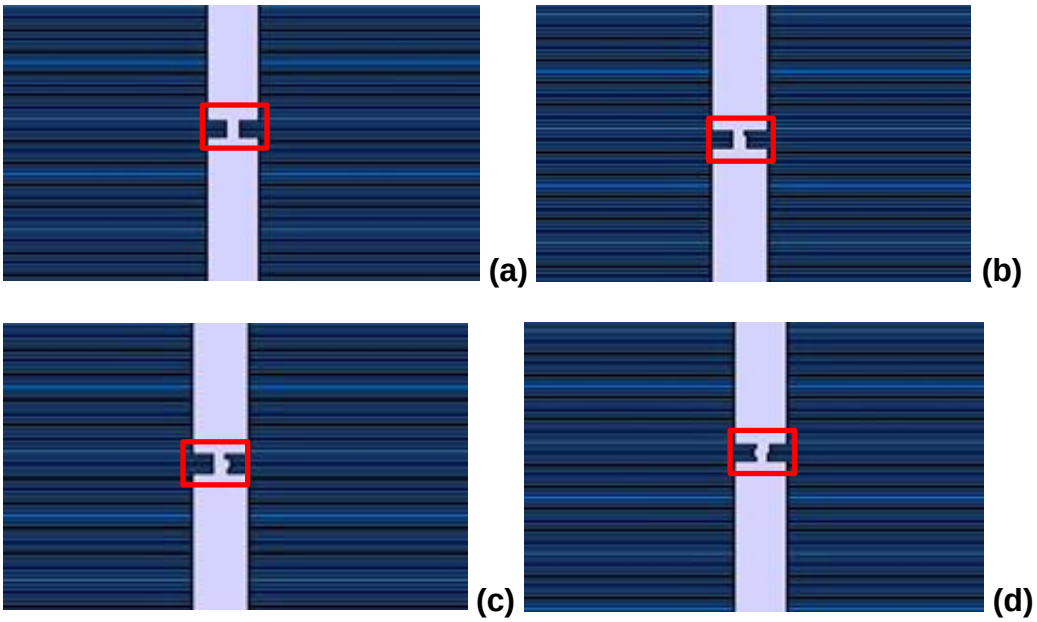

Figure 4.32a: Depicts the examples of randomly altered MLC leaf positions for Segment 10 (1 × 1 cm^2) (a) Unaltered segment; (b) within ± 1 mm alteration; (c) within ± 2 mm alteration; (d) within ± 3 mm alteration

SENSITIVITY ANALYSIS OF SEGMENT TEN

In segment ten, the misaligned segments size range depends on the allowed segment alteration limit. For the ± 3mm randomly altered case the segment area ranged between 0.743 cm^2 to 1.25 cm^2. The original unaltered segment size is exactly 1.00 cm^2. For the ± 2mm case, it ranged between 0.87 cm^2 and 1.17 cm^2. For the ± 1 mm case, there is an even spread around the 1 × 1 cm^2 field.

A. SCATTER PLOTS SENSITIVITY ANALYSIS

Fig. 4.32b shows the scatter plots of a regular segment of 1 × 1 cm^2 that was altered at random within ± 1, ± 2, and ± 3 mm regarding its individual leaf positions.

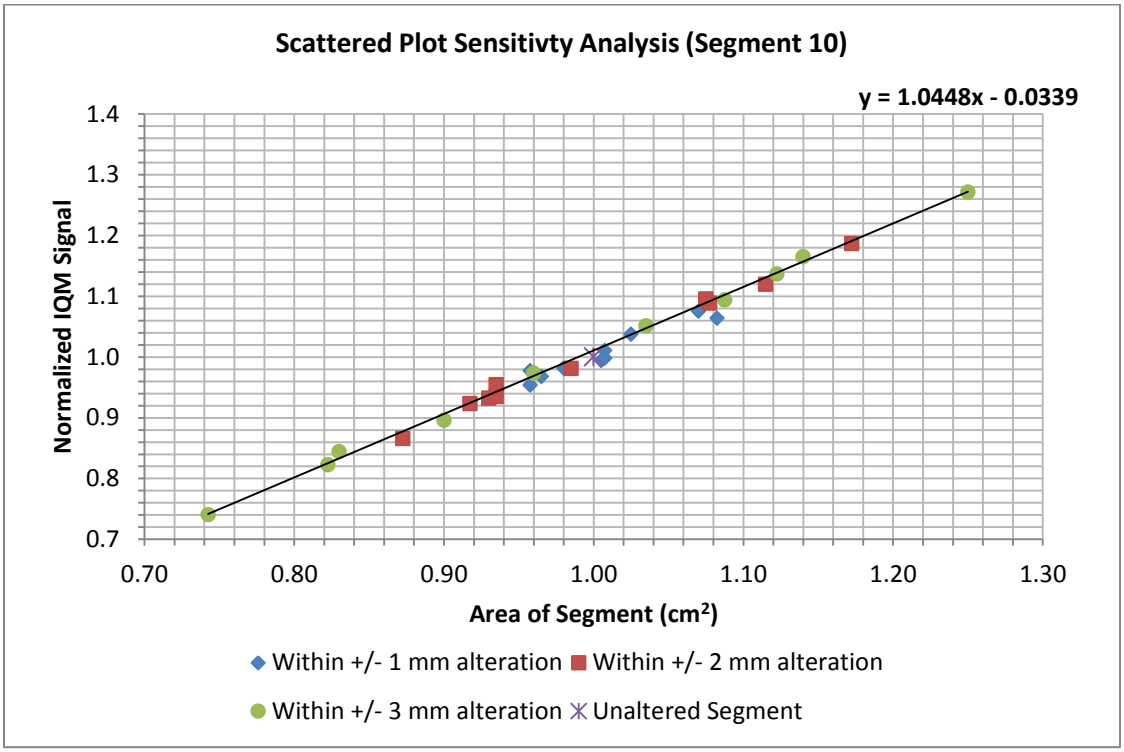

Figure 4.32b: Scatter plots Sensitivity Analysis of Segment ten, for random alterations within +/- 1, +/- 2, +/- 3 mm

On Fig. 4.32b, the scatter plots for this regular segment (area of 1 cm^2) shows a high degree of linearity with a slope of 1.0448. The IQM model is sensitive to random alteration within few millimetres. The normalised IQM signals align on the linear trend line.

B. BRUTE FORCE SENSITIVITY ANALYSIS

Fig. 4.32c shows the graph of sensitivity index against the area of the segment for altered segments of segment ten.

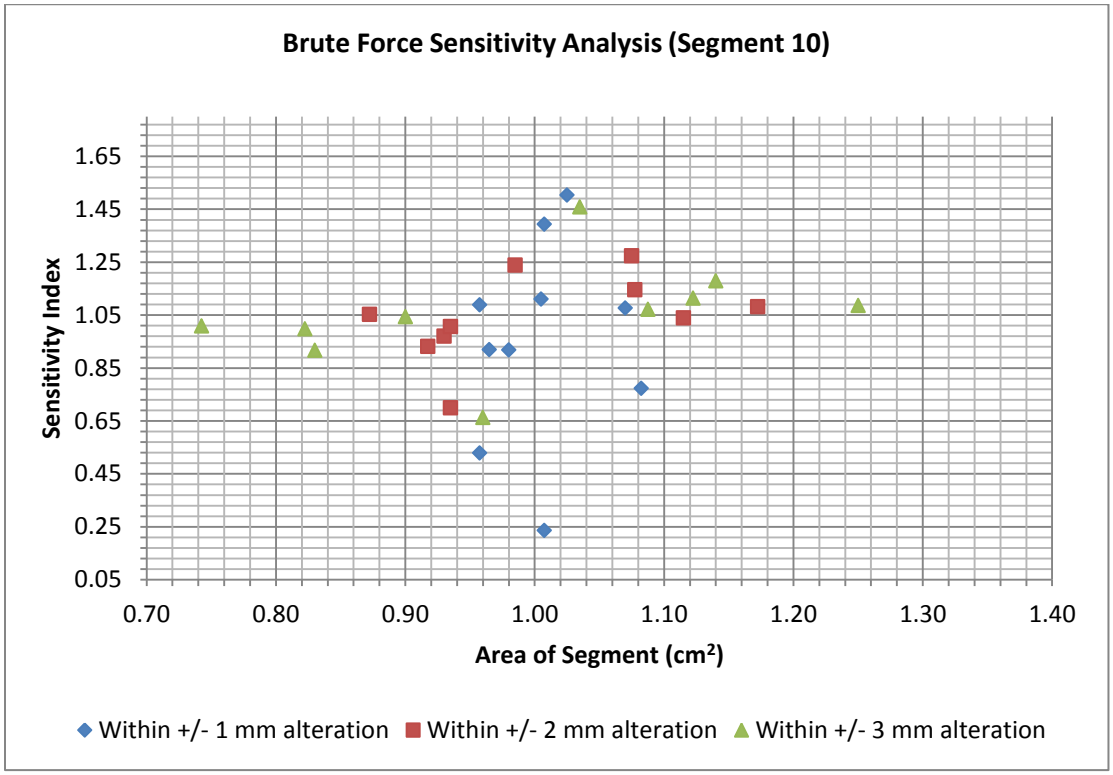

Figure 4.32c: Brute force Sensitivity Analysis of Segment ten, for random alterations within +/- 1, +/- 2, +/- 3 mm

In Fig. 4.32c, brute force analysis applied to random alterations field of 1 × 1 cm^2 shows high indices for all the entire segments altered at random. This is the effect of a linear scatter plot of segment ten (Fig. 4.31b). If the scatter plot seems to be perfectly linear, the most sensitivity index seems to spread across the graph. This shows that the IQM model is very sensitive to alterations small segments.

C. VARIANCE-BASED SENSITIVITY ANALYSIS

Fig. 4.32d shows that the variance-based sensitivity indices for all the randomly altered segments of segment ten.

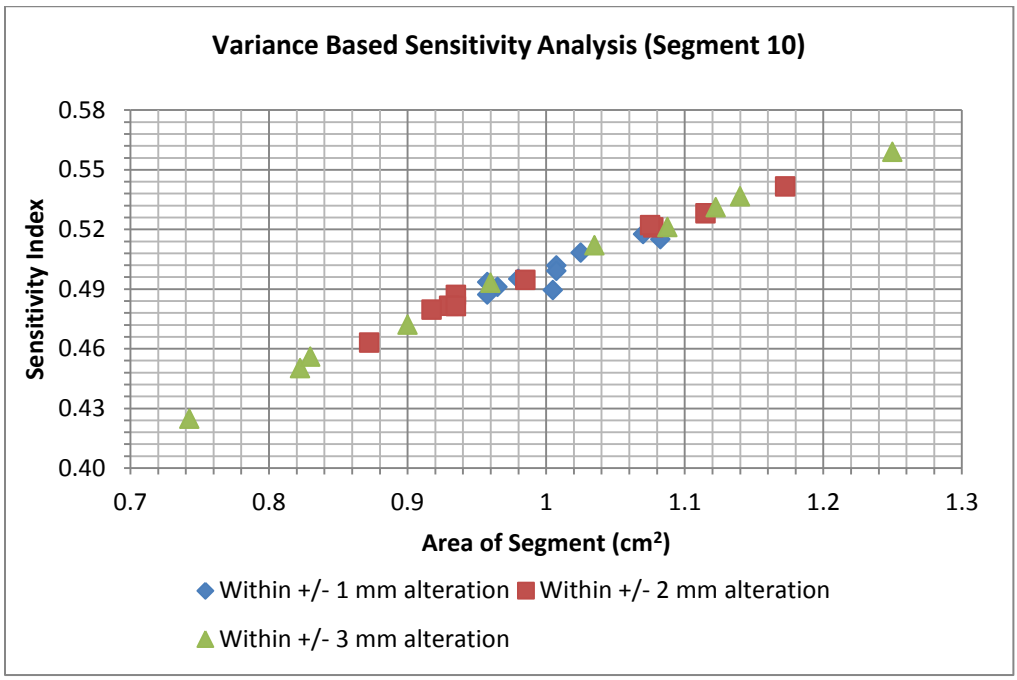

Figure 4.32d: Variance based Sensitivity Analysis of Segment ten, for random alterations within +/- 1, +/- 2, +/- 3 mm

In Fig. 4.32d, the sensitivity index shows a steep gradient and the sensitivity of the model increases with an increase in the area of the segment. The sensitivity analysis proves that the wedge-shaped chamber is sensitive to random alterations of a regular segment.

D. STANDARD REGRESSION COEFFICIENT

Fig. 4.32e shows the standard regression coefficient values for 1 × 1 cm^2 field that was altered randomly within ±1, ±2 and ±3 mm.

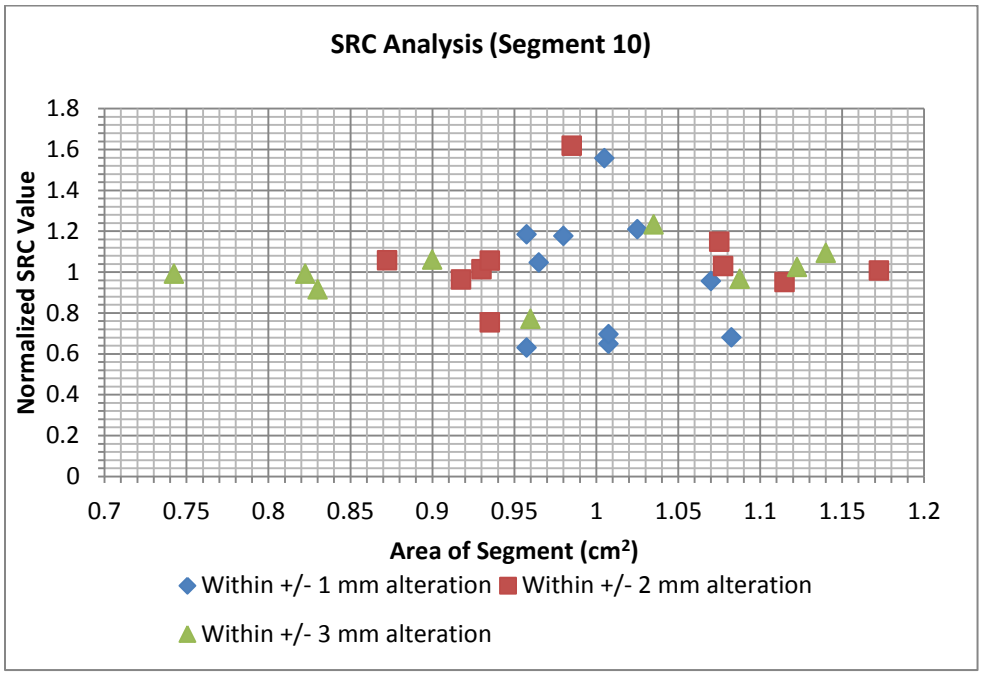

Figure 4.32e: SRC graph of Segment ten, for random alterations within +/- 1, +/- 2, +/- 3 mm

In Fig. 4.32e, the SRC value for 1 × 1 cm^2 field that was altered randomly are significantly high and seems to be uniform. This is expected of a perfectly linear scatter plots as shown in Fig 4.32b. It means that all the input parameters (altered segments) of segment ten are very sensitive as determined by its SRC values which agreed with other sensitivity analyses considered in this study. These analyses proved that the sensitivity of the IQM model is more pronounced in small fields.

4.3.3.11 SEGMENT ELEVEN

Segment eleven is an irregular segment. It was altered randomly within few millimetres. The IQM signal of the altered segments was normalised to the unaltered segment which has a segment area of 38.74 cm^2. Fig. 4.33a shows the example of an unaltered field, and the examples of fields altered at random within ±1, ±2, and ±3 mm regarding its individual leaf positions.

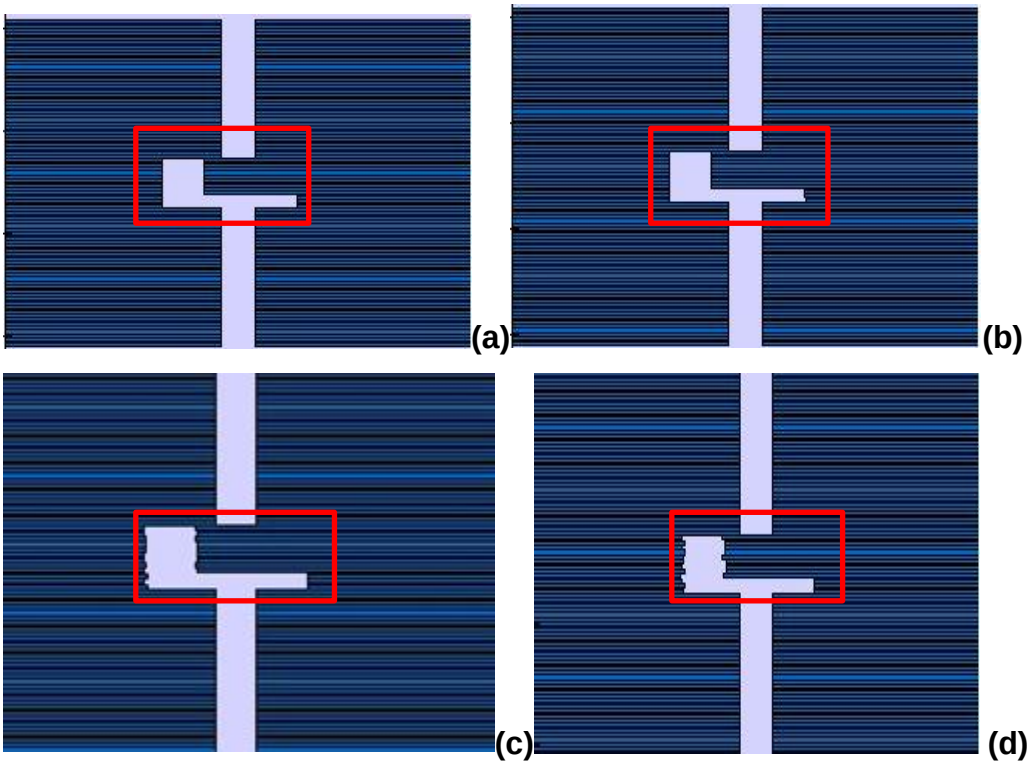

Figure 4.33a: Depicts the examples of randomly altered MLC leaf positions for Segment 11 (area of 38.74 cm^2) (a) Unaltered segment; (b) within ± 1 mm alteration; (c) within ± 2 mm alteration; (d) within ± 3 mm alteration

SENSITIVITY ANALYSIS OF SEGMENT ELEVEN

In segment eleven, alterations of the segment were able to randomly generate 10 data points between 37.72 cm^2 and 39.57 cm^2 for ± 3 mm leaf positioning error. The ± 2 mm leaf positioning errors caused 10 data values that ranged between 38.21 cm^2 to 39.45 cm^2, where ± 1 mm positional errors randomly produce 10 data points between 38.52 cm^2 and 39.00.

A. SCATTER PLOTS SENSITIVITY ANALYSIS

Fig. 4.33b shows the scatter plots of an irregular segment that was altered at random within ±1, ±2, and ±3 mm regarding its individual leaf positions.

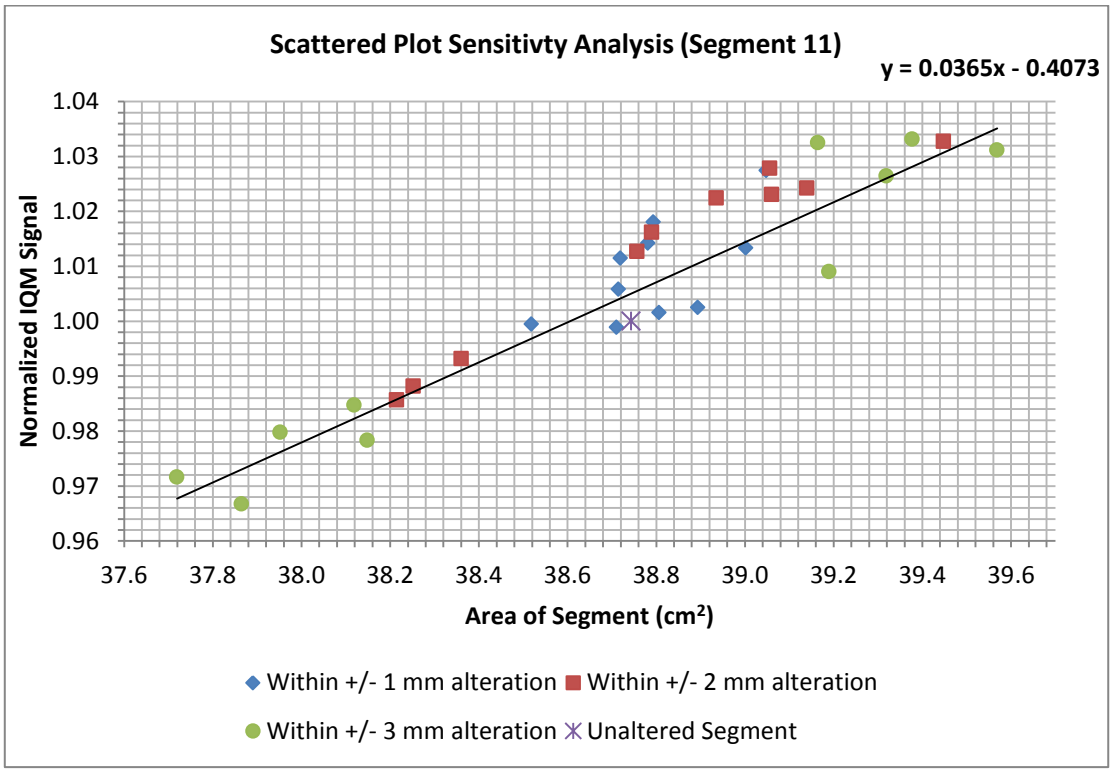

Figure 4.33b: Scatter plots Sensitivity Analysis of Segment eleven, for random alterations within +/- 1, +/- 2, +/- 3 mm

On Fig. 4.33b, the scatter plots for this irregular segment (area of 38.74 cm^2) shows a degree of linearity (0.0365). The IQM model is sensitive to random alteration within few millimetres. An increase in the area of segment causes an increase in the normalised IQM signal. The normalised IQM signals scatter around the linear trend line.

B. BRUTE FORCE SENSITIVITY ANALYSIS

Fig. 4.33c shows the graph of the brute force sensitivity index plotted against the area of the segment for the irregular segment considered in segment eleven.

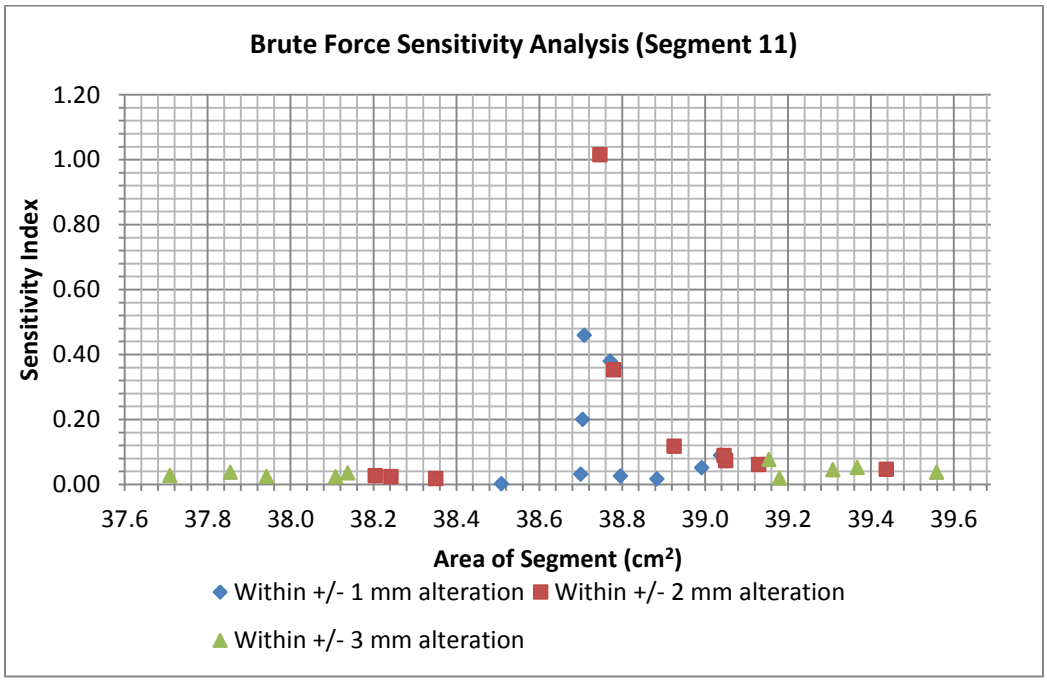

Figure 4.33c: Brute force Sensitivity Analysis of Segment eleven, for random alterations within +/- 1, +/- 2, +/- 3 mm

In Fig. 4.33c, brute force analysis on random alterations of an irregular field shows that the most sensitive altered segments are the segments with minimal alterations which are closer to the unaltered area of the segment (38.74 cm^2). This shows that the IQM is highly sensitive to minimal alterations. A large segment area gives a high magnitude of signal response, but when evaluated regarding rate of change in the IQM signal per change in the segment area (definition of brute force technique), large perturbation of the segment areas seems not to produce a huge signal difference. This is not to contradict the scatter plots analysis but to give an in-depth study of the sensitivity of the IQM model.

C. VARIANCE-BASED SENSITIVITY ANALYSIS

Fig. 4.33d shows the variance-based sensitivity indices for all the randomly altered segments of segment eleven.

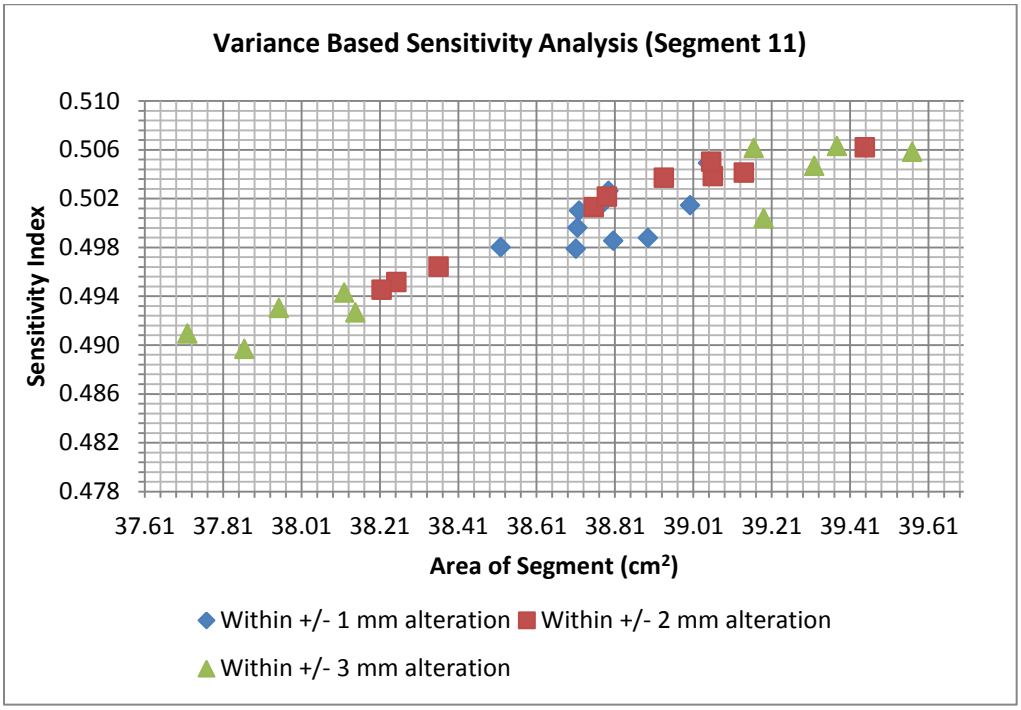

Figure 4.33d: Variance based Sensitivity Analysis of Segment eleven, for random alterations within +/- 1, +/- 2, +/- 3 mm

In Fig. 4.33d, the indices are greater than zero for all the altered segments considered. This shows that variance-based sensitivity analysis technique of random alterations of an irregular field (38.74 cm^2) for all the altered segments are sensitive.

D. STANDARD REGRESSION COEFFICIENT

Fig. 4.33e shows the standard regression coefficient values for segment eight (segment area of 38.74 cm^2) which is an irregular segment. It was randomly altered within ±1, ±2 and ±3 mm.

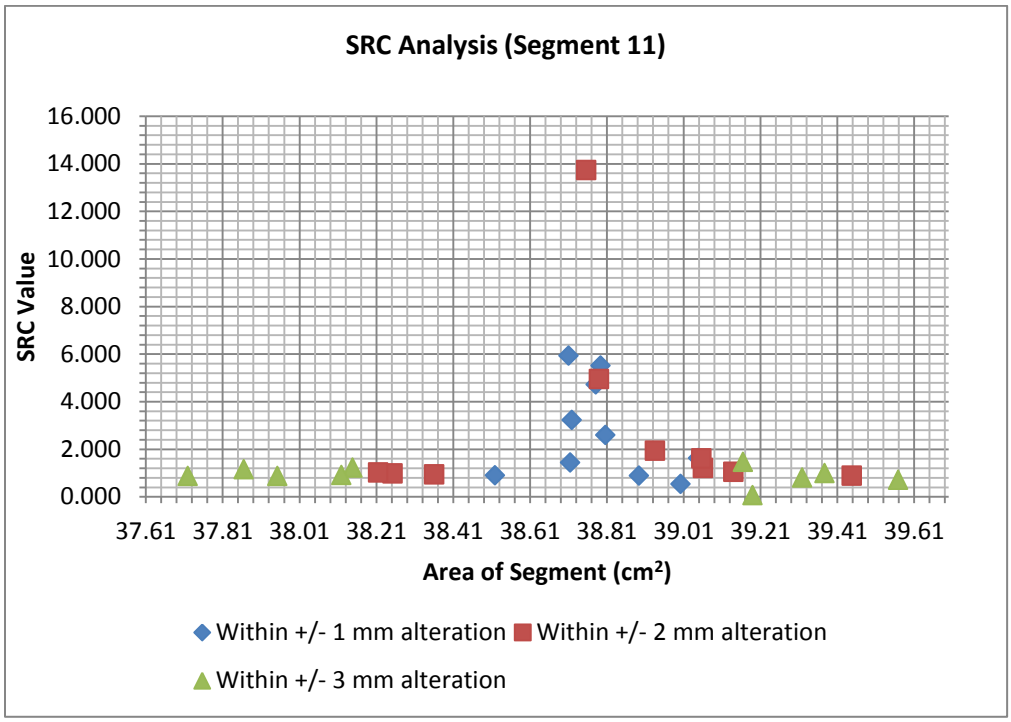

Figure 4.33e: SRC graph of Segment eleven, for random alterations within +/- 1, +/- 2, +/- 3 mm

In Fig. 4.33e, the SRC values for the input parameters around the region of the unaltered segment (segment area of 38.74 cm^2) display the highest values, which mean that are the most sensitive input parameters. The sensitivity analysis techniques used in this study proved that the wedge-shaped chamber is sensitive to random alterations of both regular and irregular segment.

CHAPTER 5

5.0 DISCUSSION

5.1 IQM COMPONENT MODULE DESIGN

A new component module (CM) namely IQM was successfully designed and was added on to the BEAMnrc code. The newly designed CM could model a wedge-shaped ionization chamber and accurately calculate dose in the air region of the IQM CM using the standard EGSnrc/BEAMnrc MC simulation. The IQM CM is efficient and user-friendly in producing an accurate spatial geometric of the wedge-shaped material as specified by the user.

The TCL/TK scripting language and MORTRAN language were used to code the IQM CM that was added to the BEAMnrc. Good understanding of programming languages, radiation transport physics, and the precise geometric definition was essential in creating this CM which was incorporated into BEAMnrc.

The flexibility of the IQM CM was to model a wedge-shaped component and create regions for dose deposition. It gives room for the user to define the dose region number, component's materials, dimensions and spatial specifications. Incorporation of the IQM CM on the BEAMnrc GUI modifies the landmarks set in the BEAMnrc software which was downloaded from the National Research Council Canada (NRCC) website. This modification must be done on the BEAMnrc codes when there is an intention to add a new CM; else access to the new CM on the interface will not be possible.

The graphical image displayed on BEAMnrc GUI and the ray-tracing technique validates the IQM geometry. The ability for geometry coordinates to be displayed according to the users' specifications validates the accuracy of the new CM codes. "Ray tracing method" as a term was not directly mentioned in BEAMnrc user manual (Rogers et al. 2011) but `nrcaux. mortran` routine performs the same function as ray tracing which is to use particle step/ interaction or particle tracking to output detailed boundaries of the simulation geometry in `egsgeom`. The ray tracing increases the computational time of simulation due to boundary cross-section scoring, and few articles have suggested MC simulation techniques for ray tracing calculation (Jacques et al. 2011; Jabbari 2008).

Successful compilation and program run authenticate the sub-routine macros of EGSnrc code in the BEAMnrc.

The IQM CM is a virtual model that will state the dosimetry potentials of the wedge-shaped ionization chamber of the IQM system. The signal of the prototype IQM system is not based on spatial dose calculation but rather on electronic signals generated during beam radiation. Since the IQM system is still in its development stage, the end point of its functionality is to calculate spatial dose as stated by the guiding articles (Paliwal et al. 1996; Chang et al. 2013; Islam et al. 2009). The calculated electronic signal in the wedge-shaped ion chamber will produce a signal of the order of nC (nano coulomb) while the MC simulation data or the calculated dose has a unit of $cGy.cm^2$ (dose-area product). Normalization allows rescaling of both outputs. The IQM CM will serve as a template for future work in real-time beam delivery check of the IQM system using EGSnrc /BEAMnrc MC Simulation. The essence of the wedge-shaped ionization chamber is to be sensitive to alterations in a patient treatment plan. If the IQM device is susceptible to plans, then an issue like output unit should be secondary. Theoretically, output unit of an ionization chamber detector should be related to the absorbed dose. MC simulation is suitable for this study since it has been accepted as dose calculation engine.

There are several MC based algorithms such as MCNP (Jabbari & Seuntjens 2014; Brown 2003), PENELOPE (Baro et al. 1995; Sempau et al. 2001) and GEANT4 (Agostinelli et al. 2003; Archambault et al. 2003) that could be used to study the IQM CM. The EGSnrc/BEAMnrc code was chosen due to its easy and free obtainability with full documentation and regular upgrade provided by the NRCC.

5.2 ACCURATE MONTE CARLO MODEL OF A LINAC

It is essential for a good linac head model to simulate the geometry of the physical linac head accurately. Generally, dose discrepancies between physical measurement and MC calculation should be limited to reasonable DD/DTA criterion as stated in AAPM report 105 (Chetty et al. 2007; J.-I. Kim et al. 2014; Low 2010; Hussein et al. 2013; Huang et al. 2014; Persoon et al. 2011). The gamma (γ) index criteria of 2% DD/2 mm

DTA and 3% DD/3 mm DTA are taken as a gold standard (Keall et al. 2000; Mesbahi 2006; Usmani et al. 2014; Mesbahi et al. 2007; Oliveira et al. 2013; Park et al. 2011; Ceberg 2013; Winiecki et al. 2009; Bak et al. 2012; Low & Dempsey 2003; Xing et al. 2015). In this research, the authors developed an MC model of an Elekta Synergy linac head equipped with Agility 160-leaf MLC using the manufacturers' specifications. Simulations were done to characterise the photon beams of 10MV for 1 × 1 cm^2 to 30 × 30 cm^2 field sizes. The MC characterised photon beams were validated by commissioning data using the following dosimetry features: percentage depth doses, lateral beam profiles, and relative output factors.

The commissioning percentage depth doses and lateral beam profiles were measured at 2 mm intervals in a homogeneous water tank. Deviations of MC calculations from commissioning data for percentage depth doses for the clinical square fields considered were calculated using 2% DD/ 2 mm DTA criterion. The majority of the MC calculated dose points passed the criterion. Failed comparison was noted at the central and penumbra region of 25 × 25 and 30 × 30 cm^2 lateral dose profiles especially at 10 and 20 cm depths in the homogeneous water phantom. The deviations of MC calculations from commissioning data for relative output factors for clinical square fields considered were majorly within 1.44% of local percentage difference.

The BEAMnrc source model of an Elekta Synergy linac head equipped with an Agility 160-leaf MLC is accurate. The MC source model of this study showed good congruent results with commissioning data like similar studies (Feng et al. 2016; Jabbari 2008; Tayalati et al. 2013; Mesbahi 2006; Mesbahi et al. 2007; Oliveira et al. 2013; Juste et al. 2007). The MLC is a complex component of a linac model. It specifies different dose distribution and penumbra for different field sizes. Complexities of Agility 160-leaf model used in this study prompted several tuning iterations and adjustments to achieve this degree of accuracy. The gamma analysis which has been accepted as an evaluation tool was used in this study for validation because it combines dose difference calculation with distance-to-agreement calculation.

The little discrepancies when benchmarked are not caused by MC beam model or radiation transport since the uncertainty of the accepted output is within 1%. It could be

as a result of additional electron source at that particular field size during measurements. The experimental uncertainty could be caused by electron sources in the linac head which are not fully accounted for or ionization chamber setup or irregular response of the ion chamber at superficial depth or at small fields since CC01 was used for small fields and CC13 was used for large fields.

The accuracy of this source model shows the potential of the model to be used for many applications such as dosimetric calculation in an advanced radiotherapy treatment techniques. In this study, the accurate source model was simulated upstream of the IQM CM for dose calculation in the IQM model. BEAMnrc CMs were used to model only the components of a full linac that contribute to its dose distributions. Despite the fact that the manufacturers provided some materials and geometries' specifications, accurate source model depends on the user. There are still parameters and modifications that would be done by the users to achieve a certain degree of accuracy. If manufacturer's specifications were fully detailed, maybe a higher degree of accuracy could have been achieved.

The number of histories required to achieve the statistical uncertainty that is within 1% in this study was above 15 billion for the largest square field (30 × 30 cm^2). BEAMDP allows the combination of several fractionated simulations to achieve the desired MC statistical uncertainty.

5.3 SENSITIVITY STUDY OF THE IQM COMPONENT MODULE

Acceptability of the IQM CM is based on its sensitivity to MLC leaf position using EGSnrc/BEAMnrc MC simulation. The IQM CM must be highly sensitive to detect leaf positioning errors in the simulated segment. The MLC leaf position quantifies the simulated IQM signal response. TG 142 and other related articles recommended that, the tolerance level for MLC misalignment of linac should be within ± 1 mm and ± 2 mm unlike TG 40 that recommended ± 5 mm for non-IMRT plans (Klein et al. 2009; Kehwar et al. 2006; Yan et al. 2009; LoSasso et al. 2001). Systematic errors were introduced by altering the MLC of several segments within few millimetres. MLC motion which was along the gradient of the IQM model was altered at random within ±1, ±2 and ±3 mm for

eleven segments. Linac head model was setup with IQM CM attached to the Linac head model at 4.5 cm from the lowest diaphragm. The spatial integral dose scored in the air chamber of the IQM CM after simulations were calculated for every alteration. Scatter plots, brute force, variance-based and standard regression coefficient sensitivity analysis techniques were carefully used to analyse the results of the mathematical model. These techniques were to show the importance of inputs on its outputs.

The calculated electronic signal and the simulated dose increase with an increase in square field size with the data closely in agreement over the range of field sizes.

In sensitivity evaluation of the IQM model to systematic positional error, alterations of 1 × 1 cm^2 field displayed a larger sensitivity when the magnitude of the IQM signal was calculated for misalignment of open leaves (1 × 1, 3 × 3, 5 × 5 and 10 × 10 cm^2) by -3, -2, -1, 1, 2, 3 mm. The wedge-shaped chamber is mostly sensitive to alterations in smaller fields than alterations in large fields, the magnitude of the IQM signal increased with an increase in the positional error of the field and decreased with a decrease in positional error of the field.

In Tab. 4.4, more offset leaves cause an increase in the normalised IQM signal and an increase in the position of leaves moved out of the field causes an increase in the IQM signal. The IQM signals were approximated to 3 decimal places which would have created an inconsistency in the outputs signals. The IQM CM is sensitive to single MLC shift of 5 × 5 cm^2

For gradient positional error analysis, the sensitivity of the IQM chamber increased along the gradient of the IQM chamber. From the MC simulations, the largest air volume region has the highest signal response. Also, different shapes with the same segment area such as 7 × 5 cm^2 and 5 × 7 cm^2 will not have the same signal response along the gradient of the IQM since they did not have the same value for trend line gradient. For each field size, the values were normalized to the unaltered field size, which does not mean that they have the same signal output. Around the region of the largest air volume of the IQM chamber, there is a noticeable plateau. This plateau is caused by loss in lateral electron equilibrium [Farrokkish's presentation also stated this idea at world medical physics conference (IUPESM 2015) (Farrokhkish et al. 2015)]. Loss of lateral

equilibrium could be as a result of the photon beam been unable to completely cover the air volume of the IQM chamber at this region (Li et al. 1995).

For random error analysis, the effect of random alterations of the Agility 160- leaf MLC model within ±1, ±2 and ±3 was marginal for bigger segments such as segment area of 49.00, 36.66, 70.82, 47.49 and 38.74 cm^2. Errors on the leaves are significant in smaller apertures compared to bigger apertures. It shows that the effects of alterations on small field sizes are more pronounced than bigger field sizes.

Scatter plots sensitivity analysis of the eleven segments shows a degree of linearity. The highest degree of linearity regarding the gradient and correlation coefficient is found in segment ten's (1 × 1 cm^2 field) scatter plots because of its' small aperture as shown in Table 5.1 and Figure 5.1. In Figure 5.1, linear function was fitted to the scatter plot (SP) correlation coefficient data as a function of original segment area (SA) *(SP = -0.0023SA+ 1.0024).* It shows that an increase in SA causes a decrease in the SP correlation coefficient that is strongly dependent on SA. An increase in segment area causes an increase in signal response of the IQM model as analysed by scatter plots. Scatter plot are quick means of checking the sensitivity of data. It does not compare the rate of change of output with the rate of change of input like the brute force sensitivity analysis.

Table 5.1: Analysis of gradients for scatter plots

Segment	Segment area (cm^2)	Gradient value
One	49.00	0.0222
Two	25.00	0.0472
Three	9.00	0.1250
Four	19.99	0.0558
Five	36.66	0.0335
Six	25.83	0.0478
Seven	70.82	0.0181
Eight	47.49	0.0298
Nine	4.00	0.2749
Ten	1.00	***1.0448***
Eleven	38.74	0.0365

Brute force sensitivity analysis for the segments considered shows that the highest sensitivity index is around the unaltered segments for large field sizes while in the small

field, the sensitivity index is commonly high for the altered segments. This shows that the IQM model is very sensitive to alterations of small fields than large fields. It is not to contradict the above discussion, but to give a detailed analysis. The brute force technique means that, if a segment is altered, the magnitude of alteration (perturbation) which is the difference between the unaltered segment area and the altered segment area must be evaluated based on the difference in magnitude of the IQM signal (output). If the minimal difference in segment area gives a significant difference in signal dose, then the model is very sensitive to such input parameter. This technique is unlike scatter plots that plot the output signal with the input parameter (segment area) alone without considering the rate of change of the unaltered parameters. It could be stated that significant difference in segment area (from unaltered to altered segment) does not necessarily lead to significant difference in IQM signal for a large segment. However, an increase in the magnitude of segment area causes an increase in the magnitude of the IQM signal. If the scatter plots seem to be perfectly linear like segment 9 and 10 which are small segments, brute force sensitivity index will display a noticeable peak across the entire altered segment which could seem to be uniform just like the brute force analysis of 2 × 2 and 1 × 1 cm^2 fields. This shows that the IQM model is very sensitive to alterations of small segments.

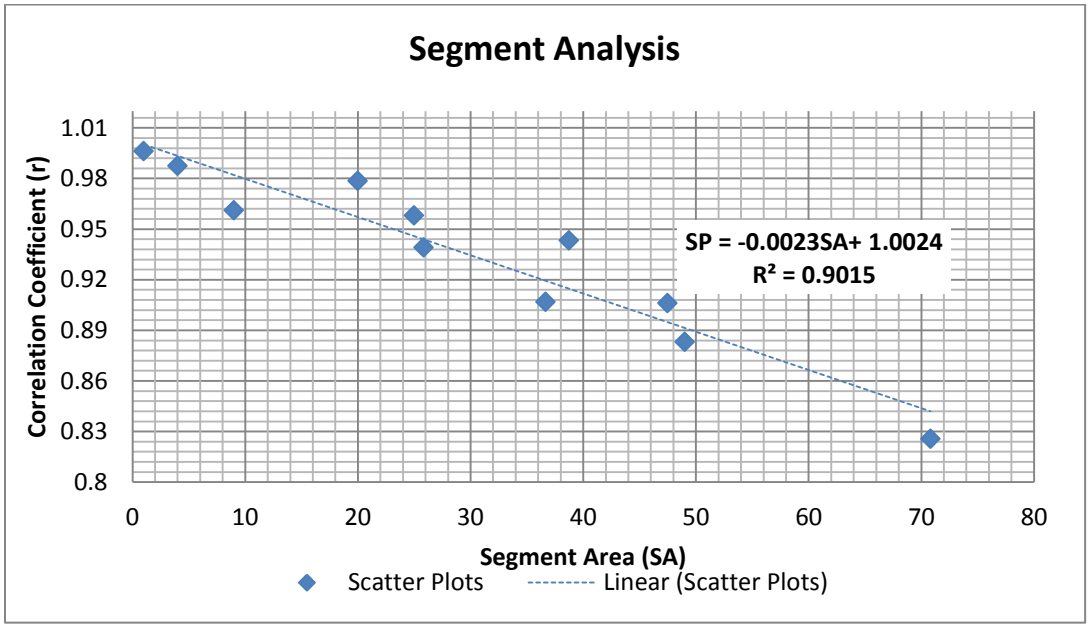

Figure 5.1: Analysis of correlation coefficient for scatter plots

Variance-based sensitivity analysis is utilised when there are correlated inputs that may have an impact on the output signals through its variance. In this study, the impact of just one input parameter (random alteration of MLC) was checked on the output signal. A sensitive parameter will not have a variance based sensitive index of zero. For the eleven segments considered, none of the segments that were altered randomly has an index of zero and the sensitive index increases with an increase in the area of the segment. The small fields correspond better than large fields. This shows that the IQM model is very sensitive to small fields. The uncertainty of the IQM signals proved that the IQM model is sensitive to segments that are altered randomly within few millimetres.

Standard regression coefficient (SRC) for the eleven segments considered displayed a maximum SRC values around the region of the unaltered segment. It could be deduced that the sensitivity of the IQM model is more pronounced for large fields with minimal alterations than for large field with maximal alterations. For small fields, maximal alterations within the offset variables considered have high SRC values in relation to minimal alterations. This means that the IQM is very sensitive to alterations of small fields than large fields. The scatter plots give a reasonable idea to this outcome. For a perfectly linear graph, the rate of change of the output value per the input variable will be uniform, which makes the SRC values to seem uniform across the altered segments of 1×1 cm^2 field considered. It could be stated that that the IQM model is very sensitive to alterations of small fields.

In total, several systematic positional error segments and three hundred and thirty (330) randomly altered segments within ±1, ±2 and ±3 mm positional errors were simulated to conclude that the IQM model is highly sensitive and the sensitivity is more pronounced in small segments than large segments. It could be hypothesised that when it comes to patient-specific TP for advanced EBRT (such as IMRT, VMAT and SRS), where all the treatment fields are not consistently small, misalignment in large fields which are of the same proportion with small field alterations will probably be delivered to patients because it will probably fall within the tolerance level of the IQM model. Since MLC positioning-errors can be quantified, maybe the tolerance level for large fields or all fields should be made stricter when IQM detector is used. This opens a further study on the sensitivity of IQM CM to patient-specific TP that covers the range of clinically

relevance and the relationship between MLC positioning-error proportion and signal output proportion for small and large field comparison.

The four sensitivity analysis techniques used in this study are independent, and each of them can be used solely to evaluate the sensitivity of a parameter. This study made use of more than one sensitivity analysis technique for an in-depth study. They all have a definite and different way of evaluating the sensitivity of a model. It should be noted that random alteration within ±3 mm does not necessarily mean that all the altered segments within ±3 mm have the lowest or highest segment area than segments that were altered within ±1 and ±2 mm. The number of leaves to be altered and leaf shifted positions were randomly defined. Therefore, it is possible to assign a positional error of -0.7 mm or 0.7 mm to segments that are meant to be altered within ±3 mm.

Photon beam of 10 MV was used for this sensitivity study. From experience, when the IQM outputs signals are normalised, increasing the beam energies it makes no huge significant difference. The IQM signal is a function of beams fluence per unit area. The IQM MC model can only calculate the MLC-defined dose and its positional errors (MC dose quantifies the leaf positioning error) when the IQM is mounted on the linac head. It cannot fully function like the IQM system which verifies the patient's identity, bunker temperature, bunker pressure, treatment gantry angles, and an alarm warning when errors are outside the tolerance corridor.

Application of MC to study the sensitivity of the wedge-shaped ionization chamber explored the potentials of MC radiation transport for dose distribution in this sophisticated ion chamber.

CHAPTER 6

6.0 CONCLUSION AND SUMMARY

6.1 CONCLUSION

This innovative research had studied the sensitivity of the prototype IQM system by using the BEAMnrc/ EGSnrc MC Simulation. It was able to develop a new CM namely IQM which was added onto the BEAMnrc. This newly developed CM is flexible enough to model the IQM system and calculate spatial dose in the air region of the wedge-shaped ionization chamber model. The IQM was modelled alongside with the linac head model as used in practice.

An accurate linac model was developed in order to avoid discrepancies upstream of the IQM model. An Elekta Synergy linac head equipped with an Agility-160 leaf MLC was modelled. It was benchmarked with measurement by using the gamma analysis of 2%/2 mm criterion.

The IQM signal was initially calculated for 1 × 1 up to 30 × 30 cm^2 fields and correlated to physical measurement. Physical measurement output is an electronic signal while simulation output is an integral dose. This study correlated the measurement and simulation by using the dose-area product and signal calculation using MC simulated MU as utilised in articles. An increase in field sizes causes an increase in IQM signal.

The MLC of the linac model were altered across a range of field shapes to have a comprehensive study. The idea behind this was to check the sensitivity of the IQM model. The purpose of the IQM system is to verify the patient treatment plan data in real-time and for this device to be used clinically, it is essential to know how sensitive it is for small segment alterations. Systematic positional errors were added and subtracted from a whole leaf bank. Secondly, the effect of moving a single leaf out of the field was studied. Thirdly, fields were moved along the gradient of the IQM model. Lastly, irregular and regular segments were altered randomly within ±1, ±2 and ±3 mm which was defined at the isocenter of 10 MV photon beam. The IQM model is sensitive to systematic and random errors introduced to the MLC leaves. This model is sensitive along its gradient and an increase in separation distance between the electrodes causes a weak signal response at the upper edge of the wedge-shaped chamber. Application of the four sensitivity analysis techniques proved that the IQM is mostly sensitive to small segment than for large segment. The smallest randomly altered

segment was 1 × 1 cm^2 field and its scatter plot showed a higher gradient of the trend line compared with other segments considered in this study. The brute force analysis of the smallest field displayed higher sensitivity indices across its altered segment than other segments that were randomly altered. The variance based sensitive indices for altered segments of 1 x 1 cm^2 field displayed a higher gradient than other segments that were altered. The smallest field considered in this study showed high standard regression coefficient values. Each of the sensitivity analysis technique is "self-sufficient" and unique in its computation. This study used more than one technique for an in-depth study and to see if the sensitivity techniques are congruent.

The sensitivity of the IQM CM in this study shows the potential of this model to be utilised for further MC study of advanced radiotherapy techniques using MC simulations. This model can also function as MLC calibration tool.

The EGSnrc/BEAMnrc MC techniques could be used reliably for dose calculation in a wedge-shaped ionization chamber. The IQM system could be integrated into the clinical workflow after the electronic signal is pre-set to dose and the IQM model can be used for further study.

6.2 SUMMARY

This thesis focused on the sensitivity study of an online beam delivery check system called integral quality monitor (IQM) using Monte Carlo simulation. It is needful to understand the potential of the IQM system in verifying patient treatment plan data in real-time treatment as done like never before. To begin with, a new component module namely IQM CM was developed to fully model the online beam delivery check system using the BEAMnrc MC code. The IQM CM could model a detailed wedge-shaped chamber that is flexible in its dose scoring volume within the air chamber of the wedge electrodes (Islam et al. 2009; iRT Systems 2014). The IQM CM was added on to the existing CMs database in BEAMnrc.

An accurate MC source model cannot be ascertained without having physical measurement data as a reference. Using the manufacturer's specifications alone does not assure the accuracy of the source model. However, articles have suggested flatness and symmetry calculation as a means of validating the MC source model (Kehwar et al. 2006; Lloyd & Gagne n.d.; Brown 2003; Tayalatia et al. 2013). Benchmarking the MC calculation with commissioning data is generally accepted as the standard means of determining the accuracy of a source model. A source model of an Elekta Synergy linac equipped with Agility 160-Leaf MLC was developed and validated with commissioning data. The source model in this study agreed with commissioning data within 2% (dose to distance) / 2mm (distance to agreement) criteria in the Gamma function.

The setup of an accurate linac model with the new IQM CM fixed below the treatment head was simulated. The spatial integral dose was scored in the air chamber of the IQM model after simulations of 15.8 billion histories for the largest field (30×30 cm^2). Sensitivity of the IQM model was deduced by adding and subtracting positional errors from individual MLC leaf or by moving segments along the gradient of the IQM CM and also through altering the MLC leaves at random within ±1, ±2 and ±3 mm in terms of its individual leaf positions as defined at the isocenter for 10 MV beams. Scatter plots, brute force, variance-based and standard regression coefficient sensitivity analysis techniques were used to analyse the sensitivity of the IQM model. Sensitivity analysing techniques used in this study proves that the IQM model is highly sensitive and the

sensitivity of the IQM model is mostly pronounced within small segments of small induced error. This makes the IQM suitable for advanced radiotherapy treatment techniques.

Application of MC techniques for dose calculation has generally been accepted as a standard method of resolving physical measurement challenges. This study was able to develop a new component module which can now serve as a basis for researchers that have an interest in MC study of wedge-shaped ionization chamber systems, especially for advanced radiotherapy pre-treatment quality control techniques. Likewise, the accurate source model achieved in this study could also be used for further study of dose calculation in treatment planning. The accurate linac source model achieved in this study was used for further study of the IQM model's sensitivity.

Keywords: Integral quality monitoring system®, Real-time monitoring, Monte Carlo Simulation, Wedge-shaped Ionization chamber, Accurate source model, Sensitivity analysis techniques

6.3 OPSOMMING

Hierdie tesis fokus op die sensitiwiteit studie van 'n aanlyn bundelverifikasie stelsel genoem integrale kwaliteit monitor (IQM) met behulp van Monte Carlo simulasie. Dit is noodsaaklik om die potensiaal van die IQM stelsel te verstaan in die verifikasie van pasiënt behandeling plan data tydens aanlyn behandeling soos nog nooit tevore gedoen kon word nie. Om mee te begin is, 'n nuwe komponent module naamlik IQM CM is ontwikkel om ten volle die aanlyn bundelverifikasie stelsel te kan modelleer met behulp van die BEAMnrc MC kode. Die IQM CM kan 'n gedetailleerde wigvormige kamer modelleer en kan aangepas word in die dosis opname streek binne die lug kamer van die wig vormige elektrode model.

‘n akkurate MC seeltjie bron model kan nie vasgestel word sonder fisiese metings data as verwysing nie. Die gebruik van die vervaardiger se spesifikasies alleen kan nie die akkuraatheid van die bron model leer nie. Alhoewel, 'n paar artikels voorgestel het dat veld platheid en simmetrie berekening as 'n middel van bekragtiging kan dien van die MC bron model. Die yking van die berekende MC data met gemete data word algemeen aanvaar as die standaard middel van die bepaling van die akkuraatheid van 'n bron model. 'n bron model van 'n Elekta Synergy toegerus met die Agility 160-MLC is ontwikkel en gevalideer met gemete data. Die bron model in hierdie studie het ooreengestem met die metings data binne 2 %/ 2 mm soos opgestel in die Gamma funksie.

'n Simuasie van 'n akkurate model met die nuwe IQM CM onder die kop vas is nageboots. Ruimtelike integrale dosis is aangeteken in die lug kamer van die IQM model na simulasies van 9.8 biljoen deeltjie lopies vir die grootste veld (30×30 cm^2) in hierdie studie. Sensitiwiteit van die IQM model is afgelei deur optelling en aftrekking posisionele foute van individuele MLC segmente, en deur bewegende segmente langs die helling van die IQM en die verandering van die MLC patroon na willekeur binne ±1, ±2 en ±3 mm in terme van sy individuele patroon posisies soos bepaal in die isosenter vir 10 MV. Verspreidingsgrafieke, brute krag, variansie-gebaseerde en standaard regressiekoëffisiënt sensitiwiteitsanalise tegnieke is gebruik om die sensitiwiteit van die IQM model ontleed. Sensitiwiteit s ontleed tegnieke in hierdie studie het bewys dat die

IQM model baie is sensitief en die sensitiwiteit van die IQM model is meestal prominent binne klein segmente deur klein geinduseerde foute. Dit maak die IQM geskik vir gevorderde bestraling behandeling tegnieke verifikasie.

Toepassing van MC tegnieke vir die berekening van dosis het oor die algemeen as 'n standaard metode van die oplossing van komplekse fisiese meting aanvaarbaar geword. Hierdie studie was in staat om 'n nuwe komponent module wat nou as basis kan dien vir navorsers wat belangstel in MC studie van wigvormige ionisasie kamer stelsels, veral vir gevorderde bestraling gehaltebeheer. Die akkurate bron model in hierdie studie kan ook gebruik word vir verdere studie van berekening van dosis in behandelingsbeplanning. Die akkurate bron model behaal in hierdie studie gebruik is vir verdere studie van sensitiwiteit die IQM model.

Sleutelwoorde: Integrale gehalte monitering System, monitering, Monte Carlo-simulasie, Wigvormige Ionisasie kamer, akkurate bron model, Sensitiwiteitsanalise tegnieke

6.4 FUTURE WORK

This study has investigated the sensitivity of the prototype wedge-shaped ionization chamber and was able to state categorically that the IQM system is sensitive to the segment which is most pronounced for small fields. It could detect positional errors in the treatment plan data. The IQM device shows the potential to be used for advanced radiotherapy techniques

As stated in this study, the IQM system is in its beta testing, which means that it could be upgraded. Firstly, further investigation is necessary on how to correlate physical measurement with MC dose for IMRT, VMAT, and SRS/SBRT treatment plan data. Secondly, since the IQM system output is an electronic signal, further study is essential on how the electronic signal can be pre-set to dose. Thirdly, Sensitivity analysis could be performed on patient-specific treatment plans.

REFERENCES

Adewuyi, S. et al., 2013. Current status of radiation oncology facilities in Nigeria. *West African Journal of Radiology*, 20(1), p.30.

Agostinelli, S. et al., 2003. Geant4—a simulation toolkit. *Nuclear Instruments and Methods in Physics Research Section A: Accelerators, Spectrometers, Detectors and Associated Equipment*, 506(3), pp.250–303.

Ahmad, S.S. et al., 2012. Advances in radiotherapy. *BMJ (Clinical research ed.)*, 345(e7765), pp.1-8.

American Cancer Society, 2011. Cancer in Africa. *Atlanta: Amercian Cancer Society*.

Amit, G. et al., 2015. Automatic learning-based beam angle selection for thoracic IMRT. *Medical Physics*, 42(4), pp.1992–2005.

Andreo, P., 1991. Monte Carlo techniques in medical radiation physics. *Physics in medicine and biology*, 36(7), pp.861–920.

Andrews, D.W. et al., 2004. Whole brain radiation therapy with or without stereotactic radiosurgery boost for patients with one to three brain metastases: phase III results of the RTOG 9508 randomised trial. *Lancet (London, England)*, 363(9422), pp.1665–72.

Archambault, L. et al., 2003. Overview of Geant4 applications in medical physics. *2003 IEEE Nuclear Science Symposium. Conference Record (IEEE Cat. No.03CH37515)*.

Attix, F.H., 1986. Introduction to Radiological Physics and Radiation Dosimetry, Wiley-Vch Verlag GmbH &Co. KGaA, p.505.

Baglan, K.L. et al., 2003. Accelerated partial breast irradiation using 3D conformal radiation therapy (3D-CRT). *International Journal of Radiation Oncology Biology Physics*, 55(2), pp.302–311.

Bak, J. et al., 2012. Modified dose difference method for comparing dose distributions. *Journal of applied clinical medical physics*, 13(2), pp.73–80.

Baro, J. et al., 1995. An algorithm for Monte Carlo simulation of the penetration and energy-loss of electrons and positrons in matter. *Nuclear Instruments and Methods in Physics Research Section A: Accelerators, Spectrometers, Detectors and Associated Equipment*, 100(1), pp.31–46.

Baskar, R. et al., 2012. Cancer and Radiation Therapy: Current Advances and Future Directions. *International Journal of Medical Science*, 9(3), pp.193–199.

Bastida-Jumilla, M.C. et al., 2011. DRR and portal image registration for automatic patient positioning in radiotherapy treatment. *Journal of Digital Imaging*, 24(6), pp.999–1009.

Becker, W. et al., 2011. Bayesian sensitivity analysis of a model of the aortic valve. *Journal of biomechanics*, 44(8), pp.1499–506.

Bedford, J.L. et al., 2016. Beam modeling and VMAT performance with the Agility 160 - leaf multileaf collimator. *Journal of Applied Clinical Medical Physics*, 14(2), pp.1–12.

Benedict, S.H., 2004. Review of Radiation Oncology Physics: A Handbook for Teachers and Students. *Journal of Applied Clinical Medical Physics*, 5(3), pp.91–92.

Bielajew, A.F., Mohan, R. & Chui, C.S., 1989. Improved bremsstrahlung photon angular sampling in the EGS4 code system. *National Research Council of Canada Report PIRS-0203*, p.22.

Bindhu, J., Supe, S. & Pawar, Y., 2009. Intensity modulated radiotherapy (IMRT) the white, black and grey: a clinical perspective. *Reports of Practical Oncology & Radiotherapy*, 14(3), pp.95–103.

Bissonnette, J.-P. et al., 2012. Quality assurance for image-guided radiation therapy utilizing CT-based technologies: a report of the AAPM TG-179. *Medical physics*, 39(4), pp.1946–63.

Blomquist, M. et al., 1998. Scanned intensity modulations for 50 MV photons. *Physics in medicine and biology*, 43(5), pp.1185–97.

Bondiau, P.-Y. et al., 2013. Phase 1 clinical trial of stereotactic body radiation therapy concomitant with neoadjuvant chemotherapy for breast cancer. *International journal of radiation oncology, biology, physics*, 85(5), pp.1193–9.

Boutilier, J.J. et al., 2015. Models for predicting objective function weights in prostate cancer IMRT. *Medical Physics*, 42(4), pp.1586–1595.

Boyer, A.L. et al., 1992. A review of electronic portal imaging devices (EPIDs). *Medical physics*, 19(1), pp.1–16.

Brent, B.W., Ken, J. & Jeffrey, H., 2003. Practical Programming in Tcl and Tk. , p.455.

Brown, F.., 2003. MCNP- A general Monte Carlo-particle transport code, version 5. , p.484.

Bucci, M.K., Bevan, A. & Roach, M., 2005. Advances in radiation therapy: conventional to 3D, to IMRT, to 4D, and beyond. *CA: Cancer journal for clinicians*, 55(2), pp.117–134.

Bucher, C., 2009. Computational Analysis of Randomness in Structural Mechanics. In *Structures and Infrastructures Book Series, volume 3*. CRC Press.

Ceberg, C., 2013. A note on the interpretation of the gamma evaluation index. *Journal of Physics: Conference Series*, 444, p.12082.

Chan, K., Saltelli, A. & Tarantola, S., 1997. Sensitivity analysis of model output: variance-based methods make the difference. In *Proceedings of the 29th conference on Winter simulation*. pp. 261–268.

Chandraraj, V. et al., 2011. Consistency and reproducibility of the VMAT plan delivery using three independent validation methods. *Journal of applied clinical medical physics / American College of Medical Physics*, 12(1), p.3373.

Chang, J. et al., 2013. A method for online verification of adapted fields using an independent dose monitor. *Medical physics*, 40(7), p.72104.

Chetty, I.J. et al., 2007. Report of the AAPM Task Group No. 105: Issues associated with clinical implementation of Monte Carlo-based photon and electron external beam treatment planning. *Medical physics*, 34(12), pp.4818–4853.

Clark, J.M., 1992. Radiology: An Illustrated History. *JAMA: The Journal of the American Medical Association*, 268(1), p.138.

Cohan, D.S. et al., 2005. Nonlinear Response of Ozone to Emissions: Source Apportionment and Sensitivity Analysis. *Environ. Sci. Technol*, 39, pp.6739–6748.

Confalonieri, R. et al., 2010. Comparison of sensitivity analysis techniques: A case study with the rice model WARM. *Ecological Modelling*, 221(16), pp.1897–1906.

Connell, P.P. & Hellman, S., 2009. Advances in radiotherapy and implications for the next century: a historical perspective. *Cancer research*, 69(2), pp.383–92.

Cook, P.J. & Burkitt, D.P., 1971. Cancer in Africa. *British Medical Bulletin*, 27(1), pp.14–20.

Coutard, H., 1934. Principles of x ray therapy of malignant diseases. *The Lancet*, 224(5784), pp.1–8.

Davis, J.N. et al., 2015. Stereotactic body radiotherapy for centrally located early-stage non-small cell lung cancer or lung metastases from the RSSearch(®) patient registry. *Radiation oncology (London, England)*, 10(1), p.113.

Depuydt, T., Van Esch, A. & Huyskens, D.P., 2002. A quantitative evaluation of IMRT dose distributions: Refinement and clinical assessment of the gamma evaluation. *Radiotherapy and Oncology*, 62(3), pp.309–319.

Dezarn, W.A., 2008. Quality assurance issues for therapeutic application of radioactive microspheres. *International journal of radiation oncology, biology, physics*, 71(1 Suppl), pp.S147-51.

Dj, K., 2014. An Overview of Image-Guided Radiotherapy (IGRT). *OMICS Journal of Radiology*, 3(4), pp.2–4.

Dorner, E., 2012. *Development and validation of multi-leaf collimator component module using a modified EGSnrc platform for Monte Carlo simulations*. Ruperto-

Carola University of Heidelberg, Germany.

Emami, B. et al., 1991. Tolerance of normal tissue to therapeutic irradiation. *International journal of radiation oncology, biology, physics*, 21(1), pp.109–22.

Farrokhkish, M. et al., 2015. Performance Study of an Automated Real Time Beam Monitoring System for SBRT Treatments. *International Journal of Radiation Oncology Biology Physics*, 93(3), p.S159.

Feng, Z. et al., 2016. Monte Carlo simulation of beam characteristics from small fields based on TrueBeam flattening-filter-free mode. *Radiation Oncology*, 11(1), pp.1–9.

Fenwick, J.D. et al., 2006. Tomotherapy and other innovative IMRT delivery systems. *Seminars in radiation oncology*, 16(4), pp.199–208.

Fix, M.K. et al., 2004. Monte Carlo source model for photon beam radiotherapy: photon source characteristics. *Medical physics*, 31(11), pp.3106–3121.

Fletcher, G.H., 1978. The evolution of the basic concepts underlying the practice of radiotherapy from 1949 to 1977. *Radiology*, 127(1), pp.3–19.

Fraass, B. et al., 1998. American Association of Physicists in Medicine Radiation Therapy Committee Task Group 53: quality assurance for clinical radiotherapy treatment planning. *Medical physics*, 25(10), pp.1773–829.

Freeman, D.E. & King, C.R., 2011. Stereotactic body radiotherapy for low-risk prostate cancer: five-year outcomes. *Radiation oncology (London, England)*, 6, p.3.

Frye, D.M. et al., 1995. Intercomparison of normalized head-scatter factor measurement techniques. *Medical physics*, 22(2), pp.249–53.

Fuangrod, T. et al., 2011. Development of EPID-based Real time Dose Verification for Dynamic IMRT. *World Academy of Science, Engineering and Technology*, 5(8), pp.609–612.

Gan, Y. et al., 2014. A comprehensive evaluation of various sensitivity analysis methods: A case study with a hydrological model. *Environmental Modelling & Software*, 51, pp.269–285.

Giraud, P. & Houle, A., 2013. Respiratory Gating for Radiotherapy : Main Technical

Aspects and Clinical Benefits. *ISRN Pulmonology- Hindawi*, (519602), pp.1–13

Greer, P.B., 2013. 3D EPID based dosimetry for pre-treatment verification of VMAT – methods and challenges. *Journal of Physics: Conference Series*, 444(1), p.12010.

Haffty, B.G. & Wilson, L.D. eds., 2009. *Handbook of radiation oncology*, Sudbury, Mass.: Jones and Bartlett Publishers.

Hakami, A., Odman, M.T. & Russell, A., 2003. High-Order, Direct Sensitivity Analysis of Multidimensional Air Quality Models. *Environ. Sci. Technol.*, 37, pp.2442–2452.

Hall, E.J., 2006. Intensity-modulated radiation therapy, protons, and the risk of second cancers. *International journal of radiation oncology, biology, physics*, 65(1), pp.1–7.

Hamby, D.M., 1994. A review of techniques for parameter sensitivity analysis of environmental models. *Environmental monitoring and assessment*, 32(2), pp.135–54.

Hansen, E.K. et al., 2006. Repeat CT imaging and replanning during the course of IMRT for head-and-neck cancer. *International journal of radiation oncology, biology, physics*, 64(2), pp.355–62.

Heath, E. & Seuntjens, J., 2003. Development and Validation of a BEAMnrc component module for accurate Monte Carlo modelling of the Varian dynamic Millennium multileaf collimator. *Physics in Medicine and Biology*, 48, pp.4045–4063.

Hellman, S., 1996. Roentgen Centennial Lecture: discovering the past, inventing the future. *International journal of radiation oncology, biology, physics*, 35(1), pp.15–20.

Helton, J.C. et al., 2006. Survey of sampling-based methods for uncertainty and sensitivity analysis. *Reliability Engineering & System Safety*, 91(10–11), pp.1175–1209.

Herman, M.G. et al., 2001. Clinical Use of Electronic Portal Imaging : Report of AAPM Radiation Therapy Committee Task Group 58. *Medical physics*, 28(5), pp.712–737.

Homma, T. & Saltelli, A., 1996. Importance measures in global sensitivity analysis of nonlinear models. *Reliability Engineering & System Safety*, 52(1), pp.1–17.

Hoyer, M. et al., 2006. Phase II study on stereotactic body radiotherapy of colorectal metastases. *Acta oncologica (Stockholm, Sweden)*, 45(7), pp.823–30.

Huang, E. et al., 2002. Intensity-modulated radiation therapy for pediatric medulloblastoma: early report on the reduction of ototoxicity. *International journal of radiation oncology, biology, physics*, 52(3), pp.599–605.

Huang, J.Y. et al., 2014. Effects of spatial resolution and noise on gamma analysis for IMRT QA. *Journal of Applied Clinical Medical Physics*, 15(4), pp.93–104.

Hussein, M. et al., 2013. A comparison of the gamma index analysis in various commercial IMRT/VMAT QA systems. *Radiotherapy and Oncology*, 109(3), pp.370–376.

Hwang, D., Byun, D.W. & Talat Odman, M., 1997. An automatic differentiation technique for sensitivity analysis of numerical advection schemes in air quality models. *Atmospheric Environment*, 31(6), pp.879–888.

IAEA, 2003. A Silent Crisis :Cancer treatment in developing countries. *IAEA in Austria, September 2003 IAEA/PI/A74 E/03-01531*, p.20.

IAEA, 1998. Design and Implementation of a Radiotherapy Programme: Clinical, Medical Physics, Radiation Protection and Safety Aspects. *IAEA-TECDOC-1040*, p 97.

IAEA, 1997. Quality assurance in radiotherapy. *(IAEA Vienna, May IAEA-TECDOC-989)*, p.249.

IBA, 2014. Dolphin® online treatment Monitoring. *Ion Beam Application (IBA) Uppsala Sweden*.

Intensity modulated radiotherapy collaborated working group, 2001. Intensity-modulated radiotherapy: current status and issues of interest. *International journal of radiation oncology, biology, physics*, 51(4), pp.880–914.

Iooss, B. & Lemaître, P., 2015. A Review on Global Sensitivity Analysis Methods. In *Uncertainty Management in Simulation-Optimization of Complex Systems*. Springer

US, pp. 101–122.

iRT Systems, 2014. Integral Quality Monitor Improving patient safety. *iRT Systems White paper presentation*.

iRT Systems, 2016. iRT | News. *i-rt.de/news/*. Available at: http://i-rt.de/news/.

Ishigami, T. & Homma, T., 1990. An importance quantification technique in uncertainty analysis for computer models. In *[1990] Proceedings. First International Symposium on Uncertainty Modeling and Analysis*. IEEE Comput. Soc. Press, pp. 398–403.

Ishihara, Y. et al., 2014. Development of a dose verification system for Vero4DRT using Monte Carlo method. *Journal of Applied Clinical Medical Physics*, 15(6), pp.160–172.

Ishikura, S., 2008. Quality assurance of radiotherapy in cancer treatment: Toward improvement of patient safety and quality of care. *Japanese Journal of Clinical Oncology*, 38(11), pp.723–729.

Islam, M.K. et al., 2009. An integral quality monitoring system for real-time verification of intensity modulated radiation therapy. *Medical physics*, 36(12), pp.5420–5428.

Jabbari, K., 2008. *Development of a fast Monte Carlo code for dose calculation in treatment planning and feasibility study of high contrast portal imaging*. McGill University Montreal.

Jabbari, K. et al., 2013. Monte Carlo Simulation of Siemens ONCOR Linear Accelerator with BEAMnrc and DOSXYZnrc Code. *Journal of medical signals and sensors*, 3(3), pp.172–9.

Jabbari, K. & Seuntjens, J., 2014. A fast Monte Carlo code for proton transport in radiation therapy based on MCNPX. *Journal of Medical Physics*, 39(3), p.156.

Jacques, R., Wong, J. & Taylor, R., 2011. Real-time dose computation : GPU-accelerated source modeling and superposition / convolution. *Medical physics*, 38(1), pp.294–305.

Jarkko, O., 2014. *Monte Carlo Simulations in Quality Assurance of Dosimetry and Clinical Dose Calculations in Radiotherapy*. Tampere University of Technology.

Jeraj, M. & Robar, V., 2004. Multileaf collimator in radiotherapy. *Radiol Oncol*, 38(3), pp.235–240.

Juste, B., Mota, M.E. & Gallardo, S., 2007. Monte Carlo Modeling of the Elekta Precise Linear Accelerator : Validation of Dose Distribution in a Heterogeneous Water Phantom. *Nuclear Applications*, pp.1–8.

Kagawa, K. et al., 1997. Initial clinical assessment of CT-MRI image fusion software in localization of the prostate for 3D conformal radiation therapy. *International Journal of Radiation Oncology Biology Physics*, 38(2), pp.319–325.

Kamp, F. et al., 2014. Variance-based sensitivity analysis of biological uncertainties in carbon ion therapy. *Physica Medica*, 30(5), pp.583–587.

Karzmark, C., 1984. Advances in linear accelerator design for radiotherapy. *Med Phys*, 11(2), pp.105–128.

Kawrakow, I., 2000. Accurate condensed history Monte Carlo simulation of electron transport. I. EGSnrc, the new EGS4 version. *Med Phys*, 27(3), pp.485–498.

Kawrakow, I., 2000. Accurate condensed history Monte Carlo simulation of electron transport . II . Application to ion chamber response simulations. *Medical physics*, 27(3), pp.499–513.

Kawrakow, I., 2002. Electron impact ionization cross sections for EGSnrc. In *Med. Phys. (abstract)*. p. 1230.

Kawrakow, I. et al., 2013. *The EGSnrc code system: Monte Carlo simulation of electron and photon transport*, NRCC PIRS-701.

Kawrakow, I. & Bielajew, A.F., 1998. On the condensed history technique for electron transport. *Nuclear Instruments and Methods in Physics Research Section B: Beam Interactions with Materials and Atoms*, 142(3), pp.253–280.

Keall, P.J. et al., 2005. Four-dimensional radiotherapy planning for DMLC-based

respiratory motion tracking. *Medical physics*, 32(4), pp.942–951.

Keall, P.J. et al., 2000. The effect of dose calculation uncertainty on the evaluation of radiotherapy plans. *Med. Phys.*, 27(3), pp.478–484.

Kehwar, T.S., Bhardwaj, A.K. & Chakarvarti, S.K., 2006. Evaluation of dosimetric effect of leaf position in a radition field of an 80-leaf multileaf collimator fitted to the LINAC head as tertiary collimator. *Journal of Applied Clinical Medical Physics*, 7(3), pp.43–54.

Kelsey, C.A., 2016. The Physics of Radiology, 4th Edition, edited by H. E. Johns and J. R. Cunningham (1984). *Medical Physics*, 11(5), pp.731–732.

Khan, F.M., 2014. *The Physics of Radiation Therapy (4th Edition)* F. M. Khan, ed., Lippincott Williams & Wilkins.

Kim, J.I. et al., 2014. The sensitivity of gamma-index method to the positioning errors of high-definition MLC in patient-specific VMAT QA for SBRT. *Radiation oncology (London, England)*, 9(167), p.12.

Kim, M. et al., 2014. Stereotactic ablative radiotherapy for oligometastatic disease in liver. *BioMed research international*, 2014, p.9.

Klein, E.E. et al., 2009. Task Group 142 report: Quality assurance of medical accelerators. *Medical Physics*, 36(9), pp.4197–4212.

Kubo, H.D. et al., 1998. High dose-rate brachytherapy treatment delivery: report of the AAPM Radiation Therapy Committee Task Group No. 59. *Medical physics*, 25(4), pp.375–403.

Kupelian, P.A. et al., 2004. Radical prostatectomy, external beam radiotherapy <72 Gy, external beam radiotherapy > or =72 Gy, permanent seed implantation, or combined seeds/external beam radiotherapy for stage T1-T2 prostate cancer. *International journal of radiation oncology, biology, physics*, 58(1), pp.25–33.

Kutcher, G.J. et al., 1994. Comprehensive QA for radiation oncology: report of AAPM Radiation Therapy Committee Task Group 40. *Medical physics*, 21(4), pp.581–618.

Langen, K.. et al., 2003. Evaluation of ultrasound-based prostate localization for image-

guided radiotherapy. *International Journal of Radiation Oncology*Biology*Physics*, 57(3), pp.635–644.

Langmack, K.A., 2001. Portal imaging. *The British journal of radiology*, 74(885), pp.789–804.

Lee, N. et al., 2002. Intensity-modulated radiotherapy in the treatment of nasopharyngeal carcinoma: an update of the UCSF experience. *International Journal of Radiation Oncology Biology Physics*, 53(1), pp.12–22.

Levin, C.V., El Gueddari, B. & Meghzifene, A., 1999. Radiation therapy in Africa: Distribution and equipment. *Radiotherapy and Oncology*, 52(1), pp.79–84.

Li, G. et al., 2008. Advances in 4D Medical Imaging and 4D Radiation Therapy. *Technology in cancer research & treatment*, 7(1), pp.67–81.

Li, G. et al., 2013. Evaluation of the ArcCHECK QA system for IMRT and VMAT verification. *Physica Medica*, 29(3), pp.295–303.

Li, X.A. et al., 1995. Lateral electron equilibrium and electron contamination in measurements of head-scatter factors using miniphantoms and brass caps. *Medical physics*, 22(7), pp.1167–70.

Liu, D. & Zou, Z., 2012. Sensitivity Analysis of Parameters in Water Quality Models and Water Environment Management. *Journal of Environmental Protection*, 3(8), pp.863–870.

Lloyd, S. a M. & Gagne, I.M., 2014. *Monte Carlo simulation of MLC-shaped TrueBeam electron fields benchmarked against measurement*. (Preprint).

Looe, H. et al., 2010. Enhanced Accuracy of IMRT Photon Fluence Profile Surveillance: Iterative Resolution Correction of the DAVID Chamber. *Medical Physics*, 37(6), pp.3227–3227.

LoSasso, T., Chui, C.S. & Ling, C.C., 2001. Comprehensive quality assurance for the delivery of intensity modulated radiotherapy with a multileaf collimator used in the dynamic mode. *Medical physics*, 28(11), pp.2209–2219.

Low, D.A. et al., 1998. A technique for the quantitative evaluation of dose distributions.

Medical physics, 25(5), pp.656–61.

Low, D.A. & Dempsey, J.F., 2003. Evaluation of the gamma dose distribution comparison method. *Medical Physics*, 30(9), p.2455.

Low, D. a, 2010. Gamma Dose Distribution Evaluation Tool. *Journal of Physics: Conference Series*, 250, p.12071.

Ma, C.-M.C., Maughan, R.L. & Orton, C.G., 2006. Within the next decade conventional cyclotrons for proton radiotherapy will become obsolete and replaced by far less expensive machines using compact laser systems for the acceleration of the protons. *Medical Physics*, 33(3), p.571.

Ma, C.M. et al., 2004. Monitor unit calculation for Monte Carlo treatment planning. *Physics in medicine and biology*, 49(9), pp.1671–87.

Madsen, M.T. & Ponto, J.L., 1992. *Medical physics handbook of nuclear medicine*, Medical Physics Handbook Of Nuclear Medicine. Madison, Wis.: Medical Physics Pub., Print.

Mayles, P., Nahum, A. & Rosenwald, I.C., 2007. *Handbook of Radiotherapy: theory and parctice*, Taylor and Francis group.

Mesbahi, A., 2006. Development a simple point source model for Elekta SL-25 linear accelerator using MCNP4C Monte Carlo code. *Iranian Journal of Radiation Research*, 4(1), pp.7–14.

Mesbahi, A., Mehnati, P. & Keshtkar, a., 2007. A comparative Monte Carlo study on 6MV photon beam characteristics of Varian 21EX and Elekta SL-25 linacs. *Iranian Journal of Radiation Research*, 5(1), pp.23–30.

Michalski, J.M. et al., 2003. Preliminary evaluation of low-grade toxicity with conformal radiation therapy for prostate cancer on RTOG 9406 dose levels I and II. *International journal of radiation oncology, biology, physics*, 56(1), pp.192–8.

Mohammadi, M. & Bezak, E., 2012. Evaluation of relative transmitted dose for a step and shoot head and neck intensity modulated radiation therapy using a scanning liquid ionization chamber electronic portal imaging device. *Journal of medical*

physics, 37(1), pp.14–26.

Mohan, R., 1995. Field Shaping for Three-Dimensional Conformal Radiation Therapy and Multileaf Collimation. *Seminars in radiation oncology*, 5(2), pp.86–99.

Most, T., 2011. Variance-based sensitivity analysis in the presence of correlatio input variables. *Lecture note, www.dynardo.de/en/library*.

Mundt, A.J. & Roeske, J.C., 2005. *Intensity Modulated Radiation Therapy: A Clinical Perspective, Volume 1*, PMPH-USA.

Myers, P. et al., 2013. VMAT monthly QA using two techniques: 2D ion chamber array with an isocentric gantry mount and an in vivo dosimetric device attached to gantry. *Journal of Radiotherapy in Practice*, 13(2), pp.240–246.

Nakamura, K. et al., 2014. Recent advances in radiation oncology: intensity-modulated radiotherapy, a clinical perspective. *International journal of clinical oncology*, 19(4), pp.564–9.

Nath, R. et al., 2009. AAPM recommendations on dose prescription and reporting methods for permanent interstitial brachytherapy for prostate cancer: report of Task Group 137. *Medical physics*, 36(11), pp.5310–22.

Nath, R. et al., 1997. Code of practice for brachytherapy physics: report of the AAPM Radiation Therapy Committee Task Group No. 56. American Association of Physicists in Medicine. *Medical physics*, 24(10), pp.1557–98.

Nath, R. et al., 1999. Intravascular brachytherapy physics: report of the AAPM Radiation Therapy Committee Task Group no. 60. American Association of Physicists in Medicine. *Medical physics*, 26(2), pp.119–52.

Nelson, W.R., Hirayama, H. & Rogers, D., 1985. The EGS4 Code System. *Report SLAC-265, Standford Linear Accelerator Centre, Standford, California*, 265.

Oh, C.E. et al., 1999. Comparison of 2D conventional, 3D conformal, and intensity-modulated treatment planning techniques for patients with prostate cancer with regard to target-dose homogeneity and dose to critical, uninvolved structures. *Medical Dosimetry*, 24(4), pp.255–263.

Oldham, M., Neal, A. & Webb, S., 1995. A comparison of conventional 'forward planning' with inverse planning for 3D conformal radiotherapy of the prostate. *Radiotherapy and oncology : journal of the European Society for Therapeutic Radiology and Oncology*, 35(3), pp.248–62.

Oliveira, A.C.H. et al., 2013. Monte Carlo Simulation of a Medical Linear Accelerator for Generation of Phase Spaces. In *International Nuclear Atlantic Conference - INAC 2013*. p. 15.

Paganetti, H. et al., 2004. Accurate Monte Carlo simulations for nozzle design, commissioning and quality assurance for a proton radiation therapy facility. *Medical Physics*, 31(7), p.2107-2118.

Paliwal, B.R. et al., 1996. A consistency monitor for radiation therapy treatments. *Med Phys*, 23(10), pp.1805–1807.

Palta, J.R., Liu, C. & Li, J.G., 2008. Current external beam radiation therapy quality assurance guidance: does it meet the challenges of emerging image-guided technologies? *International journal of radiation oncology, biology, physics*, 71(1 Suppl), pp.S13-7.

Palta, J.R., Mackie, T.R. & Chen, Z., 2003. Intensity-Modulated Radiation Therapy—The State of the Art. *Medical Physics*, 30(12), p.3265.

Park, J.-H. et al., 2011. Application of the gamma evaluation method in Gamma Knife film dosimetry. *Medical physics*, 38(10), pp.5778–87.

Parkin, D.M. et al., 2003. *Cancer in Africa—Epidemiology and Prevention* IARC press, ed., Lyon France: IARC Scientific Publications 153. Lyons: IARC Press.

Partridge, M., Ebert, M. & Hesse, B.M., 2002. IMRT verification by three-dimensional dose reconstruction from portal beam measurements. *Medical physics*, 29(8), pp.1847–58.

Pawlicki, T. & Mundt, A.J., 2007. Quality in radiation oncology. *Medical physics*, 34(5), pp.1529–1534.

Persoon, L.C.G.G. et al., 2011. A fast three-dimensional gamma evaluation using a

GPU utilizing texture memory for on-the-fly interpolations. *Medical physics*, 38(7), pp.4032–4035.

Petereit, D.G., 2015. *Global Challenges in Radiation Oncology*, Frontiers in Oncology.

Plischke, E., 2012. How to compute variance-based sensitivity indicators with your spreadsheet software. *Environmental Modelling & Software*, 35, pp.188–191.

Podgorsak, E.B., 2005. Chapter 5 Treatment machines for external beam radiotherapy. *Radiation Oncology Physics: A Handbook for Teachers and Students*, pp.123–160.

Podgorsak, E.B. & Hendee, W.R., 2006. Radiation Physics for Medical Physicists. *Medical Physics*, 33(1), p.249.

Poppe, B. et al., 2010. Clinical performance of a transmission detector array for the permanent supervision of IMRT deliveries. *Radiotherapy and oncology : journal of the European Society for Therapeutic Radiology and Oncology*, 95(2), pp.158–65.

Poppe, B. et al., 2006. DAVID- A translusent multi-wire transmission ionization chamber for invivo verification of IMRT and conformal irradiation techniques. *Physics in Medicine and Biology*, 51(5), pp.1237–1248.

Poppe, B. et al., 2008. SU-GG-T-144: IMRT Pre-Treatment Plan and In-Vivo Verification with 2D-ARRAYs and Multi-Wire Ionisation Chambers. *Medical Physics*, 35(6), p.2759.

Prendergast, B.M. et al., 2013. Flattening filter-free linac improves treatment delivery efficiency in stereotactic body radiation therapy. *Journal of applied clinical medical physics*, 14(3), pp.64-71.

PTW, 2013. DAVID dose delivery QA system. Available at: http://www.ptw.de/2398.html

Riegel, A. et al., 2011. SU-E-T-430: Quantifying Alterations in Flattened and Flattening-Filter-Free Beam Characteristics from a Gantry Mounted, in Vivo Beam Delivery Verification System on a TrueBeam Linear Accelerator. *Medical Physics*, 38(6), p.3587.

Roach, M. et al., 1996. Prostate volumes defined by magnetic resonance imaging and computerized tomographic scans for three-dimensional conformal radiotherapy.

International Journal of Radiation Oncology Biology Physics, 35(5), pp.1011–1018.

Roger, E. & Critchlow, J., 1996. TCL/TK Command Reference Guide. , p.149.

Rogers, D.W.O. et al., 1995. BEAM: A Monte Carlo code to simulate radiotherapy treatment units. *Med Phys*, 22(5), pp.503–524.

Rogers, D.W.O. & Bielajew, A.F., 1990. *Monte Carlo techniques of electron and photon transport for radiation dosimetry. In K.R.Kase, B.E. Bjarngard, and F.H. Attix, editor.* V. I. The Dosimetry of ionizing Radiation, ed., Academic Press.

Rogers, D.W.O., Walters, B. & Kawrakow, I., 2011. BEAMnrc Users Manual. *Source*, 509, pp.1–260.

Roopashri, G. & Baig, M., 2013. Current advances in radiotherapy of head and neck malignancies. *Journal of international oral health : JIOH*, 5(6), pp.119–123.

Rosenberg, I., 2008. Radiation Oncology Physics: A Handbook for Teachers and Students. *British journal of cancer*, 98(5), p.1020.

Ryu, J.K. et al., 2002. Interim report of toxicity from 3D conformal radiation therapy (3D-CRT) for prostate cancer on 3DOG/RTOG 9406, level III (79.2 Gy). *International journal of radiation oncology, biology, physics*, 54(4), pp.1036–46.

Sale, C.A. et al., 2005. 2D versus 3D radiation therapy for prostate carcinoma: a direct comparison of dose volume parameters. *Acta Oncol*, 44(4), pp.348–354.

Saltelli, A. et al., 2004. *Sensitivity Analysis in Practice: A Guide to Assessing Scientific Models*, John Wiley & Sons.

Saltelli, A. et al., 2010. Variance based sensitivity analysis of model output. Design and estimator for the total sensitivity index. *Computer Physics Communications*, 181(2), pp.259–270.

Saltelli, A. & Annoni, P., 2010. How to avoid a perfunctory sensitivity analysis. *Environmental Modelling & Software*, 25(12), pp.1508–1517.

Saltelli, A. & Bolado, R., 1998. An alternative way to compute Fourier amplitude sensitivity test (FAST). *Computational Statistics & Data Analysis*, 26(4), pp.445–

460.

Saltelli, A. & Tarantola, S., 2002. On the Relative Importance of Input Factors in Mathematical Models. *Journal of the American Statistical Association*, 97(459), pp.702–709.

Satelli, A. et al., 2008. *Global Sensitivity Analysis: The Primer*, Wiley.

Sätherberg, A. & Karlsson, M., 1998. Calculation of photon energy and dose distributions in a 50 MV scanned photon beam for different target configurations and scan patterns. *Medical Physics*, 25(2), pp.236–240.

Saw, C.B., Meigooni, A.S. & Nath, R., 1998. Review of AAPM Task Group No. 43 recommendations on interstitial brachytherapy sources dosimetry. *Medical dosimetry*, 23(4), pp.259–263.

Schwieger, V., 2004. Variance-based sensitivity analysis for model evaluation in engineering survey. In *INGEO and FIG Regional central and eastern european conference on engineering survey*. Bratislava, Slovakia, pp. 11–13.

Sempau, J. et al., 2001. Monte Carlo simulation of electron beams from an accelerator head using PENELOPE. *Physics in Medicine and Biology*, 46(4), pp.1163–1186.

Señal, N.C. et al., 2008. *Internal Quality Assurance and the European Standards and Guidelines the European Standards and Guidelines*,

Sitas, F. et al., 2006. Cancer. In D. T. Jamison et al., eds. *Disease and Mortality in Sub-Saharan Africa. 2nd edition*. The International Bank for Reconstruction and Development / The World Bank.

Sobol, I.., 2001. Global sensitivity indices for nonlinear mathematical models and their Monte Carlo estimates. *Mathematics and Computers in Simulation*, 55(1–3), pp.271–280.

Spezi, E. & Lewis, D.G., 2006. Gamma histograms for radiotherapy plan evaluation. *Radiotherapy and Oncology*, 79(2), pp.224–230.

St Clair, W.H. et al., 2004. Advantage of protons compared to conventional X-ray or IMRT in the treatment of a pediatric patient with medulloblastoma. *International*

journal of radiation oncology, biology, physics, 58(3), pp.727–34.

Stelljes, T.S. et al., 2015. Dosimetric characteristics of the novel 2D ionization chamber array OCTAVIUS Detector 1500. *Medical Physics*, 42(4), pp.1528–1537.

Sawkey, D., 2012. *Introducing EGSnrc / BEAMnrc style variance reduction techniques into Geant4*, Varian Medical Systems.

Tayalati, Y. et al., 2013. Monte Carlo Simulation of 6MV Elekta Synergy Platform Linac photon beam using Gate / Geant4. *arXiv:1309.0758 [physics.med-ph]*, p.10.

Thariat, J. et al., 2013. Past, present, and future of radiotherapy for the benefit of patients. *Nature Reviews Clinical Oncology*, 10(1), pp.52–60.

Thilmann, C. et al., 2004. Inversely planned intensity modulated radiotherapy of the breast including the internal mammary chain: a plan comparison study. *Technology in cancer research & treatment*, 3(1), pp.69–75.

Thoelking, J. et al., 2016. Characterization of a new transmission detector for patient individualized online plan verification and its influence on 6MV x-ray beam characteristics. *Zeitschrift fur medizinische Physik*, 26(3), pp.200–208.

Thomadsen, B.R. et al., On the cause of the variation in tissue-maximum ratio values with source-to-detector distance. *Medical physics*, 20(3), pp.723–7.

Thwaites, D. et al., 1995. Quality assurance in radiotherapy. *Radiotherapy and Oncology*, 35(1), pp.61–73.

Tiede, C., 2005. *Integration of optimzation algorithms with sensitivity analysis with application to volcanic regions*. Daramstadt University of Technology.

Usmani, M.N. et al., 2014. Development and reproducibility evaluation of a Monte carlo-based standard LINAC model for quality assurance of multi-institutional clinical trials. *Journal of Radiation Research*, 55(6), pp.1131–1140.

Van Dyk, J. et al., 1993. Commissioning and quality assurance of treatment planning computers. *International Journal of Radiation Oncology Biology Physics*, 26(2), pp.261–273.

van Elmpt, W.J.C. et al., 2005. Experimental verification of a portal dose prediction model. *Medical physics*, 32(9), pp.2805–18.

Virnig, B.A. et al., 2002. Studying radiation therapy using SEER-Medicare-linked data. *Medical care*, 40(8 Suppl), p.IV-49-54.

Walters, B.R.B. et al., 2001. *QA tests of the EGSnrc system and comparisons with EGS4 (Draft)*, NRCC Report PIRS-703.

Weichselbaum, R.R. & Hellman, S., 2011. Oligometastases revisited. *Nature Reviews Clinical Oncology*, 8(6), pp.378–82.

Wendling, M. et al., 2006. Accurate two-dimensional IMRT verification using a back-projection EPID dosimetry method. *Medical physics*, 33(2), pp.259–73.

Wieslander, E., 2000. Verification of Dose Calculation Algorithms in Treatment Planning Systems for External Radiation Therapy - A Monte Carlo Approach. *Physics in medicine and biology*, 45, pp.2887–2896.

Williamson, J.F. et al., 2008. Quality assurance needs for modern image-based radiotherapy: recommendations from 2007 interorganizational symposium on 'quality assurance of radiation therapy: challenges of advanced technology'. *International journal of radiation oncology, biology, physics*, 71(1 Suppl), pp.S2-12.

Winiecki, J. et al., 2009. The gamma evaluation method as a routine QA procedure of IMRT. *Reports of Practical Oncology & Radiotherapy*, 14(5), pp.162–168.

Woodruff, H.C. et al., 2015. First Experience With Real-Time EPID-Based Delivery Verification During IMRT and VMAT Sessions. *International Journal of Radiation Oncology Biology Physics*, 93(3), pp.516–522.

World Health Organization Technical Manual, 2008. *Radiotherapy Risk Profile*, WHO Press, World Health Organisation, Geneva 27, Switzerland.

Wu, Q.J. et al., 2008. The impact of respiratory motion and treatment technique on stereotactic body radiation therapy for liver cancer. *Medical physics*, 35(4), pp.1440–51.

Xia, J. et al., 2000. Computer-assisted three-dimensional surgical planning and

simulation: 3D virtual osteotomy. *International journal of oral and maxillofacial surgery*, 29(1), pp.11–17.

Xiao, Y. et al., 2015. Flattening filter-free accelerators: a report from the AAPM Therapy Emerging Technology Assessment Work Group. *Journal of Applied Clinical Medical Physics*, 16(3).

Xing, A. et al., 2015. Evaluation of 3D Gamma index calculation implemented in two commercial dosimetry systems. *Journal of Physics: Conference Series*, 573, p.12054.

Xing, L. & Li, J.G., 2000. Computer verification of fluence map for intensity modulated radiation therapy. *Medical physics*, 27(9), pp.2084–2092.

Yan, G. et al., 2009. On the sensitivity of patient-specific IMRT QA to MLC positioning errors. *Journal of Applied Clinical Medical Physics*, 10(1), pp.120–128.

Zelefsky, M.J. et al., 2000. Clinical experience with intensity modulated radiation therapy (IMRT) in prostate cancer. *Radiotherapy and oncology : journal of the European Society for Therapeutic Radiology and Oncology*, 55(3), pp.241–9.

Zhao, J. & Tiede, C., 2011. Using a variance-based sensitivity analysis for analyzing the relation between measurements and unknown parameters of a physical model. *Nonlinear Processes in Geophysics*, 18(3), pp.269–276.

Zhou, X. & Lin, H., 2008. *Local sensitivity analysis*, Springer US.

Zhu, T.C. et al., 2009. Report of AAPM Therapy Physics Committee Task Group 74: in-air output ratio, Sc, for megavoltage photon beams. *Medical physics*, 36(11), pp.5261–5291.

APPENDIX

APPENDIX ONE

1.0 IQM parameter on BEAMnrc interface

Page 1

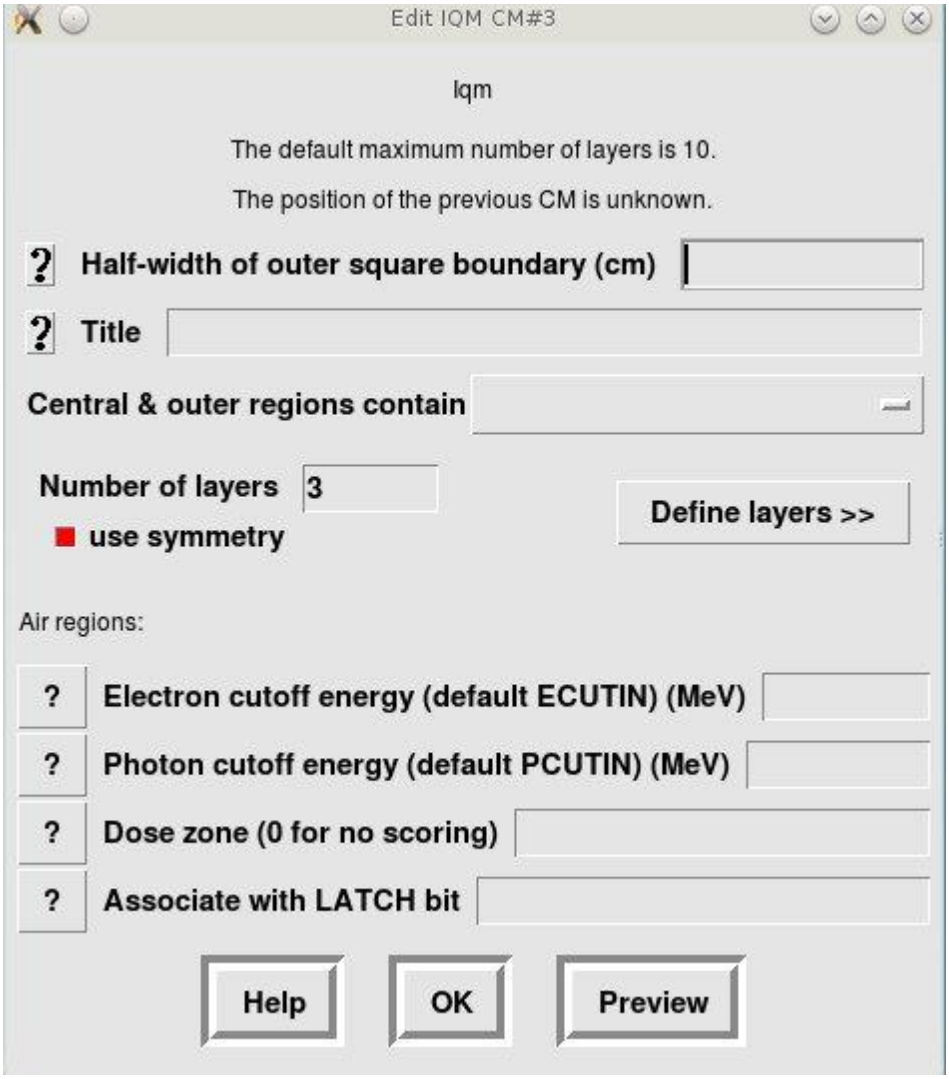

Page 2.

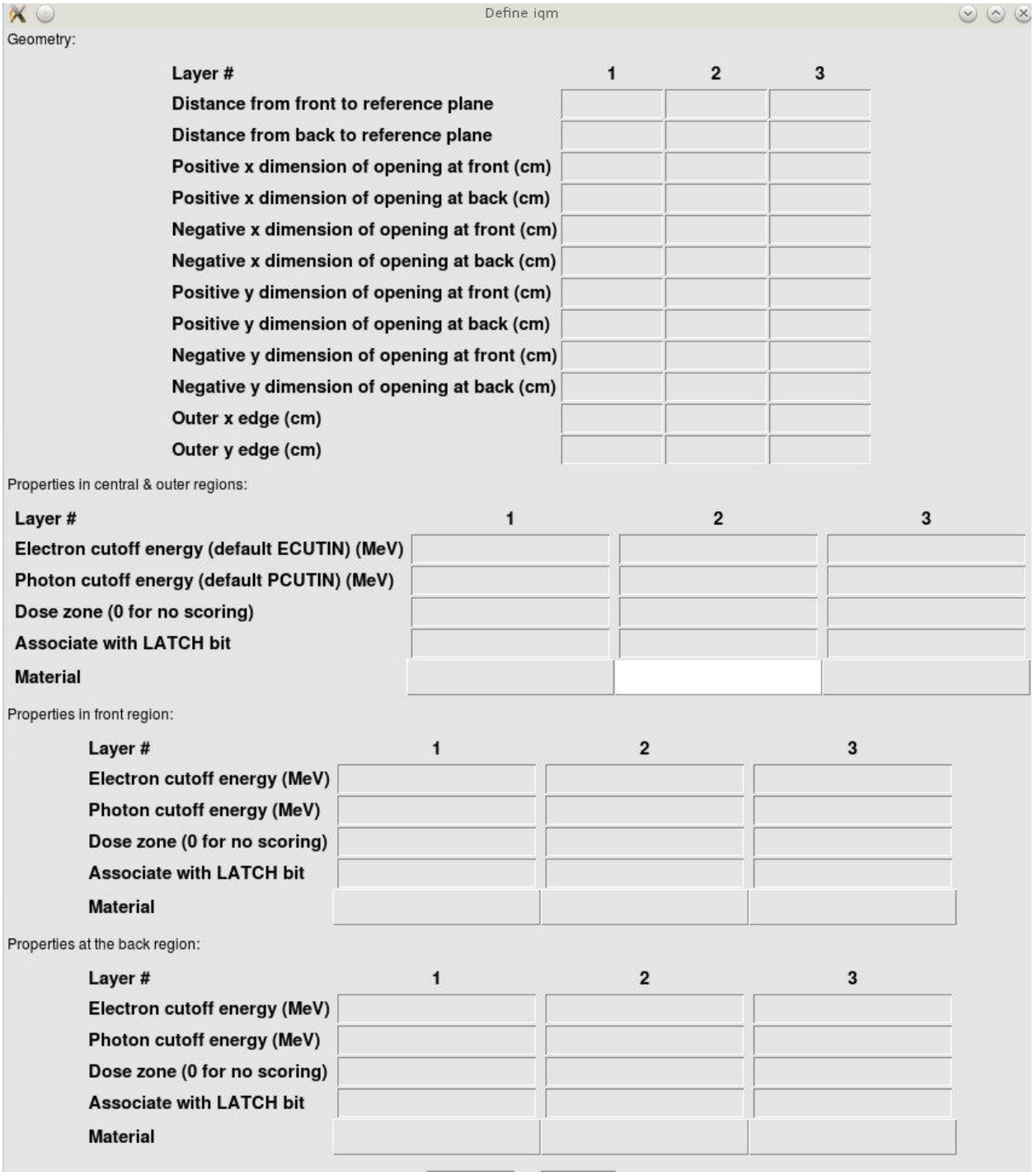
Define iqm
Geometry:
Layer # 1 2 3
Distance from front to reference plane
Distance from back to reference plane
Positive x dimension of opening at front (cm)
Positive x dimension of opening at back (cm)
Negative x dimension of opening at front (cm)
Negative x dimension of opening at back (cm)
Positive y dimension of opening at front (cm)
Positive y dimension of opening at back (cm)
Negative y dimension of opening at front (cm)
Negative y dimension of opening at back (cm)
Outer x edge (cm)
Outer y edge (cm)
Properties in central & outer regions:
Layer # 1 2 3
Electron cutoff energy (default ECUTIN) (MeV)
Photon cutoff energy (default PCUTIN) (MeV)
Dose zone (0 for no scoring)
Associate with LATCH bit
Material
Properties in front region:
Layer # 1 2 3
Electron cutoff energy (MeV)
Photon cutoff energy (MeV)
Dose zone (0 for no scoring)
Associate with LATCH bit
Material
Properties at the back region:
Layer # 1 2 3
Electron cutoff energy (MeV)
Photon cutoff energy (MeV)
Dose zone (0 for no scoring)
Associate with LATCH bit
Material

APPENDIX TWO

2.0 Application of brute force, variance-based and standard regression coefficient sensitivity analysis

Segment area (cm^2)	IQM signal	Signal variance
20.00 (unaltered)	1.5	0.91
20.3 (altered)	1.55	0.978
19.8 (altered)	1.45	0.9

Mean of the variances = 0.929

a. Brute Force:

$$S_i = \left|\frac{d(I)}{d(A)}\right|_i$$

$$S_i = \left|\frac{1.55-1.5}{20.3-20}\right|$$

$$S_i = 0.1667 Ans$$

b. Variance-based:

$$S_i = \frac{V[E(Y \mid X_i)]}{V[E(Y \mid X_i)] + E[V(Y \mid X_i)]}$$

$$S_i = \frac{0.978}{(0.978 + 0.929)}$$

$$S_i = 0.513 Ans$$

c. Standard regression coefficient:

$$SRC = \left| \frac{\frac{(Y_i - \overline{Y})}{s}}{\frac{(X_i - \overline{X})}{S_i}} \right|$$

If s (standard deviation for Y) is 1.5 and s_i (standard deviation for X) is 1.4

If Mean of Y (IQM signal) is 1.6 and mean of X (area of segment) is 2.3 for Y_i of 1.8 and X_i of 2.4

Then

$$SRC = \frac{\frac{(1.8-1.6)}{1.5}}{\frac{(2.4-2.3)}{1.4}}$$

$$SRC = 1.799 Ans$$

……to God be the glory, great things He has done.